AN ANALYTICAL MODEL TO PREDICT THE ENVIRONMENTAL FORCES ON A TENSION LEG PLATFORM AND TIME DOMAIN RESPONSE ANALYSIS

Stéphane CORNUT

Thesis submitted for a Degree of Master of Science

Department of Naval Architecture and Ocean Engineering

University of Glasgow

December 1995

ProQuest LLC.
789 East Eisenhower Parkway
P.O. Box 1346
Ann Arbor, MI 48106 – 1346

CONTENTS

CONTENTS ii

LIST OF FIGURES vii

LIST OF TABLES xii

ACKNOWLEDGEMENTS xiii

SUMMARY xv

CHAPTER 1: INTRODUCTION 1.1

1. CONCEPT AND HISTORY OF THE TENSION LEG PLATFORMS 1.1

2. PREVIOUS WORK 1.2

3. OBJECTIVES 1.3

REFERENCES OF CHAPTER 1 1.5

CHAPTER 2: FREQUENCY DOMAIN METHOD 2.1

1. INTRODUCTION 2.1

2. THE FREQUENCY DOMAIN METHOD 2.1

3. MOTION EQUATION COEFFICIENTS 2.3

4. SPECTRAL ANALYSIS 2.6

REFERENCES OF CHAPTER 2 2.9

CHAPTER 3: FIRST ORDER WAVES 3.1

1. INTRODUCTION 3.1

2. MORISON APPROACH 3.2
2.1. DIFFRACTION 3.2
2.1.1. Columns 3.3
2.1.2. Pontoons 3.5

2.2. ADDED MASS 3.7
2.2.1. Columns 3.7
2.2.2. Pontoons 3.8

3. ANALYTICAL METHOD 3.9
3.1. INTRODUCTION 3.9
3.2. HORIZONTAL PLANE 3.10
3.2.1. Diffraction 3.10
3.2.2. Radiation 3.13
3.3. VERTICAL PLANE 3.15
3.3.1. Diffraction 3.16
3.3.2. Radiation 3.20
3.4. ROLL AND PITCH 3.21
3.4.1. Diffraction 3.21
3.4.2. Radiation 3.22
3.5. PONTOONS 3.22

4. VALIDATION 3.23
4.1. SURGE AND SWAY FORCES AND MOTIONS 3.24
4.1.1. Diffraction 3.24
4.1.2. Radiation 3.25
4.1.3. Displacements 3.25
4.2. HEAVE FORCES AND MOTIONS 3.26
4.2.1. Diffraction 3.26
4.2.2. Radiation 3.26
4.2.3. Displacements 3.27
4.3. ROLL AND PITCH 3.28
4.3.1. Diffraction 3.28
4.3.2. Radiation 3.28
4.3.3. Displacements 3.28
4.4. DIRECTIONAL SEAS 3.29

5. CONCLUSION 3.29

REFERENCES OF CHAPTER 3 3.30

CHAPTER 4: SECOND ORDER WAVES 4.1

1. INTRODUCTION 4.1

2. THEORY 4.1
2.1. STEADY DRIFT 4.1
2.1.1. Single cylinder 4.2
2.1.2. Array of cylinders 4.4
2.1.3. Displacement 4.5
2.2. SLOWLY VARYING DRIFT 4.5

3. VALIDATION 4.6
3.1. DRIFT COEFFICIENT APPROXIMATION 4.6
3.2. STEADY DRIFT 4.7

3.2.1. Surge 4.8
3.2.2. Heave 4.9
3.2.3. Pitch 4.9
3.2.4. Directionality 4.10
3.3. SLOWLY VARYING DRIFT 4.10
3.3.1. Surge 4.10
3.3.2. Heave 4.11
3.3.3. Pitch 4.11

4. CONCLUSION 4.11

REFERENCES OF CHAPTER 4 4.13

CHAPTER 5: WIND AND CURRENT 5.1

1. INTRODUCTION 5.1

2. WIND 5.1
2.1. WIND FORCES 5.1
2.2. DISPLACEMENT 5.4
2.2.1. Steady Displacement 5.4
2.2.2. Fluctuating Wind Motion 5.4
2.3. WIND SPECTRA 5.5
2.3.1. The Harris wind spectrum 5.6
2.3.2. The Davenport wind spectrum 5.6
2.3.3. The Kaimal wind spectrum 5.6
2.3.4. The Ochi-Shin wind spectrum 5.7
2.3.5. The Slettringen wind spectrum 5.7
2.4. RESULTS 5.8
2.4.1. Steady response 5.8
2.4.2. Dynamic response 5.9

3. CURRENT 5.10
3.1. CONSTANT VELOCITY PROFILE 5.10
3.2. VARYING VELOCITY PROFILE 5.11
3.2.1. Tidal current 5.12
3.2.2. Storm surge current 5.12
3.2.3. Forces 5.13
3.3. STEADY RESPONSE 5.13
3.4. DISCUSSION OF THE RESULTS 5.13
3.4.1. Surge 5.14
3.4.2. Pitch 5.16

4. CONCLUSION 5.16

REFERENCES OF CHAPTER 5 5.17

CHAPTER 6: TIME DOMAIN STUDY IN REGULAR WAVES 6.1

1. INTRODUCTION 6.1

2. TIME DOMAIN ANALYSIS 6.2

3. MATHEMATICAL MODELLING 6.3
3.1. LINEAR MODEL 6.3
3.2. DEFINITION OF NON-LINEARITIES 6.4
3.2.1. Viscous damping 6.5
3.2.2. Stiffness of the tendons 6.5
3.2.3. Drag Force 6.9
3.2.4. Coupling between the different modes of motion of the platform 6.10
3.2.5. Free surface effects 6.10
3.2.6. The effects of the displacement of the structure 6.16

4. TIME DOMAIN ANALYSIS 6.17
4.1. EFFECTS OF NON LINEARITIES ON THE SNORRE TLP 6.17
4.1.1. Test 0: Linear Model 6.18
4.1.2. Test 1: Non Linear Mooring Model 6.19
4.1.3. Test 2: Viscous Damping 6.19
4.1.4. Test 3: Motion Coupling 6.19
4.1.5. Test 4: Drag Force 6.20
4.1.6. Test 5: Free Surface Effects 6.20
4.1.7. Test 6: Displacements of the TLP 6.20
4.1.8. Test 7: Fully Non Linear Model (except displacements) 6.20
4.1.9. Test 8: Fully Non Linear Model (including displacements) 6.21
4.1.10. Conclusion 6.21
4.2. EFFECTS OF NON LINEARITIES ON THE HEIDRUN TLP 6.22
4.2.1. Test 0: Linear Model 6.22
4.2.2. Test 1: Non Linear Mooring Model 6.22
4.2.3. Test 2 and 3: Viscous Damping and Motion Coupling 6.23
4.2.4. Test 4: Drag Force 6.23
4.2.5. Test 5: Free Surface Effects 6.23
4.2.6. Test 6: Displacements of the TLP 6.23
4.2.7. Test 7: Fully Non Linear Model (except displacements) 6.24
4.2.8. Test 8: Fully Non Linear Model (including displacements) 6.24
4.3. EFFECTS OF THE WAVES CHARACTERISTICS ON THE SNORRE TLP 6.24
4.3.1. Surge Response 6.25
4.3.2. Heave Response 6.25
4.3.3. Pitch Response 6.25
4.3.4. Tendon Forces 6.26
4.4. EFFECTS OF THE DIRECTIONALITY OF THE ENVIRONMENTAL FORCES 6.26
4.4.1. Tendon Force Model Analysis 6.27
4.4.2. Pretension 6.28
4.4.3. First Order Force 6.29
4.4.4. Slackness Coefficient 6.29
4.4.5. Conclusion 6.29

REFERENCES OF CHAPTER 6 6.30

CHAPTER 7: CONCLUSION AND POSSIBLE FUTURE DEVELOPMENTS 7.1

1. WAVE MODEL 7.1

2. WIND AND CURRENT MODEL 7.1

3. TIME DOMAIN MODEL 7.2

REFERENCES OF CHAPTER 7 7.4

LIST OF FIGURES

CHAPTER 1

Fig 1.1: The Hutton TLP 1.7

CHAPTER 3

Fig 3.1: Mesh of the truncated cylinder 3.31

Fig 3.2: Mesh of the array of bottom mounted cylinders 3.32

Fig 3.3: Mesh of the array of truncated cylinders 3.33

Fig 3.4: First order surge force on an array of four complete cylinders 3.34

Fig 3.5: First order surge force on an array of four truncated cylinders 3.35

Fig 3.6: First order surge force on the Snorre TLP 3.36

Fig 3.7: Surge added mass of an array of four complete cylinders 3.37

Fig 3.8: Surge potential damping of an array of four complete cylinders 3.38

Fig 3.9: Surge added mass of an array of four truncated cylinders 3.39

Fig 3.10: Surge potential damping of an array of four truncated cylinders 3.40

Fig 3.11: Surge added mass of the Snorre TLP 3.41

Fig 3.12: Surge potential damping of the Snorre TLP 3.42

Fig 3.13: Displacement in surge 3.43

Fig 3.14: Displacement in surge about natural frequency 3.44

Fig 3.15: Displacement in surge about natural frequency 3.45

Fig 3.16: First order heave force on a truncated cylinder 3.46

Fig 3.17: First order heave force on an array of four truncated cylinders 3.47

Fig 3.18: First order heave force on the Snorre TLP 3.48

Fig 3.19:	Heave added mass of a truncated cylinder	3.49
Fig 3.20:	Heave added mass of an array of four truncated cylinders	3.50
Fig 3.21:	Heave added mass of the Snorre TLP	3.51
Fig 3.22:	Heave potential damping of a truncated cylinder	3.52
Fig 3.23:	Heave potential damping of an array of four truncated cylinders	3.53
Fig 3.24:	Heave potential damping of the Snorre TLP	3.54
Fig 3.25:	Displacement in heave	3.55
Fig 3.26:	First order pitch moment on an array of four complete cylinders	3.56
Fig 3.27:	First order pitch moment on an array of four truncated cylinders	3.57
Fig 3.28:	First order pitch moment on the Snorre TLP	3.58
Fig 3.29:	Pitch added mass of the Snorre TLP	3.59
Fig 3.30:	Displacement in pitch	3.60
Fig 3.31:	First order forces on the Snorre TLP for 22.5 heading sea	3.61
Fig 3.32:	First order forces on the Snorre TLP for 45 heading sea	3.62
Fig 3.33:	Displacements of the Snorre TLP for 22.5 heading sea	3.63
Fig 3.34:	Displacements of the Snorre TLP for 45 heading sea	3.64

CHAPTER 4

Fig 4.1:	Drift Coefficient	4.14
Fig 4.2:	Convergence of the steady drift displacement in surge	4.15
Fig 4.3:	Slowly varying drift response spectra for a 20 m/s wind speed	4.16
Fig 4.4:	Slowly varying drift response spectra for a 50 m/s wind speed	4.17
Fig 4.5:	Steady drift force in surge	4.18
Fig 4.6:	Steady drift force in surge	4.19
Fig 4.7:	Steady drift force in surge	4.20
Fig 4.8:	Steady drift surge response in irregular sea	4.21

Fig 4.9:	Steady drift force in heave on the Snorre TLP	4.22
Fig 4.10:	Steady drift force in pitch	4.23
Fig 4.11:	Steady drift force in pitch	4.24
Fig 4.12:	Steady drift pitch response in irregular sea	4.21
Fig 4.13:	Steady drift forces for 22.5 heading sea	4.25
Fig 4.14:	Steady drift forces for 45 heading sea	4.26
Fig 4.15:	Slowly varying drift surge response spectra	4.27
Fig 4.16:	Significant values of the slowly varying drift surge response	4.28
Fig 4.17:	Slowly varying drift pitch response spectra	4.29
Fig 4.18:	Significant values of the slowly varying drift pitch response	4.28

CHAPTER 5

Fig 5.1:	Wind spectra for a 20 m/s Wind	5.18
Fig 5.2:	Wind spectra for a 50 m/s Wind	5.19
Fig 5.3:	Surge response spectra due to wind gusts (20 m/s Wind)	5.20
Fig 5.4:	Surge response spectra due to wind gusts (50 m/s Wind)	5.21
Fig 5.5:	Pitch response spectra due to wind gusts (20 m/s Wind)	5.22
Fig 5.6:	Pitch response spectra due to wind gusts (50 m/s Wind)	5.23
Fig 5.7:	Map of the current and wind velocities in the North Sea	5.27

CHAPTER 6

Fig 6.1:	TLP motion responses: Linear Model	6.32
Fig 6.2:	TLP tendon response: Linear Model	6.33
Fig 6.3:	TLP motion responses: Non Linear Mooring Model	6.34
Fig 6.4:	TLP tendon responses: Non Linear Mooring Model	6.35
Fig 6.5:	TLP motion responses: Drag Force	6.36

Fig 6.6:	TLP motion responses: Free Surface Effects	6.37
Fig 6.7:	TLP motion responses: Displacements	6.38
Fig 6.8:	TLP motion responses: Test 7	6.39
Fig 6.9:	TLP tendon responses: Test 7	6.40
Fig 6.10:	TLP motion responses: Fully Non Linear Model	6.41
Fig 6.11:	TLP tendon responses: Fully Non Linear Model	6.42
Fig 6.12:	Snorre surge response	6.43
Fig 6.13:	Snorre heave response	6.44
Fig 6.14:	Snorre pitch response	6.45
Fig 6.15:	Force in tendon 1 (Snorre)	6.46
Fig 6.16:	Force in tendon 3 (Snorre)	6.47
Fig 6.17:	Tendon forces (Snorre)	6.48
Fig 6.18:	Linear surge response	6.51
Fig 6.19:	Linear pitch response	6.51
Fig 6.20:	Linear tendon forces	6.51
Fig 6.21:	Non linear mooring model surge response	6.52
Fig 6.22:	Non linear mooring model heave response	6.52
Fig 6.23:	Non linear mooring model pitch response	6.52
Fig 6.24:	Non linear mooring model down-stream tendon forces	6.53
Fig 6.25:	Non linear mooring model up-stream tendon forces	6.53
Fig 6.26:	Drag force model pitch response	6.54
Fig 6.27:	Free surface effects pitch response	6.54
Fig 6.28:	Displacement model pitch response	6.54
Fig 6.29:	Test 7: surge response	6.55
Fig 6.30:	Test 7: heave response	6.55

Fig 6.31:	Test 7: pitch response	6.55
Fig 6.32:	Test 7: down-stream tendon forces	6.56
Fig 6.33:	Test 7: up-stream tendon forces	6.56
Fig 6.34:	Fully non linear model surge response	6.57
Fig 6.35:	Fully non linear model heave response	6.57
Fig 6.36:	Fully non linear model pitch response	6.57
Fig 6.37:	Fully non linear model down-stream tendon forces	6.58
Fig 6.38:	Fully non linear model up-stream tendon forces	6.58
Fig 6.39:	Wave amplitude	6.61
Fig 6.40:	Surge steady offset	6.61
Fig 6.41:	First order surge response	6.62
Fig 6.42:	Heave steady offset	6.62
Fig 6.43:	First order heave response	6.63
Fig 6.44:	Second order heave response	6.63
Fig 6.45:	Pitch steady offset	6.64
Fig 6.46:	First order pitch response	6.64
Fig 6.47:	Tendon forces pretension	6.65
Fig 6.48:	First order tendon forces	6.65

LIST OF TABLES

CHAPTER 1

Table 1.1: Snorre TLP characteristics 1.8

CHAPTER 5

Table 5.1: Steady displacement due to wind 5.24

Table 5.2: Significant surge displacement values due to dynamic wind 5.24

Table 5.3: Significant pitch displacement values due to dynamic wind 5.24

Table 5.4: Surge steady displacement due to current 5.25

Table 5.5: Pitch steady displacement due to current 5.26

CHAPTER 6

Table 6.1: TLP response: time domain simulation:
Snorre TLP, Amplitude 13.52m, Frequency 0.2rad/s, Head Sea. 6.31

Table 6.2: Heidrun TLP characteristics 6.49

Table 6.3: TLP response: time domain simulation:
Heidrun TLP, Amplitude 13.52m, Frequency 0.2rad/s, Head Sea. 6.50

Table 6.4: Linear model results for different wave frequencies:
Snorre TLP, Wind velocity: 40m/s, Current velocity: 0.6m/s 6.59

Table 6.5: Non linear model results for different wave frequencies:
Snorre TLP, Wind velocity: 40m/s, Current velocity: 0.6m/s 6.60

Table 6.6: Non colinear environmental forces
Snorre TLP, Amplitude 13.52m, Frequency 0.2rad/s. 6.66

ACKNOWLEDGEMENTS

The author is grateful for the help he got during his research study at the Department of Naval Architecture and Ocean Engineering at the University of Glasgow.

The author would like to thank the following:

Professor D. Faulkner and Professor N. Baltrop, former and present Heads of Department, for allowing him to carry out this study.

Dr. A. Incecik, Superintendent of the Hydrodynamics Laboratory, for supervising this research.

Mr R. Snell and Dr B. Corr, from the Department of Structural and Ocean Engineering at BP Exploration, for their interest in the research project.

Dr. O. Yilmaz, for his help with the time domain program, for his valuable assistance and for his stimulating discussions

Dr. H.S. Chan for allowing him to use his program, and for giving him some of his results.

Mr. A. Mac Leary for his instructive discussions.

All the other persons who supported him during the course of this research.

Finally, the financial support from British Petroleum in the form of the Molinero Scholarship is gratefully acknowledged.

DECLARATION

Except where reference is made to the work of others,
this thesis is believed to be original

SUMMARY

This thesis presents a model to predict the environmental forces on a tension leg platform. The response of the platform and the loads in the mooring lines are also formulated.

In the first part, the loading model to predict the forces due to waves, wind and current is developed.

Chapter 2 introduces the frequency domain method used for the validation of the model.

Chapter 3 presents two models for the calculation of the first order wave forces. The first one is based on a simple Morison approach, combined with the strip theory.
The second model is based on analytical solutions of the diffraction and radiation wave potentials for an array of cylinders.
These two methods are compared and validated with the results of a 3D diffraction radiation code.

In chapter 4, two models for the calculation of second order wave loads (steady and slowly varying drift) are developed. They are based on two analytical solutions of the wave diffraction potential. The models are validated with the results of a diffraction radiation code.

Chapter 5 introduces the models to predict the wind and current forces. Different formulations of wind spectra are used. The influence of the current velocity profile is investigated.

In the second part, the loading model is used in time domain simulations to calculate the responses of the TLP and the forces in the tendons.

Chapter 6 presents the time domain model used in this study. Different non linearities such as the free surface effects and the coupling due to the mooring system are taken into account.

The effects of the non linearities are investigated for two TLP designs (Snorre and Heidrun).A comparison between a linear and a non linear model is also carried out for a whole range of wave frequencies.

Finally, the effects of the directionality of the environmental forces on the tendon forces are investigated.

CHAPTER 1: INTRODUCTION

1. CONCEPT AND HISTORY OF THE TENSION LEG PLATFORMS

Most of the oil resources in shallow waters are already in production. The offshore production is now looking at deeper oil fields. The fixed platform designs are not suitable for these kinds of fields. A new design has been developed over the recent years to address this problem. The tension leg platforms are a new type of platforms that enable oil production in deep seas.

TLPs are a quite recent design as Mercier's review [1.1] shows. The first concept was tested in 1973, off the coast of California. It was only a third scale model, known as TLP-X1. The three leg platform proved the feasibility of this kind of design.

The first operational TLP was launched in 1984. It has been developed by Conoco for the Hutton field (See Figure 1). Because of the innovative design, many problems rose. The lack of rules and recommendation turned the project into a very long and expensive one. However, a lot was learned from that first experience when the second TLP, Jolliet, was developed and installed in 1986 in the Gulf of Mexico. At the time, Jolliet was the deepest production platform, with a water depth of 536m. Three more TLPs were constructed afterwards. The Snorre TLP was installed in the North sea in 1992. In 1994, the Auger TLP broke the record of Jolliet with a water depth of 872m. Finally during the summer 1995, the Heidrun TLP, was installed.

Oil companies are currently considering the use of TLPs for the developments of the fields off the Shetlands. Although, FPSO systems will be use for the early production, Mini TLPs may be used during a later stage.

There are large differences between the design of these platforms. The Hutton TLP is based on six columns connected with rectangular hulls, whereas the other ones only have four legs. The Jolliet TLP is of relatively small dimensions. The Heidrun TLP has been designed with a concrete hull instead of the usual steel. It implies very large dimensions, a large draught and a low centre of gravity. For the Shetlands' fields, TLPs of very small size are considered. If a geometry of four large circular legs and small pontoons seems to have become a rule, many possibilities are still under investigation for the TLP design.

The TLPs present several advantages compared to other platforms. They can be installed in deeper water than the conventional fixed production platforms. They are also easier to decommission. This has not been seen as such an advantage in the earlier developments, but it is becoming an important issue. Due to their very low motions in heave, the TLP are more suitable for production than other compliant designs such as semi-submersibles.

Because TLPs are different from usual platforms, new problems have risen in their design. (See Natvig et al [1.2] Nielsen et al [1.3] on this subject). A lot of importance has to be brought to dynamic effects. They condition the design of the tendons that are the most

critical part of the platform. The TLP natural periods avoid the range of the first order waves. The natural periods in the horizontal plane are about 100 seconds. They can then be excited by wind gusts and second order slowly varying waves.

In the vertical plane, the natural periods are about 2 seconds. The heave, roll and pitch motions are then excited by second order sum frequency waves, causing springing. These loads are much more difficult to calculate than the first order wave loads.

Another phenomenon that causes problems in the TLP design, is the ringing. It creates high frequency loads in the tendons, causing fatigue problems. The causes of ringing are not very well known yet. It seems to be related with steep waves causing an impact on the structure.

The TLP design presents a new challenge for the ocean engineers.

2. PREVIOUS WORK

Because of the novelty of the concept, a lot of research has been done on TLPs, during the recent years.

A lot of work has been concentrated on the determination of the second order wave loads and the corresponding response of the platform. Two different approaches have been used, an experimental one based on model testing [1.4] or a numerical one based on computer software [1.5]. The numerical methods are based on the Boundary Element Method (BEM) [1.6]. This kind of program requires heavy computations, and takes a lot of time to run. No simple way is available at the moment to approximate the second order Quadratic Transfer Function (QTF).

The first order wave loads are simpler to calculate. The strip theory [1.7], using the Morison formula, could be applied since the structure consists of circular and rectangular cylinders. For more accurate results a Diffraction/Radiation code could be used.

Kim [1.8] has been developing recently another way to calculate first order wave loads on TLPs. It is based on analytical solutions of the first order diffraction and radiation potentials for an array of vertical circular cylinders.

This kind of method was first introduced by MacCamy and Fuchs [1.9]. They calculated an analytical solution of the first order diffraction potential for a bottom mounted cylinder.

In 1971, Garrett [1.10] extended the problem to a truncated cylinder.

Then, in 1984, Chakrabarti [1.11] used the solution proposed by MacCamy and Fuchs to calculate the steady drift on a fixed bottom mounted cylinder.

Eatock-Taylor et al [1.12] proposed a formulation of the steady drift for 2 cylinders.

A major step was taken by Linton and Evans [1.13] when they proposed a solution of the first order diffraction potential for an array of fixed cylinders. The solution was then used to deduce the first order forces, the steady drift, and the free surface.

This was then extended by Kim [1.14] and [1.15], to the radiation problem. He also proposed to use a series of approximations to use this method to calculate the first order wave forces, the added mass, the potential damping and the steady drift of a TLP. This method presents the advantages that it is much quicker than the Diffraction Radiation (D/R) codes and is more accurate than the Morison approach.

Extensions of the theory are currently under way to calculate the second order QTF's and the drift damping.

The wind effects also take an important place in the design of tension leg platforms. The wind gusts, in particular, are important in the vertical plane. Several methods are available to calculate them, from a simplified single point loading, to a multiple point loading [1.16]. There are also many wind gust spectra that can be chosen [1.17]. They are all very different in their formulation and give results with large variations [1.18].

All these methods are usually applied in frequency domain based studies. However, to take into account the non-linear effects, and to calculate the tendon loads, a time domain simulation is required [1.19].

One of the main non-linear effects, that should be investigated, is the non-linear stiffness of the mooring system of the TLP. Matsui et al [1.20] proposed a way to model, up to the second order, the interactions of the tendons and the hull for the calculation of the mooring stiffness.

The second main non-linearity is the free surface effects. These are supposed to be a main cause of the ringing phenomenon. For irregular seas, a stretching method has to be applied. Indeed, the Airy theory overestimates the wave kinematics in the wave crest region [1.21]. Rainey et al [1.22] proposed an original approach. They showed that the most common approach, the Wheeler stretching, is not suitable. Mekha et al [1.21] compared different stretching methods and reached to the same conclusion. A second order stretching method seemed more appropriate.

Natvig [1.23] proposed a simple time domain method to model the free surface effects. He used a very simple stretching method, but put the emphasis on the multiple effects of the free surface. In his model, he included force, added mass, and damping variations, but also wave slapping and a term depending on the time derivative of the added mass. From this, he was able to generate through a numerical simulation, a ringing event observed during experimental model tests.

3. OBJECTIVES

The main objective of this thesis is to analyse the dynamic response of a tension leg platform in extreme weather conditions. The motions in five degrees of freedom are studied - surge, sway, heave, pitch and roll.

The effects of the different environmental loads are investigated. This includes - the first order waves, the steady drift, the slowly varying waves, the steady wind, the wind gusts and the current.

The non-linear effects are also modelled and the forces in the tendons are calculated.

The wave, wind and current are first modelled in the frequency domain. For this purpose the geometry of the Snorre TLP is used. The main characteristics of the TLP are given in Table 1.1.

The method developed by Kim is adapted, to calculate the first order wave forces, the added mass, the potential damping and the steady drift. The slowly varying drift is then deduced from the latter using Newman's approximation. The whole method is compared and validated in the frequency domain with the results from a D/R code and a Morison approach.

Both steady, and varying wind are modelled in the frequency domain. Different wind spectra are experimented for the calculation of the dynamic wind forces.

The current is also studied. Two different models are compared in terms of forces and displacements.

Having fully validated the prediction of the forces in the frequency domain, a time domain approach is developed. It simulates regular seas only. Several non-linearities are taken into account. The non-linear mooring stiffness due to the coupling of the hull and the tendons is formulated. The free surface effects are simulated following the model given by Natvig. The viscous damping, the drag forces, the large displacements of the TLP, and the coupling between the different motions are also accounted for.

The effects of each of these non-linearities on the displacements of the platform and on the tendon forces are studied. This study is first carried out for the Snorre TLP. Then, the Heidrun design is considered. The effects of the non linearities on the two TLPs are compared to see how the geometry influences the response and the tendon forces.

Then simulations are run with whole range of wave frequencies. The variation of the response and the tendon forces with the wave frequency is then analysed.

Finally, the influence of the direction of the environmental forces is investigated. The TLP responses and tendon forces are calculated for non collinear environmental forces.

REFERENCES OF CHAPTER 1

[1.1] Mercier J.A., Birell N.D., Chivvis J.C., Hunter A.F., 1991, Tension Leg Platforms - Progress and prospects, SNAME transactions Vol 99.

[1.2] Natvig B.J., Teigen P., 1993, Review of hydrodynamic challenges in TLP design, Proceedings of the third international offshore and polar engineering conference Singapore.

[1.3] Nielsen F.G., Olsen G., 1993, Hydrodynamic challenges related to large volume floating production platform, Abstract of the eighth international workshop on water waves and floating bodies, St. John's Newfoundland.

[1.4] Mathinsen T., Muren J., 1994, Snorre TLP - Analysis of measured responses, Proc. of the fourth ISOPE Conference.

[1.5] Lee C.H., Newman J.N., Kim M.H., 1993, The computation of second order wave loads on a compliant TLP, Proc. of the ISOPE Conference, Singapore.

[1.6] Lee C.H., Newman J.N., Kim M.H., Yue D.K.P., 1991, The computation of the second order wave loads, Proc. of OMAE Houston.

[1.7] Hooft J.P., 1982, Advance Dynamics of Marine Structures, Interscience publication.

[1.8] Kim M.H., Mercier R.S., Gu G., Wu C., Bothelo D., 1993, PC-based wave load computation for large volume multi-column structures, Proceedings of the third International Offshore and Polar Engineering Conference, ISOPE.

[1.9] MacCamy R.C., Fuchs R.A., 1954, Wave forces on piles: a diffraction theory, Technical Memorandum No.69, Beach Erosion Board.

[1.10] Garrett C.J.R., 1971, Wave forces on circular dock, Journal of Fluid Mechanics, Vol. 46, Part 1, p.129-139.

[1.11] Chakrabarti S.K., 1984, Steady drift force on vertical cylinder - viscous vs. potential, Applied Ocean Research, Vol. 6, No. 2.

[1.12] Eatock-Taylor R., Hung S.M., 1985, Wave drift enhancement effects in multi column structures, Applied Ocean Research, Vol. 7, No. 3.

[1.13] Linton C.M., Evans D.V., 1990, The interaction of waves with arrays of vertical circular cylinders, Journal of Fluid Mechanics, Vol. 215, p.549-569.

[1.14] Kim M.H., 1993, Interaction of waves with N vertical circular cylinders, Journal of Waterway, Port, Coastal, and Ocean Engineering, Vol. 119, No. 6.

[1.15] Kim M.H., 1992, A simple method to compute wave loads on a TLP, ASCE Conf. Ocean V, College Station.

[1.16] Kareem A., Dalton C, 1982, Dynamic Effects of wind on Tension Leg Platforms, OTC.

[1.17] Ochi M.K., Shin Y.S., 1988, Wind turbulent spectra for design consideration of offshore structures, OTC.

[1.18] Wichers J.E.W., 1992, The effect of wind spectra on the low frequency motion of a moored tanker, Maritime Research Institute Netherlands.

[1.19] Molin B, 1993, Second order hydrodynamics applied to moored structures, 19th WEGEMT School Report.

[1.20] Matsui T., Sakoh Y., Nozu T., 1993, Second order sum frequency oscillations of tension leg platforms: predictions and measurements, Applied Ocean Research Vol.15, p.107-118.

[1.21] Mekha B.B., Johnson C.P., Roesset J.M., 1994, Effects of different wave free surface approximations on the response of a TLP in deep water, Proc. of the fourth ISOPE Conference.

[1.22] Rayney R.C., Smith S., 1993, Application of slender body theory and accurate wave kynematics to ringing calculations - A critique of the Morison Wheeler methodology. Proc. of the seminar on tensioned buoyant platforms, University College London.

[1.23] Natvig B.J., 1994, A proposed ringing analysis model for higher order tether response, Proceedings of the fourth International Offshore and Polar Engineering Conference, ISOPE.

Hutton TLP

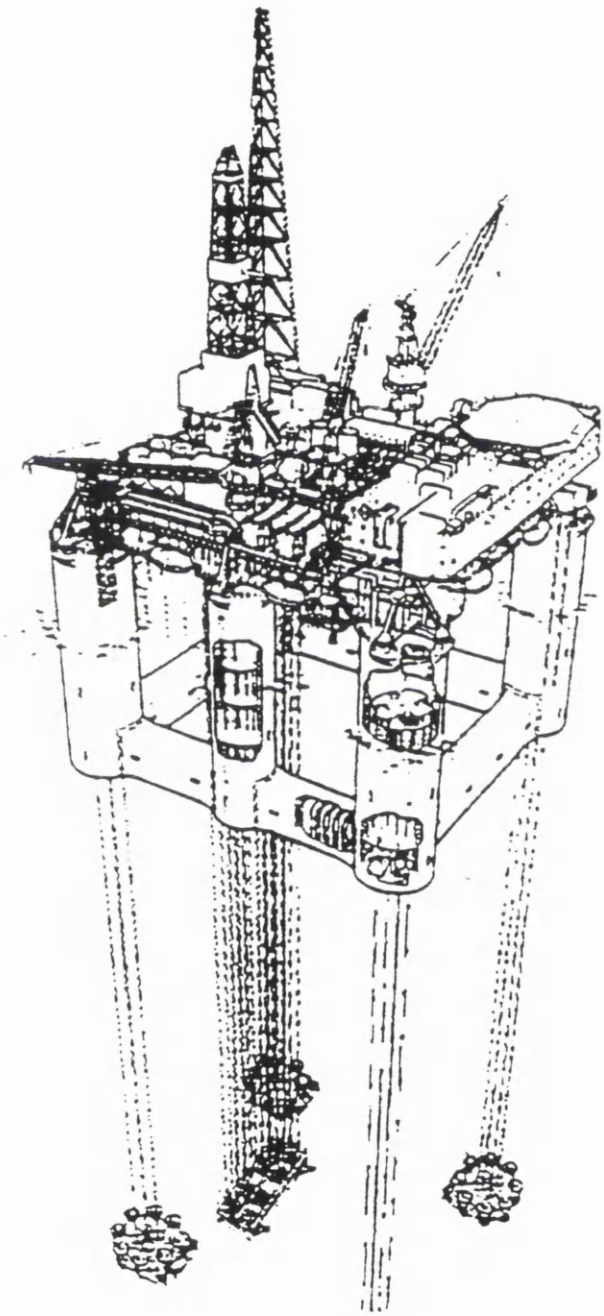

Figure 1.1

SNORRE TLP CHARACTERISTICS

Spacing between the columns centres	76 m
Columns diameter	25 m
Pontoon width	11.5 m
Pontoon height	11.5 m
Draught	37.5 m
Total Mass	8.00E+07 kg
Tether pretension	2.25E+08 N
Roll moment of inertia	1.48E+11 N.m.s^2
Pitch moment of inertia	1.48E+11 N.m.s^2
Vertical position of CoG above free surface	13.5 m
Length of the mooring tethers	310 m
Section of the tethers	1.157 m^2
Young modulus of the tethers	2.10E+11 N/m^2
Surge Stiffness	7.26E+05 N/m
Heave Stiffness	8.04E+08 N/m
Roll Stiffness	1.12E+12 N/m
Surge natural frequency	0.06 rad/s
Heave natural frequency	2.6 rad/s
Roll natural frequency	2.2 rad/s

Table 1.1

CHAPTER 2: FREQUENCY DOMAIN METHOD

1. INTRODUCTION

This chapter introduces the frequency domain method. This method is used in the following three chapters to predict the displacements of the TLP, as a function of the environment forces.

The spectral approach and the concept of significant values are also presented here.

In the first part of the study, the frequency domain approach is used to validate wave force prediction techniques developed with three dimensional diffraction/radiation code results.

The frequency domain method has certain limitations. It cannot take the non-linear phenomena into account. However, it is a simple way to calculate the displacements of the platform as a function of the forces. It is therefore suitable to validate theoretical calculations.

The other advantage of the frequency domain approach is its ability to study not only regular seas, but also irregular seas.

The time domain method, which takes non-linearities into account, is much more complex to develop.

There is not a simple way of applying the time domain based prediction tools to irregular seas.

The time domain simulation is only used in the last chapter to investigate the effect of the non-linearities in TLP motions.

2. THE FREQUENCY DOMAIN METHOD

The problem of the dynamic response of the TLP, is based on the equations of motion, given by Newton's laws.

$$\frac{d\, m\vec{v}}{dt} = \vec{F}$$
$$\frac{d\, I\vec{\omega}}{dt} = \vec{M} \qquad (2\text{-}1)$$

When these equations are applied to the TLP, it comes:

$$([M]+[M_a])\{\ddot{X}\}+[C]\{\dot{X}\}+([K_h]+[K_m])\{X\}=\{F\} \quad (2\text{-}2)$$

Where:

X: displacement vector of the platform

M: mass and inertia matrix

M_a: added mass matrix

C: damping matrix

K_h: hydrodynamic stiffness matrix

K_m: mooring stiffness matrix

F: force vector

The expression of these different components of the equation is given in the following section.

The frequency domain method gives a simple way to solve this equation, giving a direct relation between the unknown X and the forces applied to the TLP.

It is based on two main principles. The forces and motions are assumed to be harmonic, and it is assumed that the equation is linear.

Using a Fourier transformation, the equation can be expressed in term of frequency. This way, the displacements are derived from the forces using a simple transfer function.

$$X(\omega)=F(\omega)\cdot Q(\omega) \quad (2\text{-}3)$$

Where the transfer function Q can be written as:

$$Q(\omega)=\frac{1}{(K_m+K_h-\omega^2(M+M_a))-i(\omega C)} \quad (2\text{-}4)$$

In case of a steady force, Q becomes:

$$Q=\frac{1}{(K_m+K_h)} \quad (2\text{-}5)$$

Since the equation is linear, the displacements due to each environmental force can be studied independently.

The limitation of the method comes from the two main assumptions:

- harmonic forces and displacement

- linearity of the equation

It means that non-linearities such as the displacement of the platform, the coupling between the different degrees of freedom, the non-linearity of the mooring system, or the free surface effects cannot be taken into account. However, the effects of these non-linearities are studied later, in a time domain simulation.

3. MOTION EQUATION COEFFICIENTS

As stated before, the problem is based on the following motion equation:

$$([M]+[M_a])\{\ddot{X}\}+[C]\{\dot{X}\}+([K_h]+[K_m])\{X\}=\{F\} \qquad (3\text{-}1)$$

The centre of the co-ordinate system is chosen at the centre of gravity of the TLP, and the x, y, and z axes correspond respectively to surge, sway and heave.

The formulation of the added mass matrix, the potential damping matrix, and the force vector are given in chapters 3, 4, and 5, where effects of environmental forces are studied. The forces taken into account in this study are the ones due to waves, wind and current.

The wave forces studied are the first order wave forces (See Chapter 3), the second order steady and slowly varying drift (See Chapter 4), the steady and varying wind forces and the steady current force (See Chapter 5). The drag forces due to waves are not taken into account since they are small compared to the inertia forces on a structure with large cross-sectional members. Furthermore, they would have to be linearised for the frequency domain study. However, their effect is taken into account in the time domain simulation. The sum frequency force due to waves is not taken into account, because no simple theory exists to calculate them.

The study is carried out for five degrees of freedom: surge, sway, heave, roll and pitch. The original problem based on a 6x6 linear system, is simplified in a 5x5 system.

The displacement vector X then becomes:

$$\{X\}=\begin{Bmatrix} X_1 \\ X_2 \\ X_3 \\ X_4 \\ X_5 \end{Bmatrix} \qquad (3\text{-}2)$$

the components corresponding respectively to surge, sway, heave, roll and pitch.
The Mass-Inertia matrix can be written as:

$$[M]=\begin{bmatrix} M & 0 & 0 & 0 & 0 \\ 0 & M & 0 & 0 & 0 \\ 0 & 0 & M & 0 & 0 \\ 0 & 0 & 0 & I_x & 0 \\ 0 & 0 & 0 & 0 & I_y \end{bmatrix} \tag{3-3}$$

Where M is the mass of the TLP and I_x and I_y are the inertia about the x and y axis.

The damping matrix C can be split into two terms. The potential damping C_p (See chapter 3) and the viscous damping C_v.

$$[C]=\left[C_p+C_v\left(\dot{X}\right)\right] \tag{3-4}$$

The viscous damping is not linear since it depends on the squared velocity of the structure. This term is usually linearised using a first order expension of the sinus function. Another method is used here, the expression of the damping is calculated in the frequency domain, by using an iteration algorithm to solve the motion equation.
The viscous damping is usually bigger than the potential damping. It can be important for the surge motion, for which the first order waves and the slowly varying drift can excite the natural frequency.

The viscous damping matrix can be written as:

$$[C_v]=[C_{vij}] \tag{3-5}$$

Where:

$$\begin{aligned}
C_{vij} &= 0 \quad \text{for} \, i \neq j \\
C_{v11} &= \frac{1}{2}\rho\left(4\,C^c_{dx}\,D_c + 2\,C^p_{dx}\,D_{pz}\right)\left|\dot{X}_1\right| \\
C_{v22} &= \frac{1}{2}\rho\left(4\,C^c_{dy}\,D_c + 2\,C^p_{dy}\,D_{pz}\right)\left|\dot{X}_2\right| \\
C_{v33} &= \frac{1}{2}\rho\left(4\,C^c_{dz}\,D_c + 4\,C^p_{dz}\,D_{px}\right)\left|\dot{X}_3\right| \\
C_{v44} &= \frac{1}{2}\rho\left(4\,C^c_{dy}\,D_c \int_{-d-Z_G}^{-Z_G} z^2\,|z|\,dz + 2\,C^p_{dy}\,D_{pz} \int_{-L_p/2}^{L_p/2} y^2\,|y|\,dy\right)\left|\dot{X}_4\right| \\
C_{v55} &= \frac{1}{2}\rho\left(4\,C^c_{dx}\,D_c \int_{-d-Z_G}^{-Z_G} z^2\,|z|\,dz + 2\,C^p_{dx}\,D_{pz} \int_{-L_p/2}^{L_p/2} x^2\,|x|\,dx\right)\left|\dot{X}_5\right|
\end{aligned} \tag{3-6}$$

Where: ρ: water density
D_c: column diameter
d: draught
Z_G: height of the centre of gravity
D_{px} and D_{pz}: breadth and height of the pontoons
L_p: length of the pontoons
C_{di}^{c} and C_{di}^{p}: drag coefficients of the columns and the pontoons in direction i.

K_h represents the hydrostatic stiffness matrix:

$$[K_h] = \begin{bmatrix} 0 & 0 & 0 & 0 & 0 \\ 0 & 0 & 0 & 0 & 0 \\ 0 & 0 & \rho g S_{wl} & 0 & 0 \\ 0 & 0 & 0 & K_{h4} & 0 \\ 0 & 0 & 0 & 0 & K_{h5} \end{bmatrix} \tag{3-7}$$

Where:

$$\begin{aligned} k_{h4} &= \rho.g.V_w\left(\frac{1}{V_w}.\int_{S_{wl}} y^2 dS - \overline{BG}\right) \\ k_{h5} &= \rho.g.V_w\left(\frac{1}{V_w}.\int_{S_{wl}} x^2 dS - \overline{BG}\right) \end{aligned} \tag{3-8}$$

Where:
g: gravity acceleration
S_{wl}: cross section of the TLP at the water level
V_w: Wet volume
G: centre of gravity of the structure
B: buoyancy centre

K_m represents the linearised mooring stiffness matrix due to the tendons:

$$[K_m] = \begin{bmatrix} T/L_c & 0 & 0 & 0 & 0 \\ 0 & T/L_c & 0 & 0 & 0 \\ 0 & 0 & AE/L_c & 0 & 0 \\ 0 & 0 & 0 & \frac{AE}{L_c}\left(\frac{L}{2}\right)^2 & 0 \\ 0 & 0 & 0 & 0 & \frac{AE}{L_c}\left(\frac{L}{2}\right)^2 \end{bmatrix} \tag{3-9}$$

Where: T: pretension in the tendons
L_c: tendon length.
A: total section of the tendons
E: Young module of the tendons
L: spacing between the columns (centre to centre)

4. SPECTRAL ANALYSIS

In the frequency domain, the varying environmental effects are expressed in terms of energy spectra. These spectra give a relation between the amplitude of the phenomena and the frequency. For the waves for example, the wave amplitude is related to the energy spectrum S_w by the following relation:

$$A^2 = S_w(\omega)d\omega \tag{4-1}$$

Where A is the wave amplitude and ω the frequency.

Similarly for the slowly varying wind:

$$v_w^2 = S_{wind}(\omega)d\omega \tag{4-2}$$

Where v_w is the wind varying velocity.

Different formulation of wave and wind spectra are available. They are related to the wind velocity or the sea state. These formulations can be found in chapters 4 and 5 where waves and wind forces are calculated respectively.

From these spectra, force spectra can be derived for the varying forces. For the first order waves for example:

$$SF_{low}(\omega) = S_w(\omega)\left(\frac{F_{low}(\omega)}{A}\right)^2 \tag{4-3}$$

Where: SF_{low}: first order wave force spectrum
F_{low}: first order wave force

Similarly response spectra, corresponding to the displacement can be derived:

$$RS_{low}(\omega) = S_w(\omega)\left(\frac{F_{low}(\omega)}{A}\right)^2 Q^2(\omega) \tag{4-4}$$

For the varying wind:

$$RS_{wind}(\omega) = S_{wind}(\omega)\left(\frac{F_{wind}(\omega)}{v_w}\right)^2 Q^2(\omega) \tag{4-5}$$

From these spectra, one can determine two particular values useful for a design project- the significant value and the maximum value of the spectrum.

For a wave spectrum, the significant value, called $H_{1/3}$, corresponds to the mean height of the one-third of the highest waves. The maximum value H_{max} represents the average value of the highest wave of the sea state. The same values can be defined for the response spectra.

In order to calculate these values, one must introduce the moment m_n of order n of a spectrum S.

$$m_n(S) = \int_0^{\infty} \omega^n \, S(\omega) d\omega \tag{4-6}$$

The wave height, and the motions of the TLP are supposed to follow a Rayleigh distribution (narrow banded spectrum).

This assumption is true if

$$\varepsilon(S) = \sqrt{1 - \frac{m_2(S)^2}{m_0(S) \cdot m_4(S)}} \approx 0 \tag{4-7}$$

Using this assumption, the significant and maximum values of a spectrum can be calculated as follows:

For the wave spectrum:

$$\begin{aligned} H_{1/3} &= 4\sqrt{m_0(S_w)} \\ H_{max} &= 2\left[\sqrt{2 \ln N_w} + \frac{\gamma}{\sqrt{2 \ln N_w}}\right]\sqrt{m_0(S_w)} \end{aligned} \tag{4-8}$$

Where:

N_w: the number of waves appearing during the sea state (about a thousand for a three hour storm).

γ=0.5772 is the Euler constant.

For the response spectra the significant and maximum values are given by:

$$X_{1/3} = 2\sqrt{m_0(RS_x)}$$

$$X_{max} = \left[\sqrt{2\ln\frac{T}{T_{zx}}} + \frac{\gamma}{\sqrt{2\ln\frac{T}{T_{zx}}}}\right]\sqrt{m_0(RS_x)} \qquad (4\text{-}9)$$

Where:

T is the sea state duration

$$T_{zx} = 2\pi\sqrt{\frac{m_0(RS_x)}{m_2(RS_x)}} \qquad (4\text{-}10)$$

is the average upcrossing period

REFERENCES OF CHAPTER 2

[2.1] Incecik A., 1993, The effects of non-colinear wave, wind, current loading on dynamic response of a TLP, OMAE.

CHAPTER 3: FIRST ORDER WAVES

1. INTRODUCTION

Mainly, two methods may be used to calculate the forces due to first order waves on a large offshore structure, the Morison equation or Green functions through a diffraction radiation code.

The Morison equation has the advantage of being simple and of giving results quickly, needing few calculations from the computer. The major inconvenience of the formula is that it gives only a rough approximation of the loads.

The radiation codes give more precise results but require extensive computational time and are slow. The time factor is an important one if the loads have to be calculated in the time domain.

The other drawback of this method is that a mesh has to be generated for the special geometry of the platform. At the initial design stage, generating a new mesh every time the geometry is changed is not feasible.

A third method can be applied in the case of geometries based on vertical circular cylinders. This method uses analytical solutions of the first order diffraction and radiation potentials.

The Morison approach and the analytical method are developed for a TLP geometry in section 2 and section 3 to calculate the wave loads. The results based on the Morison approach and the analytical method are compared with those obtained from a diffraction radiation code in section 4.

2. MORISON APPROACH

Section 2.1 describes the calculation of the forces due to the waves. Section 2.2 presents the calculation of the added mass. The potential damping is not calculated with this method.

2.1. FORCES

The forces are calculated in the co-ordinate system (G,x,y,z), but the wave potential is written in the co-ordinate system (O,x,y,z). The origin O corresponds to the projection of the centre of gravity G, along the z axis, on the mean water level.

Following Airy theory, the first order waves are represented by a sinusoidal shape. The potential representing first order waves is given as:

$$\phi = \frac{Ag}{\omega} e^{k.z} \sin(kX - \omega t) \qquad (2.1\text{-}1)$$

Where:

$$kX = k\cos\alpha\, x + k\sin\alpha\, y \qquad (2.1\text{-}2)$$

$$k = \frac{\omega^2}{g} \qquad (2.1\text{-}3)$$

A: wave amplitude
ω: wave frequency
α: wave propagation angle

We assume here that the water depth is infinite. This assumption can be made because TLPs are moored in deep waters.

This formula is given for a regular sea. For irregular seas, we suppose that we have an infinite sum of regular waves with different frequencies and amplitudes. The potential becomes a sum of sinus:

$$\phi = \sum_i \frac{A_i g}{\omega_i} e^{k_i.z} \sin(k_i X - \omega_i t) \qquad (2.1\text{-}4)$$

Since the equations are linear, each frequency is independent of the other. So we can write the equation with only one frequency, like for a regular sea.

The acceleration of the waves, a_w is defined as:

$$\vec{a}_w = \frac{\partial}{\partial t}\left(\vec{\nabla}\phi\right) \tag{2.1-5}$$

or:

$$\begin{aligned} a_{wx} &= A\omega^2 \cos\alpha\, e^{kz} \sin(kX - \omega t) \\ a_{wy} &= A\omega^2 \sin\alpha\, e^{kz} \sin(kX - \omega t) \\ a_{wz} &= -A\omega^2 e^{kz} \cos(kX - \omega t) \end{aligned} \tag{2.1-6}$$

The wave forces are written using the Morison formula describing hydrodynamic forces on cylinders.

$$F_x = \rho C_m S_x a_{wx} + \frac{1}{2}\rho C_d D_c |u_{wx}| u_{wx} \tag{2.1-7}$$

Where: F_x is the force in the x direction for unit length cylinder of section S and diameter D_c.
a_{wx} and u_{wx} are respectively the acceleration and the velocity of the waves in the x direction.
C_m and C_d are the inertia and drag coefficients.
ρ is the water density.

As stated before, the second part of the equation, called the drag term, is neglected since it is small compared to the first one.

The formula is applied for each pontoon and column, and the sum is considered to be the total force applied on the TLP.

2.1.1. Columns

By integrating the force over the draught d of the TLP columns we get:

$$F_x^c = \rho C_m^c \frac{\pi}{4} D_c^2 A g \cos\alpha \left(1 - e^{-kd}\right) \sum_{i=1}^{4} \sin(kx_i - \omega t) \tag{2.1-8}$$

Where: $$kx_i = k\cos\alpha\, X_{ci} + k\sin\alpha\, Y_{ci} \tag{2.1-9}$$

X_{ci} and Y_{ci} are the co-ordinate of the centre of the four columns.

Similarly:

$$F_y^c = \rho C_m^c \frac{\pi}{4} D_c^2 A g \sin\alpha \left(1 - e^{-kd}\right) \sum_{i=1}^{4} \sin(kx_i - \omega t) \tag{2.1-10}$$

The vertical component of the force can not be found using the Morison formula. It is calculated by integrating the pressure over the base of the column, it corresponds to the Froude Krylov force. The pressure is simply calculated at the centre of the bottom of the column, and multiplied by the section. These approximations should give a correct result since:

- the diffraction effects are small in this region
- the dimension of the column is small compared to the length of the waves having an effect at that depth.

The pressure is given by the following formula:

$$p = -\rho \frac{\partial \phi}{\partial t} \tag{2.1-11}$$

The vertical force on the columns:

$$F_z^c = \rho \frac{\pi}{4} D_c^2 A g e^{-kd} \sum_{i=1}^{4} \cos(kx_i - \omega t) \tag{2.1-12}$$

Where all the symbols have been previously defined.

The moment in roll and pitch are given by a combination of the loads in the horizontal and vertical planes:

$$\begin{aligned} M_x^c &= \int_{base} y\, p\, dS - \int_{-d}^{0} (z - Z_G) F_y^c\, dz = M_1 + M_2 \\ M_y^c &= \int_{-d}^{0} (z - Z_G) F_x^c\, dS - \int_{base} x\, p\, dz = M_3 + M_4 \end{aligned} \tag{2.1-13}$$

Where Z_G is the height of the centre of gravity above the water level.

$$M_1 = \rho A g \frac{\pi}{4} D_c^2\, e^{-kd} \sum_{i=1}^{4} Y_{ci} \cos(kx_i - \omega t) \tag{2.1-14}$$

$$M_2 = -\rho A \omega^2 C_m^c \frac{\pi}{4} D_c^2 \sin\alpha \left(\frac{d}{k} e^{-kd} - \frac{1}{k^2}\left(1 - e^{-kd}\right) - \frac{Z_G}{k}\left(1 - e^{-kd}\right) \right) . \sum_{i=1}^{4} \sin(kx_i - \omega t) \tag{2.1-15}$$

$$M_3 = \rho A \omega^2 C_m^c \frac{\pi}{4} D_c^2 \cos\alpha \left(\frac{d}{k} e^{-kd} - \frac{1}{k^2}\left(1 - e^{-kd}\right) - \frac{Z_G}{k}\left(1 - e^{-kd}\right) \right) . \sum_{i=1}^{4} \sin\left(kx_i - \omega t\right) \tag{2.1-16}$$

$$M_4 = -\rho A g \frac{\pi}{4} D_c^2 e^{-kd} \sum_{i=1}^{4} X_{ci} \cos\left(kx_i - \omega t\right) \tag{2.1-17}$$

2.1.2. Pontoons

For the integration of the forces, the pontoons of length L_p are divided into N consecutive cylinders of length L_p/N. The Morison formula is applied on each of them, and the total force on the pontoons is equal to the sum of the forces on the strips.

The horizontal forces act only on two pontoons, so the total component of the force on the pontoons in x direction is:

$$F_x^p = \rho A \omega^2 C_m^p D_{px} D_{pz} \cos\alpha \left(e^{-k\left(d - \frac{D_{pz}}{2}\right)} \right) \frac{L_p}{N} \sum_{i=0}^{N-1} \left(\sin\left(kx_{i1} - \omega t\right) + \sin\left(kx_{i2} - \omega t\right) \right) \tag{2.1-18}$$

Where C_m^p is the inertia coefficient for the rectangular pontoons of height D_{pz} and width D_{px}.

and:

$$\begin{aligned} kx_{i1} &= k\cos\alpha\left(-\frac{L_p}{2}\right) + k\sin\alpha\left(-\frac{L_p}{2} + \frac{L_p}{2N} + \frac{iL_p}{N}\right) \\ kx_{i2} &= k\cos\alpha\left(\frac{L_p}{2}\right) + k\sin\alpha\left(-\frac{L_p}{2} + + \frac{L_p}{2N} + \frac{iL_p}{N}\right) \end{aligned} \tag{2.1-19}$$

For the y direction:

$$F_y^p = \rho A \omega^2 C_m^p D_{px} D_{pz} \sin\alpha \left(e^{-k\left(d - \frac{D_{pz}}{2}\right)} \right) \frac{L_p}{N} \sum_{i=0}^{N-1} \left(\sin\left(kx_{i3} - \omega t\right) + \sin\left(kx_{i4} - \omega t\right) \right) \tag{2.1-20}$$

Where:

$$\begin{aligned} kx_{i3} &= k\cos\alpha\left(-\frac{L_p}{2} + \frac{L_p}{2N} + \frac{iL_p}{N}\right) + k\sin\alpha\left(-\frac{L_p}{2}\right) \\ kx_{i4} &= k\cos\alpha\left(-\frac{L_p}{2} + \frac{L_p}{2N} + \frac{iL_p}{N}\right) + k\sin\alpha\left(\frac{L_p}{2}\right) \end{aligned} \tag{2.1-21}$$

Similarly, the vertical forces on the pontoons can be written as:

$$F_z^p = -\rho A\omega^2 C_m^p D_{px} D_{pz} e^{-kd} \sum_{j=1}^{4} \sum_{i=0}^{N-1} \cos\left(kx_{ij} - \omega t\right) \tag{2.1-22}$$

Where all the symbols have been previously defined.
For the moments:

$$M_x^p = \oint y F_z \, dl - \int_{-L_p/2}^{L_p/2} (z - Z_G) F_y \, dx = M_1 + M_2$$

$$M_y^p = \int_{-L_p/2}^{L_p/2} (z - Z_G) F_x \, dy - \oint x F_z \, dl = M_3 + M_4 \tag{2.1-23}$$

Where:

$$M_1 = -\rho A\omega^2 C_m^p D_{px} D_{pz} e^{-kd} \frac{L_p}{N} \left[\left(-\frac{L_p}{2} \right) \sum_{i=0}^{N-1} \left(\cos\left(kx_{i3} - \omega t\right) - \cos\left(kx_{i4} - \omega t\right) \right) + \sum_{i=0}^{N-1} \left(\left(-\frac{L_p}{2} + \frac{i L_p}{N} \right) . \sum_{j=1}^{2} \cos\left(kx_{ij} - \omega t\right) \right) \right] \tag{2.1-24}$$

$$M_2 = \left(d - \frac{D_{pz}}{2} + Z_G \right) F_y^p \tag{2.1-25}$$

$$M_3 = -\left(d - \frac{D_{pz}}{2} + Z_G \right) F_x^p \tag{2.1-26}$$

$$M_4 = \rho A\omega^2 C_m^p D_{px} D_{pz} e^{-kd} \frac{L_p}{N} \left[\left(-\frac{L_p}{2} \right) \sum_{i=0}^{N-1} \left(\cos\left(kx_{i1} - \omega t\right) - \cos\left(kx_{i2} - \omega t\right) \right) + \sum_{i=0}^{N-1} \left(\left(-\frac{L_p}{2} + \frac{L_p}{2N} + \frac{i L_p}{N} \right) . \sum_{j=3}^{4} \cos\left(kx_{ij} - \omega t\right) \right) \right] \tag{2.1-27}$$

2.2. ADDED MASS

The added mass and the potential damping correspond to the forces applied on the TLP by the radiation potential. The added mass is an important factor since it is directly linked to the natural frequency calculation.

However, the potential damping is not as important. In fact, its value is very small compared to the viscous damping.

Only the added mass is calculated here. The potential damping is considered as equal to zero.

The added mass is calculated following the method given by Hooft [3.1]. The added mass is calculated separately on the columns and the pontoons. The total added mass is obtained as the sum of the added mass of each separate element. The interaction between the different elements of the structure is neglected.

2.2.1. Columns

For a circular cylinder of unit length, the added mass in surge or sway direction is given by the following formula:

$$M_a = \rho \frac{\pi}{4} D_c^2 \tag{2.2-1}$$

The surge or sway added mass for four columns:

$$M_{ax}^c = M_{ay}^c = 4\rho \frac{\pi}{4} D_c^2 \, d \tag{2.2-2}$$

In the vertical direction, the added mass can be neglected since it is very small compared to the mass of the structure:

$$M_{az}^c = 0 \tag{2.2-3}$$

For the roll and pitch motions:

$$M_{a\Omega x}^c = M_{a\Omega x}^c = 4\rho \frac{\pi}{4} D_c^2 \int_{-d-Z_G}^{-Z_G} z^2 dz = \frac{1}{3} \rho \pi D_c^2 \left((d + Z_G)^3 - Z_G^3 \right) \tag{2.2-4}$$

The moment calculation is carried out for an angular motion about the centre of gravity G.

2.2.2. Pontoons

For the rectangular pontoons, the added mass is found by the same formula, only using a shape coefficient K_i. The value of this coefficient can be found in tables given in reference [3.2].

$$M_a = \rho K_i \frac{\pi}{4} D_p^2 \tag{2.2-5}$$

In horizontal directions, only two pontoons are taken into account, the added mass of the pontoons whose axes are parallel to the direction of oscillations is neglected:

$$M_{ax}^P = M_{ay}^P = 2 K_1 \rho \pi \left(\frac{D_{pz}}{2}\right)^2 L_p \tag{2.2-6}$$

Where K_1 is the shape coefficient of the pontoons in the horizontal directions.

For the heave, with four pontoons:

$$M_{az}^P = 4 K_2 \rho \pi \left(\frac{D_{px}}{2}\right)^2 L_p \tag{2.2-7}$$

Where K_2 is the shape coefficient of the pontoons in the vertical direction.

For the roll and pitch:

$$M_{a\Omega_x}^P = M_{a\Omega_y}^P = \rho \frac{\pi}{2} \left(K_2 D_{px}^2 \frac{L_p^3}{3} + K_1 D_{pz}^2 L_p \left(d - \frac{D_{pz}}{2} + Z_G \right)^2 \right) \tag{2.2-8}$$

Where L_p is the length of the pontoons.

3. ANALYTICAL METHOD

3.1. INTRODUCTION

An analytical method derived in this section is an alternative way to calculate the loads on a TLP. It is based on analytic solutions of oncoming, diffraction and radiation potentials of the first order waves on vertical circular cylinders. The columns of the TLP are considered as circular cylinders.

In order to calculate the loads on the pontoons, the Morison formula is used. This should yield acceptable results since the pontoons have a deep draught.

The method is here applied to a TLP configuration but it can be applied to any structure based on circular columns.

The method is based on the work developed by Linton and Evans [3.3] and Kim [3.4].

Linton and Evans give the analytical solution of the diffraction potential for an array of circular cylinders. Kim has extended the solution to the radiation problem.

The analytical solutions are correct for complete cylinders extending from the sea bed to the water surface. Kim has demonstrated that the solutions are still valid if applied to cylinders of deep draught (See references [3.4] and [3.5]). Nevertheless, the theory can only predict the forces in the horizontal plane. In order to obtain the forces applied to the columns in heave, Kim proposed to use the Froude Krylov approximation.

An alternative method is used in this study to calculate vertical forces. The results in heave are obtained using an analytical solution for one truncated circular cylinder (See Garrett [3.6]). This solution can be used to obtain the wave forces, damping and added mass. The influence of the columns on each other is neglected.

This theory can be extended to calculate the second order drift (See Chapter 4), and the diffracted free surface (See Chapter 6).

The first part presents the method used in the horizontal plane for the diffraction and the radiation problems.

In the second part, the vertical forces due to diffraction and radiation are formulated.

In the final part, the problem in roll and pitch is solved.

3.2. HORIZONTAL PLANE

In the following section, the potentials are assumed to take the following form:

$$\Phi(x, y, z, t) = \mathrm{Re}\left(\varphi(x, y, z)e^{-i\omega t}\right) \tag{3.2-1}$$

3.2.1. Diffraction

The potentials are expressed in N different polar co-ordinate systems (r_j, θ_j, z), whose origins are on the mean free surface and at the centre of the N different vertical circular cylinders extending from the sea bed to the mean free surface.

To simplify, the expressions of the potentials, we write:

$$\varphi(x, y, z) = \phi(x, y)f(z) \tag{3.2-2}$$

Where:

$$f(z) = -\frac{igA}{\omega}.\frac{\cosh k(z+H)}{\cosh kH} \tag{3.2-3}$$

Where:

H: water depth
A: wave amplitude
ω: wave frequency
k: real solution of:

$$k\tanh(kH) = \frac{\omega^2}{g} \tag{3.2-4}$$

In the *jth* co-ordinate system, the potential of the incoming wave becomes:

$$\phi_I^j = I_j.\sum_{n=-\infty}^{\infty} J_n(k.r_j).e^{in(\pi/2-\theta_j+\alpha)} \tag{3.2-5}$$

Where:

$I_j = e^{ik(X_{cj}.\cos\alpha + Y_{cj}.\sin\alpha)}$

X_{cj} and Y_{cj} are the co-ordinates of the centre of the *jth* column in the global co-ordinate system.

α: wave angle

Similarly, the diffraction potential is written:

$$\phi_D^j = \sum_{n=-\infty}^{\infty} A_n^j \, Z_n^j \, H_n\left(kr_j\right) e^{in\theta_j} \tag{3.2-6}$$

Where:

$$Z_n^j = \frac{J'_n\left(ka_j\right)}{H'_n\left(ka_j\right)}$$

J_n and H_n are respectively the Bessel functions of the first and third kind of order n.

a_j : radius of the *jth* cylinder

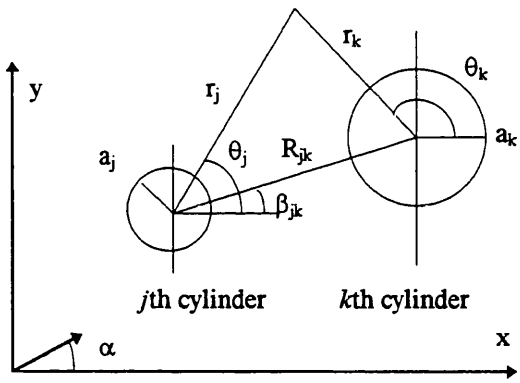

The forces on an array of N vertical circular cylinders are given by the incident and the diffraction potentials. So the total potential is written as:

$$\phi = \sum_{j=1}^{N} \phi_I^j + \phi_D^j \tag{3.2-7}$$

Using Graf's addition theorem for Bessel functions, and applying the boundary condition:

$$\frac{d\phi}{dr_k} = 0 \quad \text{on} \quad r_k = a_k, \quad k = 1,2,..,N \tag{3.2-8}$$

we obtain the following infinite system of linear equations:

$$A_m^k + \sum_{\substack{j=1 \\ \neq k}}^{N} \sum_{n=-\infty}^{+\infty} A_n^j \, Z_n^j \, e^{i(n-m)\beta_{jk}} H_{n-m}\left(kR_{jk}\right) = -I_k \, e^{im(\pi/2-\alpha)} \tag{3.2-9}$$

$$k = 1,..,N \quad -\infty < m < +\infty$$

Using this result, the potential on the *jth* cylinder becomes:

$$\phi(a_j,\theta_j) = -\frac{2i}{\pi k a_j}\sum_{n=-\infty}^{\infty}\frac{A_n^j}{H_n'(ka_j)}e^{in\theta_j} \tag{3.2-10}$$

In order to find the coefficients A_n^j, the infinite system is truncated to an N(2M+1) system of linear equations:

$$A_m^k + \sum_{\substack{j=1\\ \neq k}}^{N}\sum_{n=-M}^{M} A_n^j Z_n^j e^{i(n-m)\beta_{jk}} H_{n-m}(kR_{jk}) = -I_k e^{im(\pi/2-\alpha)} \tag{3.2-11}$$

$$k = 1,..,N \quad -M < m < +M$$

In order to obtain enough accuracy, the value of M should be taken between 6 and 12. The choice of M depends on the geometry and on the frequency. M should be increased for columns close to each other, and for high frequency.

The first order force on the *jth* cylinder is given by integrating the pressure over the surface of the cylinder:

$$F^j = \mathrm{Re}\left(X^j e^{-i\omega t}\right) \tag{3.2-12}$$

Where:

$$X^j = -i\rho\omega\int_{-d}^{0} f(z)dz\int_{0}^{2\pi}\phi(a_j,\theta_j)\begin{pmatrix}\cos\theta_j\\ \sin\theta_j\end{pmatrix}.d\theta_j \tag{3.2-13}$$

Where d is the draught of the cylinder

The upper elements of a bracketed pair refer to the force in the x-direction and the lower elements to that in the y-direction.

Evaluating the integral gives:

$$X^j = -\begin{pmatrix}i\\ 1\end{pmatrix}\frac{2\rho g A}{k^2 H_1'(ka_j)}\frac{\mathrm{sh}\,kH - \mathrm{sh}\,k(H-d)}{\mathrm{ch}\,kH}\left(A_{-1}^j\begin{pmatrix}-\\ +\end{pmatrix}A_1^j\right) \tag{3.2-14}$$

3.2.2. Radiation

The added mass and the potential damping are given by integrating the radiation potential over the surface of the cylinders.

We need first to express the radiation potential for an array of N cylinders.

For convenience, the radiation potential is written as a summation of normalised radiation potentials in each mode.

$$\varphi_R = \sum_{k=1}^{6} -i\omega\, \xi_k\, \varphi_k \tag{3.2-15}$$

Where ξ_k is the displacement in the direction k.

φ_i^j corresponding to a radiation potential for a unit velocity in direction i for the *jth* cylinder is given by:

$$\varphi_i^j(r_j,\theta_j,z) = \sum_{n=-\infty}^{\infty}\left(C_n^j\, f_0(z)\frac{H_n(k_0 r_j)}{k_0\, H_n'(k_0 a_j)} + \sum_{l=1}^{\infty} L_{nl}^j\, f_l(z)\frac{K_n(k_l r_j)}{k_l\, K_n'(k_l a_j)}\right) e^{in\theta_j} \tag{3.2-16}$$

Where:

$$f_0(z) = \frac{\cosh k_0(z+H)}{\cosh k_0 h}$$

$$f_l(z) = \frac{\cos k_l(z+H)}{\cos k_l h}$$

k_0 and k_l are respectively the solutions of:

$$k_0 \tanh(k_0 H) = \frac{\omega^2}{g} \qquad\qquad k_l \tan(k_l H) = -\frac{\omega^2}{g}$$

As previously, we use the Graf's addition theorem and the boundary condition to find the following infinite system of equations:

$$C_m^k + \sum_{\substack{j=1\\ \neq k}}^{N}\sum_{n=-\infty}^{+\infty} C_n^j \frac{J_m'(k_0 a_k)}{H_n'(k_0 a_j)} e^{i(n-m)\beta_{jk}}\, H_{n-m}(k_0 R_{jk}) = R_{mi}^k\, g_0^i(H) \tag{3.2-17}$$

$$L_{ml}^k + \sum_{\substack{j=1\\ \neq k}}^{N}\sum_{n=-\infty}^{+\infty} L_{nl}^j \frac{I_m'(k_l a_k)}{K_n'(k_l a_j)} e^{i(n-m)\beta_{jk}}\, e^{-im\pi}\, K_{n-m}(k_l R_{jk}) = R_{mi}^k\, g_l^i(H) \tag{3.2-18}$$

Where: $\qquad k = 1,..,N \quad -\infty < m < +\infty \quad 1 \le l < +\infty$

and:

$$R_{mi}^{k} = \frac{1}{2}\delta_{\pm 1,m} \quad \text{for } i = 1 \qquad \text{(surge)}$$

$$R_{mi}^{k} = \frac{-mi}{2}\delta_{\pm 1,m} \quad \text{for } i = 2 \quad \text{(sway)}$$

$$g_0^i(H) = \frac{4\cosh k_0 H\left(\sinh k_0 H - \sinh k_0 (H-d)\right)}{2k_0 H + \sinh 2k_0 H} \quad \text{for } i = 1,2$$

$$g_l^i(H) = \frac{4\cos k_1 H\left(\sin k_1 H - \sin k_1 (H-d)\right)}{2k_1 H + \sin 2k_1 H} \quad \text{for } i = 1,2$$

Where δ_{im} is the Kronecker function, and I_n and K_n are respectively the modified Bessel functions of the first and second order of order n.

In order to determine the coefficients C_m^k and L_{ml}^k, we need to truncate the system at n=M and l=L to obtain L+1 sets of N(2M+1) systems of equations. Values of M=6 and L=8 give a good accuracy for the results.

The expression of the potential on the *kth* cylinder is given by:

$$\varphi_i(a_k, \theta_k, z) = \sum_{n=-\infty}^{\infty}\left(f_0(z)\varphi_{ni}^k + \sum_{l=1}^{\infty} f_l(z)\varphi_{nli}^k\right) e^{in\theta_k} \tag{3.2-19}$$

Where:

$$\varphi_{ni}^k = \frac{1}{k_0}\left(C_n^k\left(\frac{H_n(k_0 a_k)}{H_n'(k_0 a_k)} - \frac{J_n(k_0 a_k)}{J_n'(k_0 a_k)}\right) + g_0^i(H) R_{ni}^k \frac{J_n(k_0 a_k)}{J_n'(k_0 a_k)}\right) \tag{3.2-20}$$

$$\varphi_{nli}^k = \frac{1}{k_l}\left(L_{nl}^k\left(\frac{K_n(k_l a_k)}{K_n'(k_l a_k)} - \frac{I_n(k_l a_k)}{I_n'(k_l a_k)}\right) + g_l^i(H) R_{ni}^k \frac{I_n(k_l a_k)}{I_n'(k_l a_k)}\right) \tag{3.2-21}$$

The added mass M_a and the damping C in mode i are given by the following formula:

$$M_{aij} + i\frac{C_{ij}}{\omega} = \rho \int_{Sb} \varphi_i n_j \, dS \tag{3.2-22}$$

Where n_j is the component in the direction j of the vector normal to the wet surface S_b.

After integration, the added mass and the damping on the *kth* cylinder, in mode i are given by:

$$M_{aii} + i\frac{C_{ii}}{\omega} = \sum_{n=\pm 1}\left(\varphi_{ni}^{k} Q_i + \sum_{l=1}^{\infty}\varphi_{nli}^{k} Q_{li}\right)\pi c_i a_k \rho \quad \text{for } i = 1,2$$

Where: $c_1 = 1$ and $c_2 = in\pi$

$$Q_i = \frac{\sinh k_0 H - \sinh k_0(H-d)}{k_0 \cosh k_0 H} \quad \text{for } i = 1,2$$

$$Q_{li} = \frac{\sin k_l H - \sin k_l(H-d)}{k_l \cos k_l H} \quad \text{for } i = 1,2$$

The previous analysis is exact for H=d, i.e. in the case of complete cylinders. We have assumed that the theory can be applied to deep draught cylinders with a good approximation. This point is discussed later in section 4.

3.3. VERTICAL PLANE

The previous analysis cannot be applied to predict heave forces. Since the theory has been developed for circular cylinders extending from the sea bed, it cannot be used to calculate the forces in heave.

Kim [3.4] is proposing to use the Froude Krylov approximation for the calculation of the heave forces.

A more accurate method is used here. Analytical solutions of the diffraction and radiation potentials for one truncated cylinder have been developed by Garrett [3.6]. The solutions are applied independently to the four columns of the TLP. The diffraction due to the interaction between the columns is not taken into account, but one can expect it to be small on the bottom of deep draught cylinders.

The radiation problem is solved by the same method, in order to calculate added mass and potential damping. The same assumption concerning the interaction between the columns has to be made. This may have more influence in radiation than in diffraction.

The validity of both resolutions is discussed in section 4.

The vertical forces on the pontoons are calculated with the Morison formula.

3.3.1. Diffraction

We now use a polar co-ordinate system, whose origin is the projection on sea bed along the z axis, of the centre of the cylinder (See sketch below).

The domain is divided into two areas.

1 The domain referred as inferior below the cylinder:

$$0 \le z \le Z_b \qquad \text{and} \qquad 0 \le r \le R_c$$

2 The domain referred as exterior:

$$0 \le z \le H \qquad \text{and} \qquad R_c \le r \le +\infty$$

Where Z_b is the z co-ordinate of the bottom of the cylinder, R_c the cylinder radius, and H the water depth.

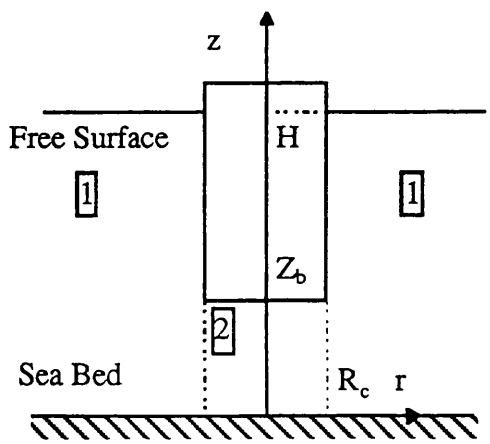

The incident potential is written as:

$$\varphi_I = -i\frac{a.g}{\omega}.\frac{ch(k_0 z)}{ch(k_0 H)}.\sum_{m=0}^{\infty}\varepsilon_m.i^m.J_m(k_0 r).\cos(m\theta) = \frac{ch(k_0 z)}{ch(k_0 H)}\sum_{m=0}^{\infty}C_{Im}.\cos(m\theta) \qquad (3.3\text{-}1)$$

Where:

$$\varepsilon_m = 2 - \delta_{m0}$$

k_0 is defined by: $\omega^2 = gk_0 \tanh(k_0 H)$

The diffraction potentials are:

For the exterior domain:

$$\varphi^e = \sum_{m=0}^{\infty} \cos(m\theta)\left(A_{m0} \frac{\cosh(k_0 z)}{\cosh(k_0 H)} H_m(k_0 r) + \sum_{n=1}^{\infty} A_{mn} \cos(k_n z) K_m(k_n r) \right) \quad (3.3\text{-}2)$$

For the interior domain:

$$\varphi^i = \sum_{m=0}^{\infty} \cos(m\theta)\left(B_{m0} \left(\frac{r}{R_c} \right)^m + \sum_{n=1}^{\infty} B_{mn} \cos(\lambda_n z) I_m(\lambda_n r) \right) \quad (3.3\text{-}3)$$

Where k_n is defined by: $\omega^2 = -gk_n \tan(k_n H)$

and λ_n is defined by: $\lambda_n = \frac{n\pi}{Z_b}$

The global potential is given by:

in the exterior domain: $\varphi = \varphi_I + \varphi^e$ (3.3-4)

in the inferior domain: $\varphi = \varphi^i$ (3.3-5)

The following matching conditions for $R = R_c$ determine the coefficients A_{mn} and B_{mn}:

for $m = 0, \infty$:

$$\begin{aligned} \varphi^i_m &= \varphi_{Im} + \varphi^e_m \qquad 0 \le z \le Z_b \\ \varphi^i_{m,r} &= \varphi_{Im,r} + \varphi^e_{m,r} \qquad 0 \le z \le Z_b \end{aligned} \quad (3.3\text{-}6)$$

To simplify the mathematical development, we rewrite the potentials redifining A_{mn} and B_{mn} as a_{mn} and b_{mn}:

$$\varphi^e(R_c, \theta, z) = \sum_{m=0}^{\infty} \cos(m\theta)\left(\sum_{n=0}^{\infty} a_{mn} f_n(z) \right) \quad (3.3\text{-}7)$$

$$\varphi^e_{,r}(R_c, \theta, z) = \sum_{m=0}^{\infty} \cos(m\theta)\left(\sum_{n=0}^{\infty} a_{mn} \alpha_{mn} f_n(z) \right) \quad (3.3\text{-}8)$$

Where: $f_0(z) = \dfrac{\cosh(k_0 z)}{\sqrt{\int_0^H \cosh^2(k_0 z)dz}}$ $\qquad$ $f_n(z) = \dfrac{\cos(k_n z)}{\sqrt{\int_0^H \cos^2(k_n z)dz}}$

$$\alpha_{m0} = k_0 \frac{H'_m(k_0 R_c)}{H_m(k_0 R_c)} \qquad \alpha_{mn} = k_n \frac{K'_m(k_n R_c)}{K_m(k_n R_c)}$$

And

$$\varphi^i(R_c, \theta, z) = \sum_{m=0}^{\infty} \cos(m\theta)\left(\sum_{n=0}^{\infty} b_{mn} g_n(z)\right) \tag{3.3-9}$$

$$\varphi^i_{,r}(R_c, \theta, z) = \sum_{m=0}^{\infty} \cos(m\theta)\left(\sum_{n=0}^{\infty} b_{mn} \beta_{mn} g_n(z)\right) \tag{3.3-10}$$

Where: $g_0(z) = \dfrac{1}{\sqrt{Z_b}}$ $\qquad$ $g_n(z) = \dfrac{\cos(\lambda_n z)}{\sqrt{\int_0^{Z_b} \cos^2(\lambda_n z)dz}}$

$$\beta_{m0} = \frac{m}{R_c} \qquad \beta_{mn} = \lambda_n \frac{I'_m(\lambda_n R_c)}{I_m(\lambda_n R_c)}$$

If we write the first matching condition as:

$$\int_0^{Z_b} \varphi^i_m \cdot g_p(z)dz = \int_0^{Z_b} \varphi^e_m \cdot g_p(z)dz + \int_0^{Z_b} \varphi_{Im} \cdot g_p(z)dz \qquad m = 0, \infty \tag{3.3-11}$$

due to the orthogonality of the functions g_n, we obtain the following linear system:

$$\{B\} = [BA].\{A\} + \{D_1\} \tag{3.3-12}$$

Where:

$$\{A\} = \left(a_{m0}, a_{m1}, \ldots, a_{mN_a}\right) \qquad \{B\} = \left(b_{m0}, b_{m1}, \ldots, b_{mN_b}\right)$$

$$[BA]_{pn} = \int_0^{Z_b} f_n(z).g_p(z).dz$$

$$\{D_1\}_p = C_{Im} \int_0^{Z_b} f_0(z).g_p(z).dz$$

If we apply the same method to the second matching condition:

$$\int_0^H \varphi^e_{m,r}.f_p(z)dz = \int_0^H \varphi^i_{m,r}.f_p(z)dz - \int_0^H \varphi_{Im,r}.f_p(z)dz \qquad (3.3\text{-}13)$$

due to the orthogonality of the functions f_n, we have:

$$\{A\} = [AB].\{B\} + \{D_3\} \qquad (3.3\text{-}14)$$

Where: $[AB]_{np} = \frac{\beta_{mn}}{\alpha_{mp}}[BA]_{pn}$ $\qquad \{D_3\} = \left(-C_{Im}\, k_0 \frac{J'_m(k_0R_c)}{J_m(k_0R_c)} \quad 0 \quad \dots \quad 0\right)$

Combining the two systems we get:

$$[I - BA.AB]\{B\} = [BA].\{D_3\} + \{D_1\} \qquad (3.3\text{-}15)$$

Where I is the identity matrix.

By solving this system, we get the coefficients b_{mn} for $n = 0, N_b$. The system has to be solved for each value of m. When the heave motion is considered, the coefficients b_{0n} are needed only. For a good accuracy, one should take values of N_a and N_b equal to 50.

The force in heave is given by integrating the pressure on the base of the column:

$$F_z = \mathrm{Re}\left(Z\, e^{-i\omega t}\right) \qquad (3.3\text{-}16)$$

Where:

$$Z = i\rho\omega \int_0^{2\pi}\int_0^{Rc} \varphi^i_{m=0}(r, Z_b)\, r\, dr\, d\theta \qquad (3.3\text{-}17)$$

After integration, it comes:

$$Z = i\rho\omega\, 2\pi\left(B_{00}\frac{R_c^2}{2} + \sum_{n=1}^{\infty} B_{0n}(-1)^n \frac{R_c}{\lambda_n} I_1(\lambda_n R_c)\right) \qquad (3.3\text{-}18)$$

This gives the force for one cylinder. If we want the force for an array of N cylinders, we have to recalculate the coefficients b_{mn} for each column, taking into account the phase of the waves at the bottom of each cylinder. This is done by multiplying the incident potential by the following factor, $\left(I_j = e^{ik_0(X_{cj}\cos\alpha + Y_{cj}\sin\alpha)}\right)$

The forces on the columns are then added together in order to obtain the total force on the structure.

3.3.2. Radiation

For heave the radiation potentials for a unit velocity, are given by:

exterior domain:

$$\varphi^e(r,z) = a'_0 f_0(z)\frac{H_0(k_0 r)}{H_0(k_0 R_c)} + \sum_{n=1}^{N_a} a'_n f_n(z)\frac{K_0(k_n r)}{K_0(k_n R_c)} \qquad (3.3\text{-}19)$$

inferior domain:

$$\varphi^i(r,z) = b'_0 g_0(z) + \sum_{n=1}^{N_b} b'_n g_n(z)\frac{I_0(\lambda_n r)}{I_0(\lambda_n R_c)} + \frac{1}{2Z_b}\left(z^2 - \frac{r^2}{2}\right) \qquad (3.3\text{-}20)$$

By applying the same method as for the diffraction, one can find the coefficients a'_n and b'_n corresponding to the following boundary conditions:

$$\begin{aligned} \varphi^i(R_c,z) &= \varphi^e(R_c,z) \qquad 0 \le z \le Z_b \\ \varphi^i_{,r}(R_c,z) &= \varphi^e_{,r}(R_c,z) \qquad 0 \le z \le Z_b \end{aligned} \qquad (3.3\text{-}21)$$

The added mass and the damping are given by the following formula:

$$M_{Az} + i\frac{C_z}{\omega} = \rho \int_{Base} \varphi^i(r,Z_b)\,dS \qquad (3.3\text{-}22)$$

After integration, it becomes:

$$M_{Az} + i\frac{C_z}{\omega} = 2\pi\rho\left(b'_0 \frac{R_c^{\,2}}{2}\frac{1}{\sqrt{Z_b}} + \frac{1}{4Z_b}\left(R_c^2 Z_b^2 - \frac{R_c^4}{4}\right) + \sum_{n=1}^{\infty} b'_n (-1)^n \sqrt{\frac{2}{Z_b}}\frac{R_c}{\lambda_n}\frac{I_1(\lambda_n R_c)}{I_0(\lambda_n R_c)}\right) \qquad (3.3\text{-}23)$$

The added mass and damping correspond here to one truncated cylinder. They should be multiplied by the number of column to obtain the total added mass and damping.

3.4. ROLL AND PITCH

By combining the loads in surge, sway and heave, the moment in roll and pitch can be calculated.

3.4.1. Diffraction

The moments on the cylinders are given by the following formula:

$$\begin{aligned} M_{Gx} &= \int_{Surface}(z p n_y - y p n_z)dS = \int_{Side} z p n_y dS - \int_{Bottom} y p n_z dS \\ M_{Gy} &= \int_{Surface}(x p n_z - z p n_x)dS = \int_{Bottom} x p n_z dS - \int_{Side} z p n_x dS \end{aligned} \qquad (3.4\text{-}1)$$

Where $\vec{n} = (n_x, n_y, n_z)$ is the vector normal to the cylinder surface and p the local pressure.

The moment on the array of cylinders can be written as:

$$M(t) = \mathrm{Re}\left((M_{side} + M_{bottom})e^{-i\omega t}\right) \qquad (3.4\text{-}2)$$

First, we integrate the pressure on the side of the *jth* cylinder:

$$\begin{bmatrix} M^j_{Side_x} \\ M^j_{Side_y} \end{bmatrix} = \begin{pmatrix} 1 \\ -i \end{pmatrix} \frac{2\rho g A}{k^3 H_1'(k a_j)} \frac{k d \,\mathrm{sh}\, k(H-d) - \mathrm{chkh} + \mathrm{ch}\, k(H-d)}{\mathrm{ch}\, kH} \left(A^j_{-1} \begin{pmatrix} + \\ - \end{pmatrix} A^j_1 \right) \qquad (3.4\text{-}3)$$

This gives the moment in the local co-ordinate system. In order to calculate the moment in the general co-ordinate system, the following formula is used:

$$\vec{M}_{/p} = \vec{M}_{/o} + \vec{PO} \times \vec{F} \qquad (3.4\text{-}4)$$

The moment due to the pressure on the bottom of the *jth* cylinder can be written as:

$$\begin{bmatrix} M^j_{Bottom_x} \\ M^j_{Bottom_y} \end{bmatrix} = i\rho\omega\pi a_j^2 \left(\frac{B_{10} a_j}{4} + \sum_{n=1}^{N_k} (-1)^n \frac{B_{1n}}{\lambda_n} I_2(\lambda_n a_j) \right) \begin{bmatrix} -\sin(\alpha) \\ \cos(\alpha) \end{bmatrix} \qquad (3.4\text{-}5)$$

The same formula as previously is used to obtain the moment in the general co-ordinate system.

3.4.2. Radiation

The added mass is calculated with the strip theory.

The potential damping is taken equal to zero. The damping is of insignificant influence on the roll and pitch motions since the natural period is far out of the range of frequencies where the waves occur most frequently.

3.5. PONTOONS

The equation derived in the previous sections are for an array of cylinders. We have to consider now how to take the pontoons into account.

Since the pontoons have a deep draught, the forces on the pontoons can be calculated by the Morison formula.

So by using Morison formulation to obtain the forces, we get a reasonable approximation.

The interaction between the pontoons and the columns is neglected. However, Berhault et al [3.9] have shown that these interactions are small compared to the other forces and can be neglected.

In the same manner, the added mass is calculated using the strip theory and the potential damping is taken equal to zero.

The formulations of the forces and the added mass for the pontoons are described in section 2 of this chapter.

4. VALIDATION

To validate the program based on the Morison formulation and the analytical solutions developed in the previous sections, a comparison is made with a 3D diffraction radiation code. The comparison is made in terms of forces, added mass, damping and displacements.

The comparisons of the forces added mass and damping are carried out for four different geometries. The first three are used only with the analytical method to validate the different assumptions made during theoretical developments. The fourth one is used with both methods, the analytical solution and the Morison approach.

- Geometry 1 is a simple truncated cylinder of 25 meters of diameter. It is used to validate the program for the vertical potentials, since the theory gives a complete analytical solution for this case. The mesh used for the diffraction radiation code can be seen in Figure 3.1.

- Geometry 2 is an array of 4 bottom mounted cylinders. The spacing between the cylinders corresponds to the position of the columns of the Snorre TLP (See below). The column height and thus the water depth has been chosen as 150m. It is used to validate the program for the horizontal potentials, since the theory gives a complete analytical solution for this case. The mesh is presented in Figure 3.2.

Disposition of the 4 cylinders

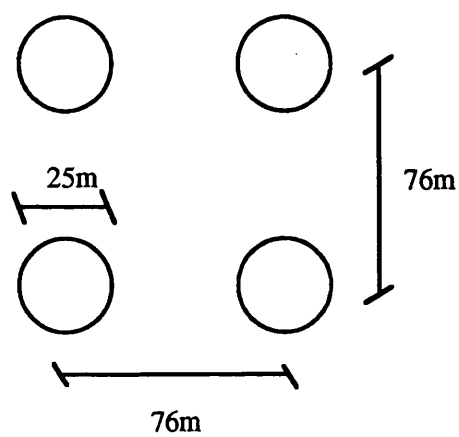

- Geometry 3 is an array of 4 truncated cylinders. The draught (37.5m) and the water depth (340m) correspond to those of the Snorre TLP. The geometry is identical to the Snorre TLP, neglecting the pontoons.

It is used to validate the following approximations of the analytical method:

For the horizontal motions, the theory can be extended from bottom mounted cylinders to deep draught cylinders.

For the vertical motions, the interaction between the cylinders can be neglected.

The corresponding mesh is presented in Figure 3.3.

- Geometry 4 is the whole Snorre TLP, columns plus pontoons. For the analytical method, it is used to check that the pontoons have little influence in waves compared to the columns therefore the use of Morison formulation and strip method lead to little inaccuracy.
  It is also used to compare the final results on a complete TLP obtained from true Morison approach, the analytical method, and the diffraction radiation code.
  The results on the Snorre TLP were calculated by Dr Hoi-Sang Chan, of the Department of Naval Architecture and Ocean Engineering at Glasgow University.

Once the forces, the added mass and the potential damping found from each theory, the displacements of the Snorre TLP are calculated in the frequency domain.

The validation is first carried out for surge and sway forces and motions, then for heave forces and motions, and finally for roll and pitch forces and motions. All these calculations use head seas with unit amplitude waves.
The last section presents calculations carried out for directional seas to complete the validation.

4.1. SURGE AND SWAY FORCES AND MOTIONS

The validation is first carried out for the diffraction problem, to check the forces. In addition the solution of the radiation problem was validated by using different methods and the results were compared, checking the added mass and the potential damping. Finally, the displacements of the Snorre TLP were calculated.

4.1.1. Diffraction

Figure 3.4 compares the first order surge forces for the geometry 2 obtained from the analytical solutions and the D/R code. We have a good agreement between the two results. For higher frequencies, a better correlation can be reached by going further in the summation of the Bessel function series in analytical solutions.

Figure 3.5 presents the same results on geometry 3. The agreement is still good and the same remark applies for high frequencies. It can be assumed that the theory based on bottom mounted cylinders can be extended to deep draught cylinders.

Finally the pontoons are taken into account using geometry 4. The results are shown in Figure 3.6. Agreement between the analytical method and the D/R code results are good. It is reasonable to calculate the forces on the pontoons with Morison formula. The influence of the pontoons is small compared to one of the columns and the error induced by the empirical formula is still quite low.

The Morison formulation does not give as a good agreement with the D/R code. It tends to overestimate the loads in high frequencies.

4.1.2. Radiation

Figures 3.7 and 3.8 show comparisons for the surge added mass and damping for the geometry 2. Good correlations between the results obtained from the analytical method and the D/R code validate the program.

The results for geometry 3 are shown in Figure 3.9 and 3.10. The agreement is still good. Thus, the radiation theory as well as the diffraction theory, can be extended from bottom mounted cylinders to deep draught cylinders.

Figure 3.11 presents the added mass comparison for geometry 4. The added mass from the pontoons calculated with strip theory was added to the results obtained from the analytical theory for the columns. The figure shows an error of approximately 12% between the two results. One should note that this error decreases to 6% of the value of the mass plus the added mass.

The value obtained from the strip theory value is also plotted. It is a straight line, since it does not take into account the variation with the frequency. However, the result gives quite a good mean value of the added mass.

Similarly, Figure 3.12 shows the potential damping for geometry 4. In this case the potential damping from the pontoons is simply neglected. This assumption is explained by the fact that the viscous damping is predominant on this part of the structure.
The correlation is good for low frequencies. The maximum values at 0.9 rad/s show a large difference between the two results. However, since the natural period is about 0.1 rad/s this difference will not have significant effect on the surge response values.

4.1.3. Displacements

The surge response results, obtained from the different theories, are very similar (See Figure 3.13). The only difference appears around the natural frequency (Between 0.05 and 0.1 rad/s). In this region the high values of the transfer function amplify the differences between the force results.

If we take a closer look at that region (Figure 3.14), we can see that the analytical solution also has a slightly higher natural frequency than the Morison formulation.

The values of the response at the natural frequency are really high because the viscous damping was not taken into account.

Figure 3.15 shows the motion response values at about the natural frequency with or without the viscous damping. It can be seen that the viscous damping has a very large influence and that it is largely more important than the potential damping in this region.

4.2. HEAVE FORCES AND MOTIONS

4.2.1. Diffraction

Figure 3.16 presents a comparison of the results for the heave force on a truncated cylinder (geometry 1). We have a good agreement between the D/R code and the correct analytical solution.

Figure 3.17 shows the forces on geometry 3. The force due to the analytical solution takes into account the phasing of the waves but not the interaction between the columns. Nevertheless, the correlation is good. As expected, for the force calculation in heave, the interaction between the different columns can be neglected.

In Figure 3.18 the force in heave for the geometry 4 is presented.

The results obtained from the analytical method and the D/R code correlate well. As with the forces in the horizontal plane, in heave, the forces on the pontoons can be taken into account with the Morison formula.

The Morison approach agrees well also for the force calculation in Heave. We notice that the solution given by the R/D code is shifted to the left compared with the two other results. This is due to the interaction between the columns which is not taken into account by the two other methods.

We can notice that the simple solution given by the Morison approach compares really well with the more complicated formulation used by the analytical method.

4.2.2. Radiation

Figure 3.19 shows the added mass in heave for geometry 1. The correlation is roughly good. The values are slightly different but the trends match well.

In Figure 3.20, the added mass is presented for geometry 3. The results indicate that, the interaction between the cylinders cannot be neglected for low frequency waves. The maximum error is about 40% for 0.1 rad/s.

However one has to note that the added mass is small compared to the mass in heave. When the mass of the platform is added, the error drops down to 6.5%.

Figure 3.21 presents the added mass for geometry 4. The shapes of the two curves given by the analytical solution and the D/R code results match well, but the values are quite different. The difference between the two sets of results is about 20%.

It should be noted that this error compared to the sum of the added mass and the structural mass is only 7.5%. This induces an error of 3.6% in the heave natural frequency calculation. Thus, approximating the added mass of the pontoons by the strip theory and neglecting the interaction between the columns gives a result of reasonable accuracy.

The added mass calculated with the strip theory, gives a really low value compared to the other two methods. This is due to the fact that the added mass of the columns has been neglected. Once again, this has to be related to the fact that the value of the added mass is small compared to the mass of the structure.

The potential damping for a single truncated cylinder, presented in Figure 3.22, shows quite different results from one theory to the other. Indeed, the analytical solution gives smaller values.

From Figure 3.23, we can see that for geometry 3, the potential dampings are completely different in term of values. Obviously, the interaction between the columns has significant importance for the damping.

Finally, in Figure 3.24, we can see that for the complete TLP the potential damping is completely different from the analytical theory to the D/R code. The interaction between the columns and between the columns and the pontoons cannot be neglected for the calculation of the potential damping in heave.

The potential damping in heave will be taken as zero for the rest of the study. This can be justified by the fact that the damping is important only for frequencies around the natural period. For the heave motion, the natural frequency (around 2.5 rad/s) is not in the range of frequencies where the first order waves are significant.
Thus taking the damping as zero should lead to a small error when calculating the motions of the TLP as described in the next section.

4.2.3. Displacements

For the Morison approach and the analytical solution, the displacements are calculated with a damping equal to zero. Nevertheless, the results agree well with D/R code (See Figure 3.25) . In fact, the damping has no influence in heave. The large variations of added mass values do not have much influence on the response of the TLP either. As stated before the added mass is small compared to the mass. Furthermore, the mooring stiffness, because of its high value, is largely predominant for the transfer function calculation, in the wave frequency range.

This high value is also the reason of the low values of the displacement in heave.

4.3. ROLL AND PITCH

4.3.1. Diffraction

Figure 3.26 presents the moments on geometry 2. Only the moment due to the horizontal forces is used in this case. The results from the analytical theory and the D/R code show good agreement, validating the theory.

On geometry 3, the bottom correction due to the vertical forces was added to the moment calculation. The agreement is mainly good (See Figure 3.27). There are small differences for low frequencies. This can be explained by the fact that in this range of frequencies the approximation on deep draught cylinders is not fully verified. Indeed, low frequency waves have a slower decay with depth and their influence at deep draught cannot be fully neglected. In the case of the moment, the error is amplified by the moment arm. However, the error is still small, and the approximation of the moment is good.

Figure 3.28 presents the moment in pitch for the complete TLP (geometry 4). The agreement is good between the D/R code and the analytical theory whereas the Morison formulation tends to overestimate the moments for higher frequencies.

4.3.2. Radiation

The added mass comparison is presented in Figure 3.29. Since the added mass for the analytical solution is calculated with the strip theory, the values obtained are not dependent of the frequency. However, the correlation is good, the maximum error being 4.2% of the added mass and 1.6% of the sum of the added mass and the inertia.

The damping approximation is very rough since the analytical solution assumes that the potential damping is zero. However, the potential damping has little significance at frequencies far from the natural frequency. For roll and pitch motions, the natural frequency of the Snorre TLP is about 2 rad/s, above the excitation frequency of any loading considered in this study.

4.3.3. Displacements

The D/R code and the analytical solution give very similar results (Figure 3.30). The Morison formulation overestimates the displacement in higher frequencies. This is clearly correlated with the same phenomenon already observed for the moment. The large difference in the damping for the two formulations does not seem to pose any problem.

It should be noticed that the amplitude of the motions is very small with a maximum of 0.023 degrees.

4.4. DIRECTIONAL SEAS

To test the validity of the program, in directional seas, the forces and the displacements have been calculated on geometry 4, with a 22.5° and a 45° heading sea.

The forces and the displacements show a good agreement in Figure 3.31 to 3.34. The same remarks as for head seas apply. In heave, the D/R code results are shifted to the left, due to the interaction between the columns. In roll and pitch small differences appear between the D/R code and the analytical theory for the low frequency region. The moments are overestimated by the Morison formula for high frequencies.

However, the results are mainly good and are validated both for head and directional seas.

5. CONCLUSION

The present study shows that the analytical solution presents a good alternative to solve the first order diffraction and radiation problems on a TLP.

It compares well with a D/R code results both for head seas and directional seas. The differences in the results for the radiation problem in heave do not have much importance on the response calculations.

The Morison approach gives reasonable results too, especially for low frequencies, but the analytical solution is more precise.

Furthermore the analytical method is much faster than the D/R code. Indeed about a minute is needed to solve the first order diffraction and radiation problems for a range of 20 frequencies. On a similar machine (DEC Alpha), the D/R code requires about 10 hours of CPU time to carry out the calculation.

The analytical method can also be extended to calculate the steady drift and the diffracted free surface. This is explained in chapters 4 and 6.

For all these reasons, the analytical method will be preferred to the two others to calculate the wave loads in the time domain explained in Chapter 6.

REFERENCES OF CHAPTER 3

[3.1] J.P. Hooft, 1982, Advance Dynamics of Marine Structures, Interscience publication.

[3.2] Atkins Research and Developement, 1978, Dynamics of marine structures: Method of calculating the dynamic response of fixed structures subject to wave and current action., Report UR8, Ciria Underwater Eng Group.

[3.3] Linton C.M., 1990, Evans D.V., The interaction of waves with arrays of vertical circular cylinders, Journal of Fluid Mechanics, Vol. 215, pp 549,569.

[3.4] Kim M.H., 1993, Interaction of waves with N vertical circular cylinders, Journal of Waterway, Port, Coastal, and Ocean Engineering, Vol. 119, No. 6.

[3.5] Kim M.H., Mercier R.S., Gu G., Wu C., Bothelo D., 1993, PC-based wave load computation for large volume multi-column structures. Proceedings of the third International Offshore and Polar Engineering Conference, ISOPE.

[3.6] Garrett C.J.R., 1971, Wave forces on circular dock, Journal of Fluid Mechanics, Vol.46, Part 1, pp 129,139.

[3.7] Molin B., 1993, Cours d'hydrodynamique, Lecture at l'Ecole Supérieure d'Ingénieurs de Marseille.

[3.8] McLachlan N.W., 1955, Bessel functions for engineers, Oxford at Clarendon Press.

[3.9] Berhault C., Molin B., Bougis J., Guevel P., Landel E., Sorasio E., 1987, Alternative methods for the numerical analysis of the linear response of semi-submersible platforms in waves. Proc. OMAE Houston.

Number of panels = 620

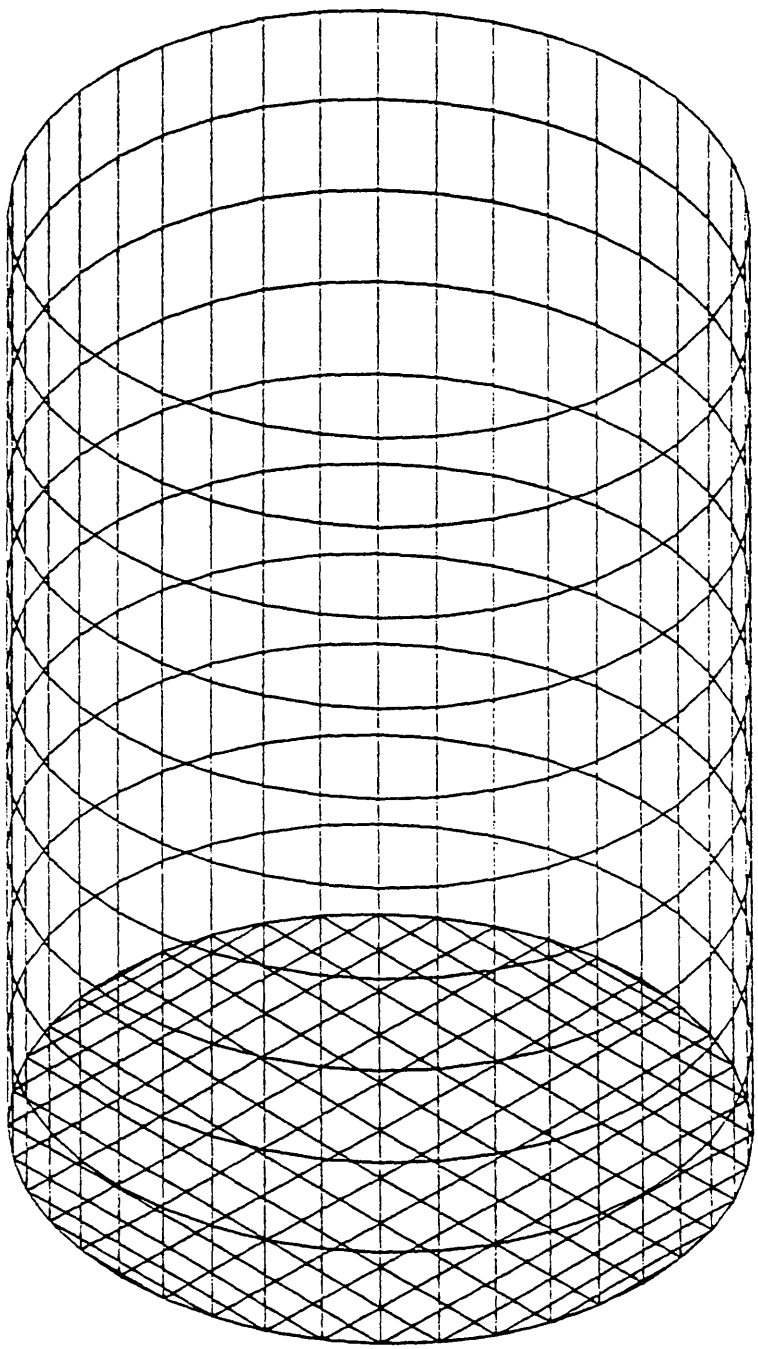

TRUNCATED CYLINDER

gure 3.1

Number of panels = 960

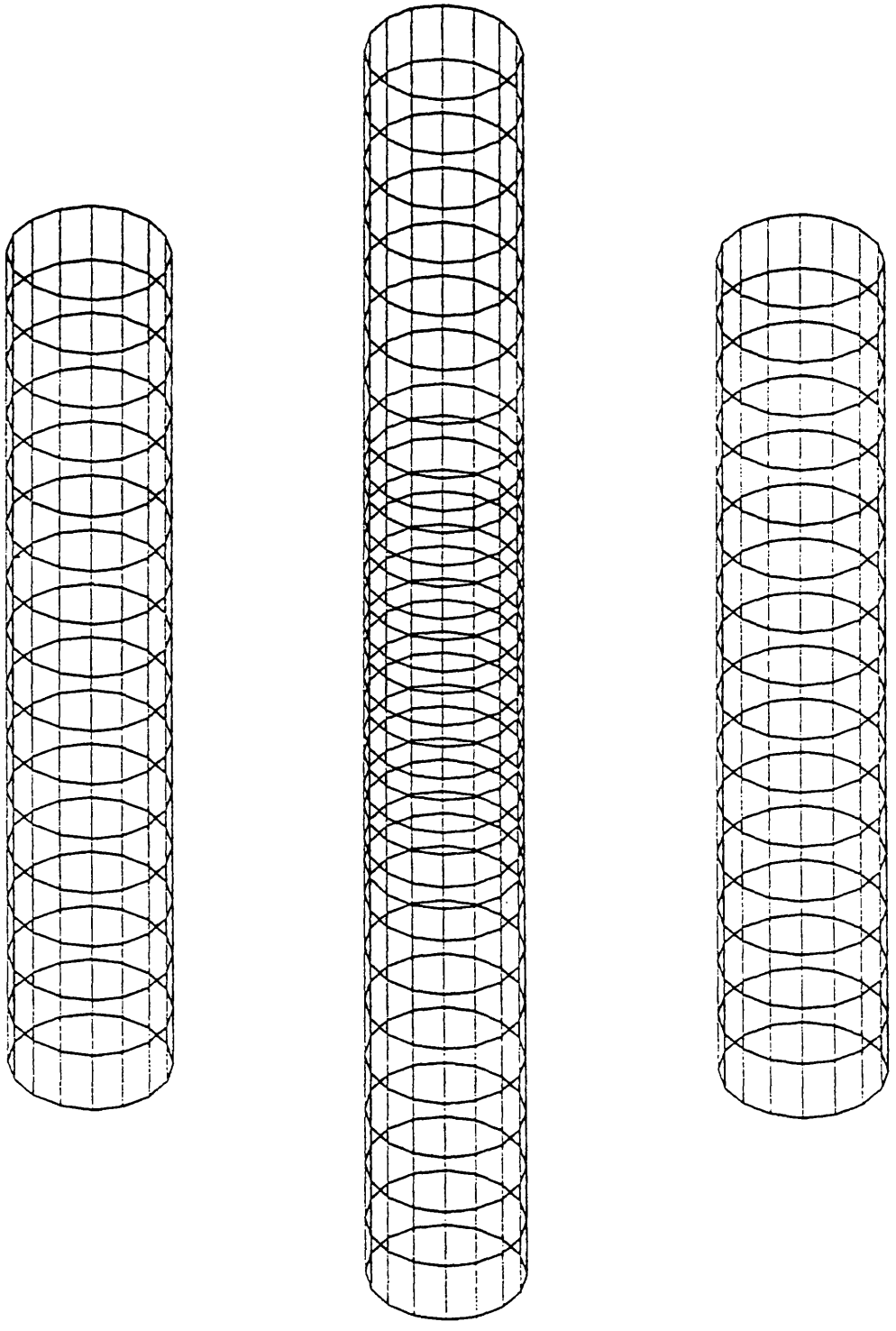

ARRAY OF 4 COMPLETE CYLINDERS

Figure 3.2

Number of panels = 796

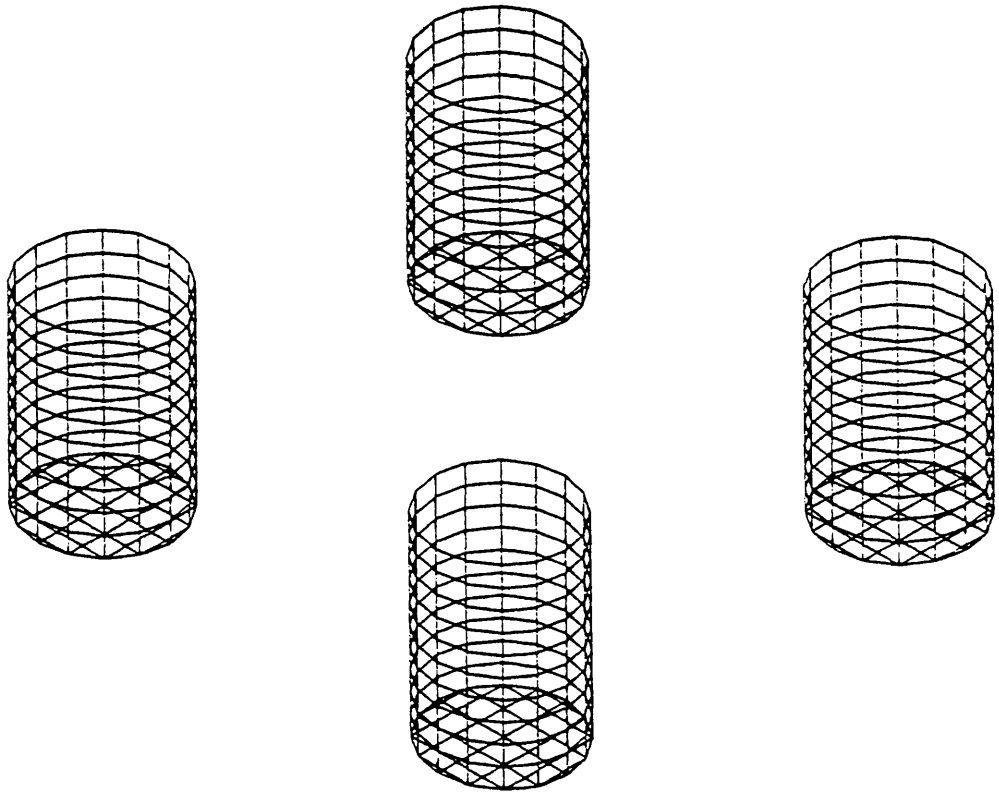

ARRAY OF TRUNCATED CYLINDERS

Figure 3.3

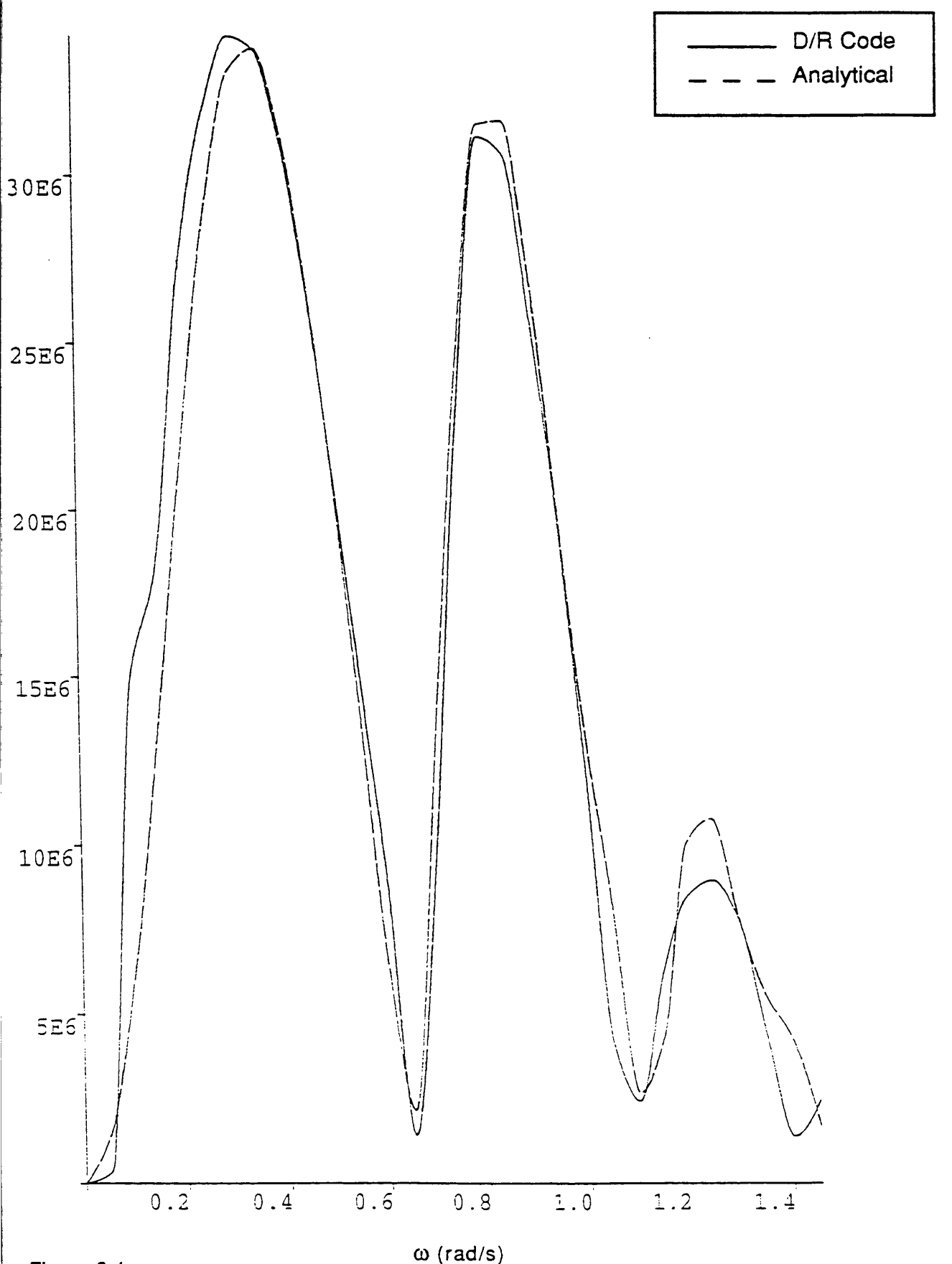
First Order Surge Force on an Array
of 4 Complete Cylinders
D/R Code
Analytical
30E6
25E6
20E6
15E6
10E6
5E6
0.2
0.4
0.6
0.8
1.0
1.2
1.4
ω (rad/s)

Figure 3.4

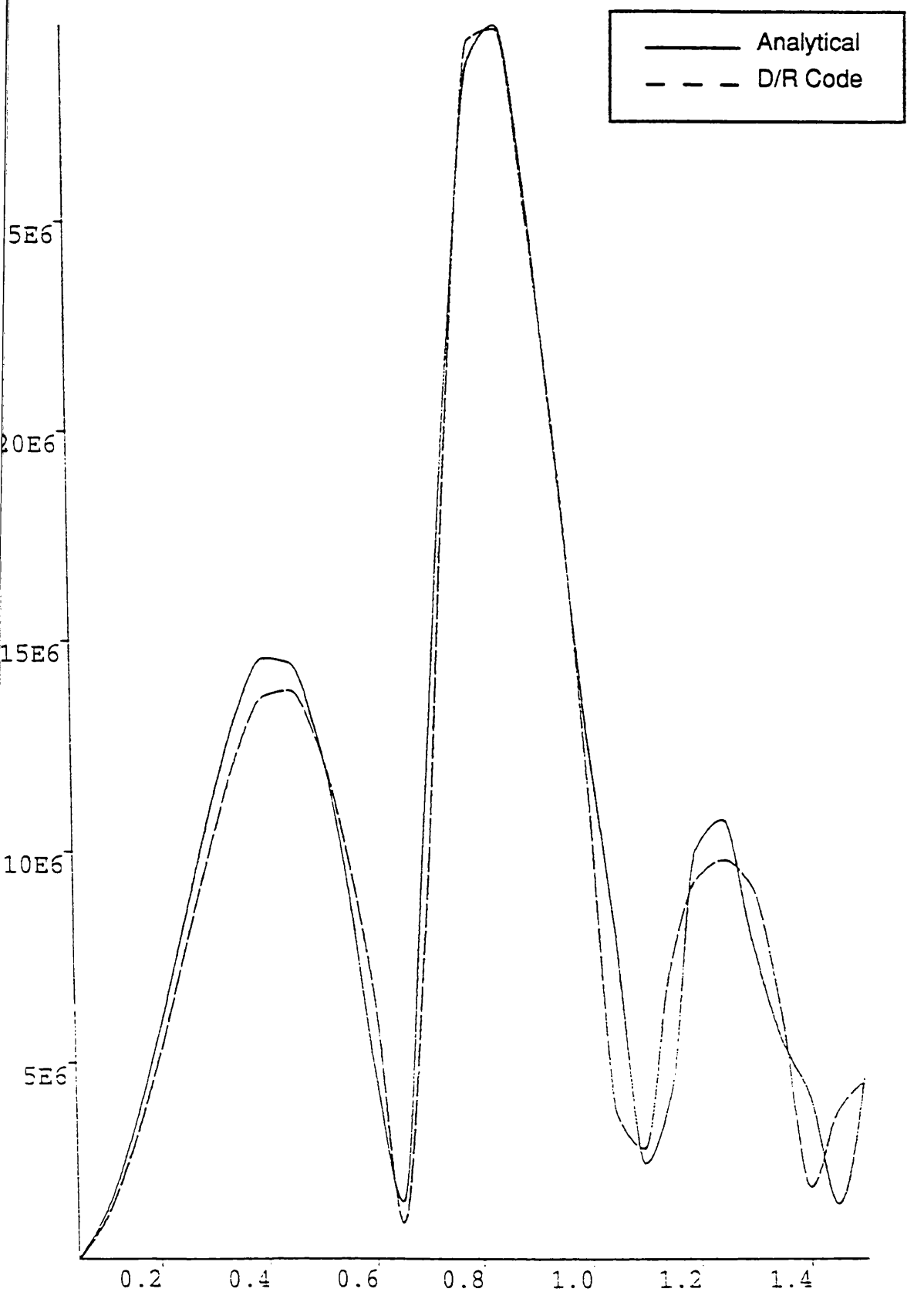
First Order Surge Force on an Array
of 4 Truncated Cylinders
Analytical
D/R Code
5E6
20E6
15E6
10E6
5E6
0.2
0.4
0.6
0.8
1.0
1.2
1.4
ω (rad/s)

Figure 3.5

First Order Surge Force on the Complete TLP.

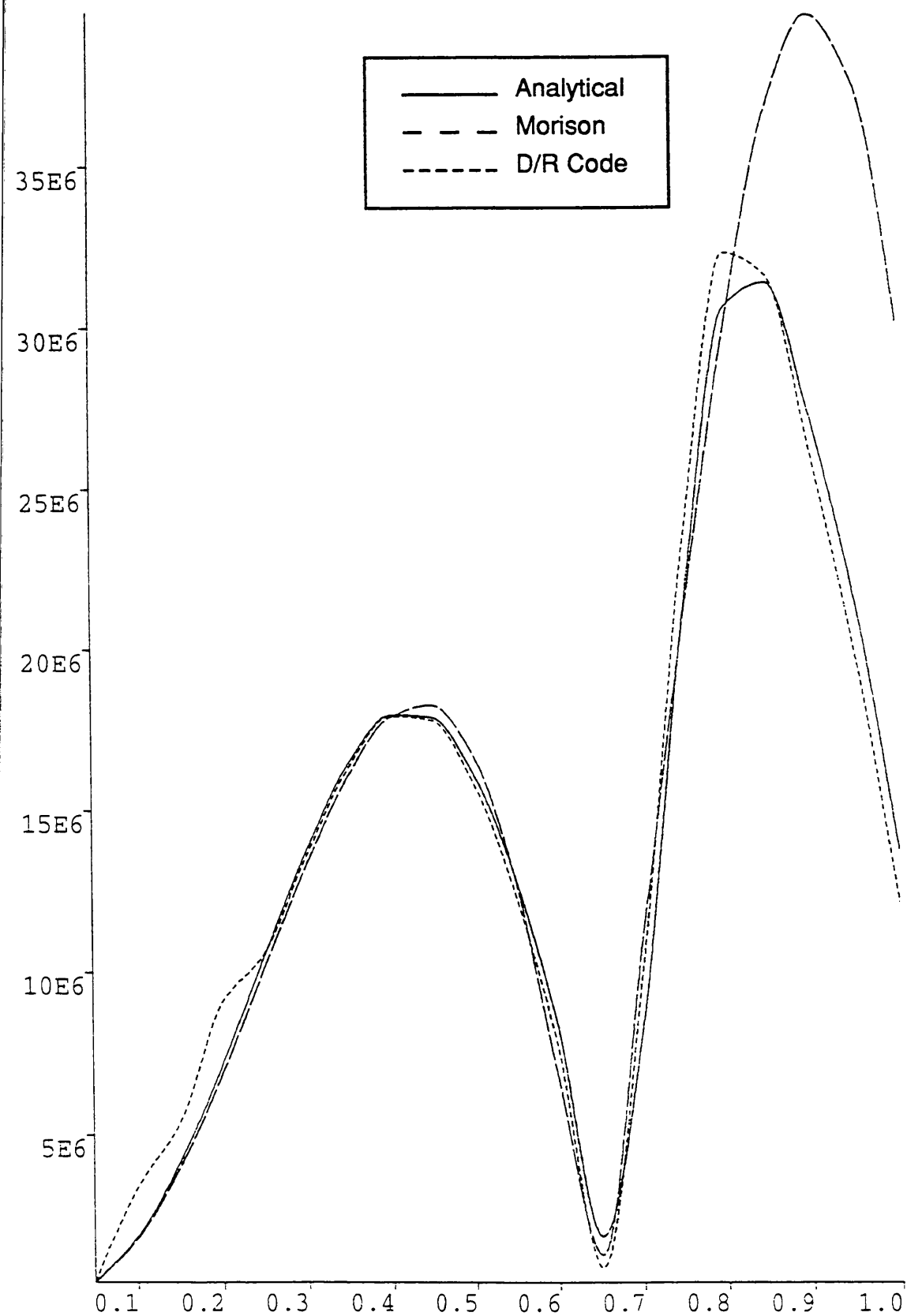

Figure 3.6

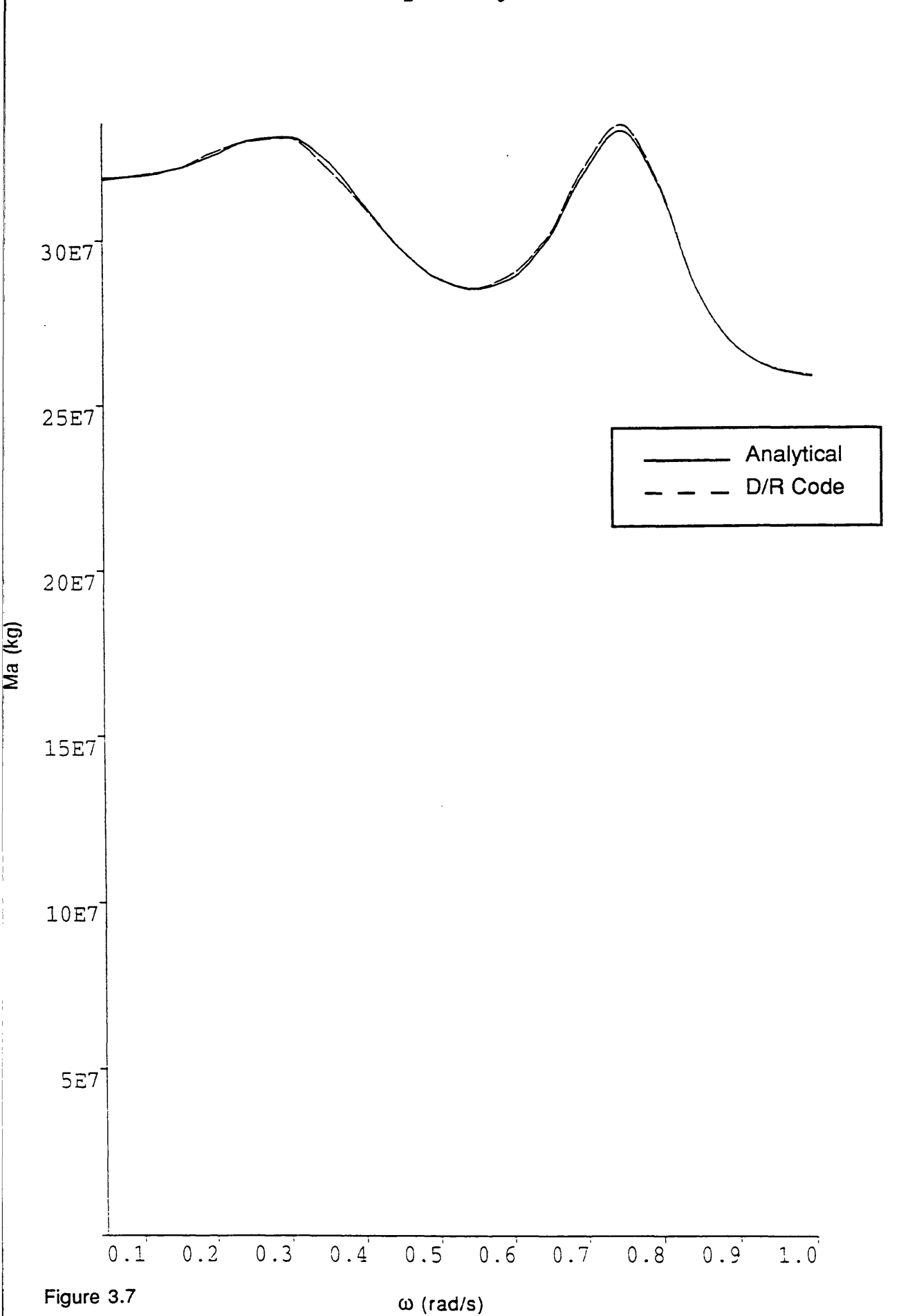
Surge Added Mass on an Array
of 4 Complete Cylinders
30E7
25E7
20E7
15E7
10E7
5E7
Ma (kg)
Analytical
D/R Code
0.1
0.2
0.3
0.4
0.5
0.6
0.7
0.8
0.9
1.0
ω (rad/s)

Figure 3.7

Surge Potential Damping on an Array of 4 Complete Cylinders

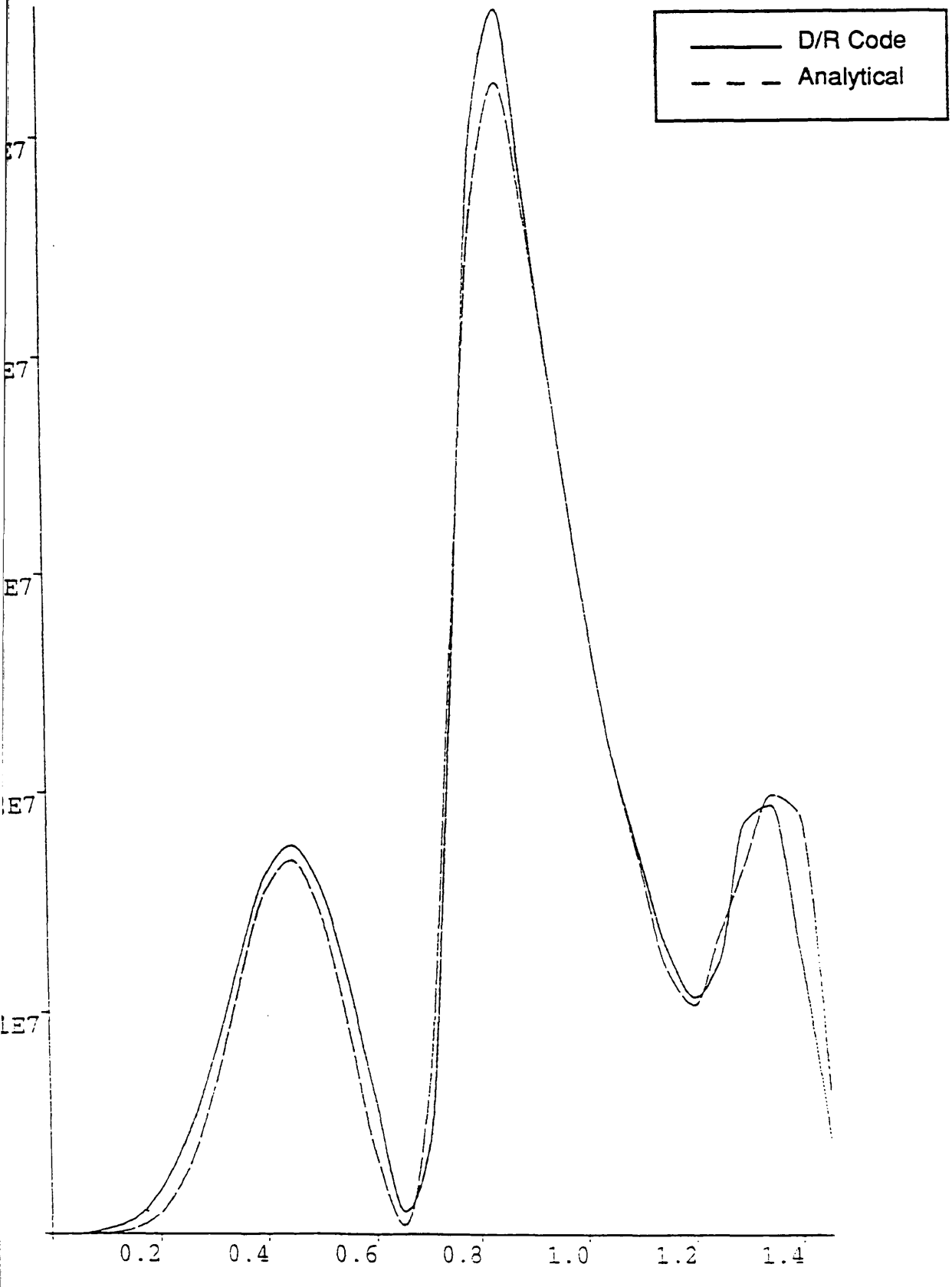

Figure 3.8

Surge Added Mass on an Array of 4 Truncated Cylinders

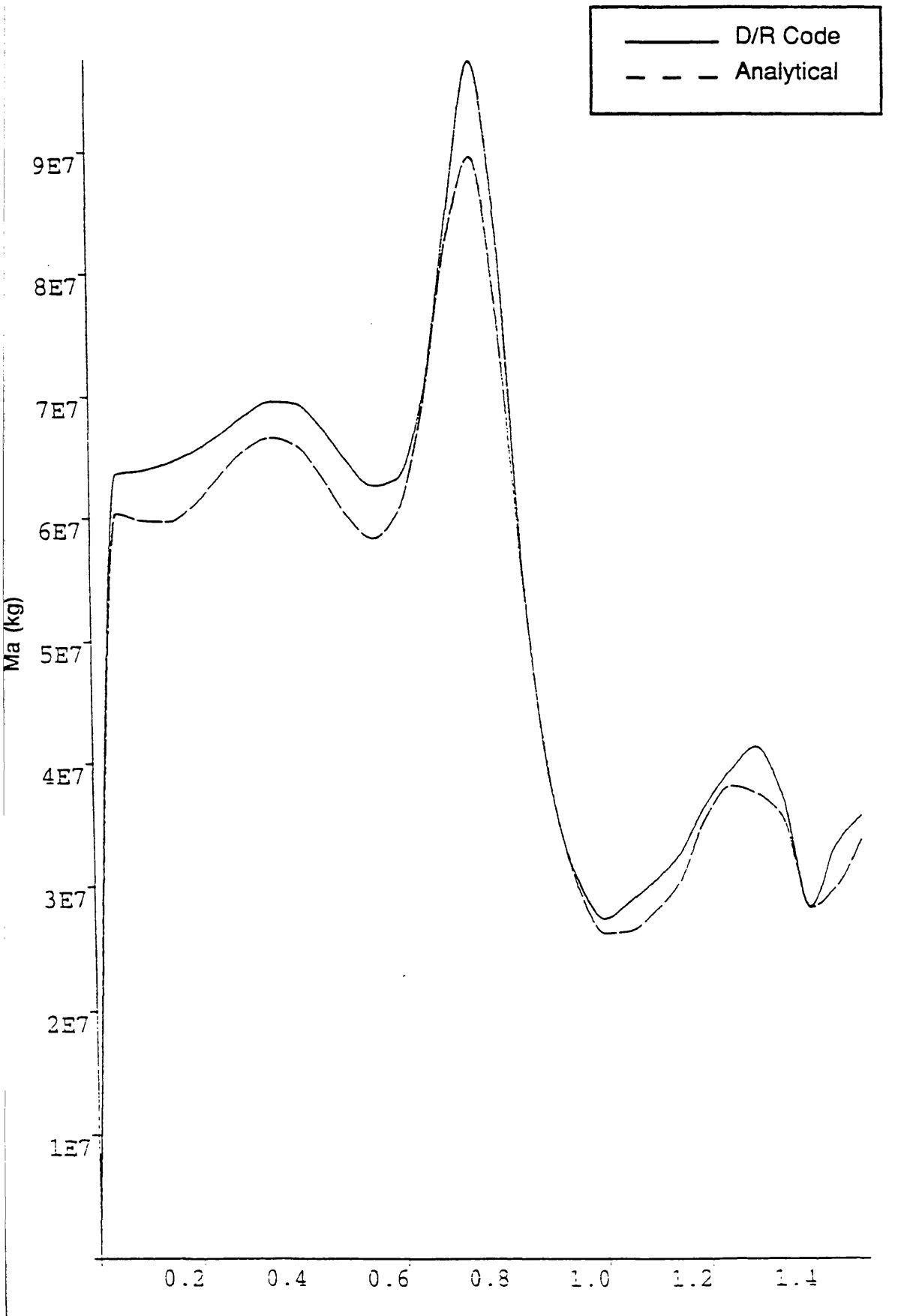

Figure 3.9

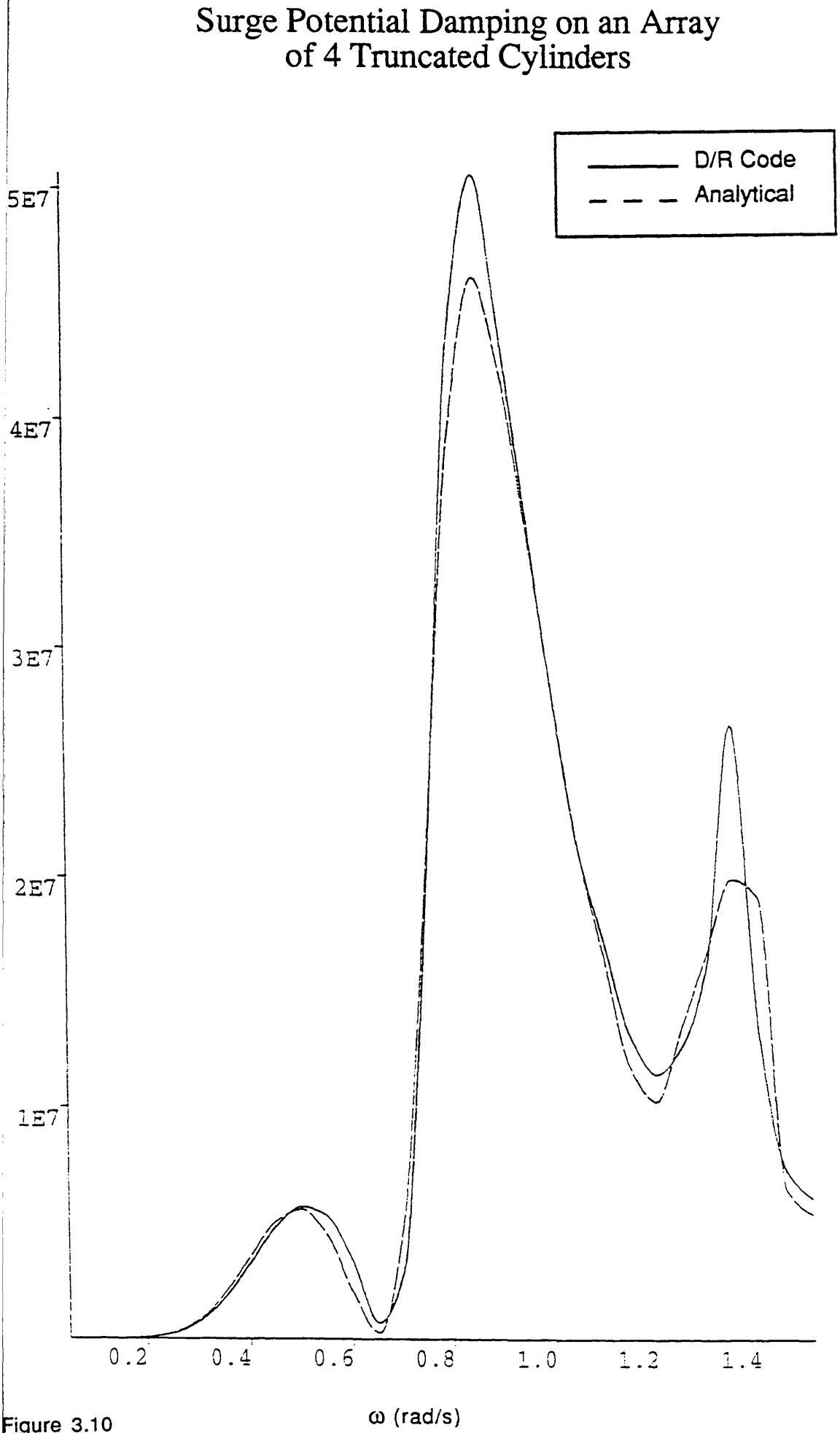
Surge Potential Damping on an Array
of 4 Truncated Cylinders
D/R Code
Analytical
5E7
4E7
3E7
2E7
1E7
0.2
0.4
0.6
0.8
1.0
1.2
1.4
ω (rad/s)

Figure 3.10

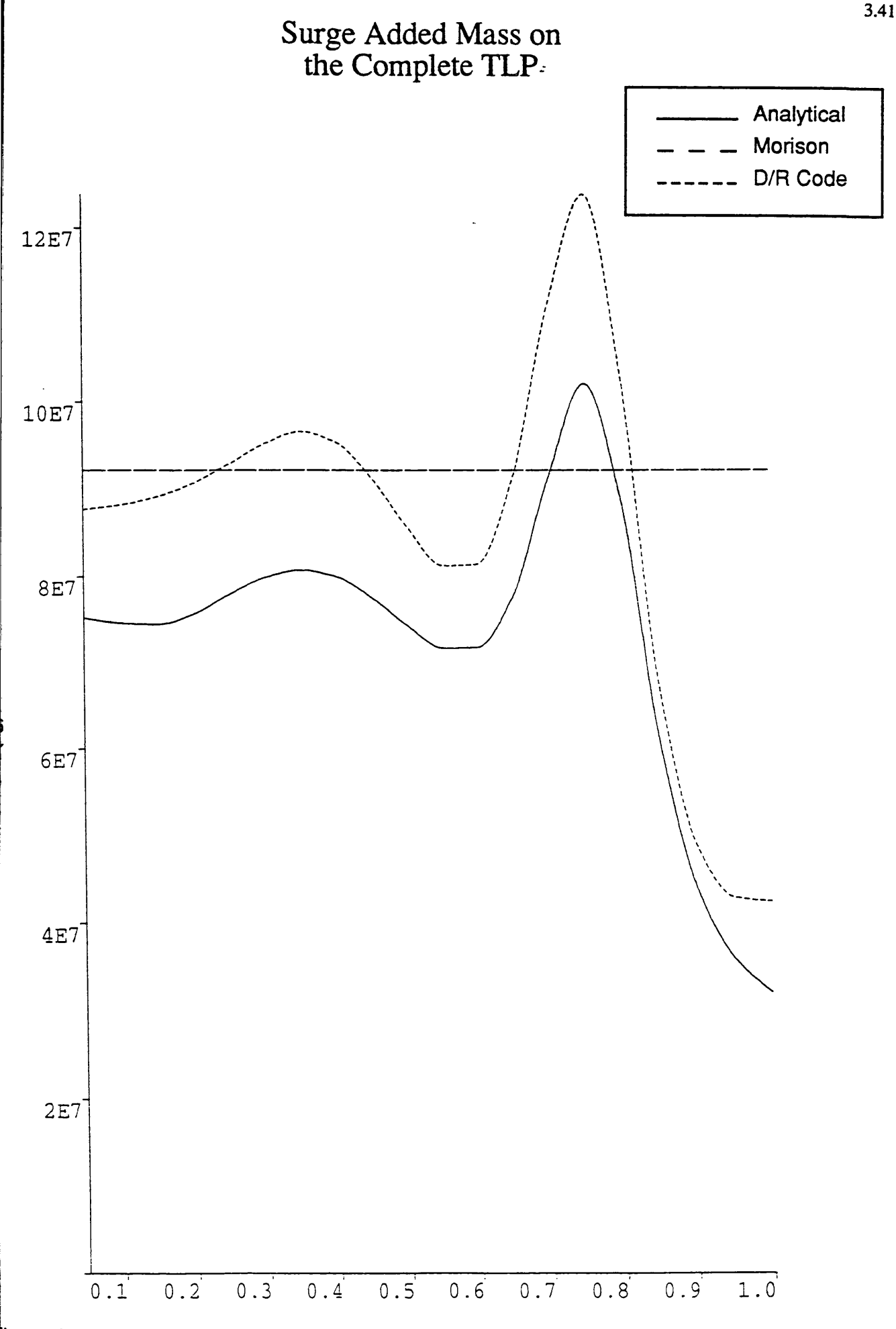
Surge Added Mass on
the Complete TLP
Analytical
Morison
D/R Code
12E7
10E7
8E7
6E7
4E7
2E7
0.1
0.2
0.3
0.4
0.5
0.6
0.7
0.8
0.9
1.0
ω (rad/s)

Figure 3.11

Surge Potential Damping on the Complete TLP

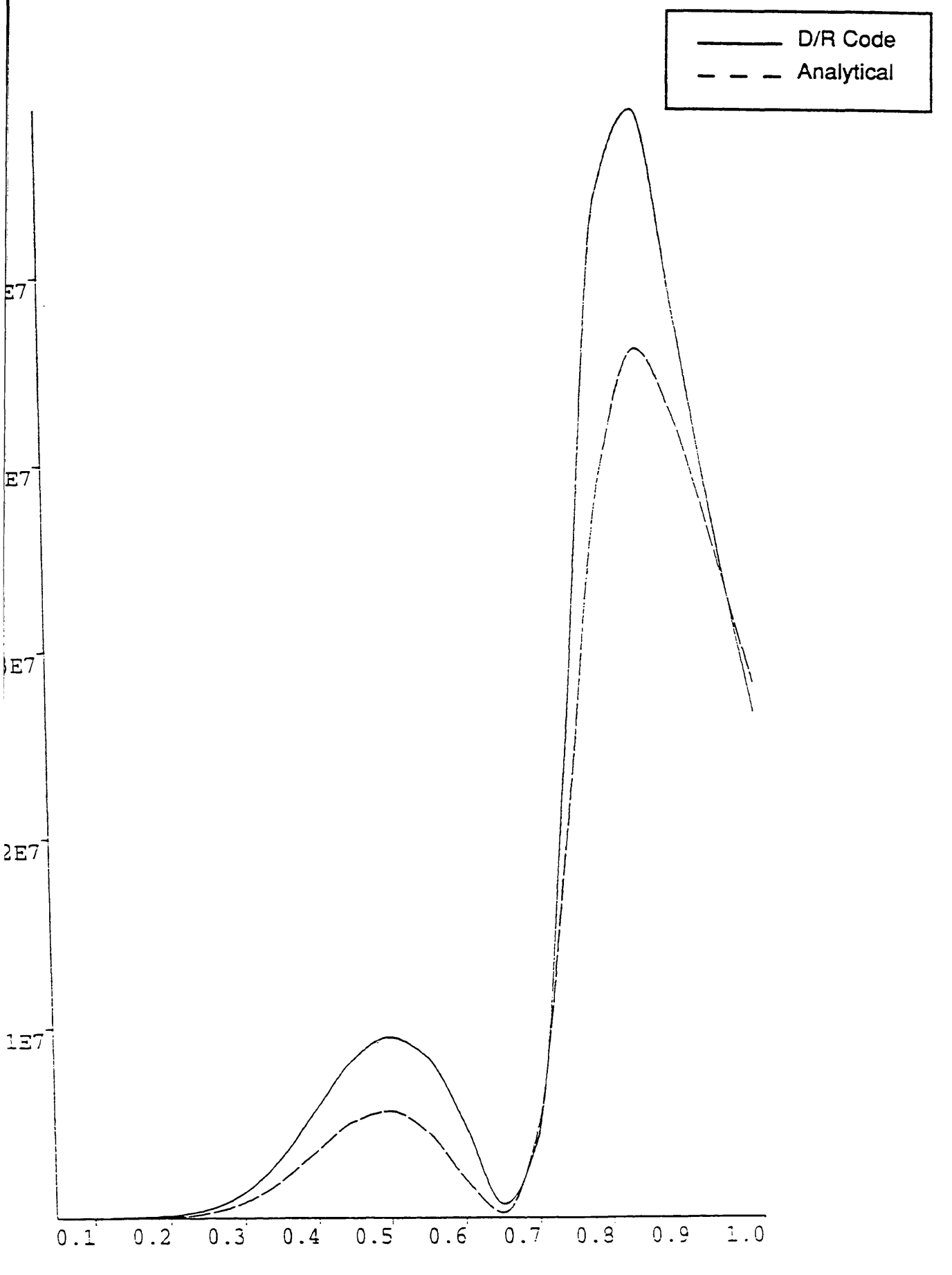

gure 3.12

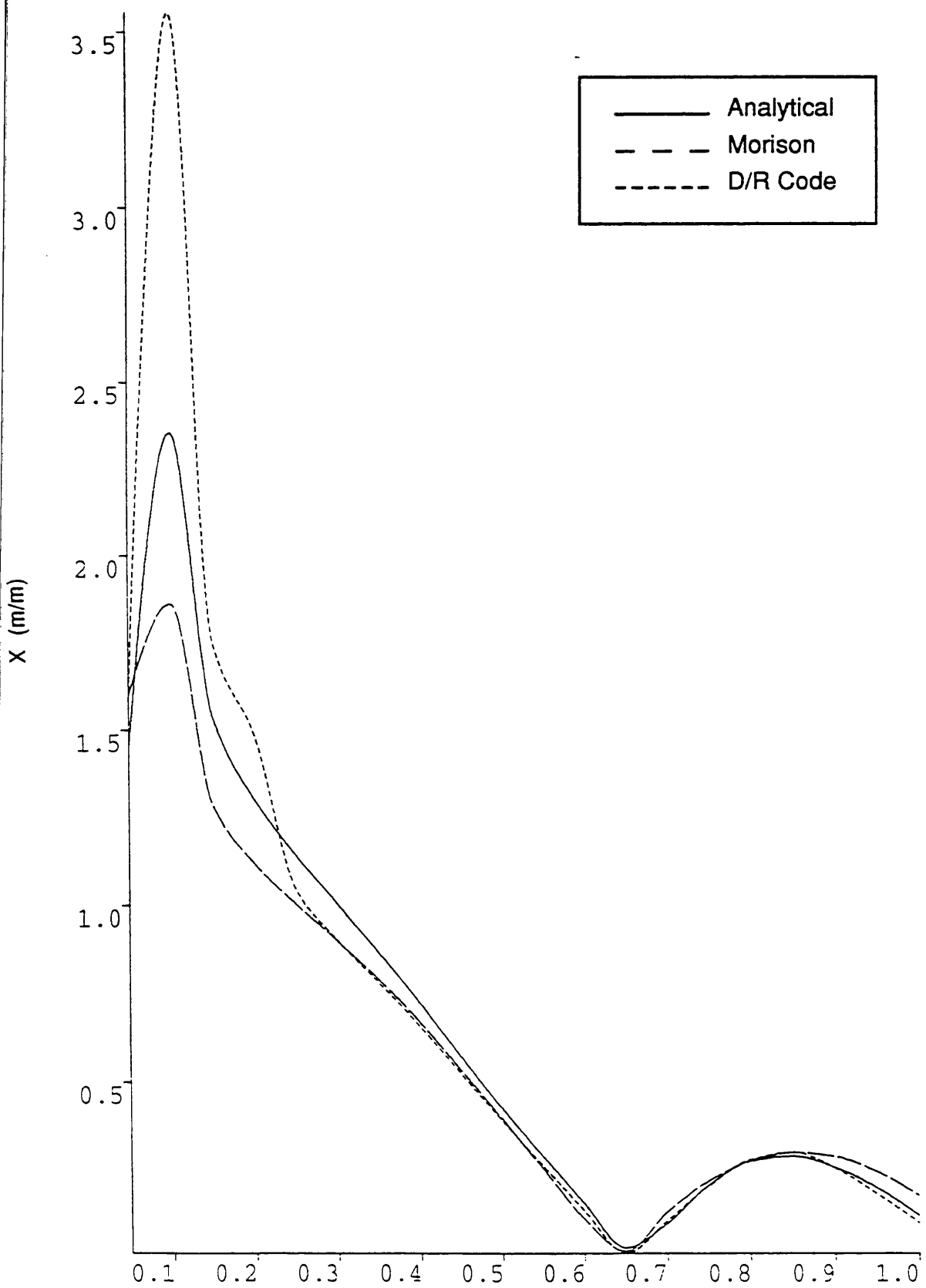
Displacement in Surge
Analytical
Morison
D/R Code
X (m/m)
3.5
3.0
2.5
2.0
1.5
1.0
0.5
0.1
0.2
0.3
0.4
0.5
0.6
0.7
0.8
0.9
1.0
ω (rad/s)

Figure 3.13

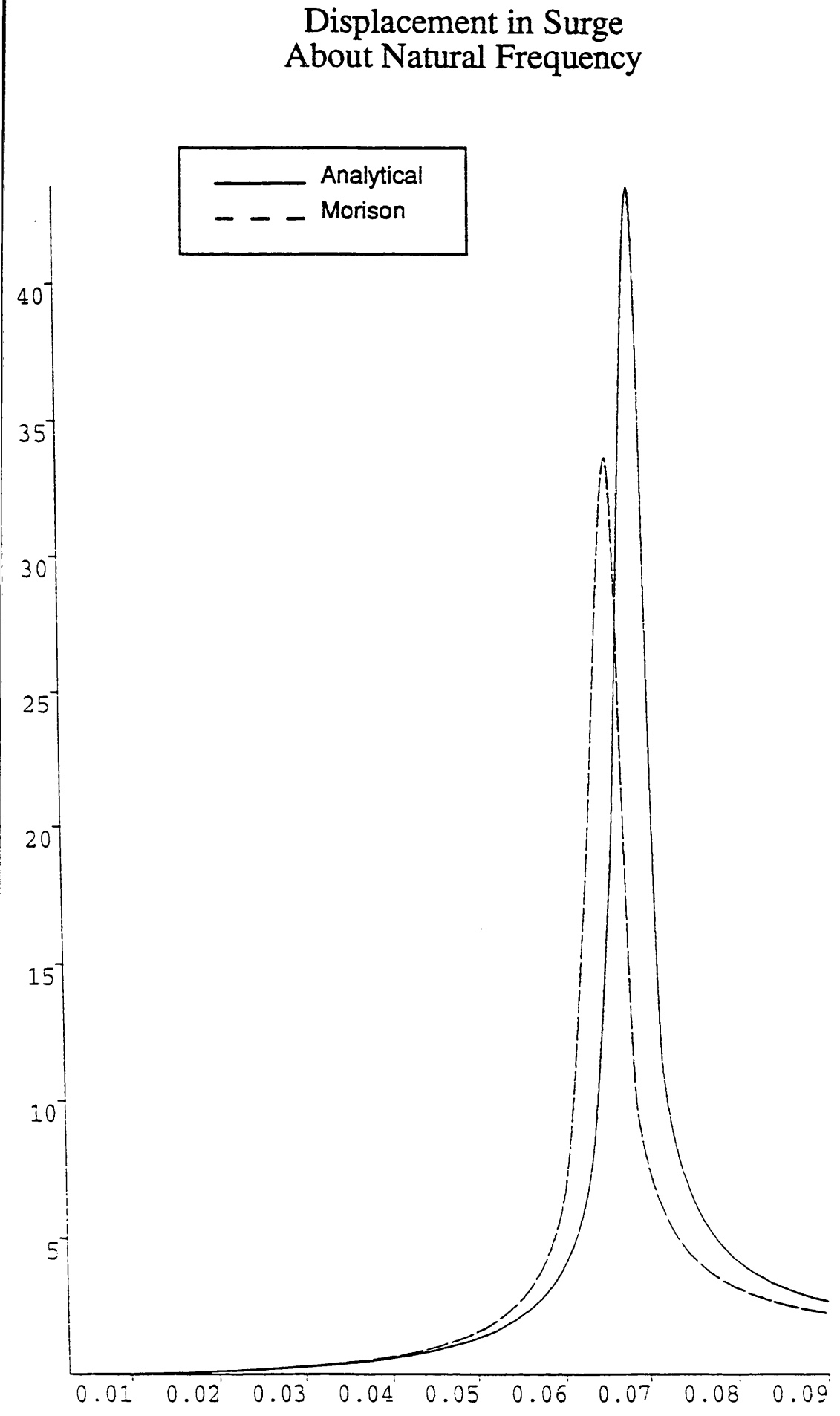
Displacement in Surge
About Natural Frequency
Analytical
Morison
40
35
30
25
20
15
10
5
0.01
0.02
0.03
0.04
0.05
0.06
0.07
0.08
0.09
ω (rad/s)

Figure 3.14

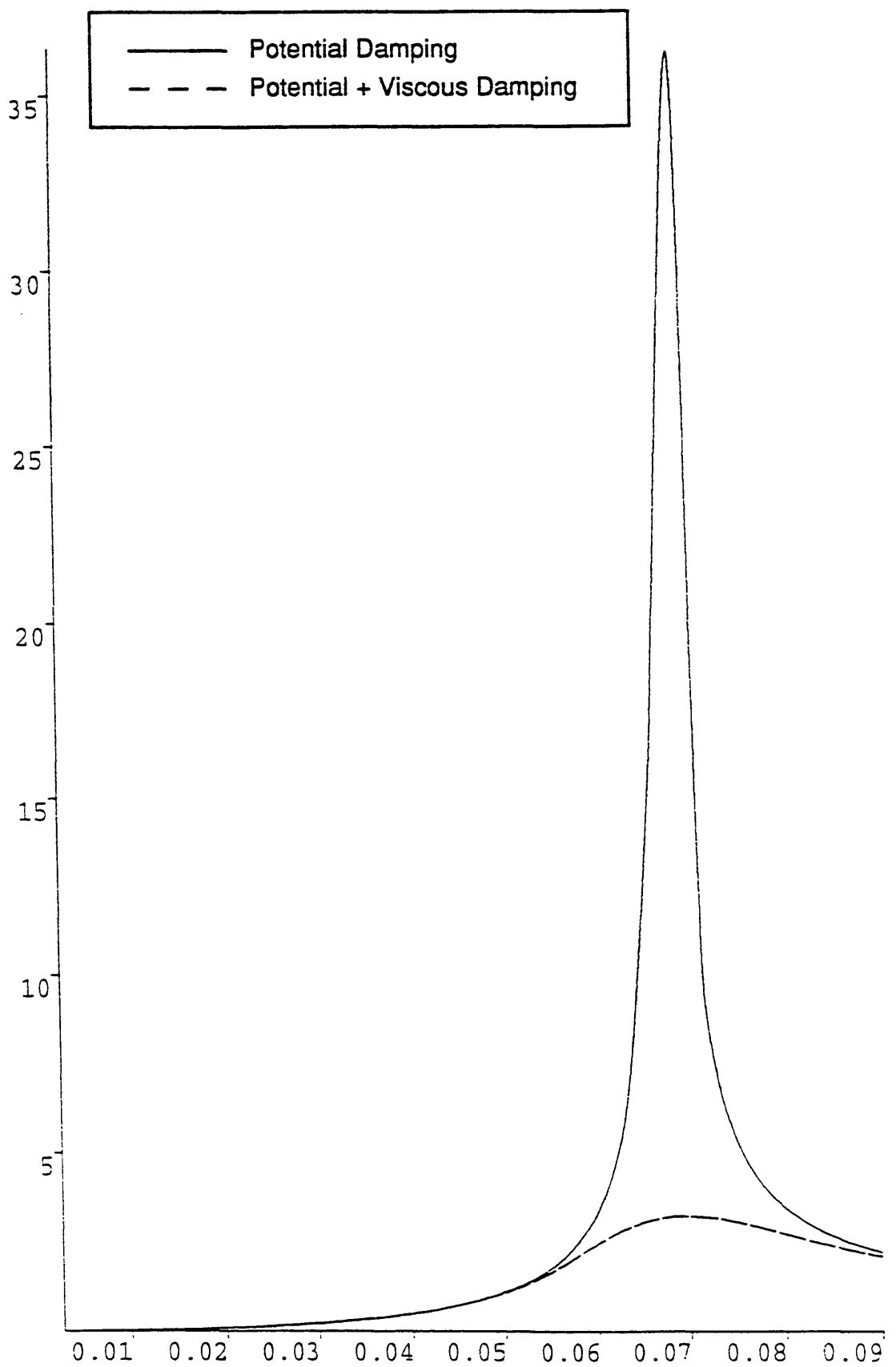
Displacement in Surge
About Natural Frequency
Potential Damping
Potential + Viscous Damping
35
30
25
20
15
10
5
0.01
0.02
0.03
0.04
0.05
0.06
0.07
0.08
0.09
ω (rad/s)

Figure 3.15

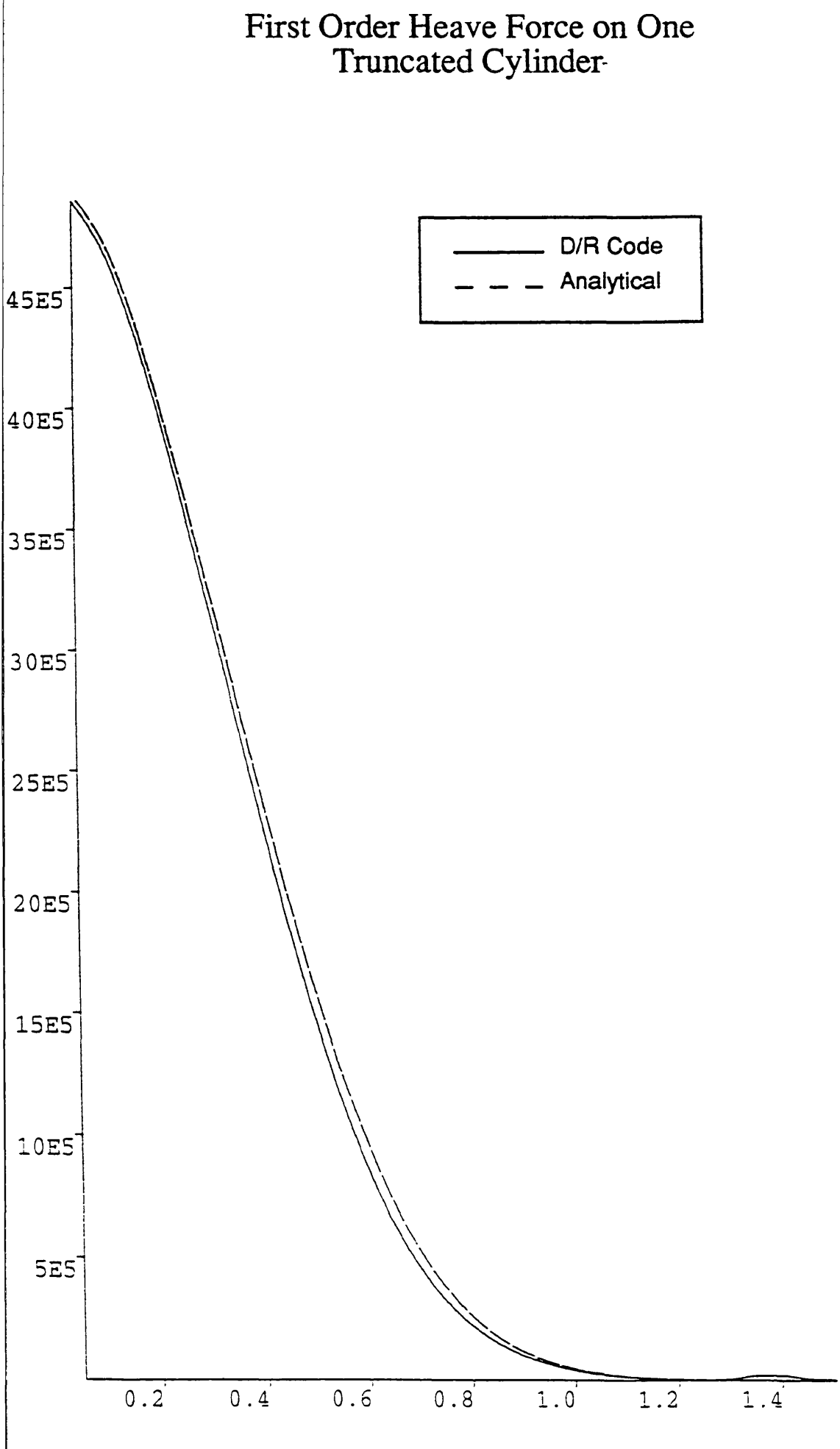
First Order Heave Force on One Truncated Cylinder
D/R Code
Analytical
45E5
40E5
35E5
30E5
25E5
20E5
15E5
10E5
5E5
0.2
0.4
0.6
0.8
1.0
1.2
1.4
ω (rad/s)

Figure 3.16

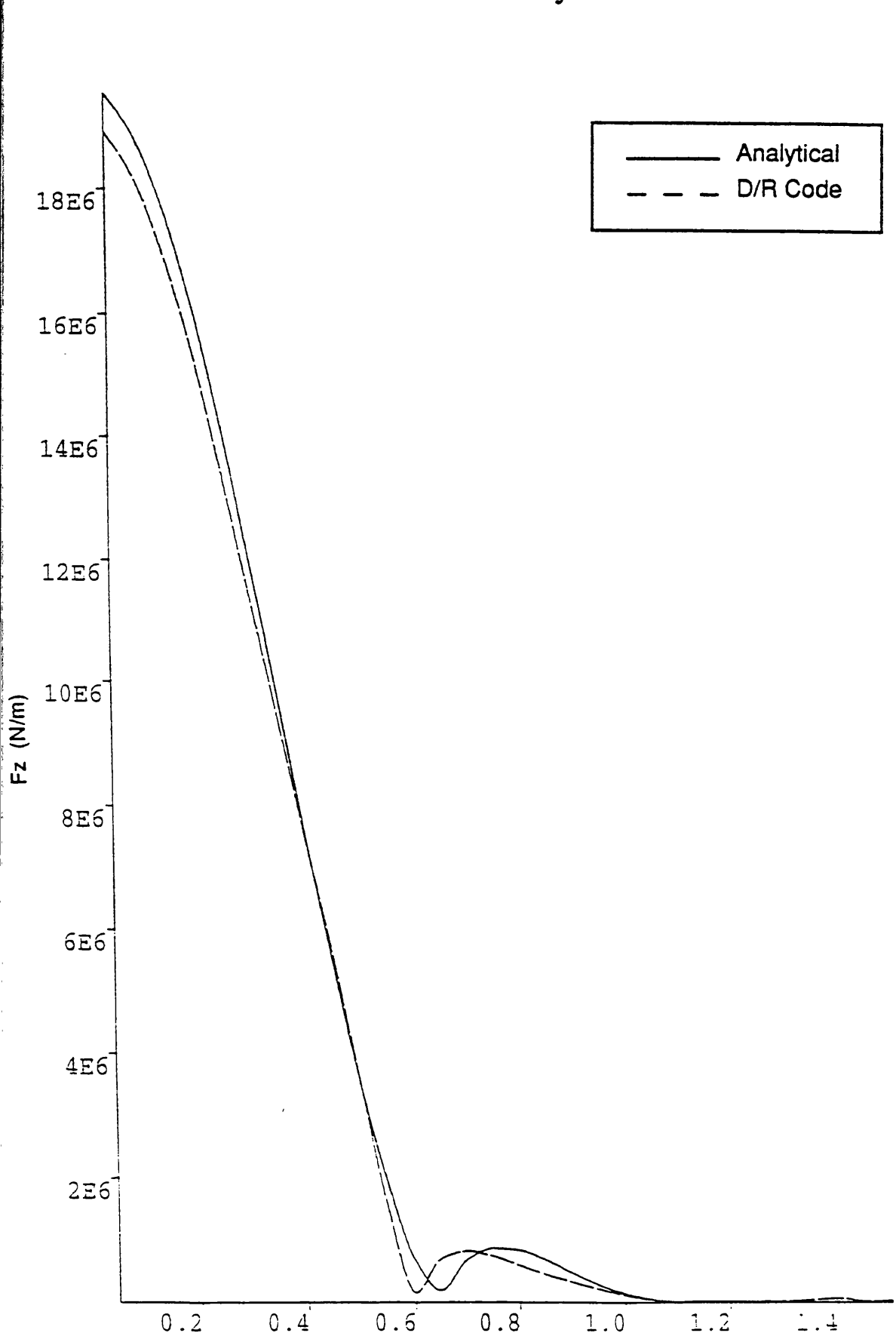
First Order Heave Force on an Array
of 4 Truncated Cylinders
Analytical
D/R Code
18E6
16E6
14E6
12E6
10E6
8E6
6E6
4E6
2E6
Fz (N/m)
0.2
0.4
0.6
0.8
1.0
1.2
1.4
ω (rad/s)

Figure 3.17

First Order Heave Force on the Complete TLP-

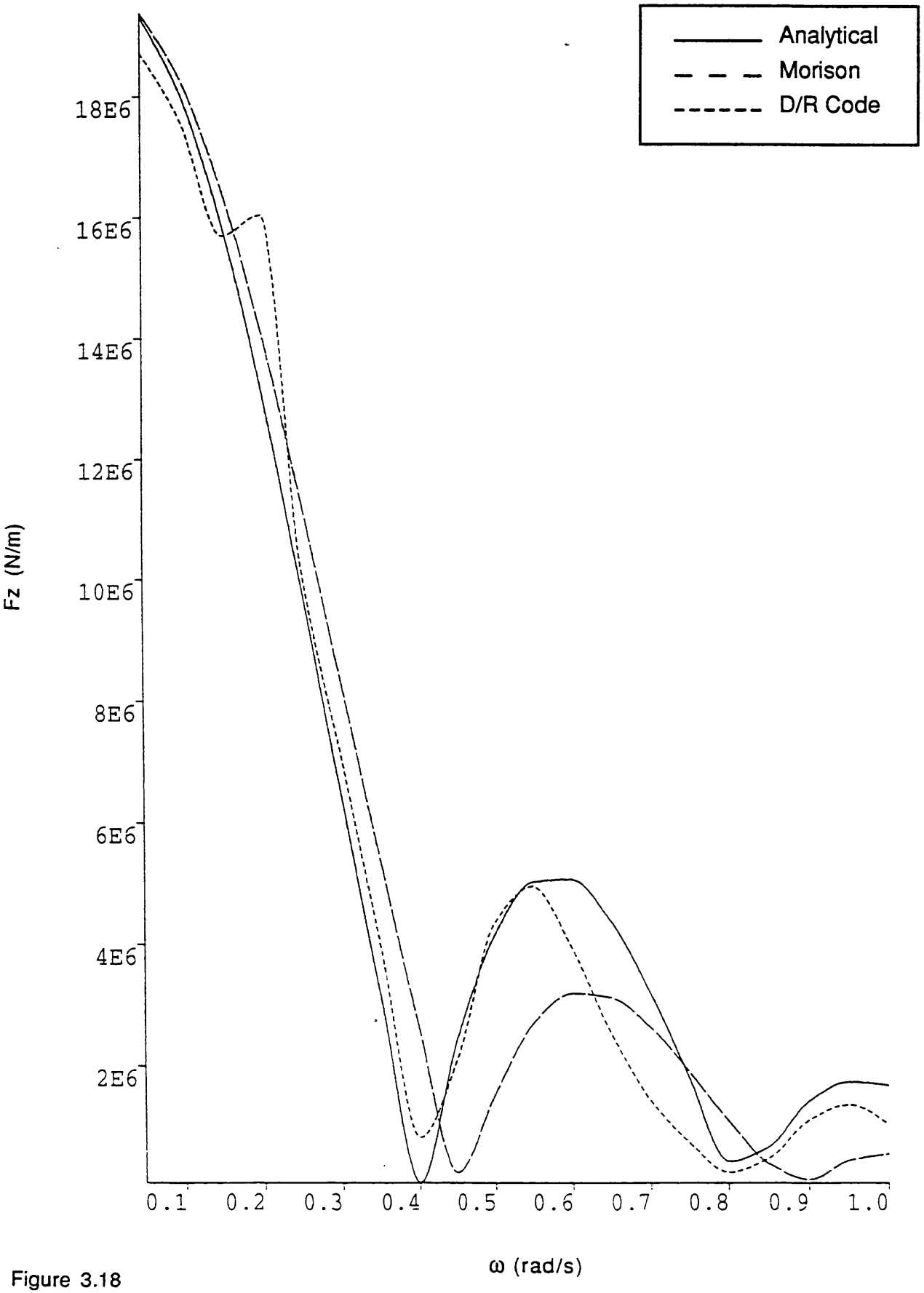

Figure 3.18

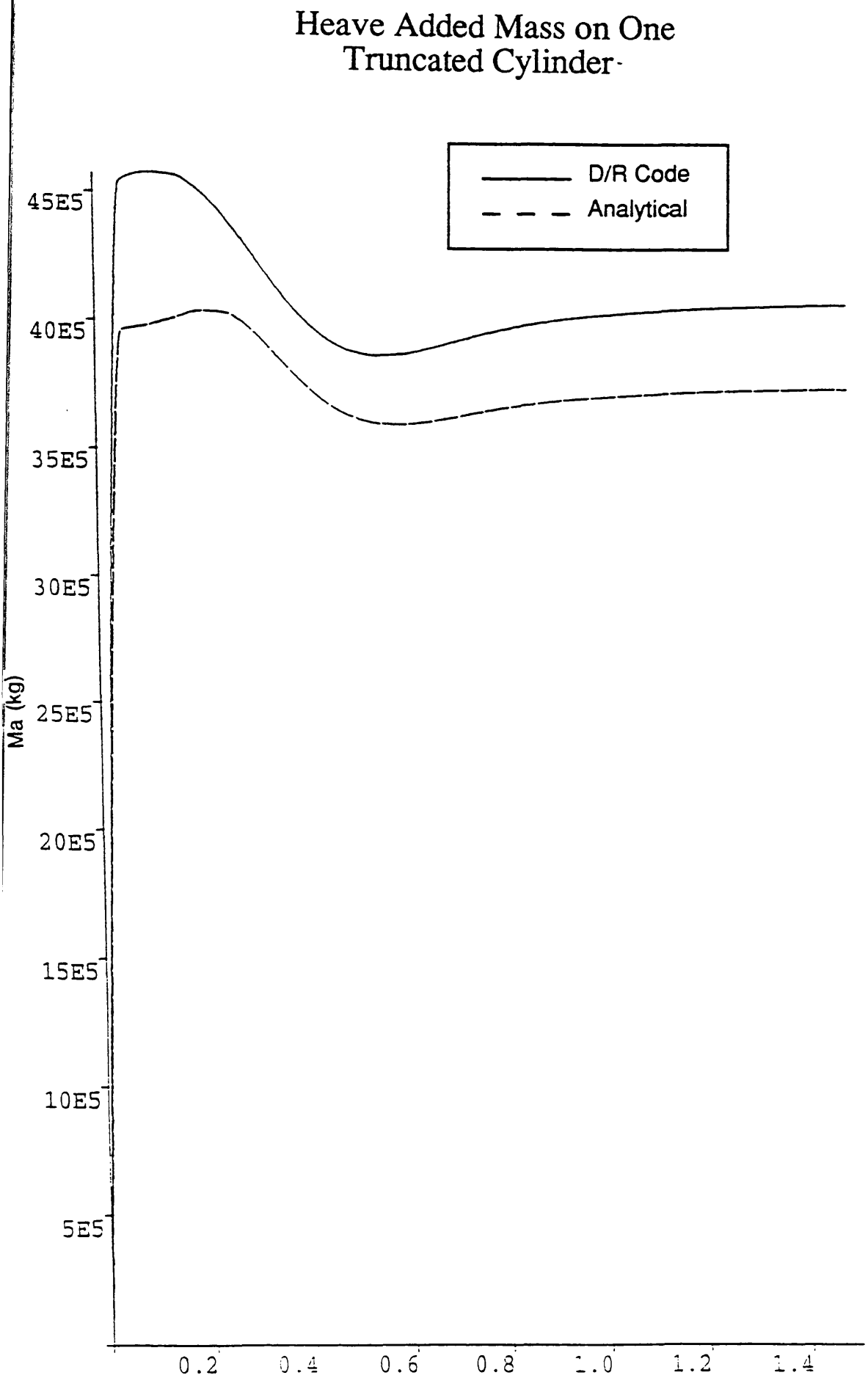
Heave Added Mass on One Truncated Cylinder
D/R Code
Analytical
45E5
40E5
35E5
30E5
25E5
20E5
15E5
10E5
5E5
Ma (kg)
0.2
0.4
0.6
0.8
1.0
1.2
1.4
ω (rad/s)

Figure 3.19

Heave Added Mass on an Array of 4 Truncated Cylinders

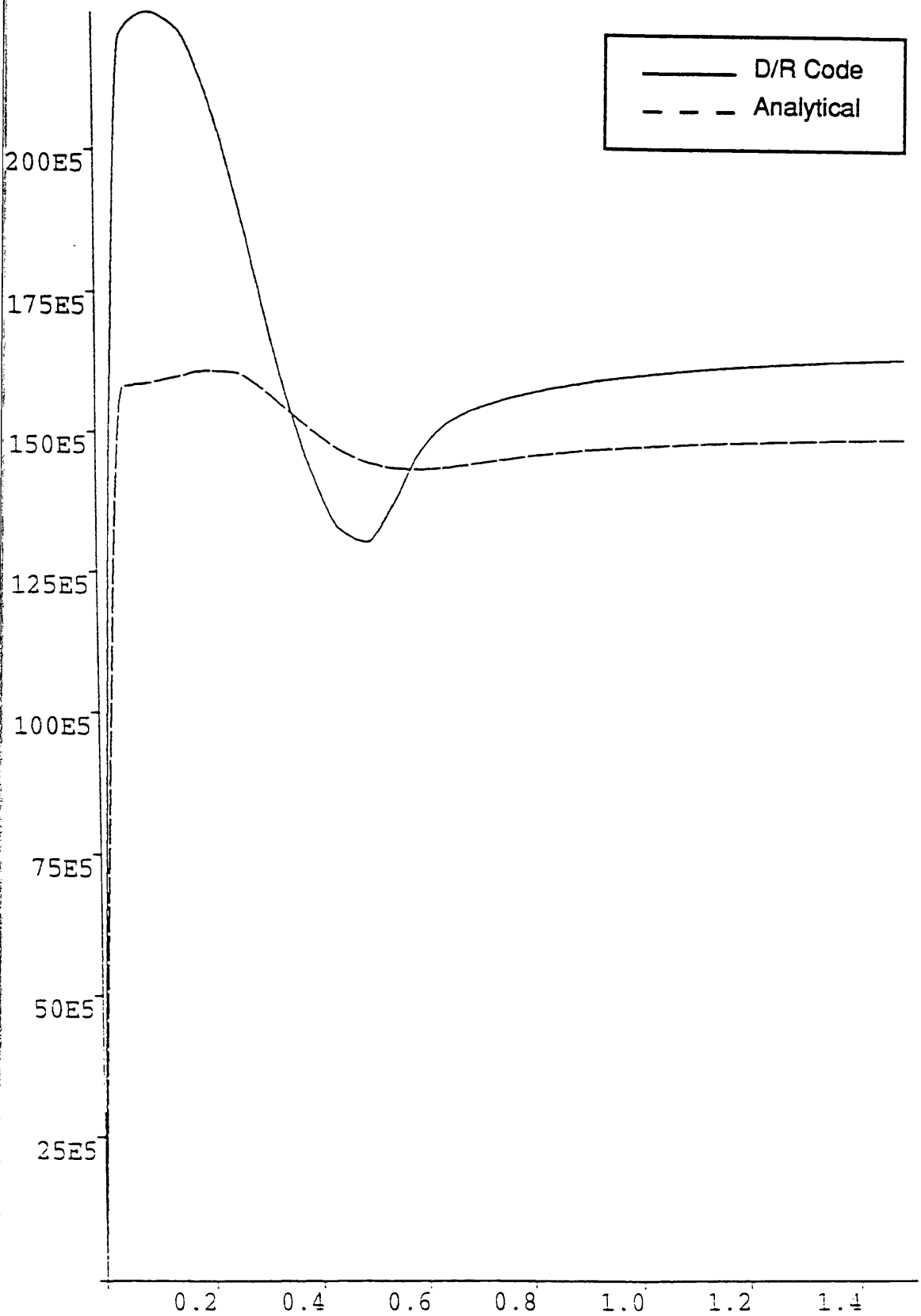

Figure 3.20

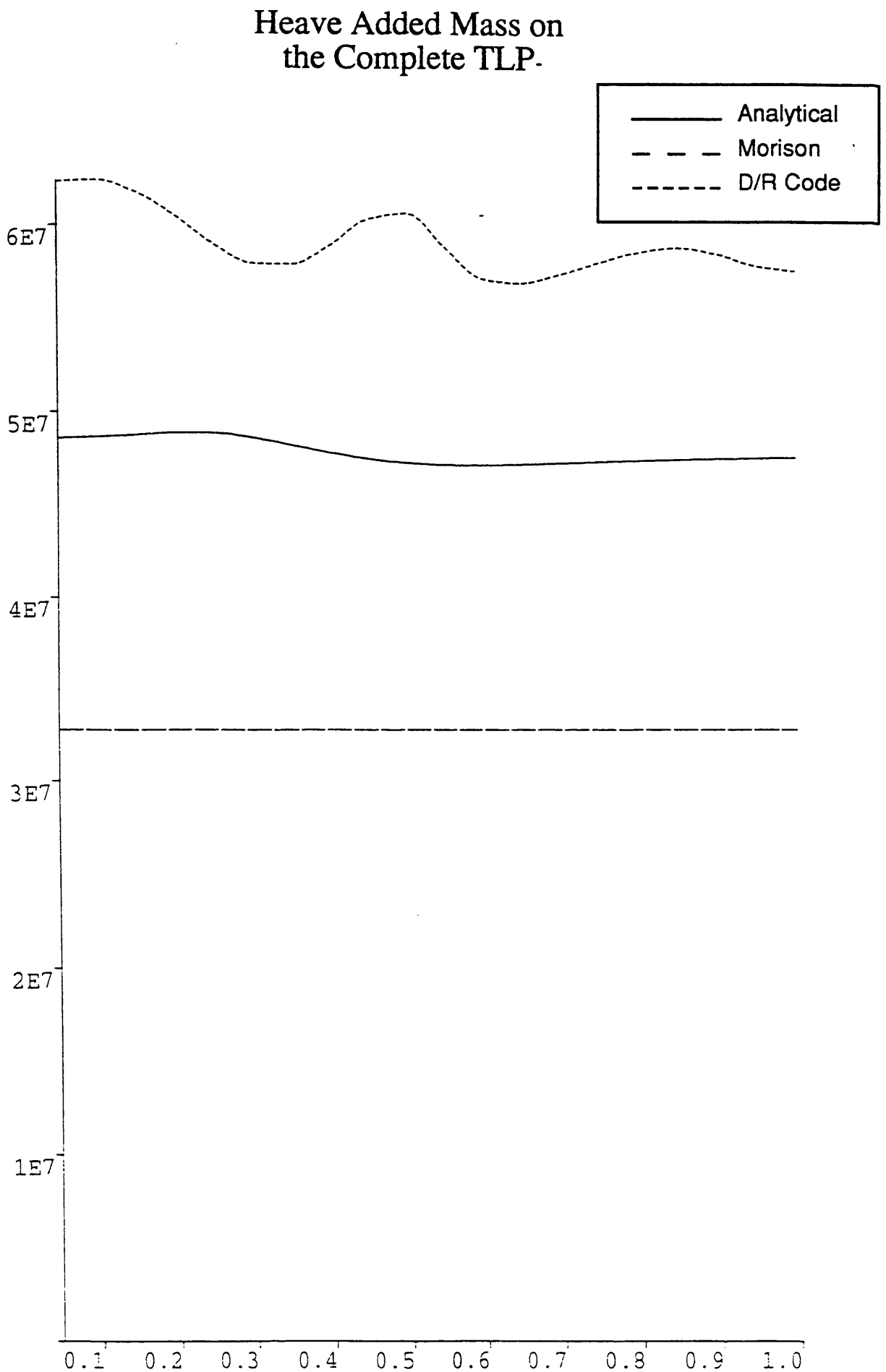
Heave Added Mass on
the Complete TLP.
Analytical
Morison
D/R Code
6E7
5E7
4E7
3E7
2E7
1E7
0.1
0.2
0.3
0.4
0.5
0.6
0.7
0.8
0.9
1.0
ω (rad/s)

Figure 3.21

Heave Potential Damping on One Truncated Cylinder

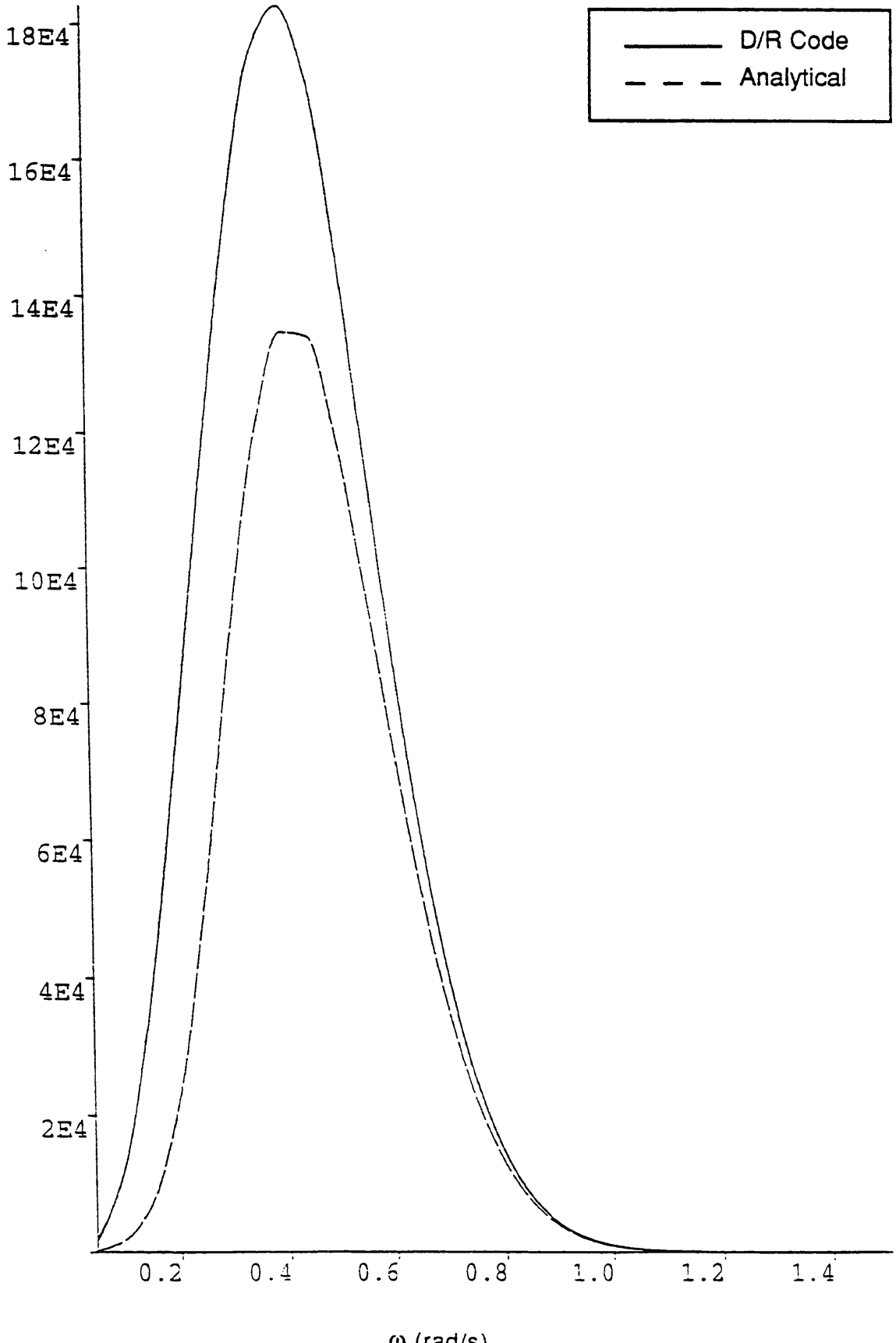

Figure 3.22

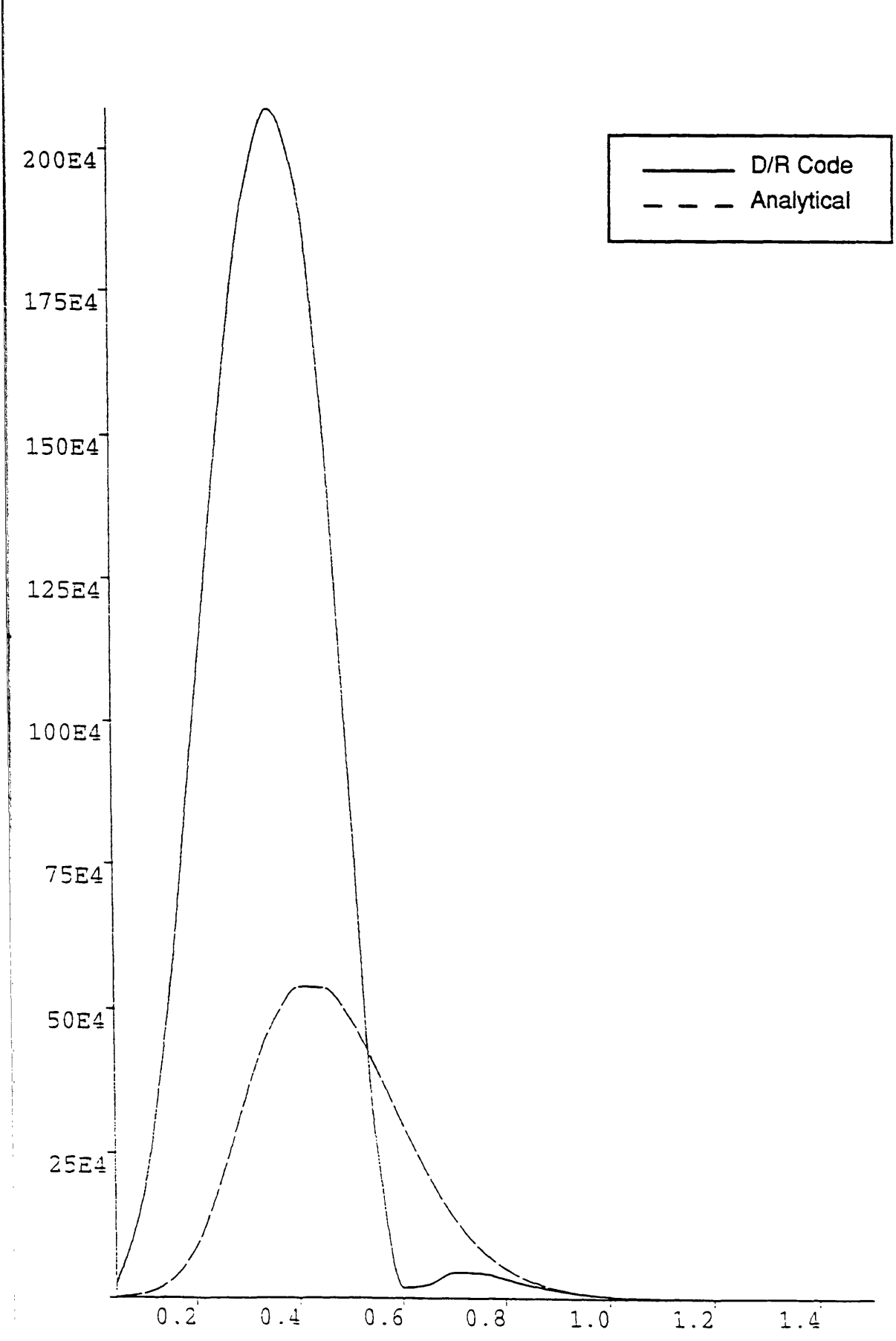
Heave Potential Damping on an Array
of 4 Truncated Cylinders
D/R Code
Analytical
200E4
175E4
150E4
125E4
100E4
75E4
50E4
25E4
0.2
0.4
0.6
0.8
1.0
1.2
1.4
ω (rad/s)

Figure 3.23

Heave Potential Damping on the Complete TLP-

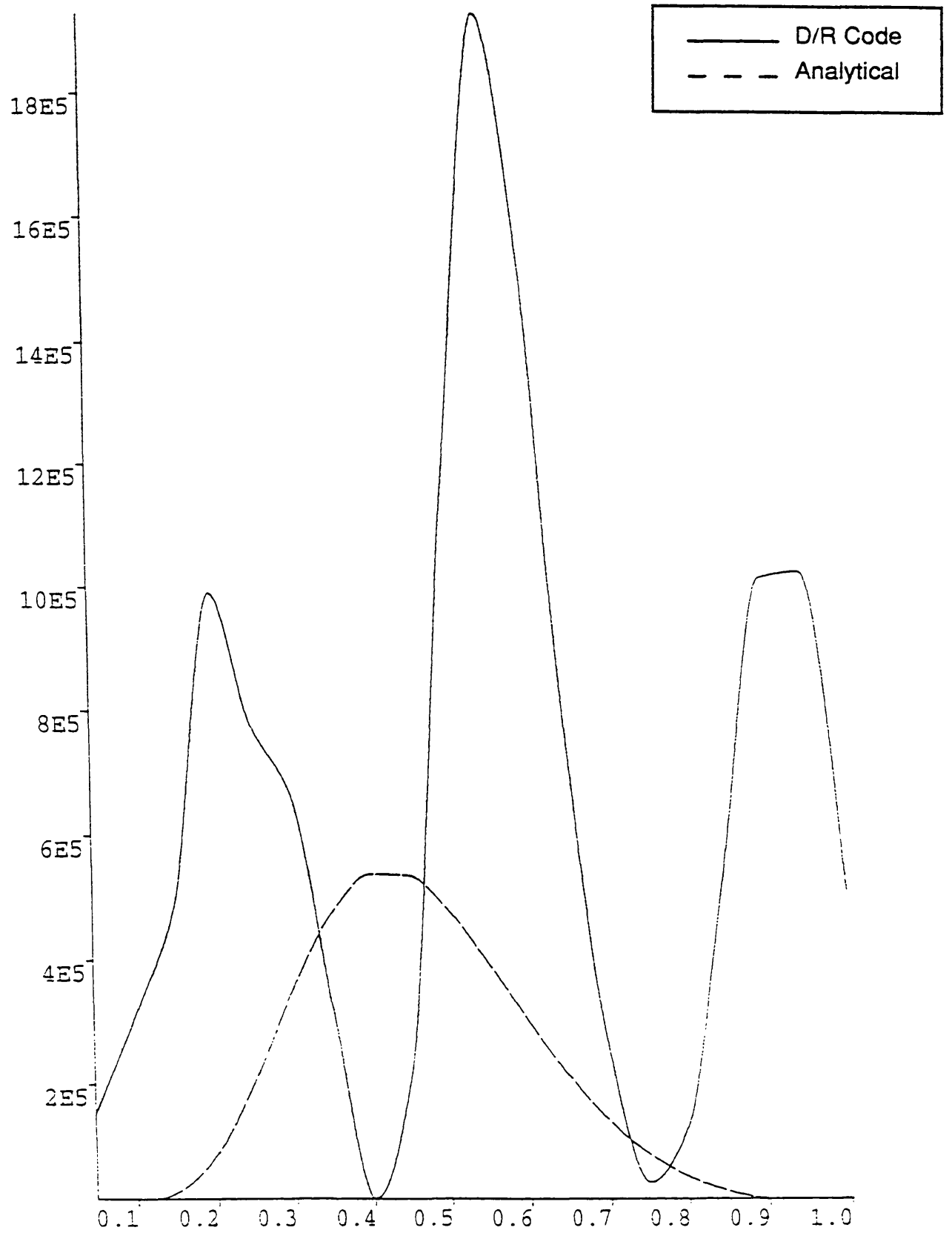

Figure 3.24

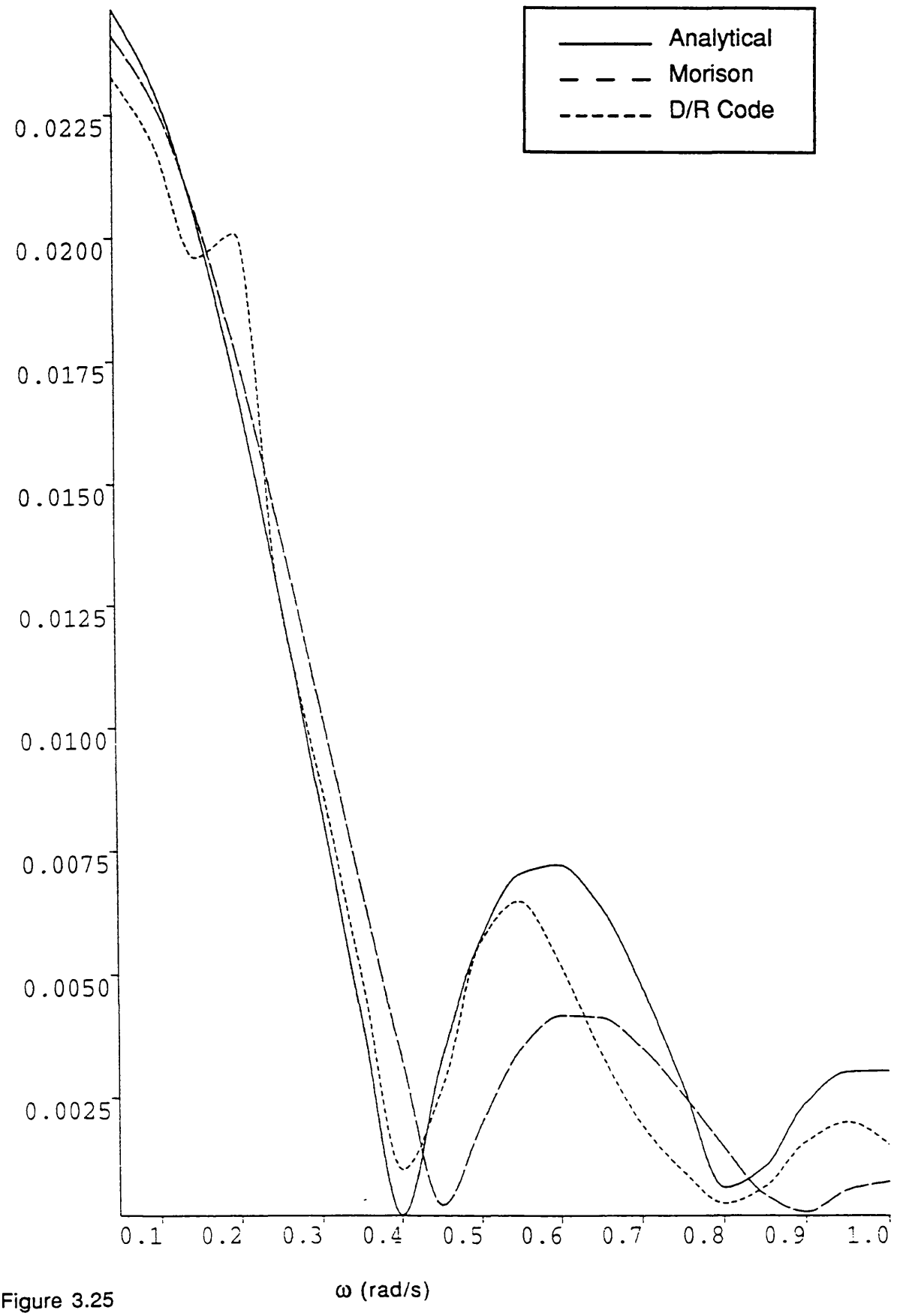
Displacement in Heave
Analytical
Morison
D/R Code
0.0225
0.0200
0.0175
0.0150
0.0125
0.0100
0.0075
0.0050
0.0025
0.1
0.2
0.3
0.4
0.5
0.6
0.7
0.8
0.9
1.0
ω (rad/s)

Figure 3.25

First Order Pitch Moment on an Array of 4 Complete Cylinders

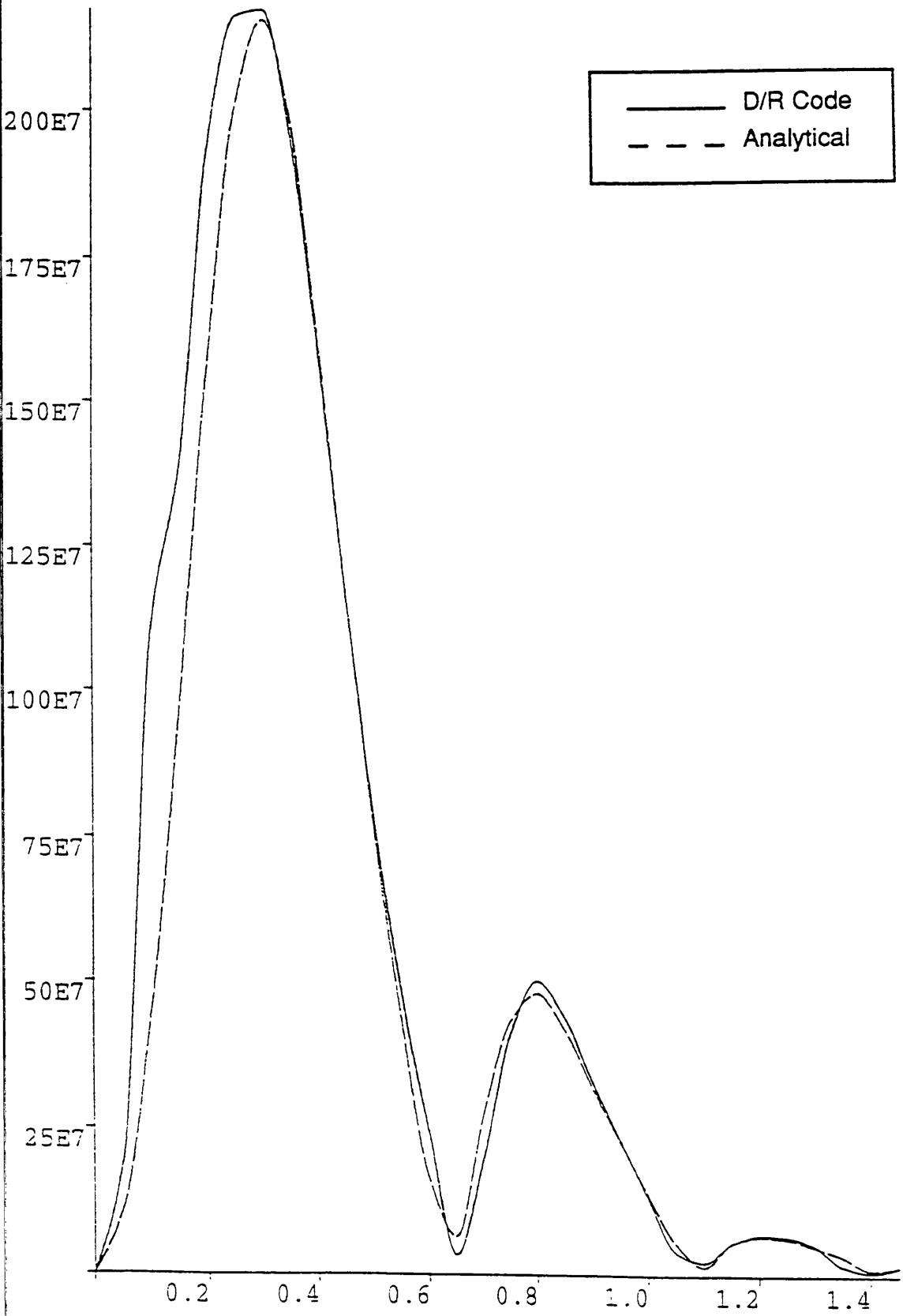

Figure 3.26

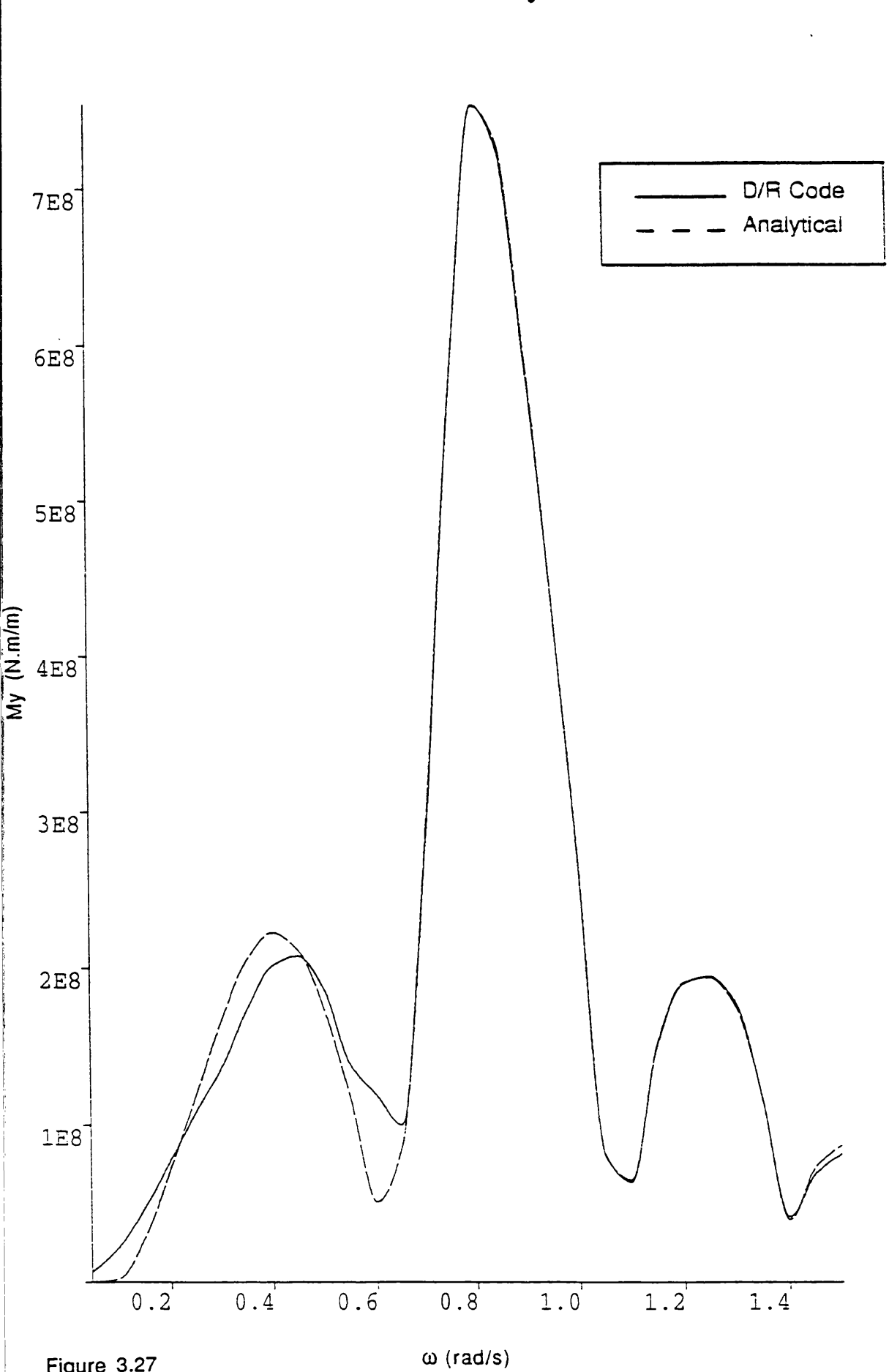
First Order Pitch Moment on an Array
of 4 Truncated Cylinders
D/R Code
Analytical
7E8
6E8
5E8
4E8
3E8
2E8
1E8
My (N.m/m)
0.2
0.4
0.6
0.8
1.0
1.2
1.4
ω (rad/s)

Figure 3.27

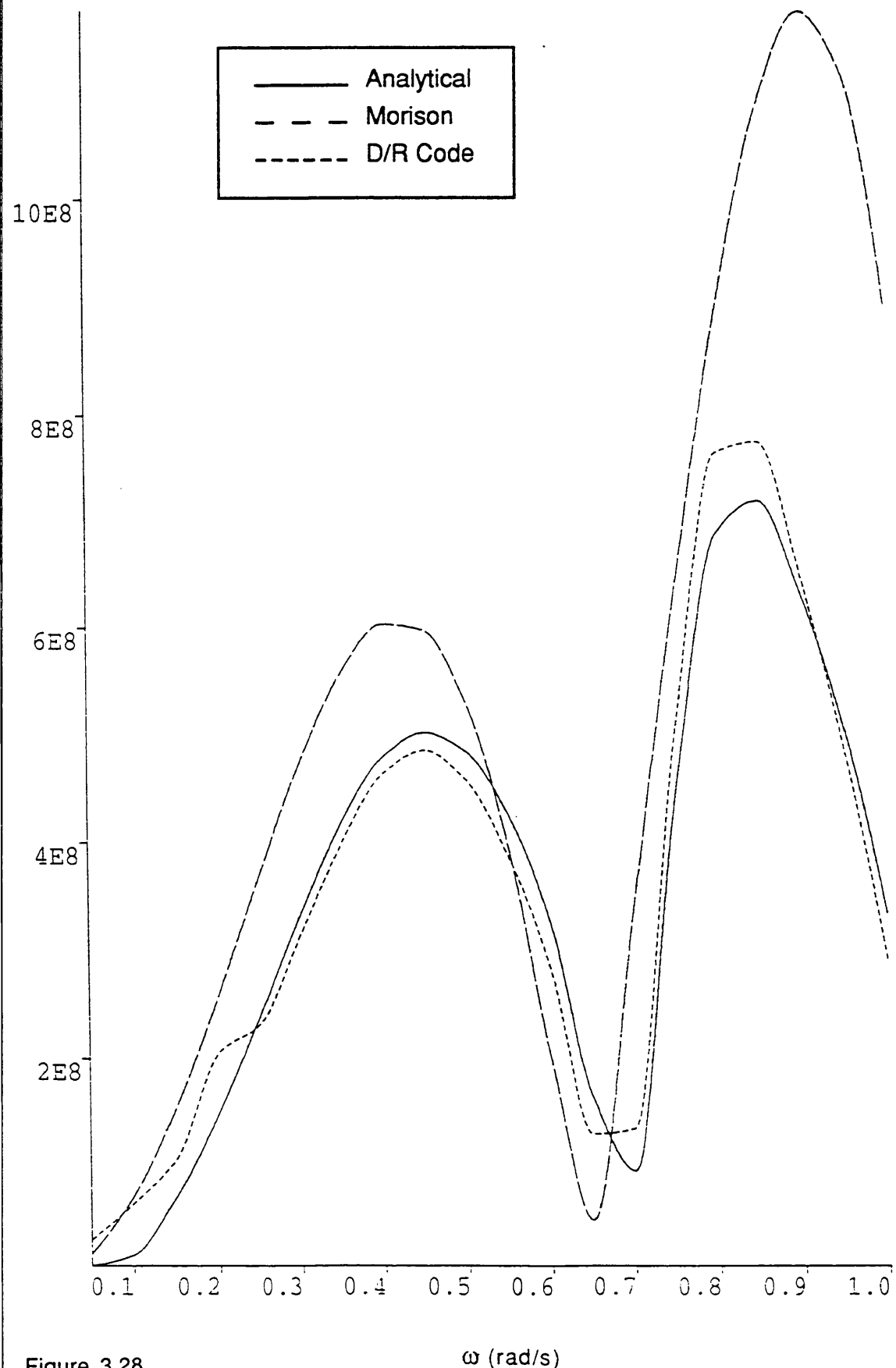
First Order Pitch Moment on
the Complete TLP
Analytical
Morison
D/R Code
10E8
8E8
6E8
4E8
2E8
0.1
0.2
0.3
0.4
0.5
0.6
0.7
0.8
0.9
1.0
ω (rad/s)

Figure 3.28

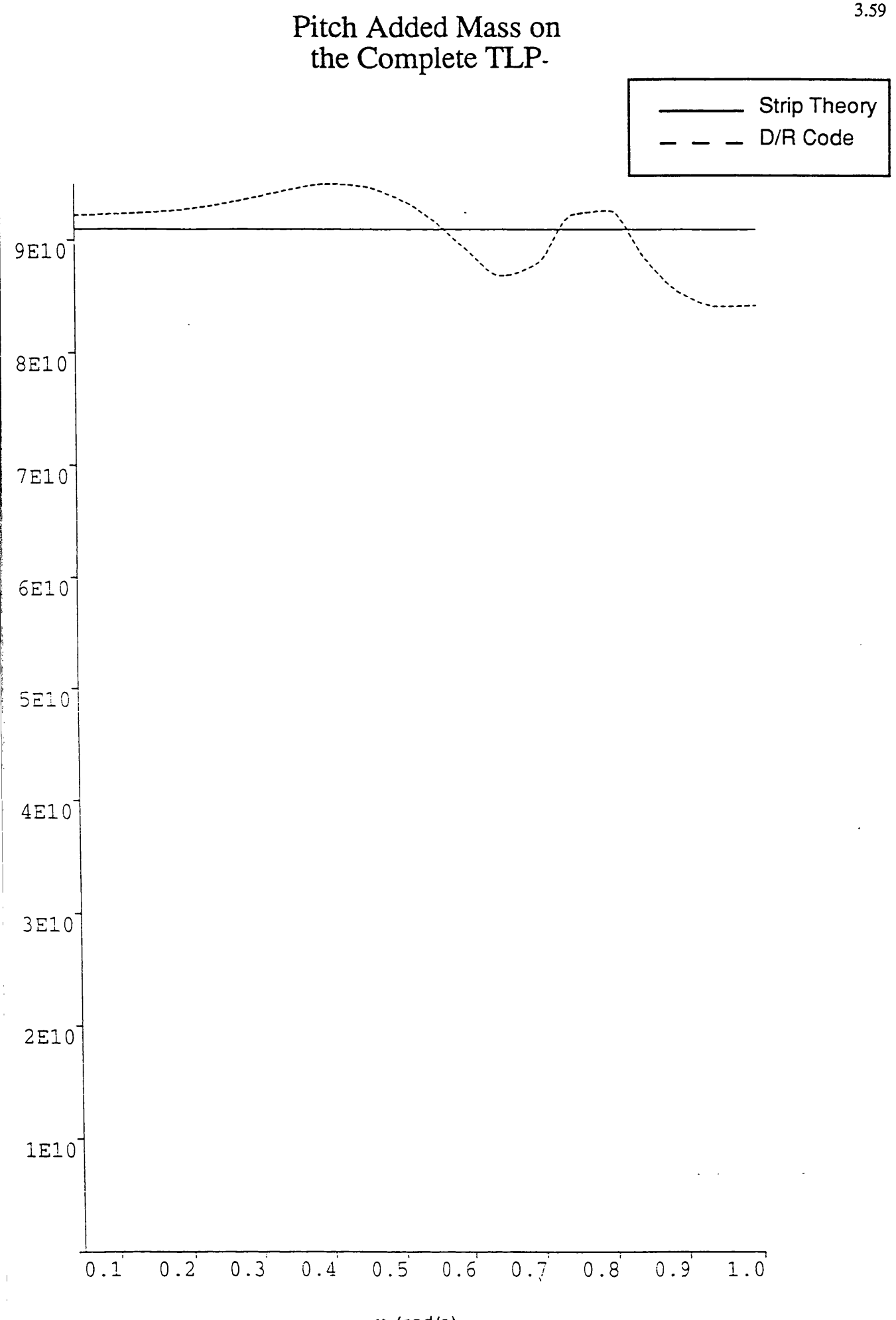
Pitch Added Mass on
the Complete TLP-
Strip Theory
D/R Code
9E10
8E10
7E10
6E10
5E10
4E10
3E10
2E10
1E10
0.1
0.2
0.3
0.4
0.5
0.6
0.7
0.8
0.9
1.0
ω (rad/s)

Figure 3.29

Displacement in Pitch

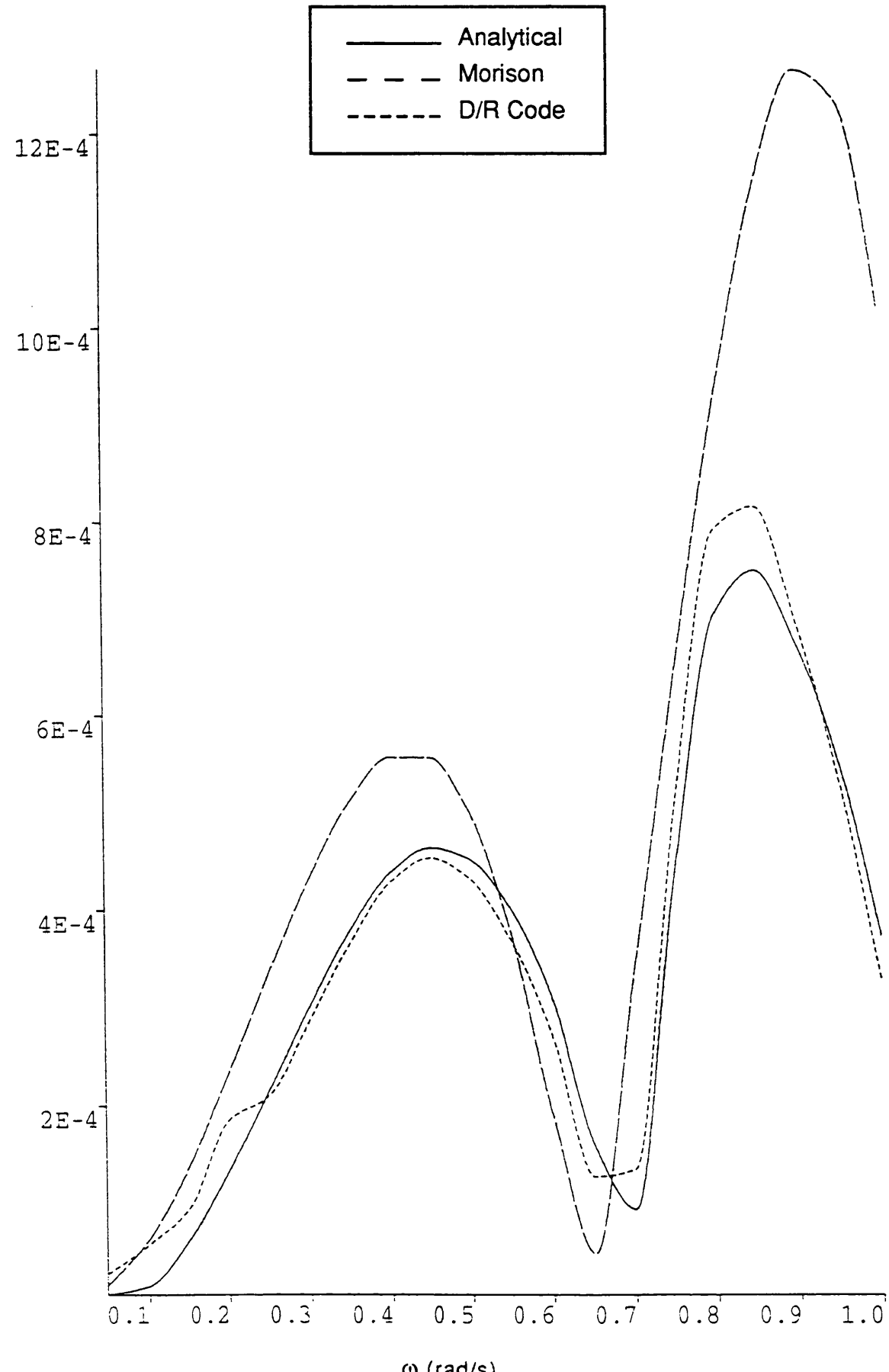

gure 3.30

First Order Forces on the complete TLP
With a 22.5° Heading Sea

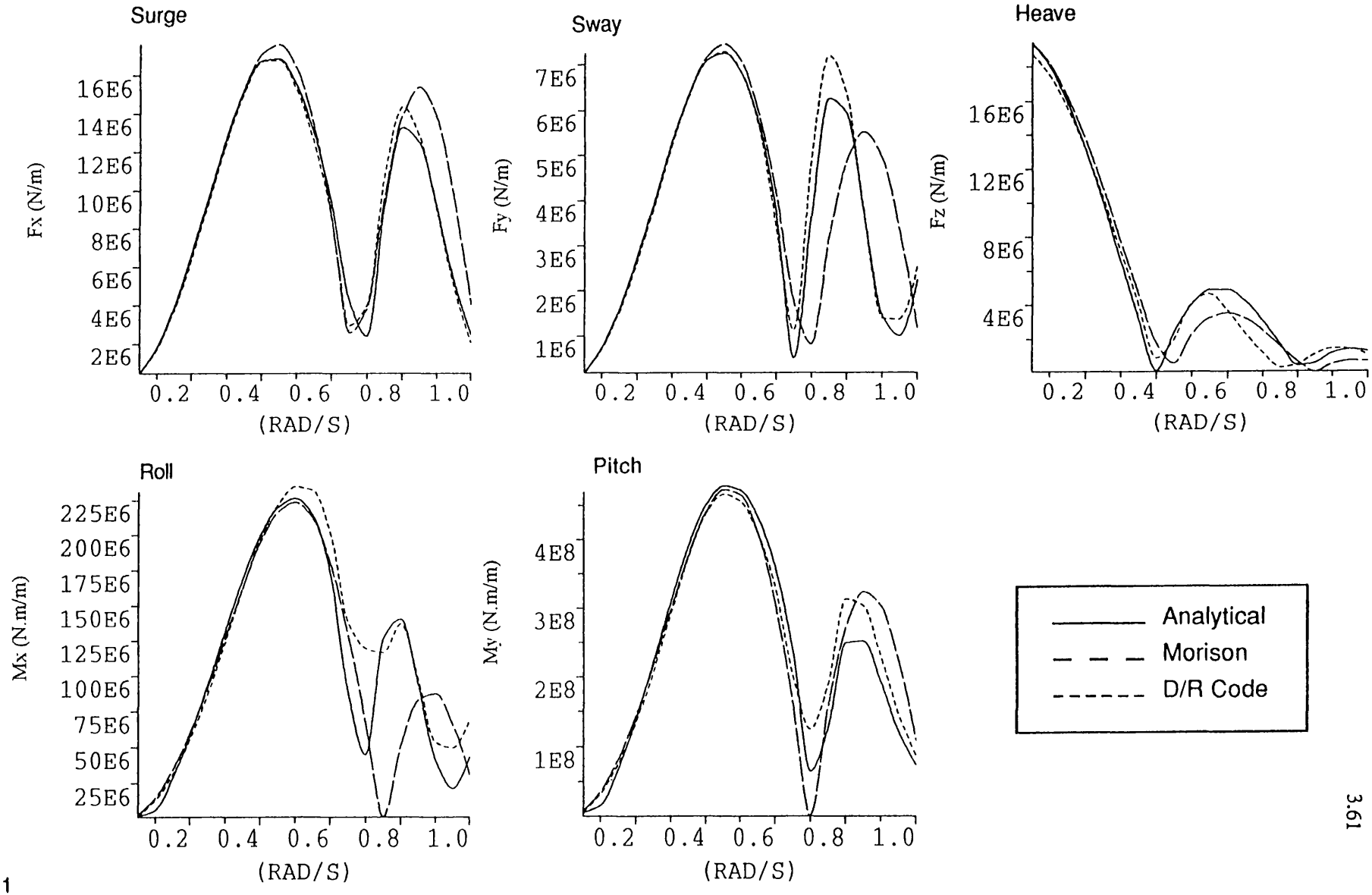

Figure 3.31

First Order Forces on the complete TLP
With a 45° Heading Sea

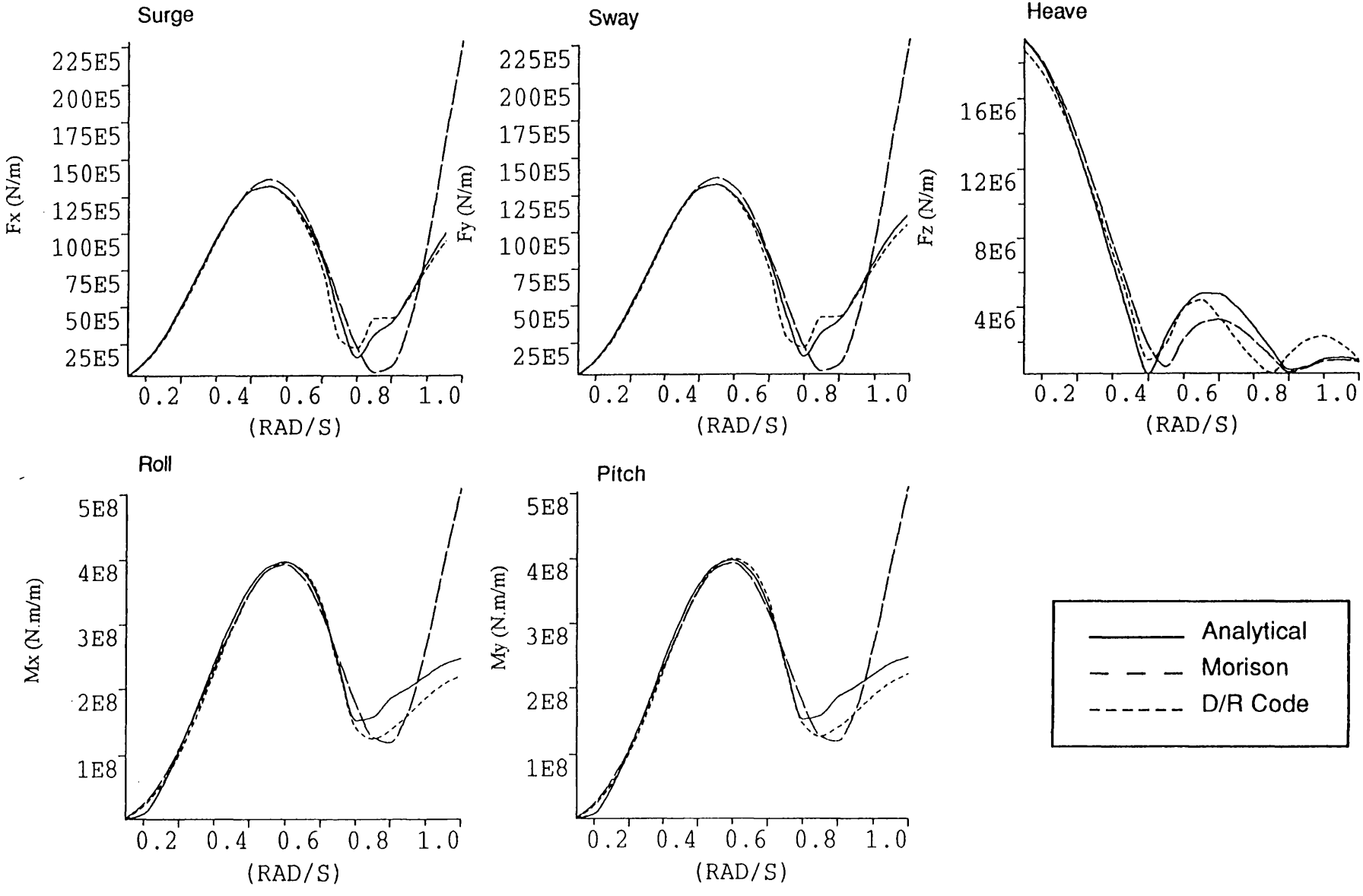

Figure 3.32

Displacements due to the First Order Forces on the complete TLP With a 22.5° Heading Sea

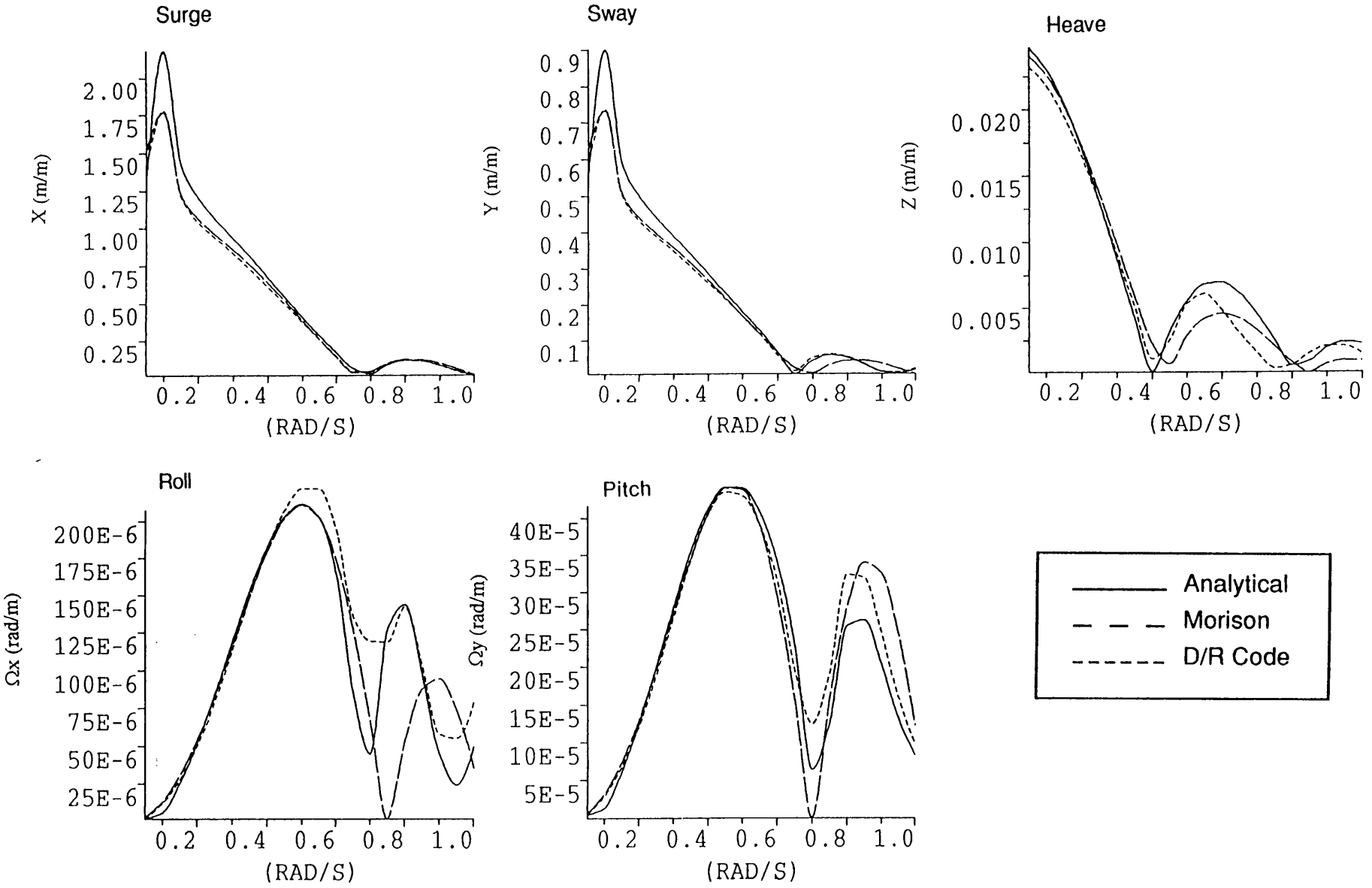

Figure 3.33

Displacements due to the First Order Forces on the complete TLP With a 45° Heading Sea

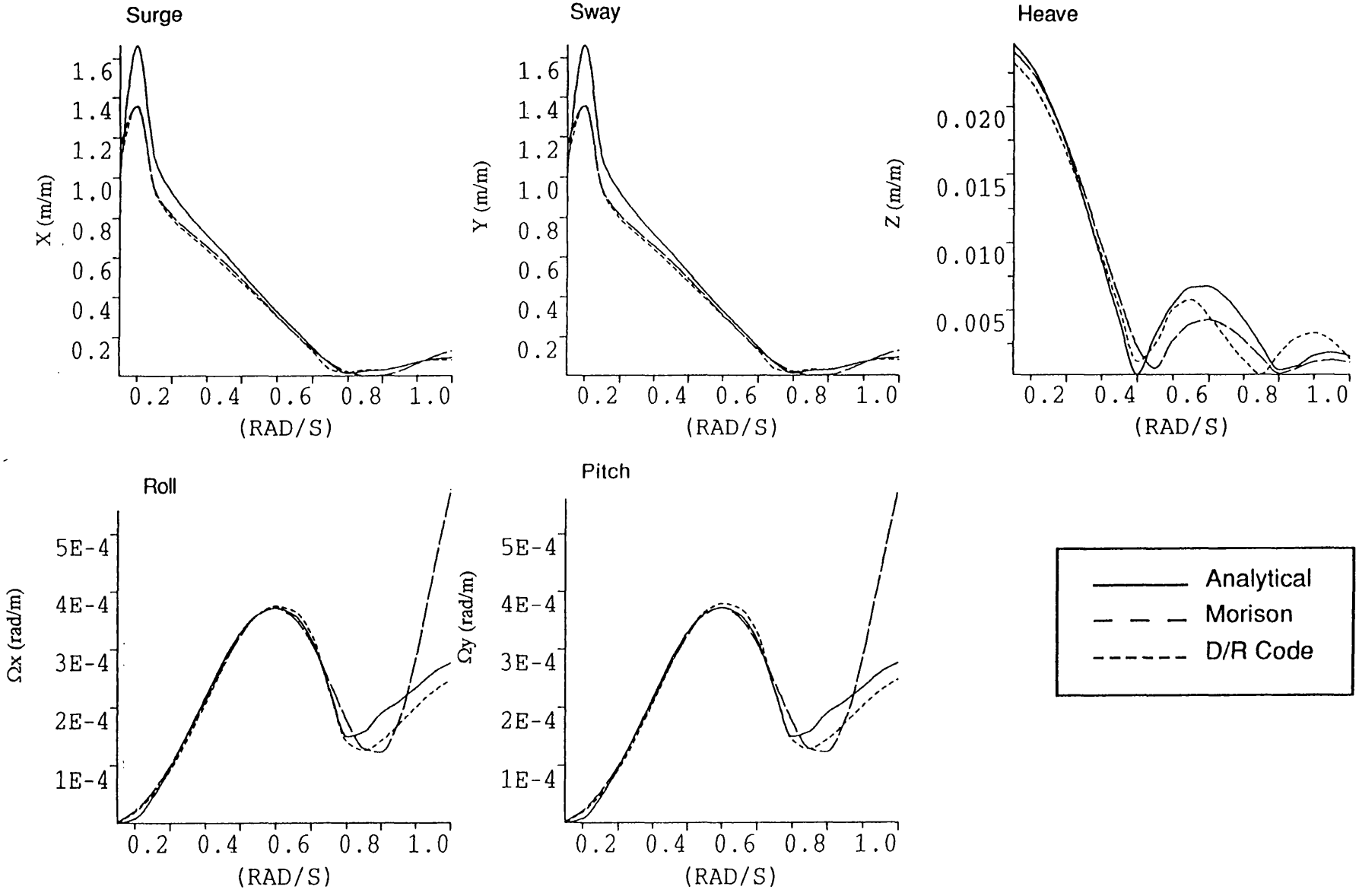

Figure 3.34

CHAPTER 4: SECOND ORDER WAVES

1. INTRODUCTION

This chapter describes the forces due to second order waves, and the corresponding motion responses of the TLP.

The steady drift force is calculated using analytical solutions. From the formulation of the steady drift, the difference frequency forces are deduced using Newman's approximation.

The sum frequency forces are not calculated since no simple theory is fully available for the moment.

In the first section, the theories underlying the calculation of the steady drift forces and their extension to the slowly varying drift forces, are presented. Two different analytical methods are used to calculate the second order forces.

In the second part, the results from both theories are validated and compared with a D/R code.

2. THEORY

2.1. STEADY DRIFT

The steady drift forces depend only on the first order potential. In the force calculations, the structural members (circular cylinders) are considered as fixed. The radiation potential is not accounted for. In this case the steady drift force is given by:

$$\vec{F}_d = \frac{1}{2T}\int_0^T dt\left\{\int_{\Gamma_o} \rho g \eta^{(1)2} \vec{n}_o \, d\Gamma_o - \iint_{S_b} \rho \nabla\Phi^{(1)2} \vec{n}_o \, dS_b\right\} \qquad (2.1\text{-}1)$$

Where:

Γ_o: waterline

S_b : wet surface

$\vec{n}_o$: vector normal to the surface

$\eta^{(1)}$: free surface elevation due to first order theory

$\Phi^{(1)}$: first order potential

T: wave period

Two theories are investigated. The first one uses the expression of the first order diffraction potential for a single circular cylinder. The force is then multiplied by the number of columns in order to obtain the total force.

The second theory is based on the first order diffraction potential for an array of vertical circular cylinders, developed in the previous chapter.

The second method is obviously more precise. However, the first one presents the advantage of being easier to develop needing simpler mathematical equations.

2.1.1. Single cylinder

The formulation is based on the extension of the work of MacCamy and Fuchs [4.1] by Chakrabarti [4.2].

The forces and moments, about Ox and Oy respectively, are calculated from the first order diffraction potential for a fixed bottom mounted cylinder.

$$F_{dx} + i\,F_{dy} = \frac{4\rho g A^2 R_c}{\pi^2 (kR_c)^3} e^{i\alpha}\left(1+\frac{2kH}{\mathrm{Sinh}(2kH)}\right)\sum_{n=0}^{\infty}\left(\frac{n(n+1)}{(kR_c)^2}-1\right)^2 \frac{1}{\left|H'_n(kR_c)\right|^2\left|H'_{n+1}(kR_c)\right|^2} \tag{2.1-2}$$

$$M_x = -\mathrm{Im}\left(\tilde{M}_d\right) \tag{2.1-3}$$

$$M_y = \mathrm{Re}\left(\tilde{M}_d\right) \tag{2.1-4}$$

Where:

$$\tilde{M}_d = \frac{-2i\rho g A^2}{\pi k R_c \,\mathrm{Sinh}(2kH)} e^{i\alpha} \sum_{n=-\infty}^{\infty}\left(\begin{array}{l}\dfrac{H^2}{2}-\dfrac{1}{4k^2}\left(\mathrm{Cosh}(2kH)-1\right)+ \\ \dfrac{n(n+1)}{(kR_c)^2}\left(-\dfrac{H^2}{2}-\dfrac{1}{4k^2}\left(\mathrm{Cosh}(2kH)-1\right)\right)\end{array}\right)\frac{1}{H'_n(kR_c)H'^{*}_{n+1}(kR_c)} \tag{2.1-5}$$

Where:

A: wave amplitude
k: wave number
α: wave angle
H: water depth
R_c: cylinder radius
H_n: first kind Hankel function of order n

In order to find the forces on the complete TLP the following assumptions are made:

- the columns are supposed to be bottom mounted. This is explained by the very fast decay of the potential with depth. The drift forces act mainly around the free surface level.

- The forces on the pontoons are neglected since no simple theory is available to predict the drift forces on pontoons. This assumption is also based on the decay of the potential. The drift has little influence on the deep draught pontoons.

The two previous assumptions are valid for surge and sway, but may be questionable in pitch and roll due to the moment arm.

- The cylinder is supposed to be fixed and only the diffraction potential is used.

- The interactions between the columns are neglected. To find the forces acting on the TLP, the force is simply multiplied by the number of columns.

- The steady drift in heave is not calculated since we consider bottom mounted cylinders. However, the steady drift force is small in heave and can be taken as zero.

This method can be simplified if one is only interested in the horizontal forces. The surge and sway forces can be written as:

$$F_{dx} + i F_{dy} = \frac{4\rho g A^2 R_c}{\pi^2 (kR_c)^3} e^{i\alpha} \left(1 + \frac{2kH}{\mathrm{Sinh}(2kH)}\right) \sum_{n=0}^{\infty} \left(\frac{n(n+1)}{(kR_c)^2} - 1\right)^2 \frac{1}{\left|H'_n(kR_c)\right|^2 \left|H'_{n+1}(kR_c)\right|^2} \tag{2.1-6}$$

Where R is the drift coefficient that can be approximated by R_{app}:

$$R = \frac{1}{\pi^2 (kR_c)^3} \sum_{n=0}^{\infty} \left(\frac{n(n+1)}{(kR_c)^2} - 1\right)^2 \frac{1}{\left|H'_n(kR_c)\right|^2 \left|H'_{n+1}(kR_c)\right|^2} \approx R_{app} = \frac{2}{3}\left(\frac{kD_c}{2}\right)^3 \tag{2.1-7}$$

This approximation is valid for kR_c smaller than 0.5, which corresponds, in the case of the Snorre TLP (R_c=12.5m), to $\omega < 0.6$rad/s.

This approach is appealing for early design stage since the drift can be calculated without having to deal with series of Bessel functions. It works only in the horizontal plane, but roll and pitch are not so important. Indeed the main action of the second

order forces appears when the slowly varying drift excites the low natural frequencies in surge and sway.

The validity of this approximation is discussed in section 3.

2.1.2. Array of cylinders

The first order diffraction potential developed in the previous chapter can be combined with Equation 2.1-1 to find the drift force on an array of bottom mounted vertical circular cylinders.
The theoretical developments can be found in references [4.3] and [4.4].

The force and moment on one column are given by:

$$F_{dx} + i F_{dy} = \frac{\rho g A^2 R_c}{\pi (kR_c)^2}\left(1 + \frac{2kH}{\mathrm{Sinh}(2kH)}\right)\sum_{n=-\infty}^{\infty}\left(\frac{n(n+1)}{(kR_c)^2} - 1\right)\frac{A_n A_{n+1}^*}{H_n'(kR_c)H_{n+1}'^*(kR_c)} \tag{2.1-8}$$

$$M_x = -\mathrm{Im}\left(\tilde{M}_d\right) \tag{2.1-9}$$

$$M_y = \mathrm{Re}\left(\tilde{M}_d\right) \tag{2.1-10}$$

Where:

$$\tilde{M}_d = \frac{2\rho g A^2}{\pi k R_c \mathrm{Sinh}(2kH)}\sum_{n=-\infty}^{\infty}\left(\begin{array}{l}\dfrac{H^2}{2} - \dfrac{1}{4k^2}\left(\mathrm{Cosh}(2kH) - 1\right) \\ + \dfrac{n(n+1)}{(kR_c)^2}\left(-\dfrac{H^2}{2} - \dfrac{1}{4k^2}\left(\mathrm{Cosh}(2kH) - 1\right)\right)\end{array}\right)\frac{A_n A_{n+1}^*}{H_n'(kR_c)H_{n+1}'^*(kR_c)} \tag{2.1-11}$$

Where A_n is the first order potential coefficient (See chapter 3).

Similar assumptions to the single body case are made:

- The columns are supposed to be bottom mounted.
- The pontoons are neglected.
- The cylinders are supposed to be fixed and only the diffraction potential is used.
- The steady drift force in heave is equal to zero.

This time the interaction between the columns is fully taken into account.

2.1.3. Displacement

From the forces, the displacement in irregular seas can be calculated using the following formula:

$$X_i = \frac{1}{K_i}\int_0^{\infty} S_w(\omega)\frac{F_{di}(\omega)}{A^2}d\omega \qquad (2.1\text{-}12)$$

Where S_w is the Pierson Moskowitz wave spectrum related to the wind velocity, K_i is the total system stiffness in the direction i and A is the wave amplitude.

The wave spectrum is given by:

$$S_w(\omega) = \frac{\alpha_{pm} g}{\omega^5} e^{-\beta_{pm}\left(\frac{g}{U_{19.5}\omega}\right)^4} \qquad (2.1\text{-}13)$$

Where:

$U_{19.5}$ is the wind velocity 19.5 meters above the sea level

α_{pm} and β_{pm} are two adimensional coefficients:

$\alpha_{pm} = 8.1\ 10^{-3}$ $\qquad$ $\beta_{pm} = 0.74$

2.2. SLOWLY VARYING DRIFT

The following method to calculate the slowly varying drift forces and displacements is developed by Molin in reference [4.5].

The slowly varying drift can be deduced from the drift force using Newman's approximation:

$$\vec{F}_-^{(2)}(\omega_1, \omega_2) = \vec{F}_d(\omega_1) \qquad (2.2\text{-}1)$$

Since the steady drift in heave is chosen as zero, the slowly varying force in that direction is equal to zero too. However, the slowly varying drift is only important at low frequencies. It has an effect mainly on surge and sway where it can excite the natural frequencies. In heave, roll and pitch, the effects are small.

The response spectrum in direction i is calculated from the following formula:

$$RS_{svdi}(\omega) = 8\int_0^{\infty} S_w(\mu) S_w(\omega+\mu) Q_i^2(\omega) \frac{F_{-i}^{(2)}(\mu, \omega+\mu)}{A_\mu A_{\omega+\mu}} d\mu \qquad (2.2\text{-}2)$$

Where Q_i is the transfer function in direction i (See Chapter 2). A_μ and $A_{\omega+\mu}$ are the wave amplitudes corresponding to frequencies μ and $\omega+\mu$ respectively.

This becomes, using Newman's approximation:

$$RS_{svdi}(\omega) = 8\int_0^\infty S_w(\mu) S_w(\omega+\mu) Q_i^2(\omega) \frac{F_{di}(\mu)}{A_\mu^2} d\mu \qquad (2.2\text{-}3)$$

From this spectrum, significant values of the response can be obtained (See chapter 2):

$$X_{1/3}^{svdi} = 2\sqrt{m_0(RS_{svdi})} \qquad (2.2\text{-}4)$$

The Newman's approximation is applied to both analytical methods and to the D/R code to obtain the slowly varying forces and the displacement.

These are compared in the next chapter.

3. VALIDATION

This chapter covers the validation of the previously developed theories.

First the drift coefficient approximation is tested.

Then, the validation of the steady drift force predictions is carried out. The assumptions used by both methods are discussed through a comparison with D/R code results. Both forces and steady displacements are compared.

Finally, the comparison is extended to the slowly varying forces and displacements.

Unless otherwise is stated, the figures presented in this section correspond to results for head seas.

3.1. DRIFT COEFFICIENT APPROXIMATION

Figure 4.1 compares the drift coefficient R with its approximation R_{app} defined in equation 2.1-7. It shows a very good agreement for frequencies below 0.6 rad/s. However, for higher frequencies, R_{app} diverge completely and cannot be used at all.

The steady drift force can be calculated accurately with the approximation for a range of frequencies between 0 and 0.6 rad/s.

If the displacement in irregular seas has to be calculated, the following formula should be applied:

$$X_{sd} = \frac{1}{K_x}\int_0^{UL} S_w(\omega)\frac{F_{dx}(\omega)}{A^2}d\omega \qquad (3.1\text{-}1)$$

The value of the upper limit of the integral, UL, is theoretically infinity. In a computer calculation, it has to be chosen to ensure acceptable convergence.

Figure 4.2 shows the values of the steady drift response calculated with the exact analytical theory for different values of the upper limit. The curves correspond to sea states due to 20m/s and 50m/s winds.

For both sea states, the convergence of the integral is reached for a value of UL above 1 rad/s.

The approximation could only be used with a maximum value of 0.6 rad/s for the upper limit. The frequency range is not wide enough to get a good numerical convergence.

The same problem appears for the slowly varying drift response spectra:

$$RS_{svdx}(\omega) = 8\int_0^{UL} S_w(\mu)S_w(\omega+\mu)Q_x^2(\omega)\frac{F_{dx}(\mu)}{A^2}d\mu \qquad (3.1\text{-}2)$$

Figures 4.3 and 4.4 show the response spectra for different values of the upper limit UL in the case of wind speed of 20 m/s and 50 m/s respectively.

A good convergence is reached for the value of UL of about 1 rad/s.

Calculating both steady drift displacement and slowly varying drift response with an upper limit value of 0.6 rad/s would largely underestimate the second order effects (by a factor varying from two to four, depending on the sea state).

The approximation cannot be applied properly for the TLP design and one has to consider the use of the exact coefficient R.

3.2. STEADY DRIFT

For the validation of the steady drift, the D/R code has been run with three different geometries:

- Geometry 1: an array of bottom mounted cylinders. This should give a validation for the analytical solution for an array of cylinders. This is used also to see the effects of the interaction between the cylinders when comparing with the analytical solution for a single cylinder.

- Geometry 2: an array of truncated cylinders, corresponding to the design of the Snorre TLP without the pontoons. The assumption over the depth of the cylinders is tested. The value of the drift force in heave is checked.

- Geometry 3: the complete Snorre TLP, with the pontoons. The effects of the pontoons are studied.

During the calculations with the D/R code, the TLP was considered as fixed, thus as the analytical solutions, it does not take into account the movements of the structure. Only the diffraction potential is used in the drift force calculation.

The steady drift forces and displacements calculated with the two analytical theories, and with the D/R code for the three different geometries are compared for surge, heave and pitch.

The computations have been carried out for a head sea and unit amplitude waves, except in the last part which validates the theory for directional seas.

3.2.1. Surge

Figure 4.5 presents the results for the surge forces calculated using the two analytical solutions, and the D/R code on geometry 1.

The solution for a single cylinder gives values of the same order as the other two but clearly present differences because it does not take into account the interaction between the cylinders.

The results from the analytical solution and the D/R code match well, validating the program.

Figure 4.6 presents the steady drift force in surge calculated from:

- D/R Code on geometry 2

- D/R Code on geometry 1

- Analytical solution for an array of 4 cylinders

The three sets of results match very well, proving that we can calculate the force on bottom mounted cylinders and extend the result to truncated cylinders.

Finally, in Figure 4.7, the analytical solution for an array of cylinders is compared with the results of D/R Code on Geometry 3.

The main difference appears in the high frequency region where the pontoons seem to have the larger influence. However, the overall results are quite well correlated.

Figure 4.8 shows the steady displacement in irregular seas due to drift as a function of the wind velocity. It compares the two analytical solutions and the R/D code results for geometry 2.

The results match well except for high velocity winds. However, the steady displacement in this range is largely dominated by the displacement due to the wind. The error can be neglected since it is small compared to the total steady displacement.

3.2.2. Heave

Figure 4.9 presents the heave force for the complete TLP calculated by the D/R Code. The value of the force does not exceed 35 kN. The corresponding value of the displacement in regular sea is about 25.10^{-6}.

In irregular sea, the displacement is about 0.025m for a 50m/s. This is very small when compared to the displacement due to the first order waves equal to 0.66 m.

This effect also appears to be very small when compared to the vertical offset of the platform when a full coupling of the tendon/TLP system is considered. The explanation of this effect can be found in the last chapter of the thesis.

The steady drift in heave is very small and its effects can be neglected.

3.2.3. Pitch

Figure 4.10 presents the steady drift in pitch calculated with the two analytical theories and the R/D code for geometry 1.

The results do not show as good agreement as in surge. The values of the moment are rather low. Indeed, the moment arm is small since the forces mainly act at the water level.

As in surge, the results of predictions for a single cylinder do not present the same shape, although magnitudes are of the same order.

In Figure 4.11, the analytical theory for an array of cylinders is compared with the results from the D/R code for geometries 2 and 3.

The results agree quite well for frequencies between 0.5 and 0.9 rad/s. For lower frequencies, the pontoons seem to have some effects on the moment. In fact, low frequency waves go deeper into the sea, and create relatively more loads on the pontoons. In the case of the moment, the effect is amplified by the moment arm.

The steady displacements created for irregular seas show few differences when calculated using different theories (See Figure 4.12). The larger differences appear for high velocity wind. However, for such values, the steady displacement in pitch due to waves is small compared to the steady displacement due to the wind.

3.2.4. Directionality

The formulations derived in this study and the D/R code take into account the directionality of the waves. To validate the wave angle dependence, the steady drift forces have been compared with the D/R code results in the case of 22.5° and 45° heading seas.

The results are presented in Figures 4.13 and 4.14. The agreement is as good as for head seas.

For the array of cylinders, surge and sway are giving good results. The heave force can be neglected since very small. The results in roll and pitch present a good approximation despite a small difference at lower frequencies.

For the single cylinder theory, the forces and moments are similar in magnitude, but not in shape, because of the interaction between the columns.

3.3. SLOWLY VARYING DRIFT

Since the quadratic transfer functions (QTF) for the difference frequency forces are not calculated by the D/R code, the Newman's approximation is also used for the calculation of the slowly varying drift utilising the steady drift force calculated by the program.

Geometry 2 has been preferred to the complete TLP for computational reasons. The D/R code was giving problems for low frequency calculations for the complete TLP. Furthermore, due to the fact that 50 different frequencies were required, a lot of time was saved by using a simpler mesh.

The integration given in equation 2.2-3 was carried out for a range of frequencies from 0.02 to 1 rad/s with a frequency step of 0.02 rad/s.

3.3.1. Surge

Figure 4.15 presents the response spectra due to the slowly varying drift forces calculated using three different methods, for the wind velocity of 50 m/s.

The responses, calculated with the analytical theory for an array of cylinders and the R/D code, show good agreement.

The solution for a single cylinder presents a lower peak at the natural frequency, underestimating the response.

Figure 4.16 presents the significant values of the responses for a range of wind speeds from 5 m/s to 50 m/s. We have a good agreement between the analytical solution for an array of cylinders and the results of the D/R code.

The solution for the single cylinder yields underestimate of the significant response for high velocity winds.

3.3.2. Heave

The slowly varying drift force and response in heave are taken as zero by both analytical solutions.

The R/D code gives a significant response of 0.04 m for 50 m/s wind. Since this is very small compared to the displacement due to other forces, it can be considered as zero.

3.3.3. Pitch

Figure 4.17 and 4.18 present the responses due to slowly varying drift forces for the wind speed of 50 m/s and the significant values of the displacement for different wind velocities.

The agreement is quite good between the analytical theory for an array of cylinders and the R/D code results for geometry 2.

As in surge, the analytical solution for a single cylinder tends to underestimate the displacements.

However, one should note that the values are very small, and that the slowly varying drift do not have much incidence on the pitch displacement.

4. CONCLUSION

The application of the analytical solution of the first order potential for an array of bottom mounted cylinders to the calculation of the steady drift, and the slowly varying drift has been presented here. This theory gives results that compare well with results from a D/R code.

The analytical theory presents a great advantage in terms of computation time, especially for the slowly varying drift that requires to cover a large range of frequencies with a small step, in order to calculate the integral with accuracy.

The theory based on the solution for a single column does not give such a good agreement. The method underestimates the movement of the TLP. However, the method is simpler to apply than the second analytical solution, and can give a quick estimation of the drift force. This estimation is important in the case of TLP's since the drift should not be neglected in the horizontal plane.

However, when this theory is applied, the exact drift coefficient should be used. The approximated coefficient, which avoids the calculation of the series of Bessel function, cannot be applied. The range of validity of the approximation is too small to calculate correctly the steady drift displacement or the slowly varying drift response.

One should note that the steady drift is mainly important for low velocity winds. For high velocity winds, the steady wind force is predominant.

For a TLP, the slowly varying drift is important mainly in the horizontal plane, where it can excite the natural frequencies. In heave and pitch, because of the high stiffness of the tendons, the natural frequencies are in the high frequency range, and cannot be excited by the slowly varying drift. Thus the slowly varying forces have very little effect on the response of the system in these directions.

REFERENCES OF CHAPTER 4

[4.1] MacCamy R.C., Fuchs R.A., 1954, Wave forces on piles: a diffraction theory, Technical Memorandum No.69, Beach Erosion Board.

[4.2] Chakrabarti S.K., 1984, Steady drift force on vertical cylinder - viscous vs. potential, Applied Ocean Research, Vol. 6, No. 2.

[4.3] Eatock Taylor R., Hung S.M., 1985, Wave drift enhancement effects in multi column structures, Applied Ocean Research, Vol. 7, No. 3.

[4.4] Linton C.M., Evans D.V., 1990, The interaction of waves with arrays of vertical circular cylinders, Journal of Fluid Mechanics, Vol. 215, pp 549,569.

[4.5] Molin B, 1993, Second order hydrodynamics applied to moored structures, 19th WEGEMT School Report.

[4.6] Molin B., 1993, Cours d'hydrodynamique, Lecture at l'Ecole Supérieure d'Ingénieurs de Marseille.

[4.7] McLachlan N.W., 1955, Bessel functions for engineers, Oxford at Clarendon Press.

Drift Coefficient

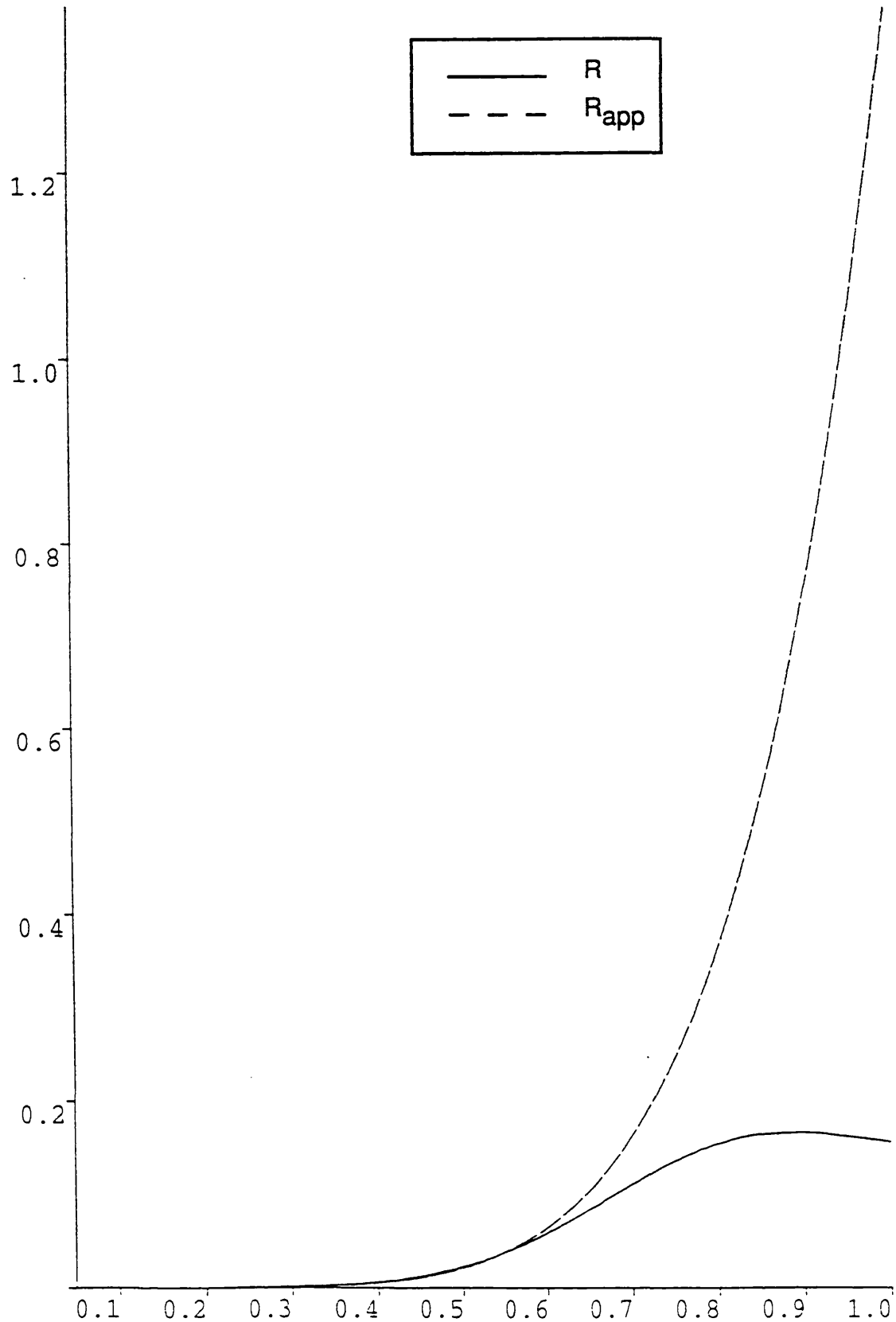

ure 4.1

Convergence of the Steady Drift Displacement in Surge

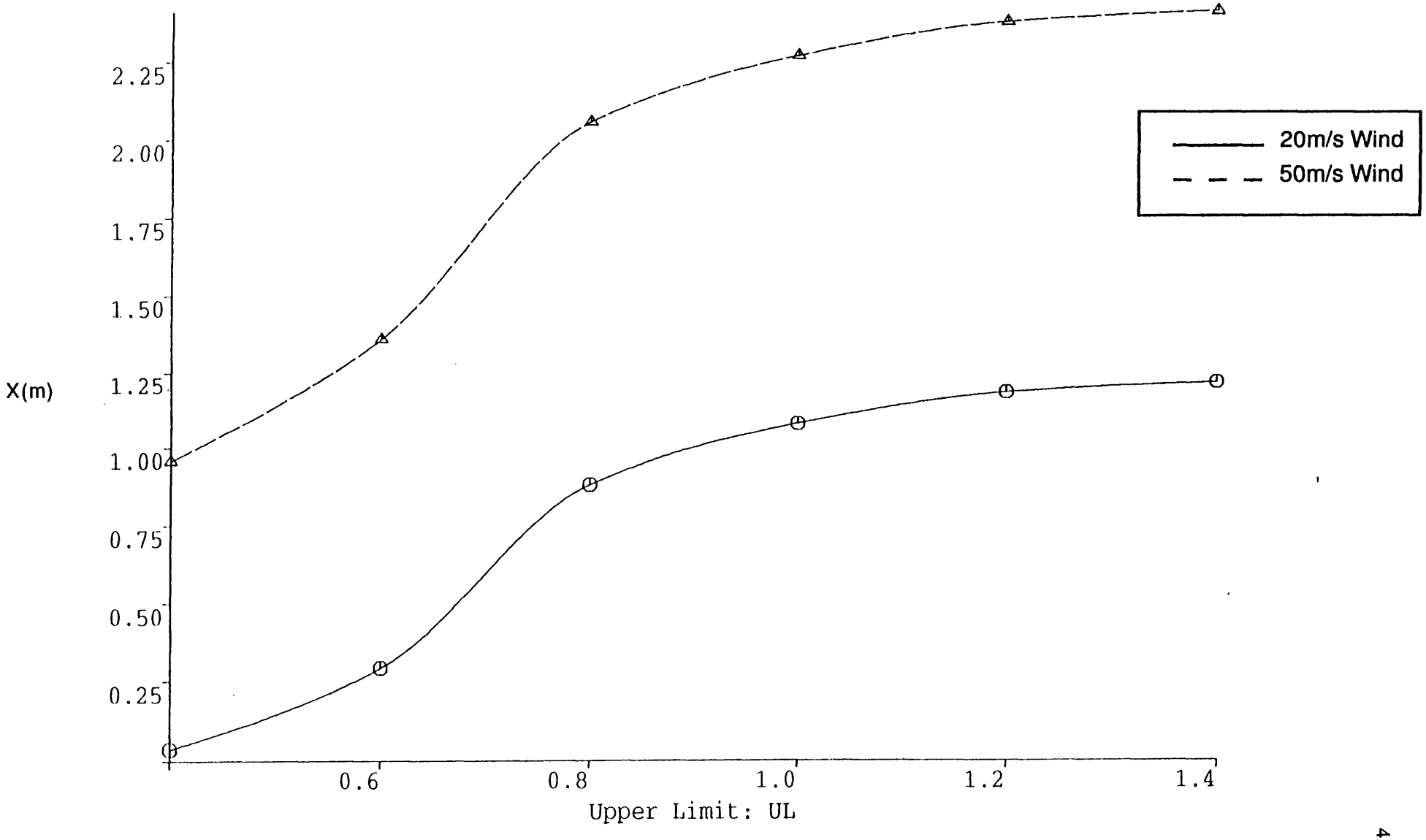

Figure 4.2

Slowly Varying Drift Response Spectra for a 20m/s Wind

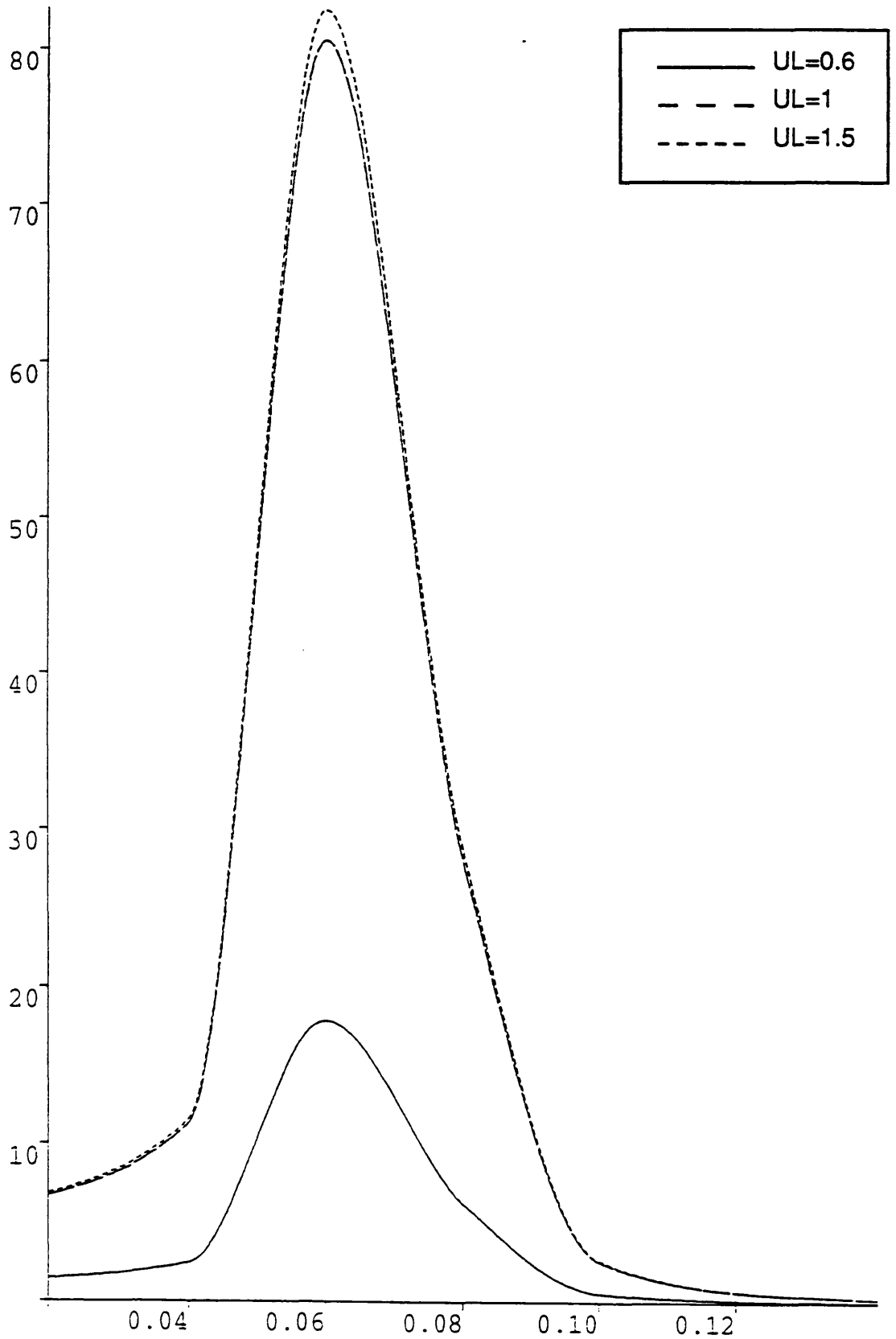

Figure 4.3

Slowly Varying Drift Response Spectra for a 50m/s Wind

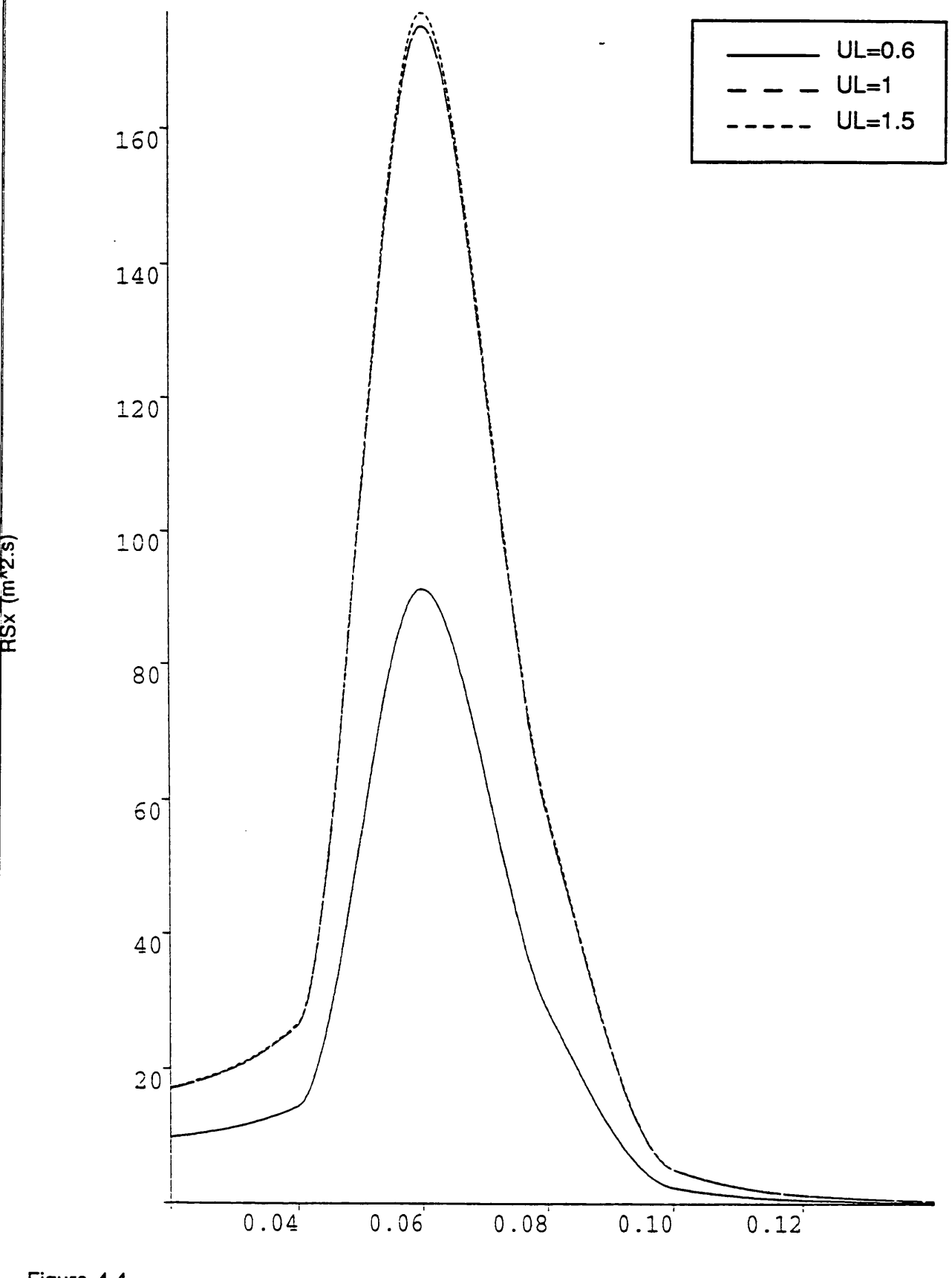

Figure 4.4

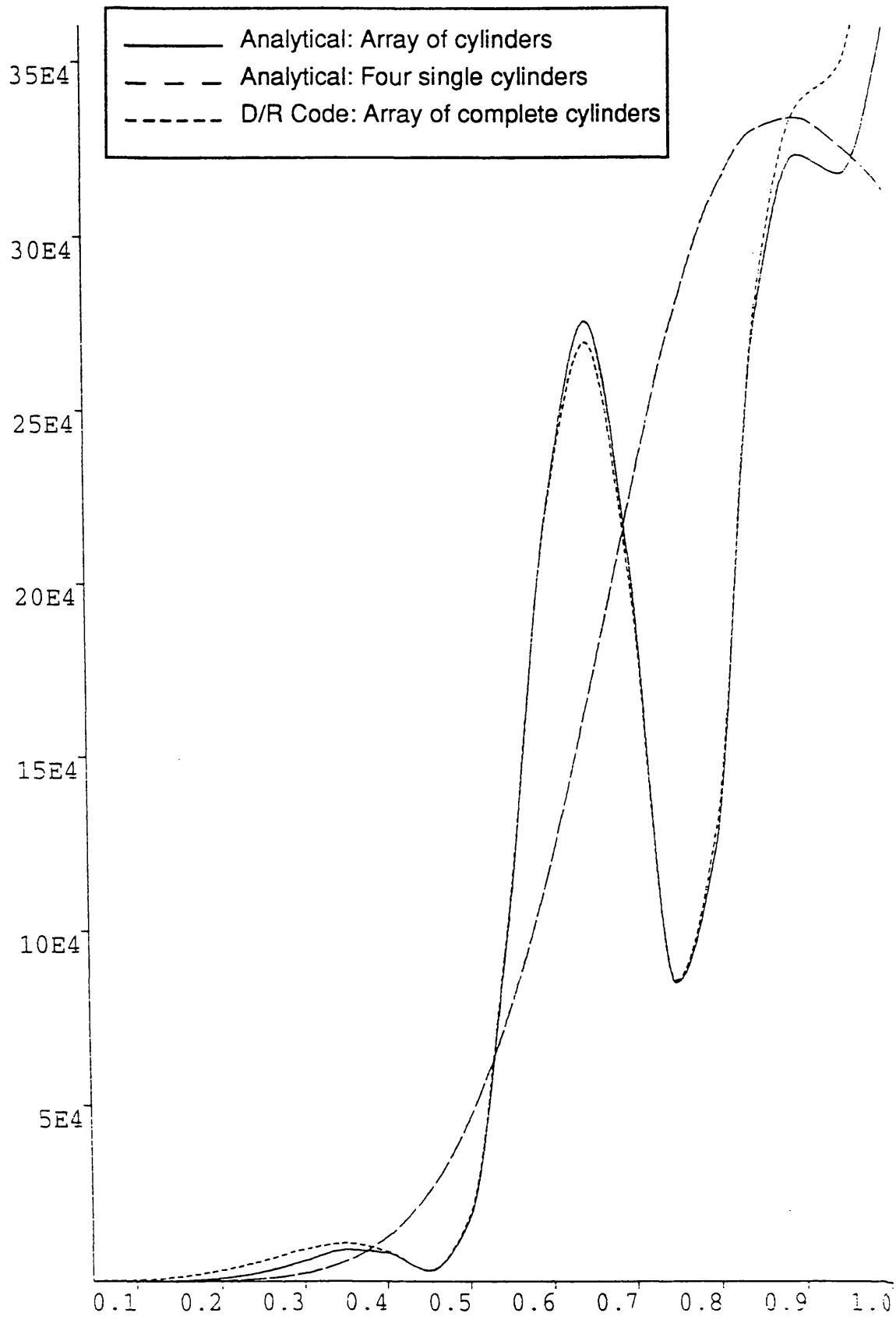
Steady Drift Force in Surge
Analytical: Array of cylinders
Analytical: Four single cylinders
D/R Code: Array of complete cylinders
35E4
30E4
25E4
20E4
15E4
10E4
5E4
0.1
0.2
0.3
0.4
0.5
0.6
0.7
0.8
0.9
1.0
ω (rad/s)

igure 4.5

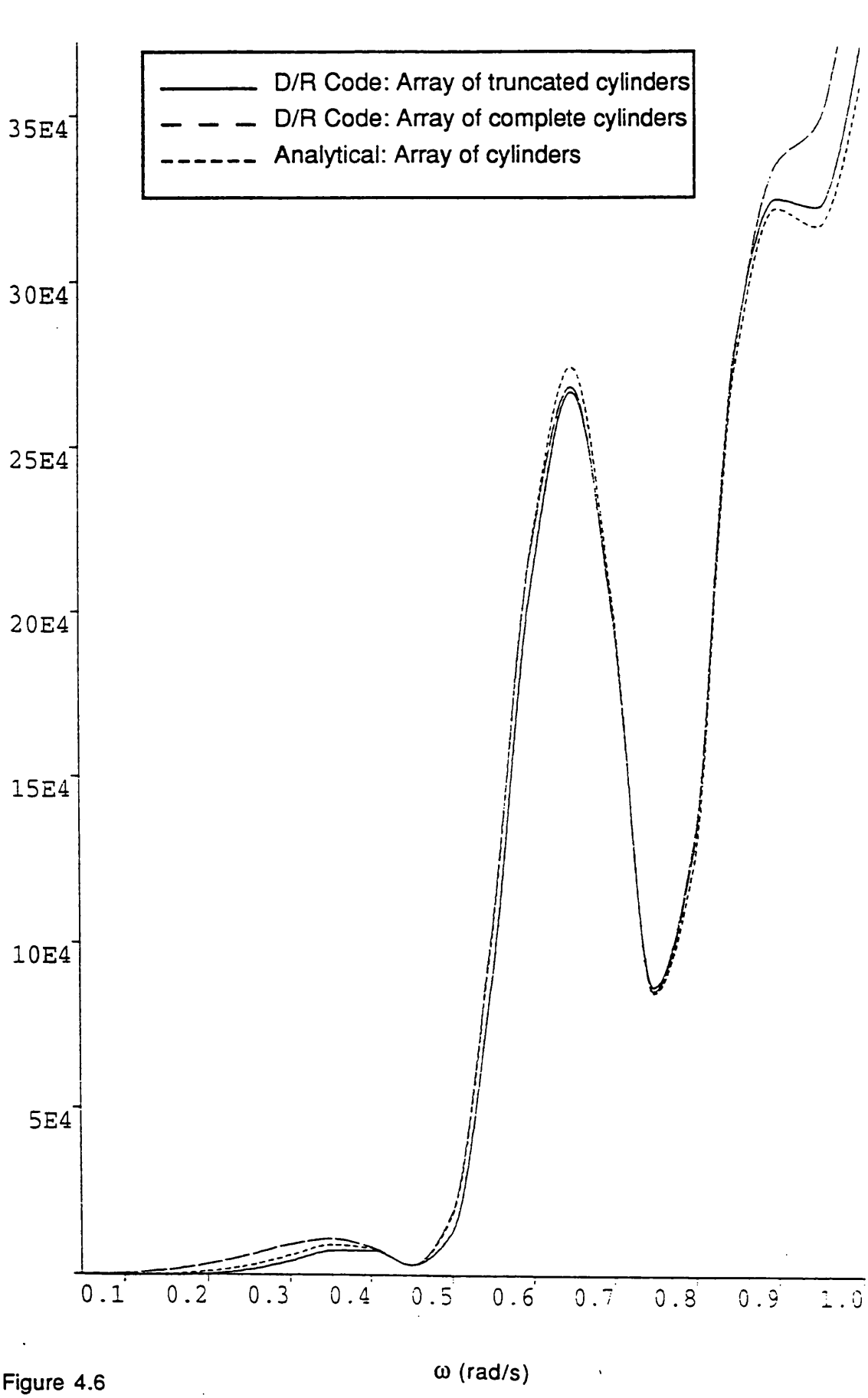
Steady Drift Force in Surge
D/R Code: Array of truncated cylinders
D/R Code: Array of complete cylinders
Analytical: Array of cylinders
35E4
30E4
25E4
20E4
15E4
10E4
5E4
0.1
0.2
0.3
0.4
0.5
0.6
0.7
0.8
0.9
1.0
ω (rad/s)

Figure 4.6

Steady Drift Force in Surge

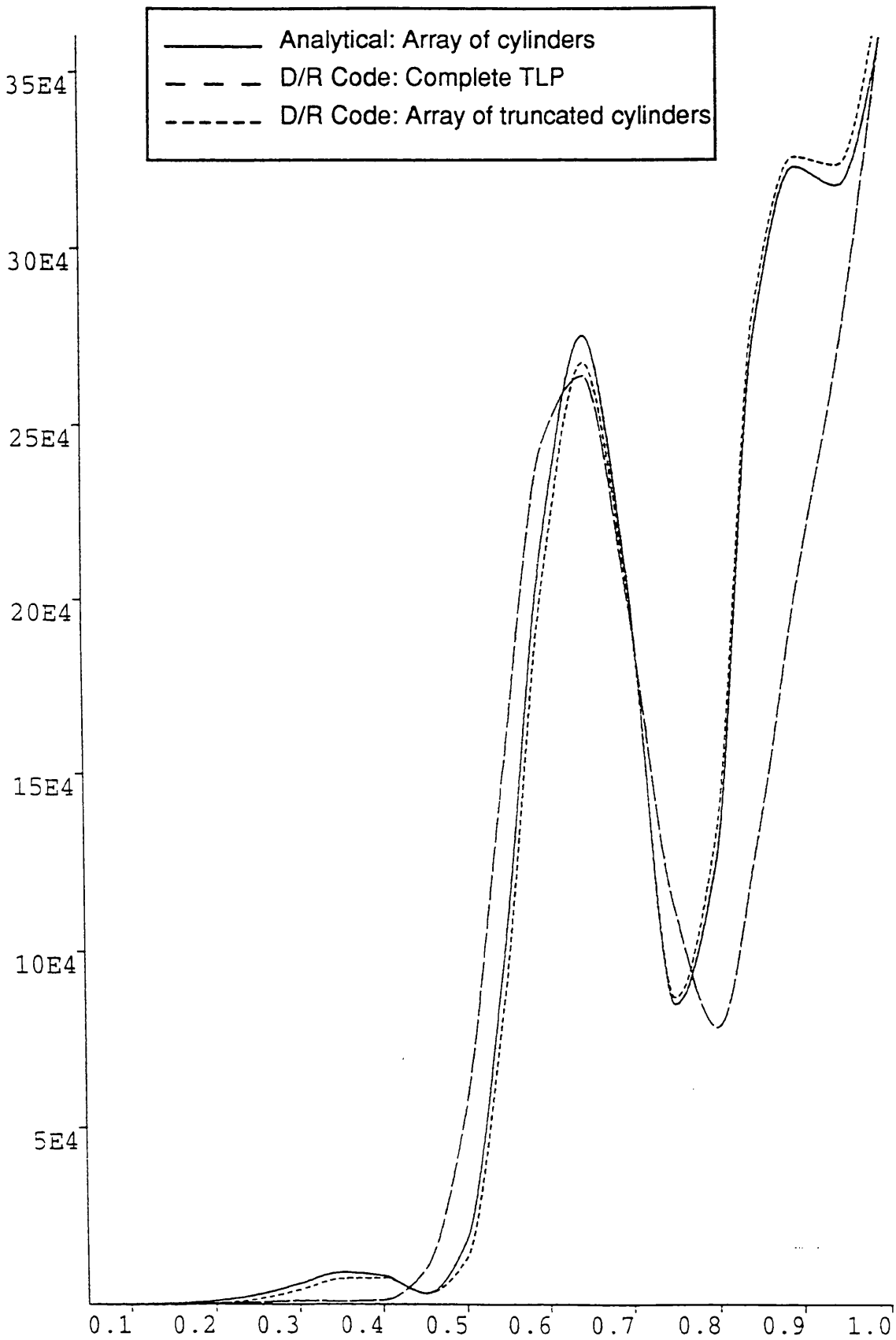

Figure 4.7

Steady Drift Response in Irregular Sea

Surge

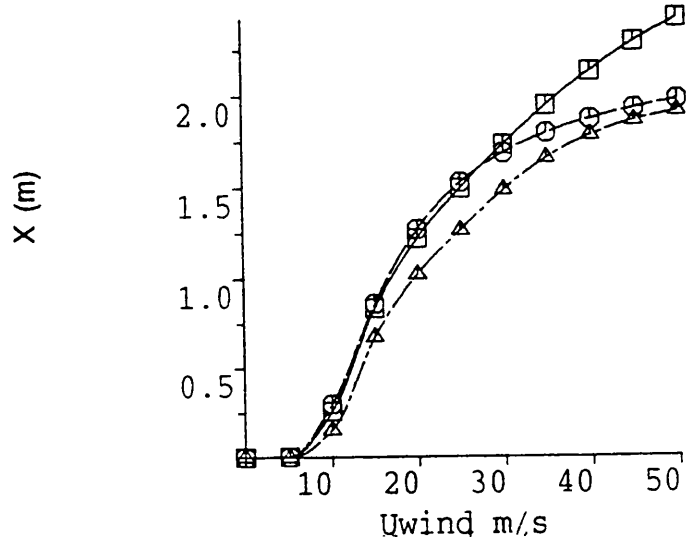

Figure 4.8

Pitch

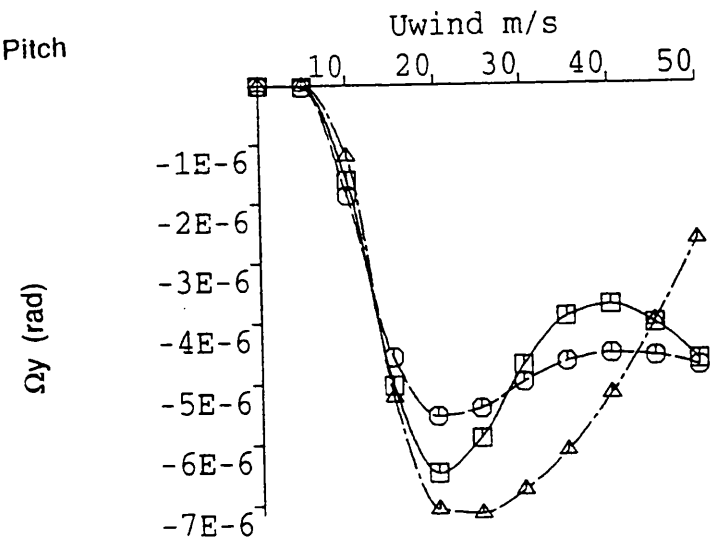

Figure 4.12

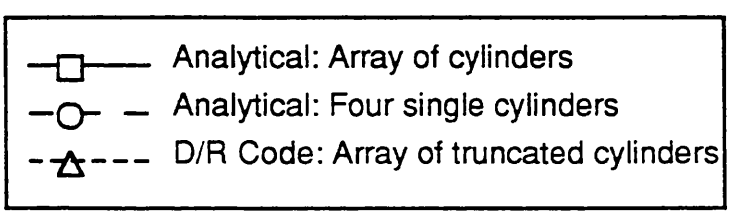

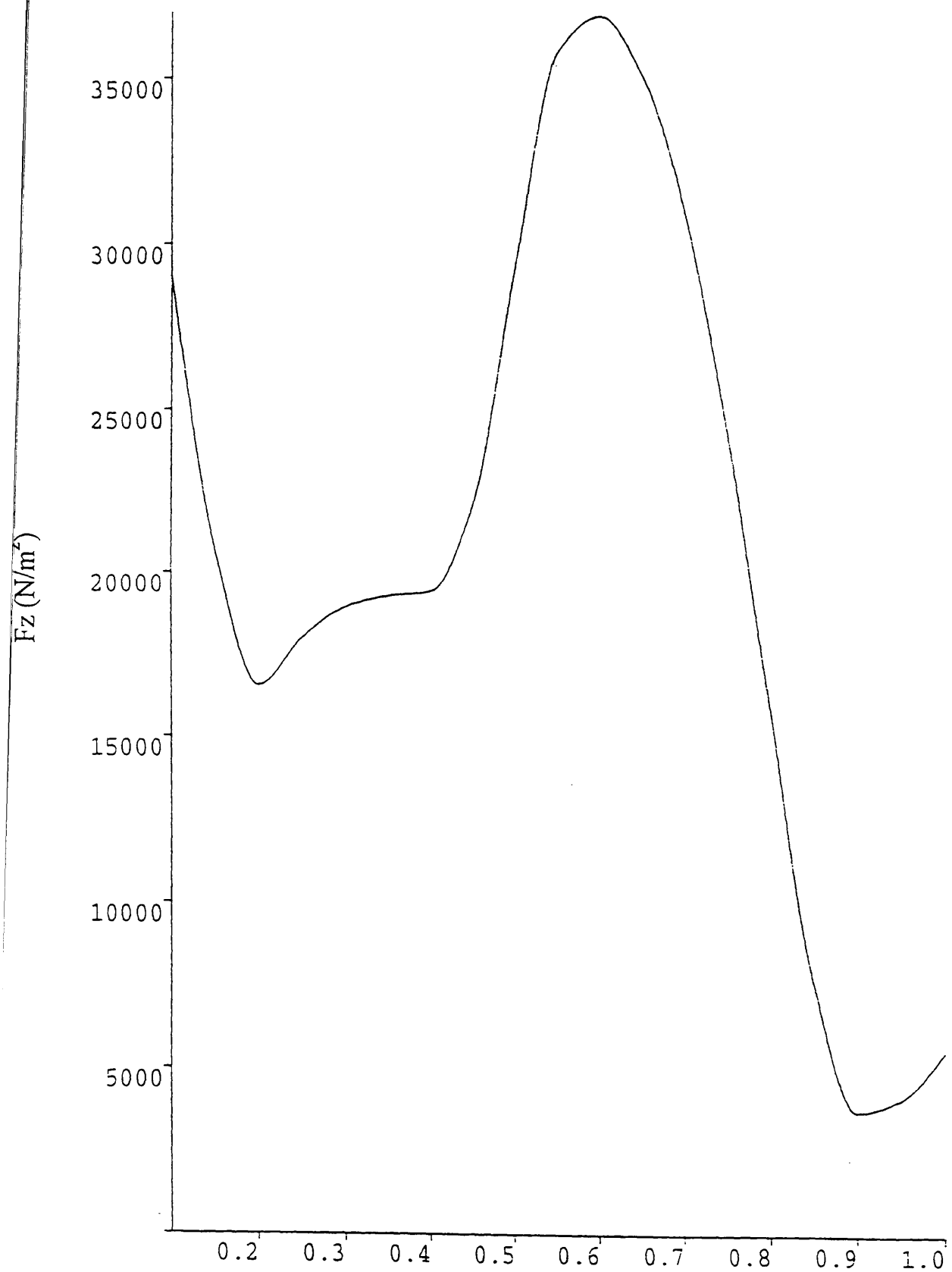
Steady Drift Force in Heave for the Complete TLP
Fz (N/m²)
35000
30000
25000
20000
15000
10000
5000
0.2
0.3
0.4
0.5
0.6
0.7
0.8
0.9
1.0
ω (rad/s)

Figure 4.9

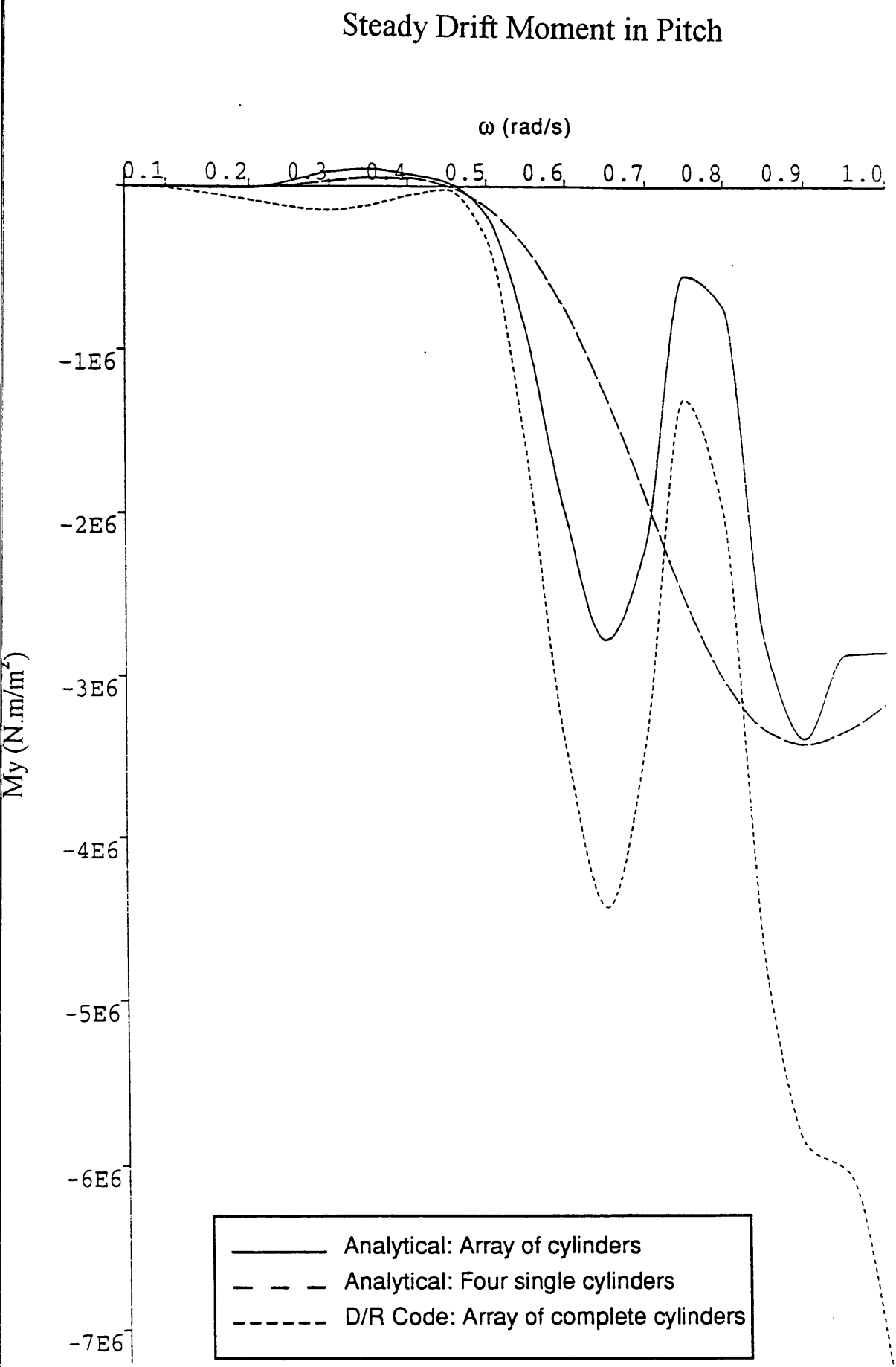
Steady Drift Moment in Pitch
ω (rad/s)
0.1
0.2
0.3
0.4
0.5
0.6
0.7
0.8
0.9
1.0
-1E6
-2E6
-3E6
-4E6
-5E6
-6E6
-7E6
My (N.m/m²)
Analytical: Array of cylinders
Analytical: Four single cylinders
D/R Code: Array of complete cylinders

Figure 4.10

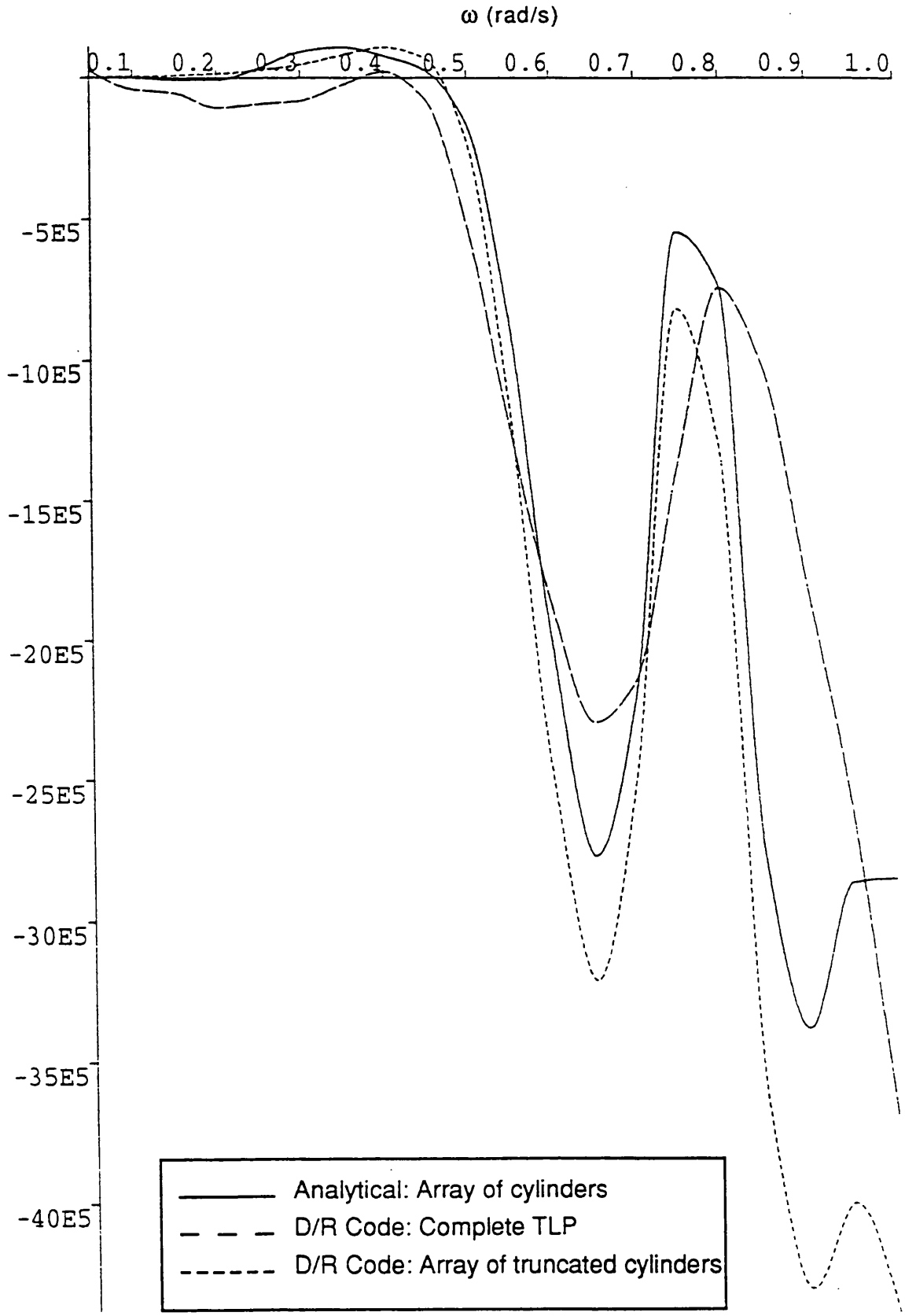
Steady Drift Moment in Pitch
ω (rad/s)
0.1
0.2
0.3
0.4
0.5
0.6
0.7
0.8
0.9
1.0
-5E5
-10E5
-15E5
-20E5
-25E5
-30E5
-35E5
-40E5
My (N.m/m²)
Analytical: Array of cylinders
D/R Code: Complete TLP
D/R Code: Array of truncated cylinders

Figure 4.11

Steady Drift Forces
With a 22.5° Heading Sea

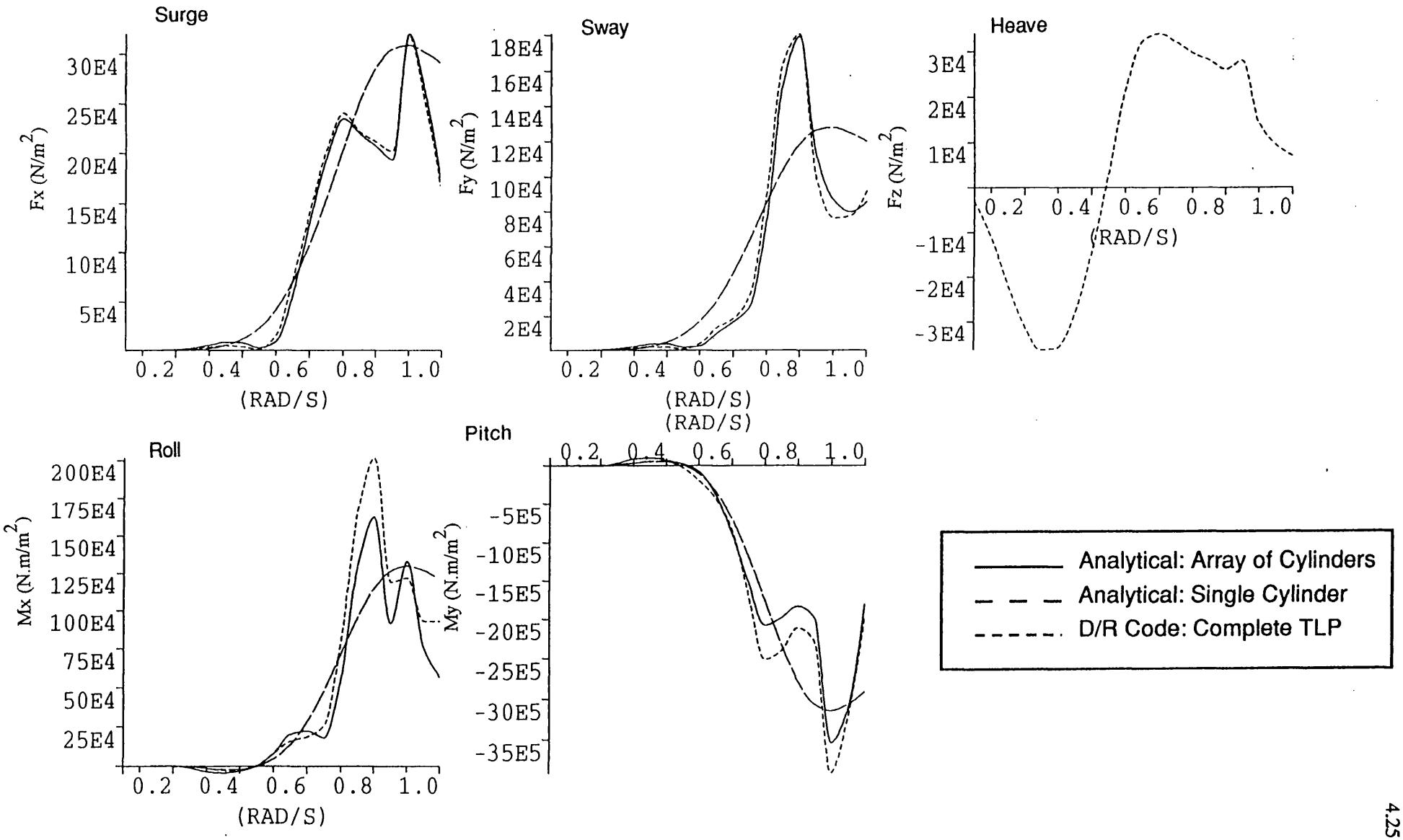

Figure 4.13

Steady Drift Forces
With a 45° Heading Sea

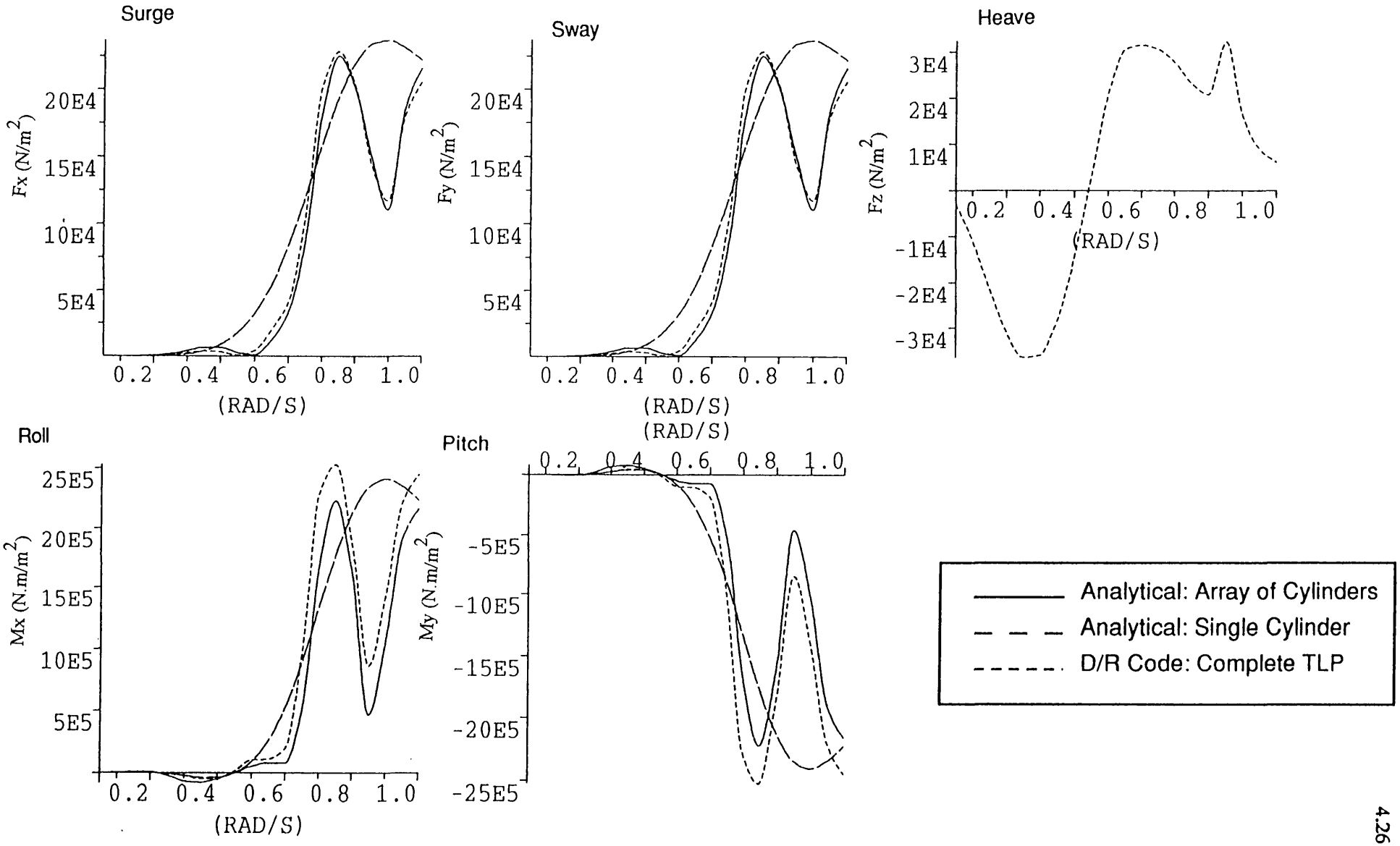

Figure 4.14

Slowly Varying Drift Surge Response Spectra

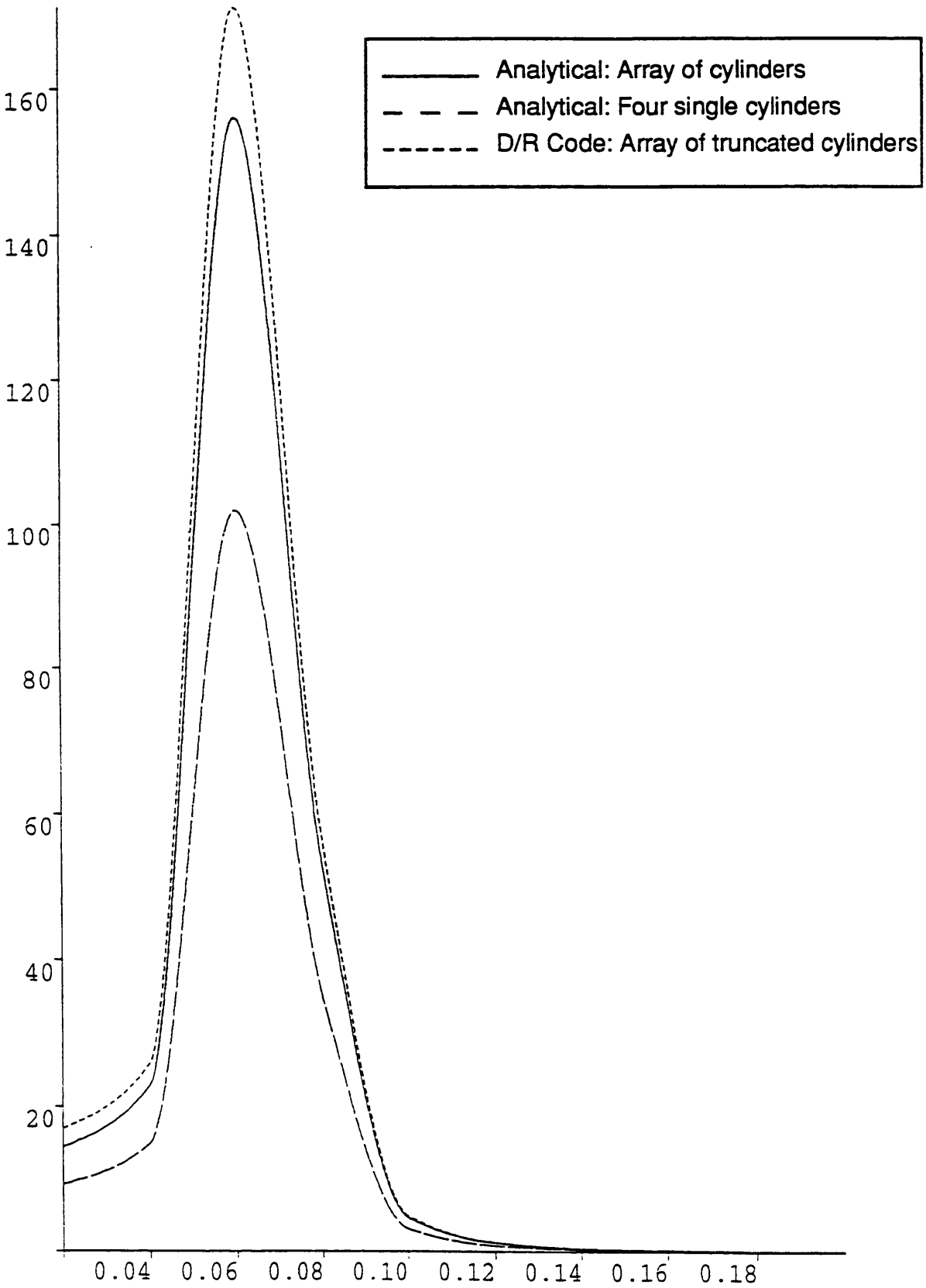

Figure 4.15

Significant Values of the Slowly Varying Drift Response

Surge

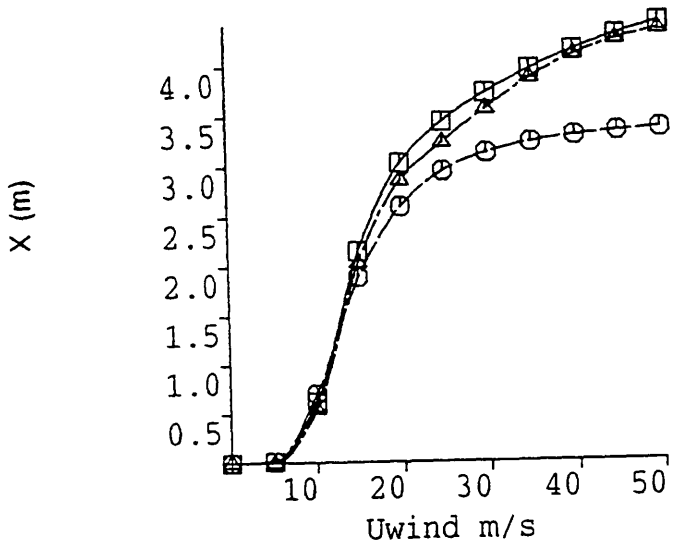

Figure 4.16

Pitch

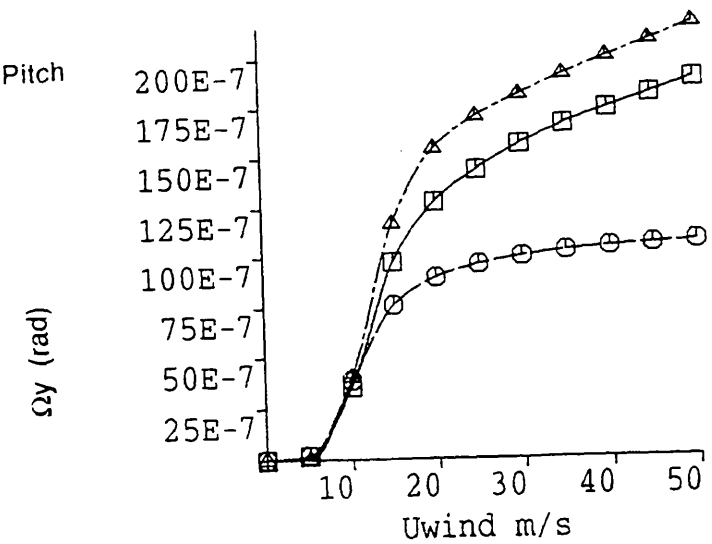

Figure 4.18

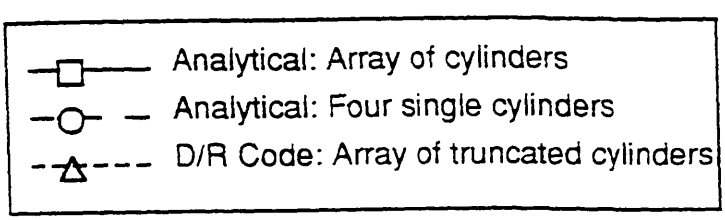

Slowly Varying Drift Pitch Response Spectra

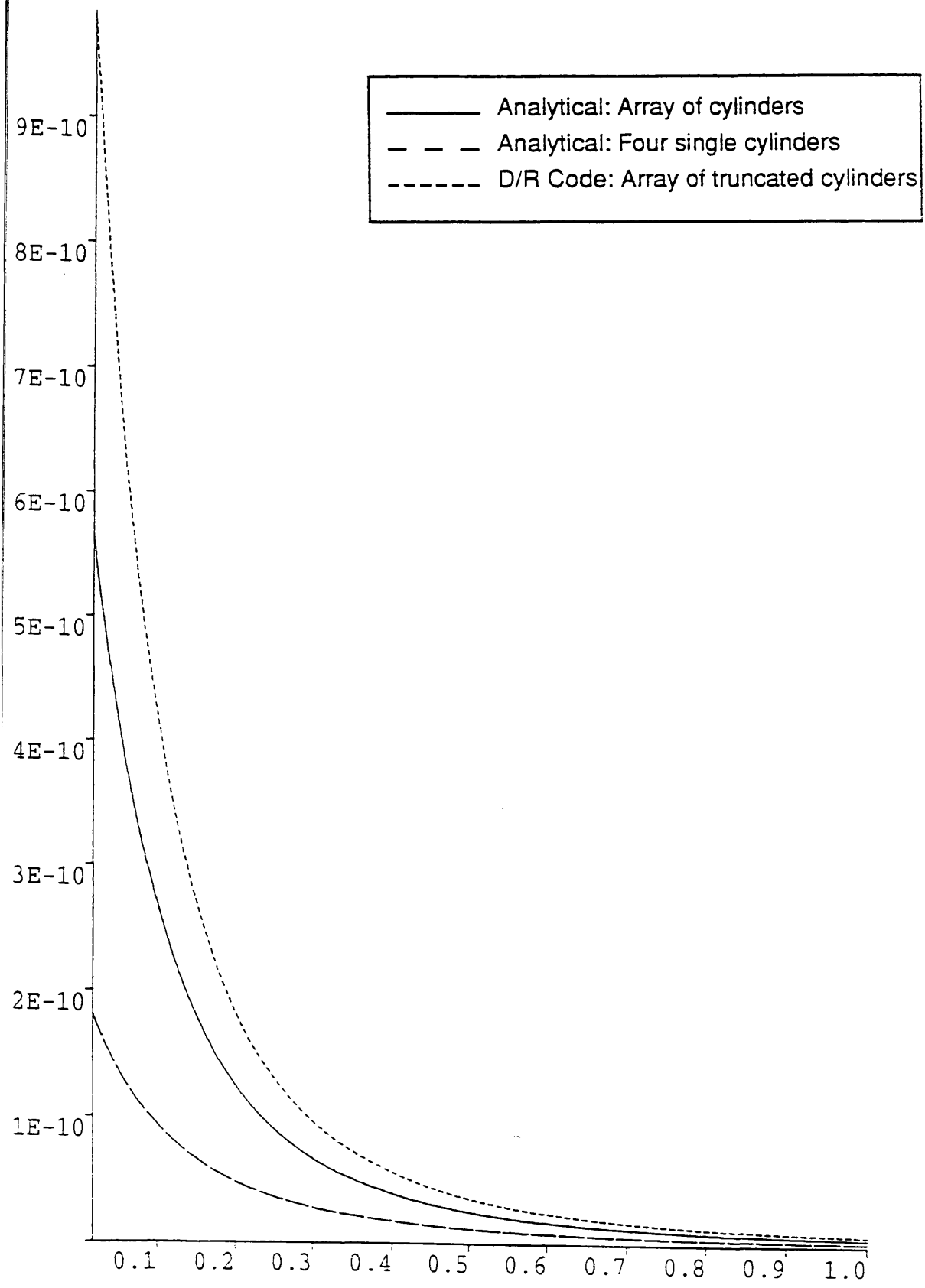

Figure 4.17

CHAPTER 5: WIND AND CURRENT

1. INTRODUCTION

Apart from the waves, two other environmental effects produce loading on offshore structures, the wind and the current. Their action should not be neglected since they can be rather important.

The wind loading can be decomposed into two components - a steady part and a slowly varying part. The steady wind force creates a steady offset of the structure. The varying force produces low frequency displacements. The second part is smaller in term of force amplitude. However, it could be important for TLP's in term of displacements, since it can excite the natural frequencies in surge and sway.

The current is quite a complicated phenomenon. A simplified formulation is used here. The current is considered as the results of tides, displacement of large volumes of water, and storm surge, surface effect due to the wind.

The first part introduces the wind effects on the TLP. Both steady and varying winds are accounted for. The forces and the displacements are calculated.

In the second part, the current effects are studied. The two different representations of the current that are used to calculate the forces and the displacements are compared.

2. WIND

In the first part of the study, the steady and varying force formulations are derived. They are then used to determine both steady and slowly varying displacements.

Five different wind spectrum formulations are presented to calculate the dynamic response. The displacement values are predicted using each of them and the results are compared. The aim is to determine the most suitable spectrum formulation for offshore structures.

2.1. WIND FORCES

The lift force due to the wind is very small and is neglected, only the drag force is considered.

The wind velocity can be divided into two parts:

$$V_w = \overline{V}_w + v_w \tag{2.1-1}$$

Where:

$\overline{V}_w$ is the mean wind speed
v_w is the fluctuating wind speed, representing the wind gusts.

The drag force due to the wind in the x direction is calculated as follows:

$$F_{wx} = \frac{1}{2}\rho_a C_d A_x \left(\overline{V}_w + v_w\right)^2 \cos^2\beta \tag{2.1-2}$$

Where:

ρ_a is the air density
C_d is the drag coefficient
A_x is projection area exposed to wind in x direction
β is direction of the wind

The force can also be divided in 2 parts:

$$F_{wx} = \overline{F}_{wx} + f_{wx} \tag{2.1-3}$$

The mean wind force:

$$\overline{F}_{wx} = \frac{1}{2}\rho_a C_d A_x \overline{V}_w^2 \cos^2\beta \tag{2.1-4}$$

and the fluctuating wind force:

$$f_{wx} = \rho_a C_d A_x \overline{V}_w v_w \cos^2\beta \tag{2.1-5}$$

The term consisting of $\frac{1}{2}\rho_a C_d A_x v_w^2 \cos^2\beta$ is neglected since it is very small compared to the others ($2v_w \overline{V}_w >> v_w^2$).

The wind velocity changes with the height z, the following formula can be used to describe these variations:

$$V_w(z) = V_w(10)\left(\frac{z}{10}\right)^{1/7} \tag{2.1-6}$$

Where $V_w(10)$ is the wind speed at 10m above the sea level.

To calculate the wind force, the loads should be integrated over the height of the structure to take the height variation into account.

The wind forces in the horizontal plane can be calculated as:

$$\overline{F}_{wx} = \frac{1}{2}\rho_a C_d D_{sy} \cos^2\beta \int_0^{H_s} \overline{V}_w^2(z)\,dz \tag{2.1-7}$$

$$f_{wx} = \rho_a C_d D_{sy} \cos^2\beta \int_0^{H_s} \overline{V}_w(z)\, v_w(z)\,dz \tag{2.1-8}$$

$$\overline{F}_{wy} = \frac{1}{2}\rho_a C_d D_{sx} \sin^2\beta \int_0^{H_s} \overline{V}_w^2(z)\,dz \tag{2.1-9}$$

$$f_{wy} = \rho_a C_d D_{sx} \sin^2\beta \int_0^{H_s} \overline{V}_w(z)\, v_w(z)\,dz \tag{2.1-10}$$

Where:

H_s: height of the structure
D_{sx} and D_{sy}: length of the structure in x and y directions.

Since no lift force is considered the force in heave is equal to 0.

$$\overline{F}_{wz} = 0 \qquad f_{wz} = 0 \tag{2.1-11}$$

The moments about the centre of gravity G are given by the following formula:

$$\overline{M}_{wx} = -\frac{1}{2}\rho_a C_d D_{sx} \sin^2\beta \int_0^{H_s} (z - Z_G)\,\overline{V}_w^2(z)\,dz \tag{2.1-12}$$

$$m_{wx} = -\rho_a C_d D_{sx} \sin^2\beta \int_0^{H_s} (z - Z_G)\,\overline{V}_w(z)\, v_w(z)\,dz \tag{2.1-13}$$

$$\overline{M}_{wy} = \frac{1}{2}\rho_a C_d D_{sy} \cos^2\beta \int_0^{H_s} (z - Z_G)\overline{V}_w^2(z)\,dz \qquad (2.1\text{-}14)$$

$$m_{wy} = \rho_a C_d D_{sy} \cos^2\beta \int_0^{H_s} (z - Z_G)\overline{V}_w(z)\,v_w(z)\,dz \qquad (2.1\text{-}15)$$

In the program, the integral is evaluated by dividing the structure into strips of small height where the wind velocity is assumed to be constant. The force on every strip is then added to obtain the total force.

2.2. DISPLACEMENT

2.2.1. Steady Displacement

The steady wind force induces a steady offset. The steady offset in the direction i is calculated as follows:

$$\overline{X}_{wi} = \frac{\overline{F}_{wi}}{K_i} \qquad (2.2\text{-}1)$$

Where K_i is the total stiffness of the system TLP/tendons in the direction i.

2.2.2. Fluctuating Wind Motion

Since every load is considered harmonic, the varying wind velocity can be written as:

$$v_w = |v_w| \sin \omega t \qquad (2.2\text{-}2)$$

As for the waves, the relation between the amplitude of the velocity and the frequency is given by a spectrum.

$$|v_w(\omega)|^2 = S_{wind}(\omega)\,d\omega \qquad (2.2\text{-}3)$$

Using the above equation, the response spectra can be calculated:

$$RS_{wi}(\omega) = S_{wind}(\omega)\left(\frac{f_{wi}}{v_w}\right)^2 Q_i^2(\omega) f_{ai}^2(\omega) \qquad (2.2\text{-}4)$$

Where f_{ai} is the aerodynamic admittance function which is introduced by Simiu et al [5.1]. It takes into account the departure from perfectly correlated flow:

$$f_{ai}(\omega) = \frac{1}{\left[1 + \frac{\omega\sqrt{A_i}}{\overline{V}_w(10)}\right]} \qquad (2.2\text{-}5)$$

Indeed, the formulation developed for the wind assumes a perfectly correlated flow. The wind field is supposed to be the same on every point of the structure. This is hardly the case in reality. One simple way to account for the variations of the perfectly correlated flow is to introduce the admittance f_a. A multiple point loading approach (See Kareem et al [5.2]) would give more accurate results. However, the method is quite complicated and does not present any real advantages in the case of a simplified geometry of the deck. This method should be used during the final design stage, when the geometry of the deck is well known and when more accurate results are needed.

2.3. WIND SPECTRA

Several wind spectrum formulations have been developed over the years. They are all based on wind measurements. However, some of them have been derived for civil engineering applications, and are based on measurements over land.

They may not be fully representative of the wind at sea, but they are used frequently in the design of offshore structures. One reason is that they were the only ones available at one time. However, new spectra have been developed recently, based on measurements at sea.

The response spectra of the varying wind are calculated with five different spectra and the results are compared in order to determine which one would be the more appropriate.

These spectra are:

- the Harris wind spectrum
- the Davenport wind spectrum
- the Kaimal wind spectrum
- the Ochi-Shin wind spectrum
- the Slettringen wind spectrum

2.3.1. The Harris wind spectrum

This spectrum has been derived by Harris [5.3] from land based data, but is widely used for the prediction of wind response of offshore structures.

$$S_{Harris}(f) = \frac{4 L_H \kappa \overline{V}_w(10)}{\left(2 + f'^2\right)^{5/6}} \tag{2.3-1}$$

Where:

L_H = 1200m at sea

$\kappa = 8 \cdot 10^{-4} + 6.4 \cdot 10^{-5} \overline{V}_w(10)$

$f' = \frac{f L_H}{\overline{V}_w(10)}$

$f = \omega / 2\pi$ is the varying wind frequency

2.3.2. The Davenport wind spectrum

This spectrum has been developed by Davenport [5.4] for land structures, and is considered to represent wind at sea not so well. In particular, the energy at low frequencies is underestimated.

However, a number of designers in the offshore industry still use it.

$$S_{Davenport}(f) = \frac{4 L_H^2 \kappa f}{\left(2 + f'^2\right)^{4/3}} \tag{2.3-2}$$

Where all the symbols have already been defined.

2.3.3. The Kaimal wind spectrum

This spectrum is very revelant since it has been derived by Kaimal [5.5] from sea based data:

$$S_{Kaimal}(f) = \frac{200 \kappa \left(f' \overline{V}_w(10)\right)^2}{f\left(1 + f'^2\right)^{4/3}} \tag{2.3-3}$$

Where:

$$f' = \frac{f z}{\overline{V}(z)}$$

Unlike the others this spectrum is function of the height z. z is taken as the centre of the surface exposed to wind.

2.3.4. The Ochi-Shin wind spectrum

This spectrum is based on data measured over a sea-way. It has been developed recently. The formulation has been given by Ochi and Shin [5.6] in 1988.

$$S(f)=583\frac{\kappa\overline{V}_w^2(10)f'}{f} \quad \text{for} \quad 0\le f'\le 0.003$$

$$S(f)=420\frac{\kappa\overline{V}_w^2(10)f'^{0.7}}{f\left(1+f'^{0.35}\right)^{11.5}} \quad \text{for} \quad 0.003\le f'\le 0.1 \qquad (2.3\text{-}4)$$

$$S(f)=838\frac{\kappa\overline{V}_w^2(10)f'}{f\left(1+f'^{0.35}\right)^{11.5}} \quad \text{for} \quad f'\ge 0.1$$

Where:

$$f'=\frac{f\,z}{\overline{V}(z)}$$

Like the Kaimal formulation, the spectrum is a function of the height z. The first part of the spectrum (for f' < 0.003) is just an artificial extension of the spectrum since wind velocities cannot be measured for such low frequencies.

2.3.5. The Slettringen wind spectrum

This is the more recent of the wind spectrum presented here. It has been developed from measurement taken at sea offshore Norway. This spectrum should be considered for offshore structures designed for the North Sea.

It is given as a reference by the NPD [5.7].

$$S_{Slett}(f)=\frac{320\left(\frac{\overline{V}_w(10)}{10}\right)^2\left(\frac{z}{10}\right)^{0.45}}{\left(1+f'^n\right)^{\frac{5}{n}}} \qquad (2.3\text{-}5)$$

Where:

$$n=0.468$$

$$f'=172\,f\left(\frac{z}{10}\right)^{\frac{3}{4}}\left(\frac{\overline{V}_w(10)}{10}\right)^{-0.79}$$

2.4. RESULTS

To calculate the wind forces, a simplified geometry of the deck has been adopted. The geometry considered for the wind calculation is presented below.

Geometry of the surface exposed to wind

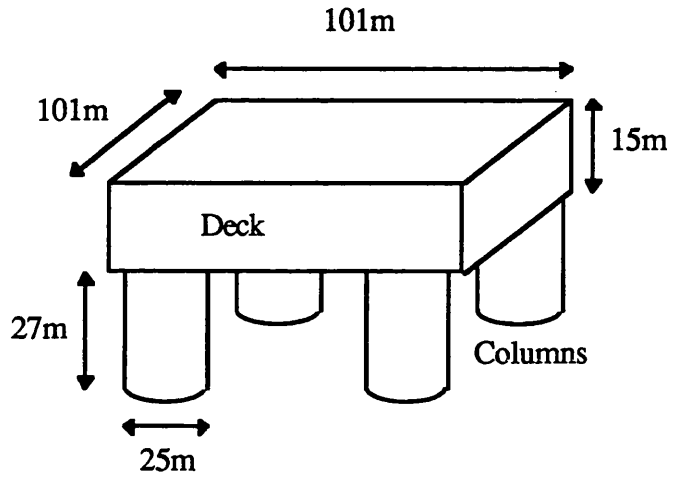

The geometrical idealisation of the deck shown above yields an approximate offset due to the wind.

The response spectra calculated with the different wind spectrum formulation are also compared.

Following the API recommendations [5.8], the drag coefficients are taken as 0.5 for the columns and 1.5 for the deck.

The area is divided into horizontal strips and the forces are computed on each of them taking into account the variation of the wind velocity with the height. (See section 2.1).

For the calculations carried out below, a zero degree heading wind has been chosen.

2.4.1. Steady response

Table 5.1 gives the steady wind displacement, in surge and pitch as a function of the wind velocity.

For high velocity winds, the surge steady displacement due to wind largely dominates the displacement due to the steady drift and the current. For lower velocity, the force due to the wind is rather small compare to the two other phenomena. The steady wind has to be calculated carefully in extreme weather conditions since it is the more important steady phenomenon.

In pitch, the importance of the wind is less significant. This is largely due to the high level of the centre of gravity of the Snorre TLP, which decreases the moment arm. One should note that in the case of the moments, the effects of the wind and the steady drift and the current cancel each other.

2.4.2. Dynamic response

The different wind gust spectra are plotted in Figures 5.1 and 5.2 for the mean wind speed of 20 and 50 m/s. Whilst they show a very good agreement at high frequencies, they present very large differences in terms of shape and values for low frequencies.

One should look closely at the region between 0.04 and 0.1 rad/s. Indeed, it is this part of the spectra that excite the natural frequencies in the horizontal plane, and produces the bigger displacements of the TLP.

The Ochi-Shin spectrum gives very high response values compared to those obtained from other spectra. The Slettringen spectrum presents a similar shape. This spectrum can reach high values at low frequencies, but is comparable to the Kaimal spectrum for higher frequencies.

The Harris spectrum and the Kaimal spectrum present quite similar shapes, although the latter yields smaller response values.

The Davenport spectrum is the only spectrum which approaches zero at low frequencies. It seems to underestimate the energy carried by the wind at low frequencies.

One should note, in Figure 5.2, the flat region of the Ochi-Shin spectrum. This part does not represent any physical phenomenon. In this region, the frequencies are too low to obtain any reliable measurements. Therefore the spectrum has been extended arbitrarily by a straight line. This implies that we are not able to model the actual wind energy distribution in the low frequency region which is important for accurate prediction of the motion response due to dynamic wind. The differences experienced due to the use of different wind spectra become more predominant as the wind velocity increases.

Figures 5.3 and 5.4 present the surge response spectra of the TLP due to dynamic wind forces. It is very clear from these figures that the main response appears at the natural frequency (0.06 rad/s). The difference between the response clearly increases as the wind velocity increases. Higher response values are obtained from the Ochi-Shin and the Slettringen spectra.

These figures can be correlated with Table 5.2 that presents the significant values of the response spectra for different wind velocities. The spectra present different behaviour depending on the wind velocity. The Ochi-Shin spectrum always gives the highest motion responses. However, the Slettringen spectrum gives smaller motion responses than the Harris spectrum for low wind velocities. Whereas for the wind speed greater than 20 m/s, the Slettringen spectrum yields larger response values. A similar kind of behaviour can be observed between the Kaimal and Davenport spectra. The Kaimal spectrum gives higher response values for high velocity winds.

The differences in term of significant values found in this study are large for high velocity wind, but they can be correlated with the calculations carried out by Wichers [5.9]. From the calculation of wind loads on a tanker, Wichers found a factor of 1.5 between the significant values of the response calculated with the Ochi-Shin and the Harris spectra, for 30 m/s mean wind.

Figures 5.5 and 5.6 show the pitch response spectra. The dynamic wind does not have the same importance for pitch response predictions as it has for surge response.

The natural frequency is in the high frequency region (over 2 rad/s), and is not excited by the dynamic wind. The response is then quite small.

Table 5.3 presents the significant pitch response values. They vary from one spectrum to another, but not in such an extend as in surge.

Finally, one should note that the significant motion response values due to dynamic wind are of the same order of magnitude as the displacement values of the steady wind. They can even be bigger in surge for high wind velocities. Thus, the dynamic wind response cannot be neglected in predicting the behaviour of compliant structures such as a TLP.

The choice of a correct wind spectrum is not easy, due to significant differences between the different models. However, since the dynamic wind behaviour is poorly modelled, conservative models should be used. In this case, the Ochi-Shin and Slettringen spectra appear to be an appropriate choice. Furthermore, they are the more recently developed spectra, and are based on sea measurements.

3. CURRENT

The current is a complicated phenomenon. A series of simplifications is used to model the current. The current occurs as the result of the tide and storm surge. The velocity profile is considered, constant in time. Thus, only the steady drag forces are taken into account, and the current loads can be calculated independently from the wave forces.

Two simplified geometries of the velocity profile are used and the displacement values obtained using two different current profiles are compared. The first geometry is based on a velocity profile constant over the water depth, and the second is based on a velocity profile varying over the water depth which approximates the effects of the storm surge and the tides. These current profile definitions are given in the guidance notes of the Department of Energy [5.10].

3.1. CONSTANT VELOCITY PROFILE

The current force in the x direction is calculated as follows:

$$F_{cx} = \frac{1}{2}\rho C_d A_x . \overline{U}_c^2 \cos^2\theta \qquad (3.1\text{-}1)$$

Where:

$\overline{U}_c = \overline{U}_t + \overline{U}_s$: constant current velocity.
$\overline{U}_t$: mean tidal current velocity
$\overline{U}_s$: mean storm surge current velocity
C_d: drag coefficient
θ: direction of current
A_x: surface exposed to current in x direction
ρ: water density

Similarly, for the y direction

$$F_{cy} = \frac{1}{2}\rho C_d A_y . \overline{U_c^2} \sin^2\theta \qquad (3.1\text{-}2)$$

There is no component of the force in the vertical direction z.

$$F_{cz} = 0 \qquad (3.1\text{-}3)$$

The moments in roll and pitch are:

$$M_{cx} = (Z_G - Z_B)F_{cy} \qquad (3.1\text{-}4)$$

$$M_{cy} = -(Z_G - Z_B)F_{cx} \qquad (3.1\text{-}5)$$

Where:

Z_B: Z co-ordinate of the buoyancy centre.
Z_G: Z co-ordinate of centre of gravity G.

3.2. VARYING VELOCITY PROFILE

The varying current velocity profile is the sum of the profiles of the storm surge current and the tidal current. The resulting form of the profile is presented in the sketch below. The storm surge current, due to wind, presents a higher velocity near the free surface. The tidal current velocity decreases near the bottom of the sea. This formulation of the current is not directly related to the physic of the problem, it is an empirical formulation based on measurements at sea.

Current Velocity Profile:

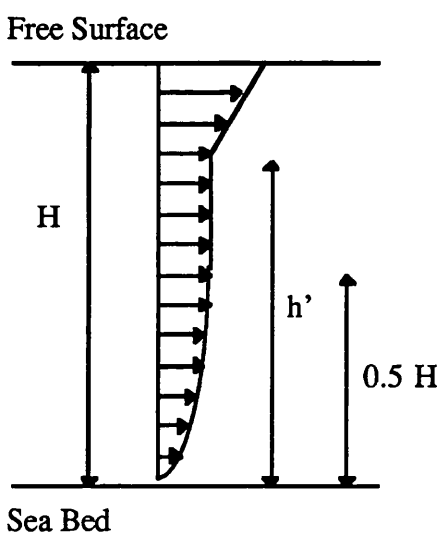

3.2.1. Tidal current

The tidal current velocity profile is defined by reference [5.10] as follows:

$$U_t(s) = \left(\frac{s}{0.32H}\right)^{1/7} \overline{U}_t \quad \text{for} \quad 0 \le s \le 0.5H$$
$$U_t(s) = 1.07\,\overline{U}_t \quad \text{for} \quad 0.5H \le s \le H \qquad (3.2\text{-}1)$$

Where:

$U_t(s)$: the velocity of the tidal current at a height s above the sea-bed

$\overline{U}_t$: depth-averaged speed of the tidal current

H: water depth

3.2.2. Storm surge current

The storm surge current velocity profile is defined by reference [5.10] as follows:

$$U_s(s) = \left(\frac{s-h'}{10}\right)U_W + \overline{U}_s \quad \text{for} \quad h' \le s \le H$$
$$U_s(s) = \overline{U}_s \quad \text{for} \quad 0 \le s \le h' \qquad (3.2\text{-}2)$$

Where:

$U_s(s)$: storm surge current velocity at a height s above the sea-bed

$\overline{U}_s$: depth-averaged velocity of the storm surge current

$h' = H - 10(U_w - \overline{U}_s)$ height above the sea-bed at which the current profile changes slope

U_W = 0.03xWind speed

In the case of $\overline{U}_s > U_W$, the velocity profile becomes:

$$U_s(s) = \overline{U}_s \quad \text{for} \quad 0 \le s \le H \qquad (3.2\text{-}3)$$

In order to keep the value of the depth averaged velocity constant, the following multiplying factor has to be introduced throughout the bilinear profile.

$$\left[\frac{5(U_W - \overline{U}_s)^2}{H \cdot \overline{U}_s} + 1\right]^{-1} \qquad (3.2\text{-}4)$$

3.2.3. Forces

Due to the varying current profile, the formulation of the forces becomes:

$$F_{cx} = \frac{1}{2}\rho C_d \cos^2\theta \int_{A_x} \left(Ut(s) + Us(s)\right)^2 dy\, ds \tag{3.2-5}$$

$$F_{cy} = \frac{1}{2}\rho C_d \sin^2\theta \int_{A_y} \left(Ut(s) + Us(s)\right)^2 dx\, ds \tag{3.2-6}$$

$$F_{cz} = 0 \tag{3.2-7}$$

$$M_{cx} = -\frac{1}{2}\rho C_d \sin^2\theta \int_{A_y} (s - H - Z_G)\left(Ut(s) + Us(s)\right)^2 dx\, ds \tag{3.2-8}$$

$$M_{cy} = \frac{1}{2}\rho C_d \cos^2\theta \int_{A_x} (s - H - Z_G)\left(Ut(s) + Us(s)\right)^2 dy\, ds \tag{3.2-9}$$

In order to calculate the above integration, the method used for the wind force formulations, is used. The structure exposed to the current is divided into small strips where the velocity is assumed to be constant. The total force is obtained by summing the forces on all the strips.

3.3. STEADY RESPONSE

Since the current velocity is constant in time, the displacement in the direction i is given by the following formula:

$$X_{ci} = \frac{F_{ci}}{K_i} \tag{3.3-1}$$

Where K_i is the total stiffness of the system.

3.4. DISCUSSION OF THE RESULTS

Table 5.4 and 5.5 show the steady displacements in surge and roll induced by the current at seven different locations in the North Sea (see Figure 5.7). For these locations, the following data are obtained from measurements at sea:

- $\overline{U}_t$ the average tidal current velocity over the water depth

- $\overline{U}_s$ the average storm surge current velocity over the water depth

- $\overline{U}_{wd}$ the hourly mean wind velocity

The results are given using methods based on a constant velocity profile, and a varying velocity profile.

The constant current velocity is the sum of the average velocity over the water depth of the tidal current and the storm surge current.

$$\overline{U}_{cur} = \overline{U}_t + \overline{U}_s \tag{3.4-1}$$

The direction of the current is taken as zero degree for all the computations.

3.4.1. Surge

Two different current profile definitions yield displacements which differ from each other from 26.5% to 6.43%. The following explains why the correlation between the two methods varies so much.

The tidal velocity can be written as:

$$U_t = \overline{U}_t + \Delta U_t \tag{3.4-2}$$

Where:

$$\Delta U_t = 0.07\,\overline{U}_t$$

Similarly, the storm surge velocity becomes:

$$U_s = \overline{U}_s + \Delta U_s \tag{3.4-3}$$

Where:

$$\Delta U_s = \left(\frac{s - h'}{10}\right).U_w$$

$$h' = H - 10\left(U_W - \overline{U}_s\right)$$

We neglect the factor:

$$\left[\frac{5(U_W - \overline{U}_s)^2}{H \cdot \overline{U}_s} + 1\right]^{-1}$$

since $H_w.\overline{U}_s >> 5.\left(U_w - \overline{U}_s\right)^2$

If we neglect the second order term, the force becomes:

$$F_c = \overline{F}_c + \Delta F_t + \Delta F_s \tag{3.4-4}$$

Where:

$$\Delta F_t = \rho C_d A_x (\overline{U}_s + \overline{U}_t) \Delta U_t \tag{3.4-5}$$

$$\Delta F_s = \rho C_d A_{xs} (\overline{U}_s + \overline{U}_t) \Delta U_s \tag{3.4-6}$$

Where:

A_x is the total area exposed to current

A_{xs} is the area exposed to the modified profile of storm surge current, depending on variable h'.

Table 5.4 gives the values of displacements due to ΔF_t and ΔF_s

$$\Delta X_t = \frac{\Delta F_t}{K_x} \qquad \Delta X_s = \frac{\Delta F_s}{K_x} \tag{3.4-7}$$

These values are also compared with the displacement due to varying profile current, and expressed as a percentage:

$$\frac{\Delta X_t}{X_{vp}} \quad \text{and} \quad \frac{\Delta X_s}{X_{vp}}$$

Where X_{vp} is the displacement due to the varying profile current.

The column called "verification" gives the value $X_{cp} + \Delta X_t + \Delta X_s$, where X_{cp} is the displacement due to the constant profile current. The correlation with the displacement due to the varying profile current is good. The values are a little higher than X_{vp} because the correcting factor is neglected in the storm surge profile.

Large variations between the results given by the two current profiles are not due to the tidal current. Indeed, the largest displacement ΔX_t, occurring at location 3, corresponds with a small difference between the two computations.

The differences between the results given by the two methods, are mainly due to the storm surge current. These differences seem to be correlated with the factor $U_w - \overline{U}_s$ which is used to calculate the height h' over which the storm surge current has a greater velocity profile. High values of the factor give large differences between the results of the two methods.

However, the biggest variations are observed when the response of the TLP to the current is at the smallest value. In these cases, the displacement due to the current is

relatively small compared to the displacement due to the wind. Thus, the error is finally small when compared to the total steady displacement. The two profiles do not give such a big difference in terms of total steady surge displacement.

3.4.2. Pitch

The same comparison has been carried out for pitch. The results can be seen in Table 5.5. The difference between the two methods varies from 19% to 15%. The variation between the two methods is not so much due to the storm surge. Indeed, the variation due to the tide is now quite important because it takes place at a larger water depth where the moment arm is larger. The steady displacements in pitch are small due to the high stiffness of the system. However, in pitch, the current has the largest contribution to the steady displacement compared to the wave drift and wind.

This is due to the particular geometry of the Snorre TLP. Because of its high centre of gravity (13.5 m above the sea level), which gives a large moment arm.

4. CONCLUSION

Wind and current load calculations for a TLP structure have been presented in this chapter.

The steady wind calculations can easily be carried out. However, the modelling of dynamic wind is more complex. The choice of a wind gust spectrum requires a careful consideration. Indeed, the spectrum formulations are all very different and give large variations in the results from one to another. Three main reasons lead to the choice of the Ochi-Shin or the Slettringen spectra. They give more conservative results. They were derived from recent measurements and finally, the measurements were obtained at sea.

A multiple point loading method for the wind load calculations could be considered for more precise results.

The study has shown that the wind effects on a TLP should not be neglected. In extreme weather conditions, the mean wind is responsible for the largest part of the offset of the structure.

In the same weather conditions, the varying wind loading creates a high surge response. The dynamic wind response is, at least, as important as the steady response.

In surge, the geometry of the current profile does not seem to be really important.

The differences are larger in pitch. In the case of the Snorre platform, the steady response in pitch is dominated by the current load. This is purely due to the geometry of the TLP. The centre of gravity being high above the water level, the current forces yield large pitching moments due to a large moment arm.

In other geometrical forms, it is very likely to have a steady pitch displacement dominated by the wind effects. The steady wave drift is not likely to produce large moments, because forces mainly act near the free surface level.

REFERENCES OF CHAPTER 5

[5.1] Simiu E., Scanlan R.H., 1978, Wind effects on structures, Wiley Interscience Publication.

[5.2] Kareem A., Dalton C , 1982, Dynamic effects of wind on Tension Leg Platforms, OTC.

[5.3] Harris R.I., 1970, The nature of the wind, Proc. of the seminar on the modern design of wind sensitive structures, The Inst. of Civil Engineers.

[5.4] Davenport A.G., 1967, Gust loading factors, Journal of the Structural Division, ASCE, Vol.93, no.ST3.

[5.5] Kaimal J.C. et al, 1972, Spectral characteristics of surface layer turbulence, Journal of Royal Meteorological Society, Vol.98.

[5.6] Ochi M.K., Shin Y.S., 1988, Wind turbulent spectra for design consideration of offshore structures, Proc. of the Offshore Technology Conference.

[5.7] Acts, regulations and provisions for the petroleum activity, 1994, Vol.2, NPD.

[5.8] Draft Recommended Practice for Planning, Designing and Constructing Fixed Offshore Platforms- Load and Resistance Factor Design, API Recommended Practice 2A-LRFD (RP 2A-LRFD) ,1989, First Edition.

[5.9] Wichers J.E.W., 1992, The effect of wind spectra on the low frequency motion of a moored tanker, Maritime Research Institute Netherlands.

[5.10] Offshore installations, 1990: Guidance on Design, Construction and Certification, Department of Energy, Fourth Edition, London.

Wind Spectra for a 20m/s Wind

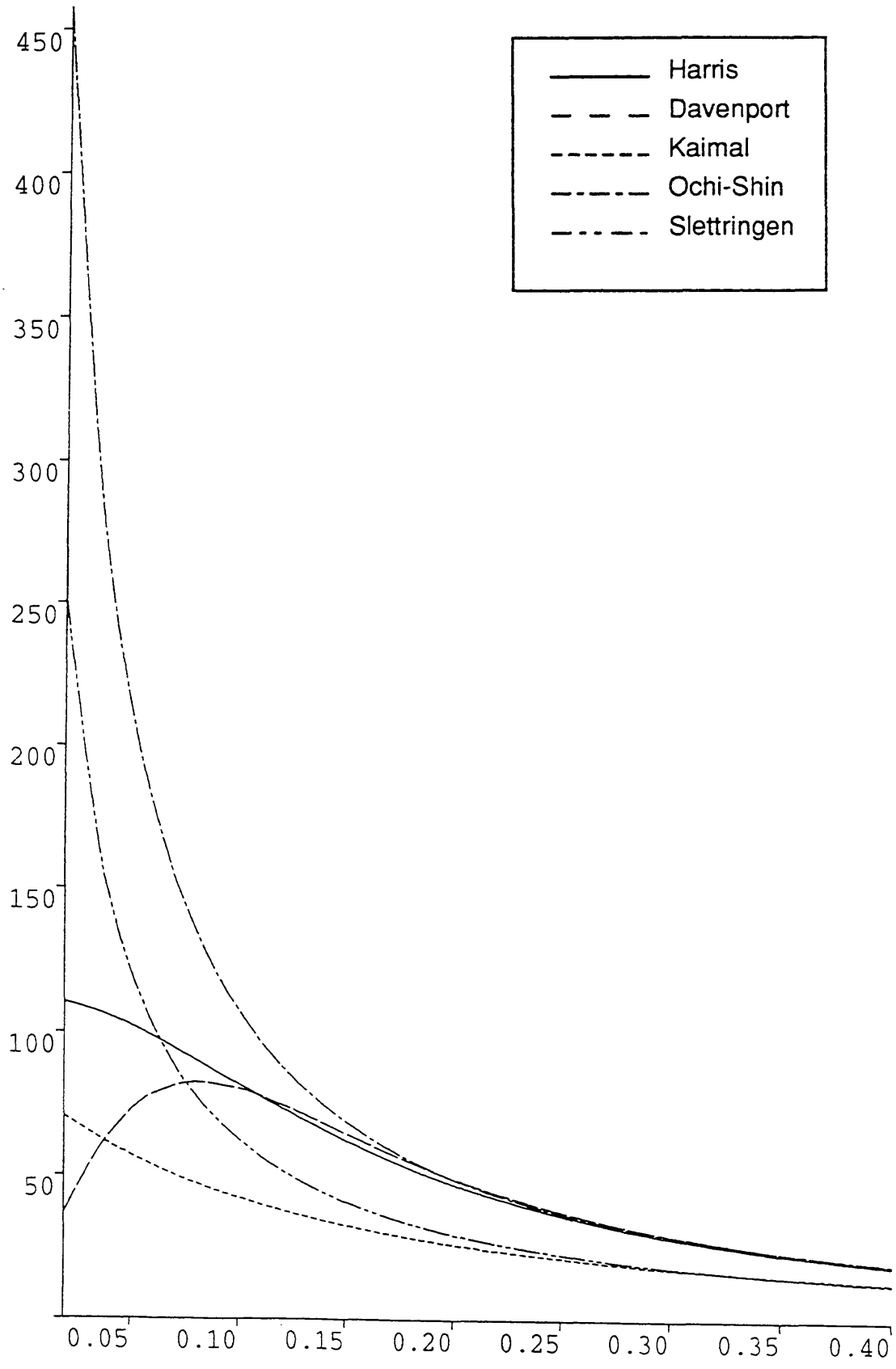

e 5.1

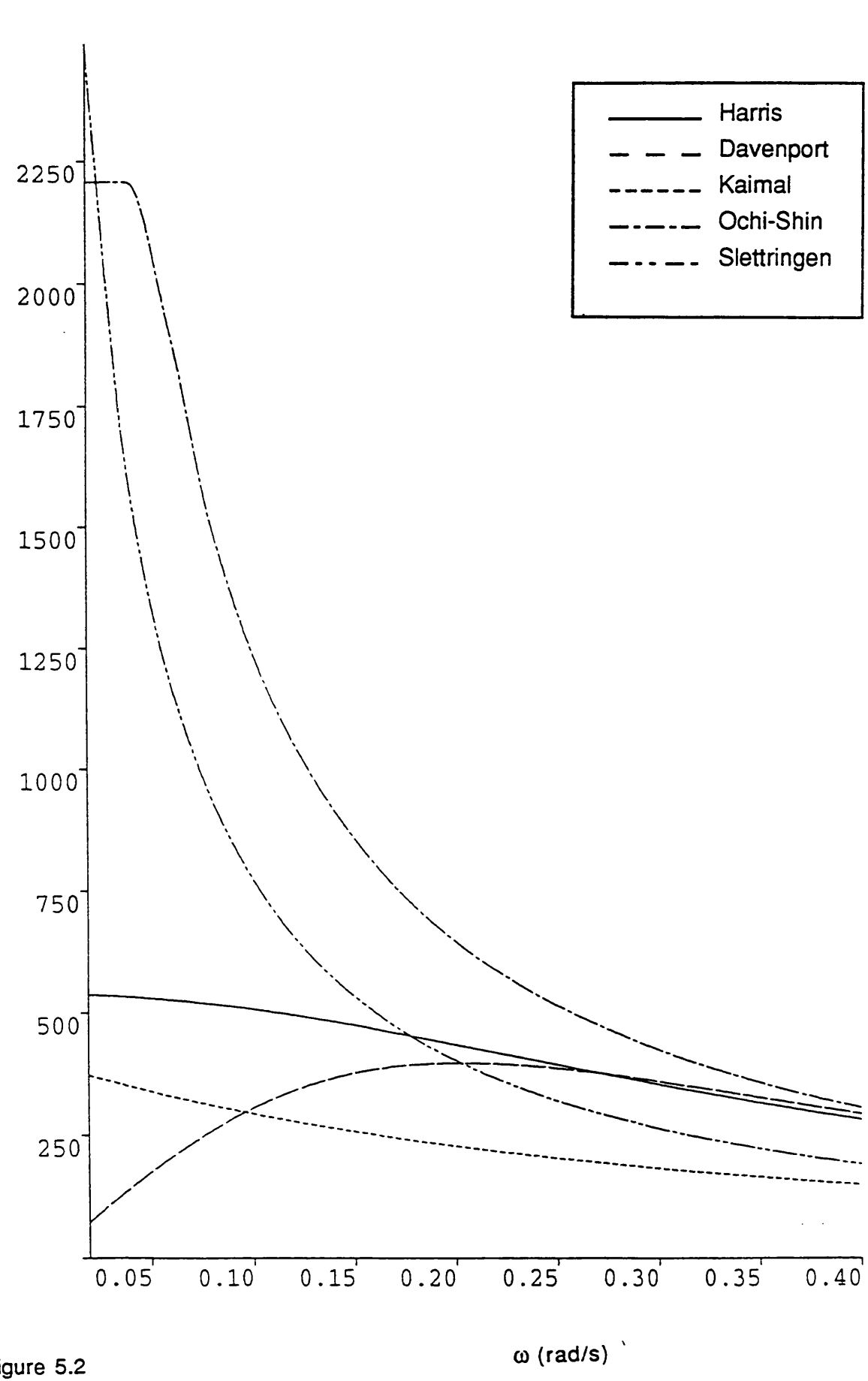
Wind Spectra for a 50m/s Wind
Harris
Davenport
Kaimal
Ochi-Shin
Slettringen
2250
2000
1750
1500
1250
1000
750
500
250
0.05
0.10
0.15
0.20
0.25
0.30
0.35
0.40
ω (rad/s)

Figure 5.2

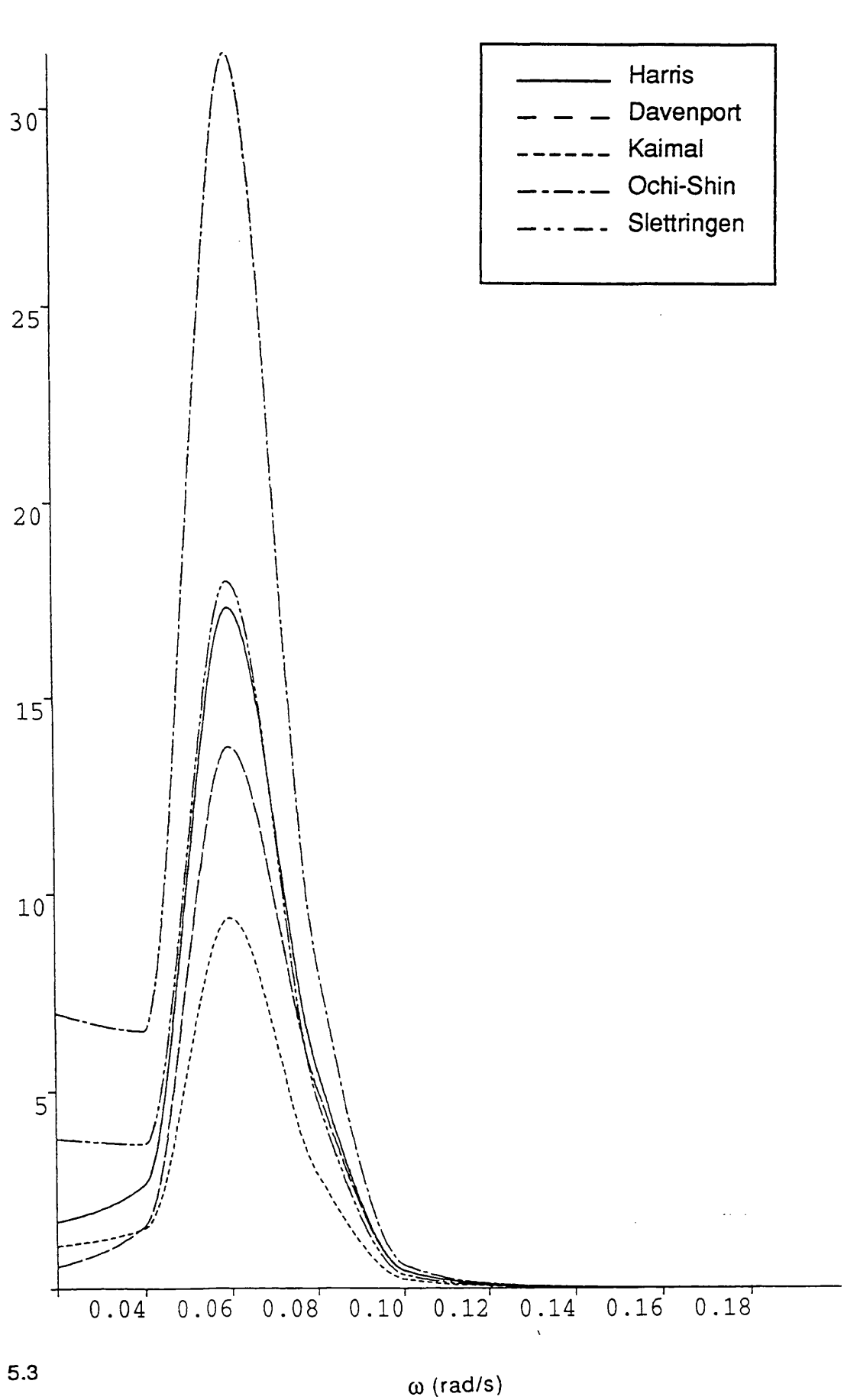
Surge Response Spectra
due to Wind Gusts (20m/s Wind)
Harris
Davenport
Kaimal
Ochi-Shin
Slettringen
30
25
20
15
10
5
0.04
0.06
0.08
0.10
0.12
0.14
0.16
0.18
ω (rad/s)

Figure 5.3

Surge Response Spectra due to Wind Gusts (50m/s Wind)

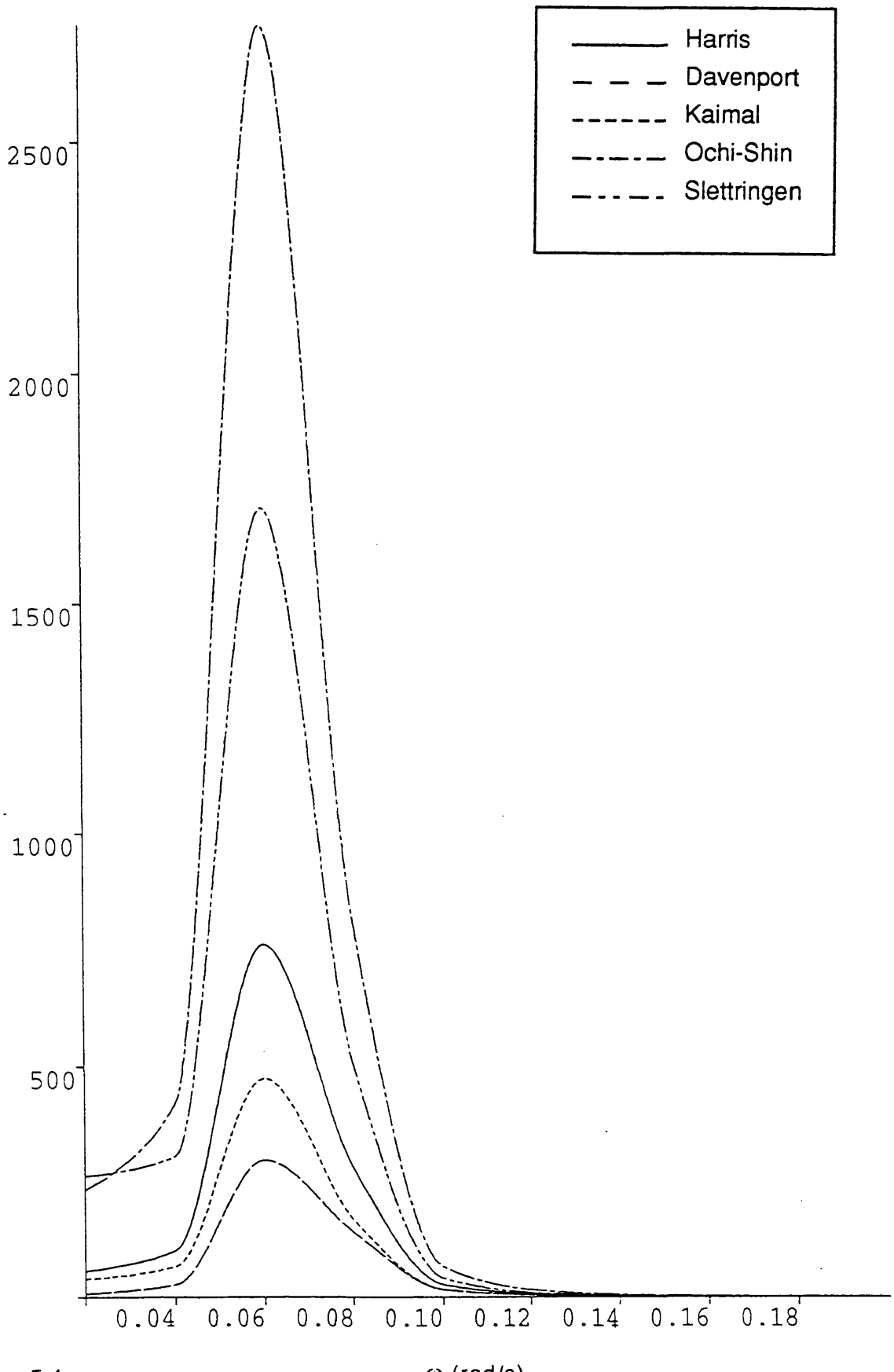

ıre 5.4

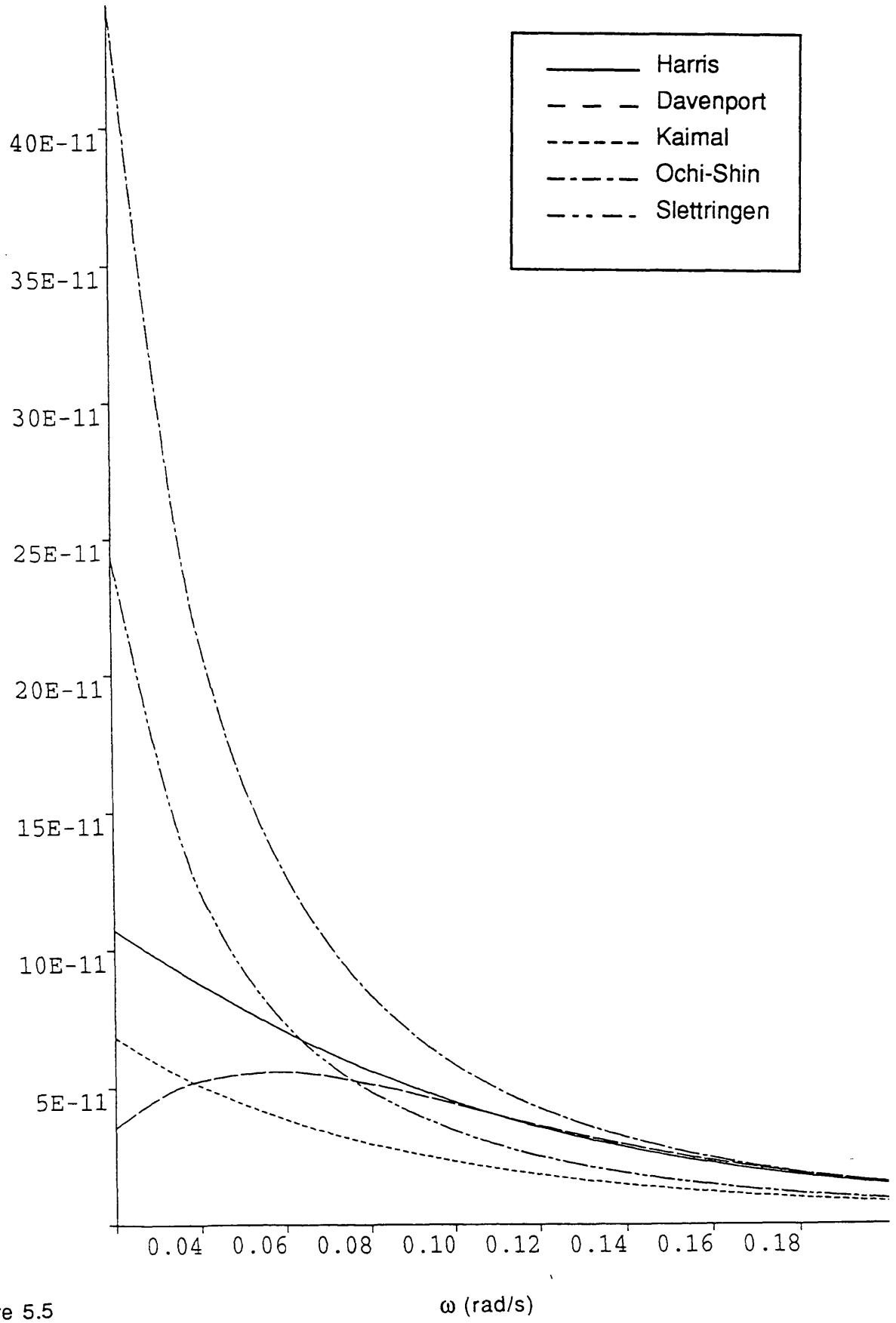
Pitch Response Spectra
due to Wind Gusts (20m/s Wind)
Harris
Davenport
Kaimal
Ochi-Shin
Slettringen
40E-11
35E-11
30E-11
25E-11
20E-11
15E-11
10E-11
5E-11
0.04
0.06
0.08
0.10
0.12
0.14
0.16
0.18
ω (rad/s)

Figure 5.5

Pitch Response Spectra due to Wind Gusts (50m/s Wind)

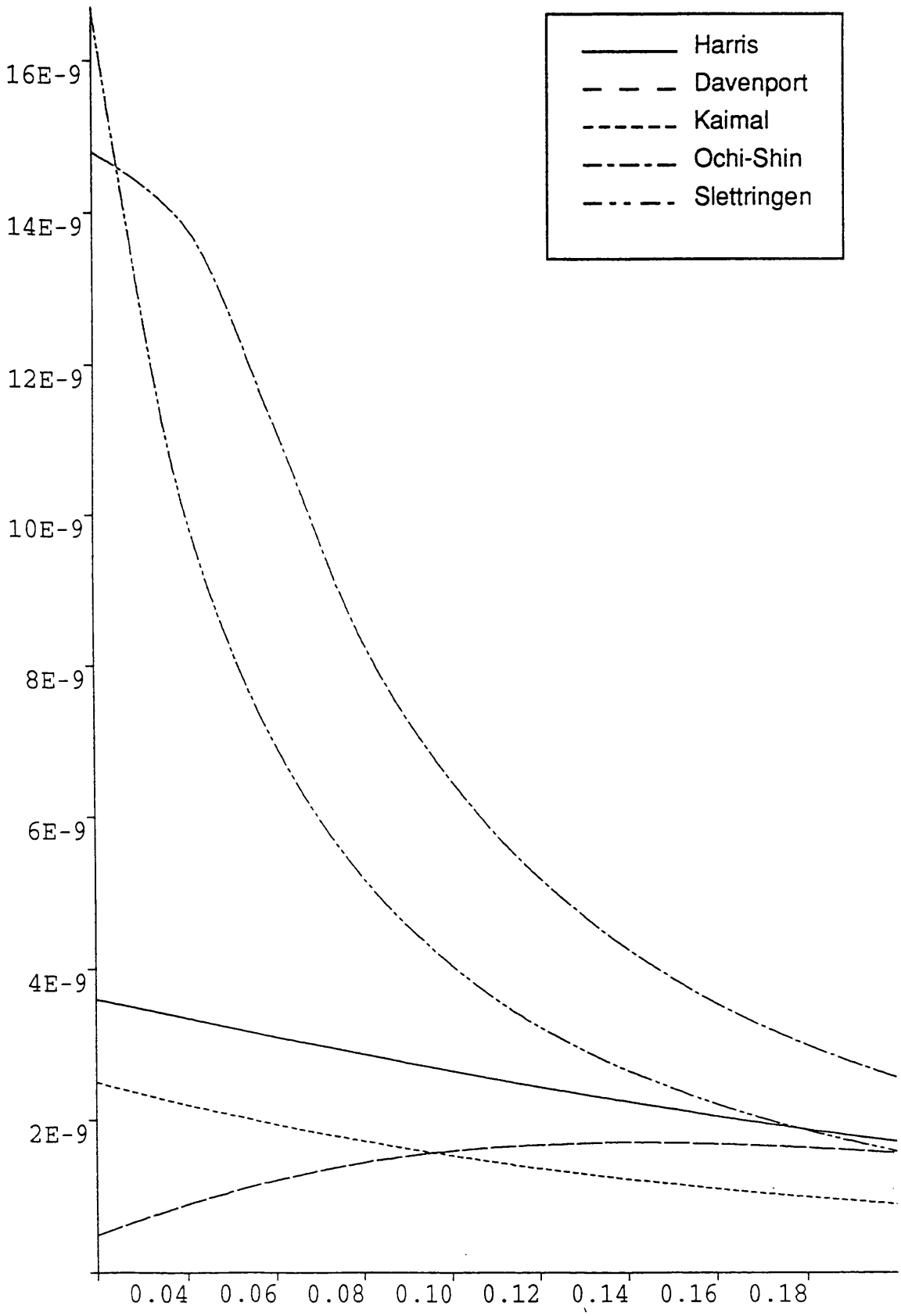

Figure 5.6

STEADY DISPLACEMENT

Uwind (m/s)	5	10	15	20	25	30	35	40	45	50
X0 (m)	8.66E-02	0.346	0.779	1.38	2.16	3.12	4.24	5.54	7.01	8.66
W0 (10^-5 rad)	0.0814	0.326	0.733	1.3	2.036	2.93	3.99	5.21	6.39	8.14

Table 5.1

SURGE SIGNIFICANT VALUES (m)

Uwind (m/s)	5	10	15	20	25	30	35	40	45	50
Harris	4.75E-02	0.282	0.727	1.37	2.21	3.24	4.46	5.87	7.465	9.25
Davenport	0.0481	0.281	0.688	1.22	1.85	2.55	3.33	4.16	5.045	5.98
Kaymal	0.036	0.204	0.528	1.01	1.65	2.46	3.42	4.55	5.831	7.28
Ochi Shin	0.0493	0.319	0.906	1.87	3.23	5.05	7.33	10.12	13.34	17.06
Slettringen	0.0308	0.223	0.667	1.41	2.49	3.94	5.77	8	10.65	13.74

Table 5.2

PITCH SIGNIFICANT VALUES (10^-5 rad)

Uwind (m/s)	5	10	15	20	25	30	35	40	45	50
Harris	0.0212	0.119	0.319	0.641	1.1	1.72	2.51	3.48	4.65	6.04
Davenport	0.0212	0.115	0.298	0.587	0.98	1.54	2.24	3.09	4.123	5.34
Kaymal	0.0159	0.0891	0.239	0.483	0.834	1.3	1.91	2.65	3.544	4.6
Ochi Shin	0.0231	0.143	0.406	0.848	1.49	2.36	3.49	4.89	6.547	8.5
Slettringen	0.0142	0.1	0.3	0.644	1.16	1.87	2.79	3.93	5.329	6.98

Table 5.3

SURGE DISPLACEMENT DUE TO CURRENT: a comparison between constant and varying profile

		Location 1	Location 2	Location 3	Location 4	Location 5	Location 6	Location 7
Tide velocity	Ut (m/s)	0.2	0.4	0.6	0.2	0.2	0.3	0.6
Storm Surge Velocity	Us (m/s)	0.4	0.6	0.8	0.6	0.4	0.4	0.8
Wind Velocity	Uwd (m/s)	40	39	39	38	37	36.5	34
Constant Current Vel.	Ucur (m/s)	0.6	1	1.4	0.8	0.6	0.7	1.4
Surge Displacement	Constant profile (m): Xcp	1.17	3.248	6.37	2.08	1.17	1.59	6.37
	Varying profile (m): Xvp	1.44	3.57	6.83	2.25	1.37	1.85	6.78
Surge displacement difference (%): (Xvp-Xcp)/Xcp		22.9	9.8	7.2	8.2	17.1	16.1	6.4
Displacement:	ΔXt (m)	0.055	0.182	0.382	0.073	0.055	0.095	0.382
	ΔXs (m)	0.217	0.184	0.108	0.132	0.171	0.191	0.038
Verification: Xcp+ΔXt+ΔXs (m)		1.44	3.61	6.86	2.28	1.40	1.88	6.79
Importance of profile variation:								
due to tide	ΔXt/Xvp (%)	3.69	5.05	5.58	3.20	3.90	5.11	5.63
due to storm surge	ΔXs/Xvp (%)	15.10	5.15	1.59	5.86	12.48	10.35	0.56
Importance of the factor Uw-Us:								
	(Xvp-Xcp)/Xcp (%)	22.9	9.8	7.2	8.2	17.1	16.1	6.4
	Uw-Us (m/s)	0.8	0.57	0.37	0.54	0.71	0.695	0.22

Table 5.4

ROLL DISPLACEMENT DUE TO CURRENT: a comparison between constant and varying profile

		Location 1	Location 2	Location 3	Location 4	Location 5	Location 6	Location 7
Tide velocity	Ut (m/s)	0.2	0.4	0.6	0.2	0.2	0.3	0.6
Storm Surge Velocity	Us (m/s)	0.4	0.6	0.8	0.6	0.4	0.4	0.8
Wind Velocity	Uwd (m/s)	40	39	39	38	37	36.5	34
Constant Current Vel.	Ucur (m/s)	0.6	1	1.4	0.8	0.6	0.7	1.4
Roll Displacement	Constant profile (deg): Ωcp	1.55E-03	4.33E-03	8.48E-03	2.77E-03	1.55E-03	2.12E-03	8.48E-03
	Varying profile (deg): Ωvp	1.85E-03	5.01E-03	9.74E-03	3.15E-03	1.84E-03	2.51E-03	9.74E-03
Roll displacement difference (%): (Ωvp-Ωcp)/Ωcp		19.1	15.9	14.9	13.9	18.5	18.3	14.9
Displacement:	ΔΩt (deg)	7.28E-05	2.43E-04	5.10E-04	9.71E-05	7.28E-05	1.27E-04	5.10E-04
	ΔΩs (deg)	1.30E-04	1.05E-04	5.93E-05	7.49E-05	1.01E-04	1.12E-04	2.02E-05
Verification: Ωcp+ΔΩt+ΔΩs (deg)		1.76E-03	4.67E-03	9.05E-03	2.94E-03	1.73E-03	2.36E-03	9.01E-03
Importance of profile variation:								
due to tide	ΔΩt/Ωvp (%)	3.86	4.84	5.23	3.08	3.96	5.08	5.23
due to storm surge	ΔΩs/Ωvp (%)	6.91	2.10	0.61	2.38	5.48	4.48	0.21

Table 5.5

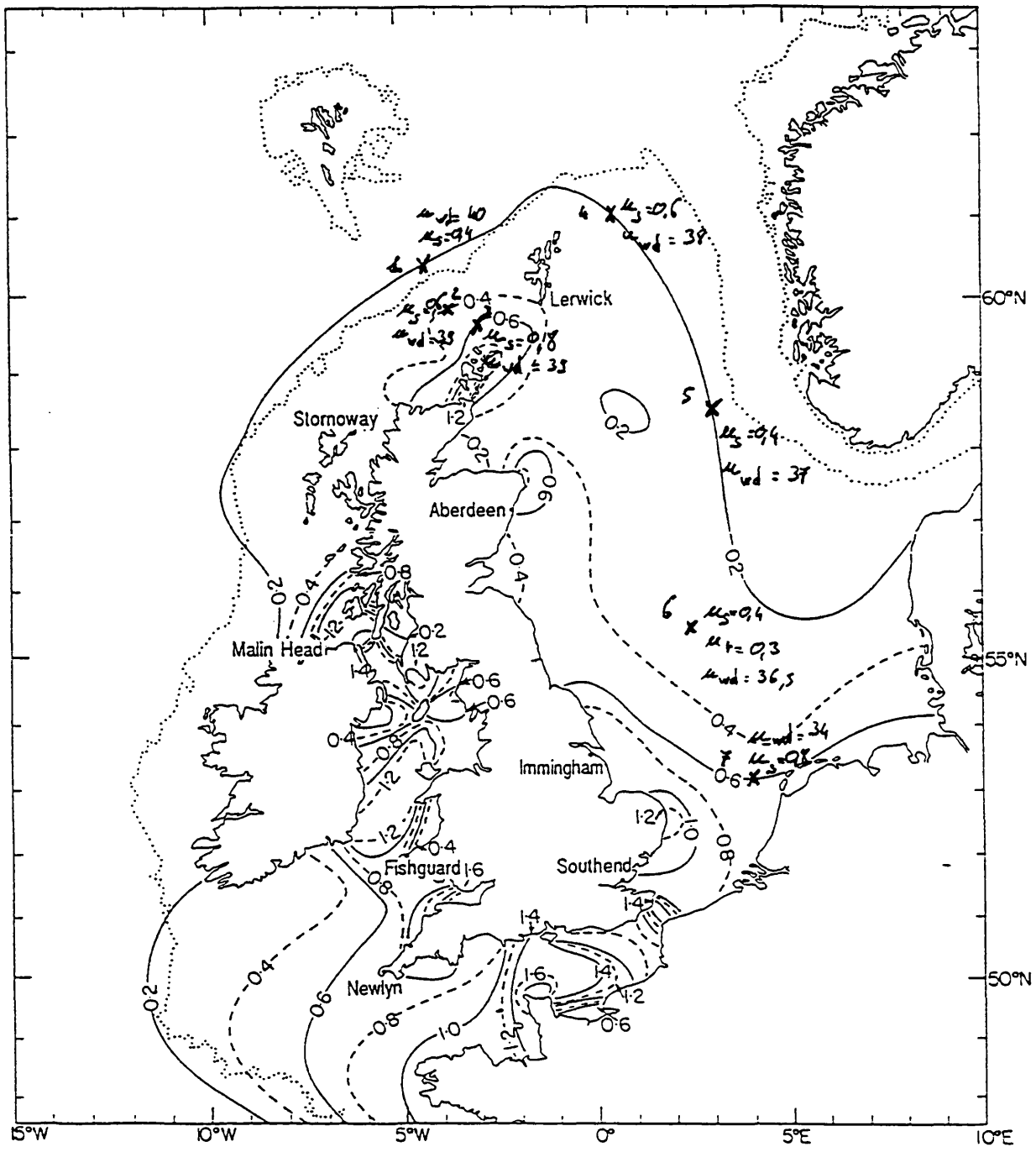

FIG. 4 : **Estimates of maximum depth-averaged flow of an average spring tidal current**

Contours are in m/s

See Section 6 for definition of spring tidal current

Dotted line is the 100 fathom (183 m) depth contour

Source: Observations (OTH 89 299)

Figure 5.7

u_s
u_s
u_{wd}
} are in m / s

CHAPTER 6: TIME DOMAIN STUDY IN REGULAR WAVES

1. INTRODUCTION

The main environmental effects have been modelled and tested in the frequency domain. The simplicity of the method allows quick calculations and is ideal for validation. However, if one wants to take into account non-linearities and to calculate the loads in the mooring lines, he has to carry out the study in the time domain. Thus, the model developed for the frequency domain is converted into the time domain. The equations of motion controlling the movements of the platform do not have to be linear, and the loads are not considered as harmonic. The differential equations are solved numerically for every time step. This kind of method is more complicated to implement and it requires high computational time.

The method presented here has been developed for a regular sea only. Due to the non-linearities, the extension to irregular seas is more complicated than in the frequency domain. This model is helpful to try to understand the effects of the different non-linearities and to check their relative importance. An extension to an irregular sea may be carried out later but is out of the scope of this study.

This chapter is divided into 5 sections. First, the principle of the time domain method is explained.

Then, a mathematical model to predict the non linear forces and motions in time domain is developed.

Finally, in section 4, four separate analyses are carried out. First, the effects of different non-linearities introduced in the model are investigated in terms of responses and tendon forces using the Snorre design.

The same study is carried out using the Heidrun TLP. The influence of the geometry of a platform on non linear responses is investigated by comparing the results obtained from the Heidrun analysis with those obtained from the Snorre analysis. The results are rather different since Heidrun is a much larger structure. In particular, its response in pitch as expected is different due to a lower centre of gravity.

Then, the response characteristics of Snorre and the forces in its tendons are investigated for a range of different regular sea states. For each of these sea states, the linear and non linear models are compared.

Finally, the influence of directionality of the environmental forces is investigated. The response values and the tendon forces are calculated for non collinear wave, wind and current. The aim of this part of the study is to investigate the worst weather conditions in term of loading in the tendon lines.

2. TIME DOMAIN ANALYSIS

The time domain analysis, developed to calculate the motions of the TLP and the forces in the tendons, can be described in three steps as summarised in the following diagram.

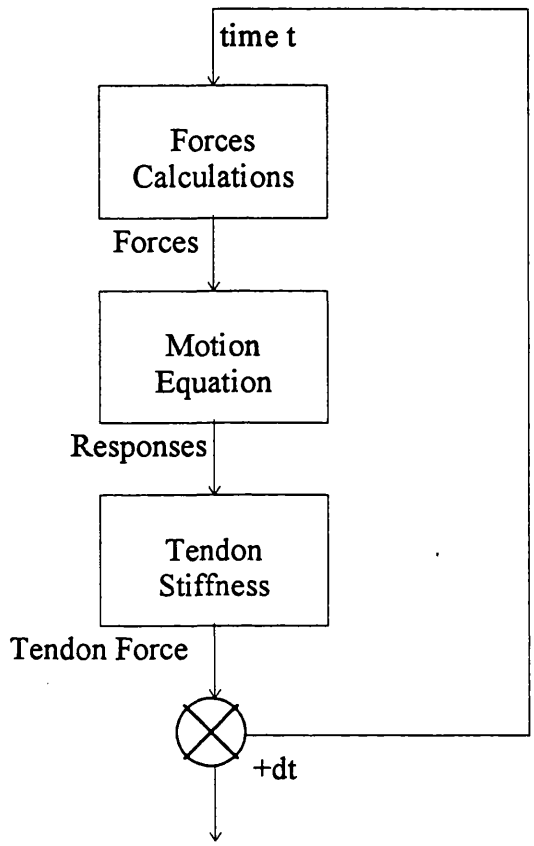

For the instant t:

1. Different forces acting on the platform are calculated at time t.

2. Response values are deduced from the differential motion equations:

$$\frac{d(M\bar{a})}{dt} = \bar{F}(t) \qquad (2\text{-}1)$$

The equations are solved numerically using a predictor corrector method. The expension of equation 2.1 in the case of a TLP is described in section 3.

3. Displacements are used to calculate the forces in the tendons.

Once these three calculations have been carried out for the instant t, the program goes through the same process again for the instant t+dt.

The final results of the analysis are produced in the form of time histories. For a more practical interpretation, the time series form of the results were processed through Fourier analysis and the response and force values are presented in the frequency domain. This process also enables us to identify super-harmonics corresponding to high order responses.

3. MATHEMATICAL MODELLING

This chapter introduces the formulation of the problem in the time domain.
The environmental loads considered are almost the same as in the frequency domain:

- First order waves
- Second order drift
- Steady wind
- Steady current

However, the slowly varying wind is not accounted for. Since the sea is taken as regular, the effects of the slowly varying drift do not appear in the model.

The model description is divided into two sections. The first presents the linear part of the model, which corresponds to the frequency domain model. A first formulation of the tendon forces is also described. It corresponds to a linear stiffness.

The second part describes different non-linearities that are included in the model. The physical effects are explained and the developments of mathematical models are detailed.
An alternative formulation of the tendon forces based on a non-linear stiffness of the mooring system is also given.

3.1. LINEAR MODEL

In the linear model the motion equation can be written as:

$$\left([M]+[M_a(\omega)]\right)\{\ddot{X}\}+[C_p(\omega)]\{\dot{X}\}+([K_m]+[K_h])\{X\}=\{F(t)\} \qquad (3.1\text{-}1)$$

Where:

M: mass-inertia matrix.
M_a: added mass matrix.
C_p: potential damping matrix.

K_m and K_h: the mooring and hydrostatic stiffness matrices.
F(t): linear force vector applied to the structure.
$\ddot{X}$, $\dot{X}$ and X: acceleration, velocity and displacement vectors of the structure.

The coefficients such as mass and stiffness are defined in the frequency domain.
The first order wave forces, added mass and potential damping are calculated at the wave frequency, using the analytical solutions developed in Chapter 3.3.

In the frequency domain, each force was studied separately. This is not the case in the time domain. The force vector F includes all the forces applied to the structure. In the linear model, it corresponds to the time dependent forces such as the wave exciting force, as well as the steady forces due to the drift, the current, and the wind.

In the linear model, the mooring system is considered as one linear spring. Since the set down is neglected the elongation of the tendons is given by:

$$dL = \frac{Z}{\cos\alpha_c} \tag{3.1-2}$$

Thus, the force in the tendons becomes:

$$F_{Tend} = T + \frac{AE}{L_c}\frac{Z}{\cos\alpha_c} \tag{3.1-3}$$

Where α_c is the cable angle given by:

$$\alpha_c = \arctan\left(\frac{\sqrt{X^2+Y^2}}{L_c+Z}\right) \tag{3.1-4}$$

And:

X, Y, Z: displacements in surge, sway and heave
A: total section of the tendons
E: Young modulus of the tendons
L_c: length of the tendons
T: initial pretension

3.2. DEFINITION OF NON-LINEARITIES

Several non-linearities are added to the first linear model:

- the viscous damping: this factor is due to the resistance water during oscillations of the structure.

- the stiffness of the tendons: the mooring system is not linear because of the coupling between the different motion of the platform. For example, the surge displacements create a set down in heave.

- the drag force: this force which is due to the viscous effects is quadratic and will create a force of higher order.

- the coupling of the movements of the platform: due to the rotations of the platform, the different motions are coupled together.

- the effects of the free surface: The forces and coefficients are normally calculated up to the mean water level. In order to investigate the non linearities due to free surface effects, the integration is carried up to the free surface level. This may have some importance in the case of steep waves.

- the effect of the motions of the structure on the wave load prediction. In the linear model, the TLP is supposed to be fixed in formulating the wave forces. In the non linear model, the wave forces are not calculated at a fixed reference position anymore, but at the actual position of the TLP.

3.2.1. Viscous damping

The viscous damping is the only non-linearity that was taken into account in the frequency domain study through an iteration process (see Chapter 2). In the time domain, its expression is straight forward. The quadratic term is directly included in the equation:

$$([M]+[M_a(\omega)])\{\ddot{X}\}+([C_p(\omega)]+[C_v]\{|\dot{X}|\})\{\dot{X}\}+([K_m]+[K_h])\{X\}=\{F(t)\} \tag{3.2-1}$$

3.2.2. Stiffness of the tendons

In the frequency domain, the tendons were considered as one linear spring. In the time domain, it is possible to model the stiffness of the tendons and their coupling with the TLP in a more precise way.

In the equations of motion, the linear mooring stiffness is replaced by the restoring forces F_M.

$$([M]+[M_a(\omega)])\{\ddot{X}\}+([C_p(\omega)]+[C_v]\{|\dot{X}|\})\{\dot{X}\}+[K_h]\{X\}=\{F(t)\}+\{F_M(t,X)\} \tag{3.2-2}$$

The following method describes the calculation of these restoring forces induced by the mooring system on the TLP. The coupling between the tendons and the TLP is fully taken into account.

A formulation of the forces in the tendons is also given.

The assumptions made are:

- The tendons have an elastic behaviour.
- The hydrodynamic effects on the tendons are neglected.
- The tendons are massless.

1. Calculation of the movements at the connection point C between the TLP and the tendons, in the co-ordinate system centered on G, centre of gravity.

$$\{X_c\} = \{X_G\} + [T_\Omega]\{\hat{X}_c\} \tag{3.2-3}$$

Where:

$$T_\Omega = \begin{bmatrix} \text{Cos}\,\Omega_y & 0 & \text{Sin}\,\Omega_y \\ \text{Sin}\,\Omega_y\,\text{Sin}\,\Omega_x & \text{Cos}\,\Omega_x & -\text{Sin}\,\Omega_x\,\text{Cos}\,\Omega_y \\ -\text{Sin}\,\Omega_y\,\text{Cos}\,\Omega_x & \text{Sin}\,\Omega_x & \text{Cos}\,\Omega_x\,\text{Cos}\,\Omega_y \end{bmatrix} \tag{3.2-4}$$

X_c: displacement at point C
X_G: displacement at point G centre of gravity of the platform
$\hat{X}_c$: co-ordinates of the point C
Ω_x, Ω_y: displacements in roll and pitch respectively

The displacement is different at the bottom of each column. Thus, the system is modelled with four non-linear springs.
In the following, we consider the system formed by one column and one of the springs representing the tendons.

2. Change of co-ordinate system

To simplify the problem, a new co-ordinate system (C_0, x', y', z) is considered. It is chosen so that the vertical axis remains the same and the displacement along y' is equal to 0. C_0 is the original position of the point C. (See sketch below).

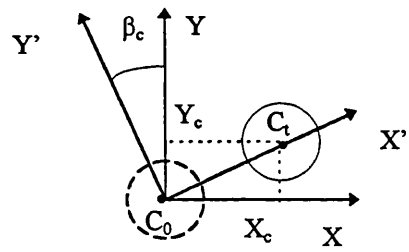

The angle β_c between the axis X and X' is given by:

$$\beta_c = \arctan\left(\frac{Y_c}{X_c}\right) \tag{3.2-5}$$

The displacement in the new co-ordinate system then becomes:

$$X'_c = \frac{X_c}{\mathrm{Cos}\,\beta_c} \tag{3.2-6}$$

The restoring forces in surge and sway are given by:

$$\begin{aligned} F_{Mx} &= F_{Mx'}\,\mathrm{Cos}\,\beta_c \\ F_{My} &= F_{Mx'}\,\mathrm{Sin}\,\beta_c \end{aligned} \tag{3.2-7}$$

3. Restoring Forces

The following sketch shows the geometry of the mooring system and a representation of the forces applied to the tendons.

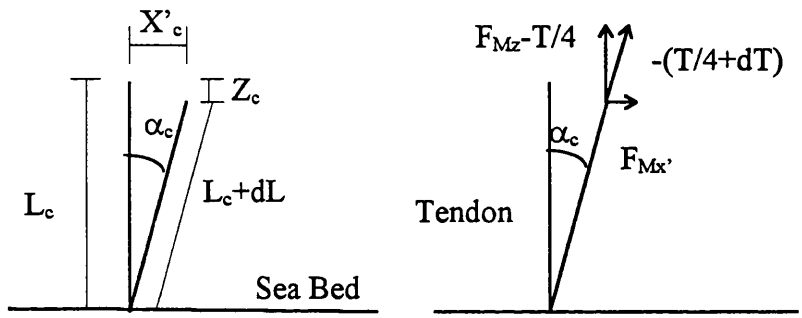

From the geometry of the system we have:

$$\begin{aligned} \mathrm{Sin}\,\alpha_c &= \frac{X'_c}{L_c + dL} \\ \mathrm{Cos}\,\alpha_c &= \frac{L_c + Z_c}{L_c + dL} \\ \mathrm{Tan}\,\alpha_c &= \frac{X'_c}{L_c + Z_c} \end{aligned} \qquad (3.2\text{-}8)$$

Where dL is the elongation of the tendons.

The equilibrium of the forces gives:

$$\begin{aligned} F_{Mx'} &= -\left(\frac{T}{4} + dT\right)\mathrm{Sin}\,\alpha_c \\ F_{Mz} - \frac{T}{4} &= -\left(\frac{T}{4} + dT\right)\mathrm{Cos}\,\alpha_c \end{aligned} \qquad (3.2\text{-}9)$$

Where T is the original pretension and dT is the variation of the pretension.

Assuming that the tendons have an elastic behaviour:

$$dT = \frac{A\,E}{4\,L_c}\,dL \qquad (3.2\text{-}10)$$

Where: A: total sectional area of the tendons
E: Young Modulus of the tendons

From Equation 3.2-8, we can calculate the angle of the cable:

$$\alpha_c = \arctan\left(\frac{X'_c}{L_c + Z_c}\right) \qquad (3.2\text{-}11)$$

and the elongation of the tendons:

$$dL = \frac{L_c + Z_c}{\mathrm{Cos}\,\alpha_c} - L_c \qquad (3.2\text{-}12)$$

Then, the forces become:

$$F_{Mx'} = -\frac{1}{4}\left(T + \frac{AE}{L_c}dL\right)\frac{X_c'}{L_c + dL}$$
$$F_{Mz} = -\frac{1}{4}\left(T + \frac{AE}{L_c}dL\right)\mathrm{Cos}\,\alpha_c + \frac{T}{4} \qquad (3.2\text{-}13)$$

Using Equation 3.2-7, the restoring forces in surge and sway become:

$$F_{Mx} = -\frac{1}{4}\left(T + \frac{AE}{L_c}dL\right)\frac{X_c'}{L_c + dL}\mathrm{Cos}\,\beta_c$$
$$F_{My} = -\frac{1}{4}\left(T + \frac{AE}{L_c}dL\right)\frac{X_c'}{L_c + dL}\mathrm{Sin}\,\beta_c \qquad (3.2\text{-}14)$$

The restoring moments in roll and pitch are given by:

$$M_{Mx} = Y_c F_{Mz} - Z_c F_{My}$$
$$M_{My} = Z_c F_{Mx} - X_c F_{Mz} \qquad (3.2\text{-}15)$$

The force in the tendons is simply given by:

$$F_{Tend} = \frac{T}{4} + \frac{AE\,dL}{4L_c} \qquad (3.2\text{-}16)$$

Where dL is calculated in Equation 3.2-12.

3.2.3. Drag Force

The drag forces were neglected in the frequency domain study. These forces can be linearised, but since the inertia forces are predominant, the drag forces are not of great interest.

However, in the time domain, it is possible to take into account the drag forces to study the high order excitations.

The effects of current and waves can be combined in the following drag force equation:

$$F_d = \frac{1}{2}\rho C_d D_c \int_{-d}^{0} \left|U_{Cur} + U_{Wave}\right|\left(U_{Cur} + U_{Wave}\right)dz \qquad (3.2\text{-}17)$$

Where U_{cur} and U_{wave} are the current and wave velocities.

The drag force is calculated using the following coefficients:.

$$C_{dx}^{c} = C_{dy}^{c} = 0.6 \qquad C_{dz}^{c} = 0.82$$

$$C_{dx}^{p} = C_{dy}^{p} = C_{dz}^{p} = 2$$

3.2.4. Coupling between the different modes of motion of the platform

The rotation of the platform in roll and pitch induces coupling between the different motions of the TLP.

This effect is modelled by a force added to the right hand side of the motion equation.

The motion equation becomes:

$$\left([M]+[M_a(\omega)]\right)\{\ddot{X}\}+\left([C_p(\omega)]+[C_v]\{|\dot{X}|\}\right)\{\dot{X}\}+[K_h]\{X\}=\{F(t)\}+\{F_M(t,X)\}+\{F_d(t)\}+\{F_{coup}(t,\dot{X})\} \tag{3.2-18}$$

Where F_{coup} represents the coupling between the different modes of motion and is written as:

$$\{F_{coup}\}=-M\begin{bmatrix}\dot{\Omega}_y\,\dot{Z}\\ -\dot{\Omega}_x\,\dot{Z}\\ -\dot{\Omega}_y\,\dot{X}+\dot{\Omega}_x\,\dot{Y}\\ 0\\ 0\end{bmatrix} \tag{3.2-19}$$

Where $\dot{X},\dot{Y},\dot{Z},\dot{\Omega}_x,\dot{\Omega}_y$ are the velocities of the TLP in surge, sway, heave, roll, and pitch respectively.

3.2.5. Free surface effects

In the frequency domain, the water level is taken as the mean water level, neglecting the effects of the free surface. In the case of steep waves, significant changes can appear if the water level is taken as the free surface level.

The free surface has an effect on the calculation of several forces and coefficients of the motion equation. Its effects are large and complex.

The solution proposed here is based on a simple model proposed by Natvig [6.1]. Only the non-linear terms that he found significant are taken into account. With this model, he was able to simulate numerically a ringing phenomenon that he recorded during model testing.

The non-linear terms accounted for are:

- the diffraction force correction
- the drag force correction
- the added mass correction
- the potential and viscous damping correction

The free surface also creates the following terms:

- the derivative of the added mass
- the wave slapping

The first four terms represent the difference between the value of these forces and coefficients when they are calculated up the free surface level instead of the mean water level.

The fifth one is due to the fact that the added mass becomes time dependent when calculated taking into account the free surface.

The last one represents the force due to the impact of waves on the structure.

These effects are expressed as forces added to the right hand side of the motion equation.

$$\left([M]+[M_a(\omega)]\right)\{\ddot{X}\}+\left([C_p(\omega)]+[C_v]\{|\dot{X}|\}\right)\{\dot{X}\}+[K_h]\{X\}=\{F(t)\}+\{F_m(t,X)\}+\{F_d(t)\}+\{F_{coup}(t,\dot{X})\}+\{F_{fscor}(t,X,\dot{X})\} \quad (3.2\text{-}20)$$

Where:

$$F_{fscor}=\Delta F_{inertia}+\Delta F_{drag}-\Delta F_{Ma}-\Delta F_{Cp}-\Delta F_{Cv}+\Delta F_{\dot{M}_a}+\Delta F_{Slap} \quad (3.2\text{-}21)$$

First, the free surface level has to be calculated. For that purpose, the first order diffraction potential is used. Its formulation is given in chapter 3. The effects of the pontoons and the movement of the TLP are neglected.

3.2.5.1. Diffracted free surface

The free surface is given by:

$$\eta=-\frac{1}{g}\frac{d\Phi}{dt}\bigg|_{z=0} \quad (3.2\text{-}22)$$

Where $\Phi = \Phi_I + \Phi_D$ is the sum of the incident and the diffracted potentials. Around the jth column the potential Φ becomes:

$$\Phi^j(R_c,\theta_j) = \mathrm{Re}\left(\frac{-2i}{\pi\, kR_c} f(z) \sum_{n=-\infty}^{\infty} \frac{A_n^j}{H_n'(kR_c)} e^{in\theta_j} e^{-i\omega t}\right) \tag{3.2-23}$$

Where:

$$f(z) = \frac{-i\,A\,g}{\omega} \frac{\cosh(k(z+H))}{\cosh(kH)} \tag{3.2-24}$$

and:

k: wave number
ω: wave frequency
A: wave amplitude
H: water depth
R_c: the column radius
H_n: the Hankel function of the first kind of order n
A_n^j: the diffraction coefficient

The free surface around the ith column becomes:

$$\eta^j(R_c,\theta_j) = \mathrm{Re}\left(\frac{-2iA}{\pi\, kR_c} \sum_{n=-\infty}^{\infty} \frac{A_n^j}{H_n'(kR_c)} e^{in\theta_j} e^{-i\omega t}\right) \tag{3.2-25}$$

For the free surface corrections, the average of the free surface around the column is used, this mean value is given by:

$$\overline{\eta}^j = \frac{1}{2\pi R_c} \int_0^{2\pi} \eta^j(R_c,\theta_j) R_c\, d\theta_j = \mathrm{Re}\left(\frac{-2iA}{\pi\, kR_c} \frac{A_0^j}{H_0'(kR_c)} e^{-i\omega t}\right) \tag{3.2-26}$$

3.2.5.2. Diffraction force corrections

The force correction represents the difference between the force expressed up to the mean water level and the force expressed up to the free surface level. This force is positive if the free surface is above the mean water level and negative if below. Only the forces on the columns are subject to the variation of free surface. The forces on the pontoons remain the same.

The correction is implemented using the diffraction potential already used to formulate the forces on the columns.

$$\Delta F_{\mathrm{Inertia}\,x} = \mathrm{Re}\left(\int_0^{2\pi}\left(\int_0^{\overline{\eta}} -\rho \frac{d\Phi}{dt} dz\right) R_c \cos\theta\, d\theta\right) \tag{3.2-27}$$

The correction terms come as:

$$\Delta F^{j}_{Dif\,x} = Re\left(\frac{-2\,i\,\rho\,g\,A}{k^2 H_1'(kR_c)} \frac{Sinh\left(k(\overline{\eta}+H)\right) - Sinh\,kH}{Cosh\,kH} \left(A^{j}_{-1} - A^{j}_{1}\right) e^{-i\omega t} \right)$$

$$\Delta F^{j}_{Dif\,y} = Re\left(\frac{-2\rho\,g\,A}{k^2 H_1'(kR_c)} \frac{Sinh\left(k(\overline{\eta}+H)\right) - Sinh\,kH}{Cosh\,kH} \left(A^{j}_{-1} + A^{j}_{1}\right) e^{-i\omega t} \right)$$

$$\Delta F^{j}_{Dif\,z} = 0$$

$$\Delta M^{j}_{Dif\,x} = Re\left(\frac{2\rho\,g\,A}{k\,H_1'(kR_c)} Q_z \left(A^{j}_{-1} + A^{j}_{1}\right) e^{-i\omega t} \right) + Z_G\,\Delta F^{j}_{Inertia\,y} \qquad (3.2\text{-}28)$$

$$\Delta M^{j}_{Dif\,y} = Re\left(\frac{-2\,i\,\rho\,g\,A}{k\,H_1'(kR_c)} Q_z \left(A^{j}_{-1} - A^{j}_{1}\right) e^{-i\omega t} \right) - Z_G\,\Delta F^{j}_{Inertia\,x}$$

Where:

$$Q_z = \frac{1}{k^2\,Cosh(kH)} \left(k\overline{\eta}\,Sinh\,k(\overline{\eta}+H) - Cosh\,k(\overline{\eta}+H) + Cosh\,kH\right) \qquad (3.2\text{-}29)$$

This formulation is based on the assumption that the wave particle kinematics can be defined in the free surface zone as defined in the rest of the fluid. This gives a good approximation for regular seas. Nevertheless, in the free surface zone, a stretching formula should be applied since the velocity and acceleration values in the wave crest are overestimated.

3.2.5.3. Drag force corrections

The corrections for the drag force are calculated following the same principles. They are:

$$\Delta F_{Drag} = \frac{1}{2}\rho\,C_d\,D_c \int_0^{\overline{\eta}} \left|U_{Waves} + U_{Current}\right| \left(U_{Waves} + U_{Current}\right) dz$$

$$\Delta M_{Drag} = \frac{1}{2}\rho\,C_d\,D_c \int_0^{\overline{\eta}} \left|U_{Waves} + U_{Current}\right| \left(U_{Waves} + U_{Current}\right) \left(Z_G - z\right) dz \qquad (3.2\text{-}30)$$

3.2.5.4. Added mass corrections

The use of radiation potentials to calculate the variations in added mass for each time step is very time consuming.

Instead, the strip theory formulation of the added mass is used, where the added mass coefficient is directly deduced from the result of the analytical theory:

$$M_a = C_m(\omega)\rho\frac{\pi D_c^2}{4}d \tag{3.2-31}$$

Where: D_c: column diameter
d: draught
C_m: frequency dependent added mass coefficient for the columns deduced from the radiation potential.

This way the correction can be expressed as:

$$\begin{aligned}
\Delta F_{Max} &= C_m(\omega)\rho\frac{\pi D_c^2}{4}\overline{\eta}\ddot{X} \\
\Delta F_{May} &= C_m(\omega)\rho\frac{\pi D_c^2}{4}\overline{\eta}\ddot{Y} \\
\Delta F_{Maz} &= 0 \\
\Delta M_{Max} &= C_m(\omega)\rho\frac{\pi D_c^2}{4}\overline{\eta}\left(\frac{\overline{\eta}}{2}-Z_G\right)^2\ddot{\Omega}_x \\
\Delta M_{May} &= C_m(\omega)\rho\frac{\pi D_c^2}{4}\overline{\eta}\left(\frac{\overline{\eta}}{2}-Z_G\right)^2\ddot{\Omega}_y
\end{aligned} \tag{3.2-32}$$

3.2.5.5. Potential and viscous damping corrections

The same principle is used to calculate the potential damping corrections. From the analytical solution, we now derive the frequency dependent coefficient C_{pd}.

$$C_p = C_{pd}(\omega)\rho\frac{\pi D_c^2}{4}d \tag{3.2-33}$$

Since the potential damping is taken as zero for heave, pitch and roll motions, the corrections only occur in surge and sway motions:

$$\begin{aligned}
\Delta F_{C_p x} &= C_{pd}(\omega)\rho\frac{\pi D_c^2}{4}\overline{\eta}\dot{X} \\
\Delta F_{C_p y} &= C_{pd}(\omega)\rho\frac{\pi D_c^2}{4}\overline{\eta}\dot{Y}
\end{aligned} \tag{3.2-34}$$

The corrections for the viscous damping follow the same principle as the drag forces. It becomes:

$$\begin{aligned}
\Delta F_{Cvx} &= \frac{1}{2}\rho C_d D_c \overline{\eta}\left|\dot{X}\right|\dot{X} \\
\Delta F_{Cvy} &= \frac{1}{2}\rho C_d D_c \overline{\eta}\left|\dot{Y}\right|\dot{Y} \\
\Delta F_{Cvz} &= 0 \\
\Delta M_{Cvx} &= \frac{1}{2}\rho C_d D_c \overline{\eta}\left(\frac{\overline{\eta}}{2} - Z_G\right)^2 \left|\frac{\overline{\eta}}{2} - Z_G\right| \left|\dot{\Omega}_x\right| \dot{\Omega}_x \\
\Delta M_{Cvy} &= -\frac{1}{2}\rho C_d D_c \overline{\eta}\left(\frac{\overline{\eta}}{2} - Z_G\right)^2 \left|\frac{\overline{\eta}}{2} - Z_G\right| \left|\dot{\Omega}_y\right| \dot{\Omega}_y
\end{aligned} \tag{3.2-35}$$

3.2.5.6. Derivative of the added mass

Due to the free surface corrections, the added mass becomes time dependent. Thus, a new term appears, the derivative of the added mass with respect to time.

According to Natvig [6.1], it has a major importance for modelling the ringing phenomenon. It comes:

$$\begin{aligned}
\Delta F_{\dot{M}_a\begin{pmatrix}x\\y\end{pmatrix}} &= -C_m(\omega)\frac{\pi D_c^2}{4}\frac{d\overline{\eta}}{dt}\begin{pmatrix}\dot{X}\\\dot{Y}\end{pmatrix} \\
\Delta F_{\dot{M}_a z} &= 0 \\
\Delta F_{\dot{M}_a\begin{pmatrix}\Omega_x\\\Omega_y\end{pmatrix}} &= -C_m(\omega)\frac{\pi D_c^2}{4}\frac{d\overline{\eta}}{dt}\left(\left(\frac{\overline{\eta}}{2} - Z_G\right)^2 + \overline{\eta}\left(\frac{\overline{\eta}}{2} - Z_G\right)\right)\begin{pmatrix}\dot{\Omega}_x\\\dot{\Omega}_y\end{pmatrix}
\end{aligned} \tag{3.2-36}$$

3.2.5.7. Wave slapping

This force represents the impact force of the wave crests on the structure. For cylinders, it can be written as:

$$\begin{aligned}
\Delta F_{Slap\begin{pmatrix}x\\y\end{pmatrix}} &= \frac{1}{2} C_s C_m(\omega)\rho D_c \Delta\eta\left(U_{waves} - \dot{X}\right)^2 \\
\Delta F_{Slap\,z} &= 0 \\
\Delta F_{Slap\begin{pmatrix}\Omega_x\\\Omega_y\end{pmatrix}} &= \begin{pmatrix}-1\\1\end{pmatrix}\left(\frac{\overline{\eta}}{2} - Z_G\right)\Delta F_{Slap\begin{pmatrix}x\\y\end{pmatrix}}
\end{aligned} \tag{3.2-37}$$

Where:

C_s=1.151: slamming coefficient (See below)

C_m: added mass coefficient, introduced here to take into account the interaction between the columns

D_c: diameter of the columns

$\Delta\eta$: slope of the diffracted wave across the column

U_{waves}: diffracted velocity of the waves

The above empirical formula is given by Faltinsen [6.2]. The coefficient C_s is deduced from the experimental work carried out by Campbell et al [6.3] for horizontal cylinders.

The slope of the wave, $\Delta\eta$, is calculated by the difference of elevation between the front and the rear of the column.

The introduction of the coefficient C_m is not necessary, since the interaction of the columns is already taken into account in the diffracted wave velocity.

A full study of the effect of slamming on a TLP structure may be interesting. However, this is out of the scope of this thesis. We will use this simple formula, that can be easily used in the time domain.

3.2.6. The effects of the displacement of the structure

So far, the wave forces have been formulated assuming that the TLP is fixed. This assumption may not be acceptable for the large amplitude motions. In the case of TLP, this means that the surge and sway motions should be taken into account in formulating the wave excitation forces and moments. Displacements in heave, roll and pitch are very small and their influence is neglected.

Large amplitude motions are considered to modify the formulation of:

- first order forces
- drag forces
- free surface

The differential equation becomes:

$$\left([M]+[M_a(\omega)]\right)\{\ddot{X}\}+\left([C_p(\omega)]+[C_v]\{|\dot{X}|\}\right)\{\dot{X}\}+[K_h]\{X\}=\{F(t,X)\}+\{F_m(t,X)\}+\{F_d(t,X)\}+\{F_{coup}(t,\dot{X})\}+\{F_{fscor}(t,X,\dot{X})\} \quad (3.2\text{-}38)$$

The non-linear terms slow down the time domain program considerably since the first order forces should be recalculated for every time step. If the structure is considered as stationary, the spatial dependent part of the force can be calculated once for all. Then, the only calculation required to obtain the forces at time t, is the multiplication of the force amplitudes by sin ωt.

One should note that the steady drift formulation has not been modified. One could also take into account the displacement of the structure in the formulation of the steady drift forces. However, the whole calculation would have been slowed down even more. Furthermore, this would not change the results significantly. Indeed, we are considering extreme weather conditions, where the wind clearly dominates all other steady forces.

4. TIME DOMAIN ANALYSIS

Four different analyses have been carried out with the time domain program.

The first one studies the effects of each non linearity on the motions and tendon loads of the Snorre TLP.

The second analysis studies similar effects using the Heidrun design. The effects of different geometries on the non linearities are investigated.

In the third study, the time domain program is run for a whole range of wave frequencies. The aim is to investigate the influence of the different components of an irregular sea state.
For each frequency, a comparison between the linear and the non linear model is carried out.

Finally, in the last part, the effects of the directionality of the environmental forces are studied in terms of displacements and tendon loads.

The last two analyses are carried out with the Snorre design.

4.1. EFFECTS OF NON LINEARITIES ON THE SNORRE TLP

The simulation is carried out for a regular head sea. The wave frequency and the wave amplitude are taken as 0.2 rad/s and 13.52 m.
Wind and current are collinear with the waves and their velocities are respectively 40 m/s and 0.6 m/s.

Nine different tests are run during this study.

Test 0 uses the linear model described in the previous section. This was done to establish a reference during the analysis of the non linearities.

The six following tests are carried out with one of the six non linearities at a time.

Test 1 introduces the non linear stiffness of the mooring system.

Test 2 is carried out with the viscous damping.

Test 3 takes into account the coupling between the motions of the TLP.

Test 4 applies the drag forces on the structure.

Test 5 considers the free surface effects.

Test 6 takes into account the large amplitude motions of the TLP in force calculations.

Finally the last two tests combine the different non linearities:

Test 7 is run for a model which takes into account every non linearities except for the large amplitude motions of the TLP

Test 8 is the same as test 7, but includes the non linearities due to the displacement of the platform.

Test 7 is important because when the non-linear simulations based on the large amplitude motion model are run, computational time required becomes excessive. If the displacements of the structure could be neglected, a lot of computation time could be saved.

During the analysis, the time history of the responses and the loads are transformed to the frequency domain using a fast Fourier transform (FFT).
The responses and the forces are then divided into four components:

- The steady response/force (offset or pretension)
- The first order response/force corresponding to the response occurring at the wave frequency (here, 0.2 rad/s).
- The second order response/force taking place at twice the wave frequency (0.4 rad/s).
- The third order response/force at three times the wave frequency (0.6 rad/s)

The results of the different tests are given in Table 6.1. The results presented here are in three degrees of freedom - surge, heave and pitch. The loads in the up-stream and down-stream tendons are also included.

4.1.1. Test 0: Linear Model

This test corresponds to a frequency domain analysis where no non linearities are taken into account. The response has only two components, a steady one corresponding to the steady forces, and a first order one corresponding to the harmonic wave forces.

The time history and the FFT of the responses and tendon forces can be seen in Figures 6.1 and 6.2.

4.1.2. Test 1: Non Linear Mooring Model

This test presents large differences in the motion responses and the tendon forces from test 0. (See Figures 6.3 and 6.4)

The displacement in surge is only slightly changed. A second response can be noticed but it is still very small compared to the first order response (1%).

Large changes can be seen in heave. Due to the set down, a large offset is present. The first order response is increased by 80%. Finally, a large second order excitation appears. These three values are of the same order of magnitude.

The response in pitch is also affected. The steady response is largely increased, but is still quite small compared to the first order response. The first order response is increased by about 30%. Finally, a second order response can be observed, it corresponds to about 10% of the first order response.

Due to a new formulation of the tendon loads, an asymmetry now appears between the forces in the up-stream and down-stream tendons.

The maximum pretension value represents a 7% increase over the linear pretension. Similarly, the maximum first order force is 11% higher than the prediction of the linear model.

A second order response is also visible in the frequency plot of the response. It corresponds to 5% of the first order response. However, it remains quite small considering the large second order responses both in heave and pitch.

4.1.3. Test 2: Viscous Damping

The viscous damping has an insignificant effect on the response of the TLP. The only noticeable difference with the linear model is a smaller first order surge response (about 2% difference).

Being far from the natural frequency, it is expected that the damping would have no effect on TLP responses.

4.1.4. Test 3: Motion Coupling

The coupling has no significant effect neither on the displacement of the TLP nor on the tendon forces.

This is due to the very small value of the rotational velocity, because of the high value of the stiffness in roll and pitch.

4.1.5. Test 4: Drag Force

The drag forces induce some changes in the steady responses and first order response of the TLP. The surge offset increases by 15%, whereas the pitch steady response decreases by 54%. This however remains quite small compared to the overall response. The first order responses are also increased, 1.5% in surge and heave and 6% in pitch.

The higher order response induced by the drag force appears at three times the wave frequency (See Figure 6.5). Nevertheless, they are very small compared to the first order response.

The effect on the tendons is small too. The induced third order force is only 4% of the first order load.

The effects of the drag forces on the tendons are underestimated by the linear mooring model that does not take into account the rotation of the TLP.

4.1.6. Test 5: Free Surface Effects

The main influence of the free surface effects appears in pitch. The amplitude of the first and steady response are slightly decreased. More important is the presence of super-harmonics (See Figure 6.6). The second order response is significant (about 10% of the first order displacement), whereas the third order response is still very small.

As stated before, the linear mooring model does not take the rotation into account for the calculation of the forces in the tendons. Thus, the free surface effects have to be coupled with the non linear mooring model to fully account for their effects on the tendons.

4.1.7. Test 6: Displacements of the TLP

Heave is left unchanged, and surge shows very little difference.

In pitch a second order response appears (Figure 6.7), but remains small. The offset is reduced by 15%.

This effect has to be coupled with the non linear mooring model to see significant changes in the tendon loads.

4.1.8. Test 7: Fully Non Linear Model (except displacements)

The time history and the FFT of the responses are presented in Figure 6.8.

Insignificant changes appear in the surge response.

The heave response is very similar to the one observed in test 1, with a steady, a first order, and a second order response of the same order of magnitude. However, the first order response is about 20% higher.

The pitch response is also very similar to test 1. The second order is quite important corresponding to about 18% of the first order response.

The values of the pretension are close to the one observed in test 1.

Larger differences in the values of the first order forces between the upstream and downstream tendons can be observed. This is due to the changes in the pitch steady offset.

The second order effects are also larger (See Figure 6.9), this is due to the second order responses in pitch due to the free surface effects. These responses represent respectively 6% and 7.5% of the first order responses in the down-stream and up-stream tendons.

4.1.9. Test 8: Fully Non Linear Model (including displacements)

Figure 6.10 shows that the responses are very similar to the ones of test 7. The main changes are a 10% rise in the surge offset, and the first order heave response.

Insignificant changes are noticeable in the tendon forces (See Figure 6.11).

4.1.10. Conclusion

A graphic presentation of table 6.1 is presented in Figures 6.12 to 6.17. The 3D charts represent each of the four components of the response for the nine tests.

Figure 6.12 shows that the surge response is hardly modified by the non linearities.

The bigger difference appears in the offset of the platform, but the effects of the drag force and the non linear mooring model cancel each other.

Figure 6.13 clearly shows that the non linear mooring model completely changes the heave response of the TLP. This effect is by far the most important one.

Figure 6.14 shows how the pitch response is affected by the non linear mooring model, and how the free surface effects, the displacements of the TLP, and to a lower extend, the drag force create super-harmonics.

Figures 6.15 and 6.16 present the forces in the down-stream and the up-stream tendons. The forces are mainly changed by the non linear mooring model.

A larger pretension can be observed in the up-stream tendon. A larger first order force appears in the down-stream tendon. The non linearities also induce super-harmonics at two and three times the wave frequency.

Finally, Figure 6.17 shows the asymmetry of the forces in the tendons for tests 1, 7 and 8. The tendon force resulting from the linear model is given as a reference.

From this analysis, it clearly appears that the most important effect on both the TLP responses and the forces in the tendons is the non linear model of the mooring system.

It produces a very different heave response, and induces an asymmetry in the tendon loading.

The drag forces, by increasing the values of the steady offset in surge and pitch, also have an effect on this asymmetry of tendon forces.

The free surface effects to a lower extend are also important since they create second order responses both in pitch response and in tendon loading.

The effects of the displacement are also noticeable but are nevertheless quite small and may be neglected if computation time savings are needed.

4.2. EFFECTS OF NON LINEARITIES ON THE HEIDRUN TLP

In this section, the same study as before is carried out for the Heidrun TLP. Since this TLP is rather different from Snorre, it is interesting to know if the non linearities have the same effects on the two platforms, or if noticeable changes can be observed.

Heidrun is much bigger structure. Its main characteristics can be found in table 6.2. Due to its concrete hull, the columns are bigger, and the draught is larger. The behaviour in pitch may also change due to the position of the centre of gravity that is much lower than on the Snorre TLP.

The same nine tests are carried out on the new geometry. The results are presented in table 6.3, under the same format. The sea state conditions also remain the same.

4.2.1. Test 0: Linear Model

The comparison of the displacements of Snorre and Heidrun shows that the responses are of the same order.

Figures 6.18 and 6.19 show a comparison of the distribution of the responses between the different frequency components for the two TLPs. Each component of the response (steady, first, second and third order) is given as a percentage of the overall response. The surge responses are about the same. The steady offset of the pitch motion for Heidrun is more important than for Snorre.

The tendon forces are greater for the Heidrun design, however the distribution of the loads between pretension and first order response is the same. (See Figure 6.20)

4.2.2. Test 1: Non Linear Mooring Model

Insignificant changes appear in surge compare to test 0, as it was observed in the case of Snorre. (See Figure 6.21)

In heave, the response has the same characteristics as for Snorre: a large offset and second order response. Figure 6.22 shows the distribution of the response between the different frequencies. It compares well with the results obtained for Snorre despite a smaller second order response.

The response in pitch is a little different from the response of Snorre. The offset is bigger whereas the second order effects are not as important. (See figure 6.23)

However, the same overall effects are observed, an increase in the offset, the first order and the second order response.

The tendon forces compare also well. (See Figures 6.24 and 6.25). The second order forces are smaller but the difference is minimal compared to the overall loading.

4.2.3. Test 2 and 3: Viscous Damping and Motion Coupling

As with Snorre, these two non linearities have very little effect on the response of Heidrun or on the forces induced in its tendons.

4.2.4. Test 4: Drag Force

As with Snorre, the surge offset is increased by about 15% and the heave motion is left unchanged.

The main difference with the Snorre response appears at the third order pitch motion. It does not increase up to the same extend.

However, in both cases this component is very small compared to the overall response. (See Figure 6.26)

The non linear mooring model would have to be applied to see any significant changes in the tendon forces.

4.2.5. Test 5: Free Surface Effects

The only significant effects appear in pitch. The pitch offset is increased, whereas it decreases in the case of Snorre. This is due to the position of the centre of gravity.

The effects on the first and second order response remain the same (a small increase).

As with the linear model, the main difference is a larger contribution of the offset in the pitch response of Heidrun. (See Figure 6.27).

The contribution of the second and third order effects are the same for both platforms.

4.2.6. Test 6: Displacements of the TLP

As before, the main differences appear in pitch. The relative second order response induced by the non linearity is smaller for Heidrun than it is for Snorre. (See Figure 6.28).

4.2.7. Test 7: Fully Non Linear Model (except displacements)

Figure 6.29 shows that in surge, the distribution of the response is very similar. The super-harmonics are very small. The results on Heidrun show a slightly larger contribution of the offset.

In heave (See Figure 6.30) the main difference appears in the second order response. It is smaller for the Heidrun design. However, the responses are quite similar.

The bigger difference between the responses of the two TLPs appears in pitch (Figure 6.31). The Heidrun response presents a larger offset and smaller super-harmonics.

In terms of tendon forces, the results are quite similar, although Heidrun has a larger offset and smaller second and third order components. (See Figures 6.32 and 6.33).

The asymmetries between the up-stream and down-stream tendons present significant differences. The difference of pretension between the two sets of tendons is about 15% of the total pretension for Heidrun. For Snorre, the same value is about 7%.

In terms of first order forces, the asymmetry is about 9.5% for Heidrun and 19% for Snorre.

These effects can be directly linked with the difference in the pitch response, where the steady offset is larger for Heidrun and the first order response is larger for Snorre.

4.2.8. Test 8: Fully Non Linear Model (including displacements)

Figures 6.34 to 6.38 show that the configuration observed in test 7 is not changed significantly by effects of the displacements. The same remarks still apply on the TLP responses and the tendon forces.

4.3. EFFECTS OF THE WAVE CHARACTERISTICS ON THE SNORRE TLP

In this section, the influence of different waves on the response of Snorre and on its tendon forces is investigated. Each wave is considered with a heading of zero degrees. The wind and the current are collinear with the waves. Their respective velocities are taken as 40 m/s and 0.6 m/s.

First, a set of waves is generated. They are characterised by a frequency and an amplitude. The relation between these two values is based on a Pierson Moskowitz spectrum for a 40 m/s wind velocity.

$$A = \sqrt{S(\omega)\,d\omega} \qquad (4.3\text{-}1)$$

Where A is the wave amplitude and S the Pierson Moskowitz wave spectrum. $d\omega$ has been taken as 0.05 rad/s.

Figure 6.39 shows the wave amplitudes plotted as a function of the frequency.

Two time domain simulations are carried out for each wave. One using the linear model (same as test 0 in the previous analyses). The second simulation used the same non linear model as described in test 7. The displacements of the TLP are not taken into account in the force calculations because the computations require too much time. However, it as been observed before that these effects are relatively small.

Tables 6.4 and 6.5 present the results of these two analyses. The wave frequency varies from 0.15 rad/s to 0.7 rad/s. For each wave the surge, heave and pitch responses as well as the tendon forces are given in terms of frequency components.

4.3.1. Surge Response

Figure 6.40 presents the predictions of the linear and non linear models for the surge offset.

The linear model gives a constant offset. The small fluctuations are due to numerical imprecision during the Fourier transform.

The value of the offset calculated with the non linear model varies significantly for frequencies between 0.15 and 0.4 rad/s. This range corresponds to the waves of largest amplitudes. For smaller waves, however, the value remains more or less constant. This value is about 13% higher than the prediction of the linear model.

Figure 6.41 shows that the results of the two models for the first order surge response are very similar.

4.3.2. Heave Response

Three components are important in the heave response, the offset, the first and the second order responses.

Since no steady force is present in heave, the heave offset calculated with the linear model is equal to zero. (See Figure 6.42).

However, the non linear model takes the set down effect into account and thus gives an offset in heave. Its value reaches a maximum of 33 cm for the highest wave. Then it decreases to a constant value of 12.5 cm.

Figure 6.43 shows that the non linear model gives higher values of the first order response in heave. This difference is amplified for the largest waves. The maximum difference between the two predictions is about 30 cm for a 0.25 rad/s wave.

At twice the wave frequency, the linear model predicts no response. However, the non linear model shows significant values for the highest waves. This response rapidly decreases as the amplitude of waves is reduced. (See Figure 6.44)

4.3.3. Pitch Response

The offset calculated with the non linear model is bigger than the value predicted by the linear model (See Figure 6.45). The behaviour of the offset is similar to what has been observed in surge. The linear model predicts a constant offset over the range of frequencies. Whereas the value calculated by the non linear model varies for the highest waves, and is constant for the smallest ones.

For the first order pitch response, the two models give close results. Only a small difference can be observed in the low frequency range. (See Figure 6.46)

4.3.4. Tendon Forces

An important remark that has been made before in the comparison of the two models, is that the non linear model do not predict the same load in every tendon.

One tendon force is plotted for the linear model whereas the forces in both the upstream and the downstream tendons are plotted for the non linear model in the Figures 6.47 and 6.48.

Figure 6.47 presents the results of the two models in terms of pretension.

The value is directly linked to the values of the offset of the platforms. The linear model gives a constant pretension whereas the non linear results show a variation in the pretension for the larger waves.

The variations between the two sets of results are quite significant. Compared to the linear model results, the pretension is 3% smaller in the down stream tendon and 5% larger in the up-stream tendon.

The values of the first order tendon forces are presented in Figure 6.48. Once again, the two models show significant differences. For the highest waves, the linear model predicts a force that is close to the up-stream tendon force. But at lower frequency, the linear model underestimates the forces both in the up-stream and the down-stream tendons. At 0.4 rad/s, the difference reaches a maximum of 18.5 Mega-Newtons.

Finally, one should note that the asymmetry of the forces decreases when the waves become smaller.

4.4. EFFECTS OF THE DIRECTIONALITY OF THE ENVIRONMENTAL FORCES

So far, the environmental forces have always been taken as collinear, and only head seas have been considered.

In this section, the influence of the direction of the three environmental forces on the Snorre TLP is investigated.

Several tests have been carried out with the time domain program for four different wave, wind and current angles - 0, 45, 90 and 135 degrees.

The sea state is represented by a regular wave of 13.52 m amplitude and 0.2 rad/s frequency. The wind and current velocities are respectively 40 m/s and 0.6 m/s.

The time domain program uses the same non linear model as in the previous section. All the non linear terms implemented in the developed model are used except for the displacements of the platform because of computational time limitations.

Table 6.6 presents the results in terms of responses and tendon forces for different combinations of the loading.

The displacements are given in five degrees of freedom in terms of steady offset and first order response. For heave, the second order response is also included.

The loads in the four tendons are given in terms of pretension and first order force.

The numbering of the tendons (1 to 4) corresponds to following geometry:

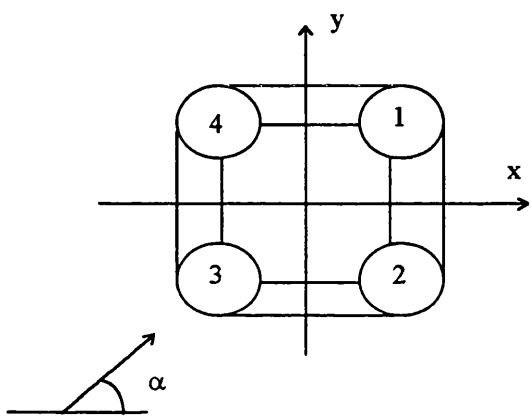

The row labelled "Fo-F1", represents the difference between the pretension and the first order force amplitude. The closer this coefficient comes to zero, the closer the tendons are to become slack. This value is referred to as the slackness coefficient later in the analysis.

Finally, the last three rows of the table give the total pretension in the four tendons, the mean value of the first order force in the four tendons, and the mean value of the slackness coefficient over the four tendons.

4.4.1. Tendon Force Model Analysis

In order to understand the loading in the tendon, it is useful to relate the tendon force to the offset and the first order responses of the TLP.

The offset at the tendon connection (point C) is given by the following relation:

$$\bar{x}_{0C} = \bar{x}_{0G} + \bar{\Omega}_0 \times \bar{X}_C \qquad (4.4\text{-}1)$$

Where x_{0G} is the offset at the centre of gravity
X_C is the position of point C
Ω_0 is the steady rotation

In the same way, the first order displacement is given by:

$$\vec{x}_{1C} = \vec{x}_{1G} + \vec{\Omega}_1 \times \left(\vec{X}_C + \vec{x}_{0C}\right) \tag{4.4-2}$$

which becomes after developments:

$$\vec{x}_{1C} = \vec{x}_{1G} + \vec{\Omega}_1 \times \vec{x}_{0G} + \vec{\Omega}_1 \times \left(\vec{X}_C + \vec{\Omega}_0 \times \vec{X}_C\right) \tag{4.4-3}$$

The pretension in the tendons can be written as:

$$F_0 = T_0 + \vec{K} \cdot \vec{x}_{0C} \tag{4.4-4}$$

Where: T_0 is the original pretension
K is the linear stiffness vector equal to:

$$\vec{K} = \begin{pmatrix} T_0 / L_c \\ T_0 / L_c \\ EA / L_c \end{pmatrix} \tag{4.4-5}$$

Similarly, the first order force becomes:

$$F_1 = \vec{K} \cdot \vec{x}_{1C} \tag{4.4-6}$$

More details regarding these developments, can be found in reference [6.4].

From this analysis, it appears that the asymmetry in the pretension and first order force are due to the second term of equations 4.4-1 and 4.4-3.

The pretension is directly related with the value of the offset. The offset is mainly due to the steady wind force. We will then be looking for a relation between wind direction and pretension.

The influence of the offset in the value of the first order force is small. Thus, the first order force is mainly related to the wave inertia force. The heading of the wave should be the most important factor for the first order forces in the tendons.

4.4.2. Pretension

The total pretension in the four tendons remains more or less the same in each of the tests carried out in this study. The main differences appear in the distribution of the loads among the different tendons.

The pretension values are almost constant in tendons 1 and 3. They correspond to the down-stream and up-stream tendons in terms of wind loading.

Tendons 2 and 4 show more significant variations. As expected, they are directly related to the wind angle. The pretension is maximum ($\cong$ 62 MN) in tendon 4 and minimum in tendon 1 (58 MN) for a 0 degree wind heading.

For a 90 degree wind angle, we observe an inversion of the forces, about 62 MN in tendon 1 and 58 MN in tendon 4.

For 45 degrees, the loads in both tendons are equal (about 60 MN).

4.4.3. First Order Force

The mean values of the first order tendon force show insignificant changes with the angle of the environmental forces.

However, the distribution of the loads in the different tendons changes. They are directly related to the wave angle.

Tendon 1 and 3 have roughly constant values for 0 and 90 degrees heading seas - about 47 MN for tendon 1 and 39 MN for tendon 3.

For quartering seas, this value increases by 6% and 7.5% in tendons 1 and 3 respectively.

However, this effects is compensated by a decrease in the loads of tendons 2 and 4.

4.4.4. Slackness Coefficient

The mean value of this coefficient over the four tendons is very similar in every test.

Yet, the slackness coefficient varies significantly from one tendon to another, depending on the wave angle.

The smaller values appear for quartering seas in the down-stream tendon. This corresponds to tendon 1 for a 45 degree wave and tendon 4 for a 135 degree wave.

4.4.5. Conclusion

The overall tendon loads do not vary significantly depending on the angle of the wave, wind and current.

Yet significant differences, in the forces can be observed between the different tendons. The loads in the tendons are related to only one of the environmental forces. The pretension is sensitive mainly to the wind angle. Similarly, the first order forces changes significantly only with the direction of the waves.

What has been called the slackness coefficient, the difference between the pretension and the amplitude of the first order force, shows a minimum in the down-stream tendon for quartering seas.

REFERENCES OF CHAPTER 6

[6.1] Natvig B.J., 1994, A proposed ringing analysis model for higher order tether response, Proceedings of the fourth International Offshore and Polar Engineering Conference, ISOPE.

[6.2] Faltinsen O.M., 1990, Sea loads on ships and offshore structures, Ocean Technology Series, Cambridge University Press.

[6.3] Campbell I.M., Weynberg P.A., 1980, Measurements of parameters affecting slamming, Technology Reports Centre, No. OT-R-8042, Southampton University.

[6.4] Matsui T., Sakoh Y., Nozu T., 1993, Second order sum frequency oscillations of tension leg platforms: predictions and measurements, Applied Ocean Research Vol.15, p.107-118.

TLP RESPONSE: TIME DOMAIN SIMULATION
Snorre TLP Amplitude=13.52m Frequency=0.2rad/s Head sea

Motion	Frequency	Linear Test 0	Non Linear Stiffness Test 1	Viscous Damping Test 2	Acceleration Coupling Test 3	Drag Forces Test 4	Free Surface Effects Test 5	Displacement Test 6	All Effects (-Disp) Test 7	All Effects Test 8
	Offset	8.01	6.81	7.996	8.01	9.22	8.27	8.39	7.97	8.82
Surge	0.2 rad/s	15.98	16.04	15.53	15.98	16.209	16.02	15.95	15.61	15.7
Response (m)	0.4 rad/s	2.38E-02	1.82E-01	2.12E-02	2.38E-02	2.87E-02	7.83E-02	1.31E-01	1.45E-01	5.43E-02
	0.6 rad/s	1.04E-02	1.09E-02	8.87E-02	1.04E-02	3.56E-02	1.41E-02	1.14E-02	4.97E-02	5.15E-02
	Offset	0.000	-0.320	0.000	0.000	0.000	0.000	0.000	-0.332	-0.356
Heave	0.2 rad/s	0.204	0.367	0.204	0.204	0.207	0.204	0.204	0.437	0.48
Response (m)	0.4 rad/s	6.03E-04	0.245	6.03E-04	7.17E-04	6.09E-04	6.04E-04	6.03E-04	0.234	0.236
	0.6 rad/s	3.02E-04	5.82E-03	3.02E-04	2.10E-04	7.46E-03	3.02E-04	3.02E-04	7.59E-03	8.30E-03
	Offset	5.26E-05	3.16E-04	5.26E-05	5.22E-05	2.44E-05	5.00E-05	4.46E-05	2.77E-04	2.91E-04
Pitch	0.2 rad/s	1.64E-03	2.16E-03	1.64E-03	1.64E-03	1.73E-03	1.60E-03	1.64E-03	2.10E-03	2.12E-03
Response (rad)	0.4 rad/s	2.66E-06	2.13E-04	2.61E-06	3.40E-06	3.26E-06	1.65E-04	7.80E-05	3.69E-04	2.89E-04
	0.6 rad/s	3.23E-06	5.34E-06	1.37E-06	1.65E-06	5.11E-05	3.67E-05	5.20E-06	5.35E-05	5.69E-05
Force	Offset	5.85E+07	5.78E+07	5.85E+07	5.85E+07	5.85E+07	5.85E+07	5.85E+07	5.82E+07	5.82E+07
in	0.2 rad/s	3.99E+07	4.22E+07	3.99E+07	3.99E+07	4.05E+07	4.00E+07	3.99E+07	4.73E+07	4.76E+07
Tendon 1 (N)	0.4 rad/s	1.19E+05	1.99E+06	1.20E+05	1.35E+05	1.35E+05	1.20E+05	1.20E+05	2.93E+06	2.36E+06
(Down-Stream)	0.6 rad/s	8.28E+04	1.04E+05	8.53E+04	5.59E+04	1.59E+06	8.29E+05	8.20E+04	1.81E+06	1.89E+06
Force	Offset	5.85E+07	6.25E+07	5.85E+07	5.85E+07	5.85E+07	5.85E+07	5.85E+07	6.23E+07	6.25E+07
in	0.2 rad/s	3.99E+07	4.42E+07	3.99E+07	3.99E+07	4.05E+07	4.00E+07	3.99E+07	3.92E+07	3.88E+07
Tendon 3 (N)	0.4 rad/s	1.19E+05	1.85E+06	1.20E+05	1.35E+05	1.35E+05	1.20E+05	1.20E+05	2.93E+06	2.47E+06
(Up-Stream)	0.6 rad/s	8.28E+04	1.14E+05	8.53E+04	5.59E+04	1.59E+06	8.29E+05	8.20E+04	1.42E+06	1.37E+06

Table 6.1

TLP MOTION RESPONSES

SURGE

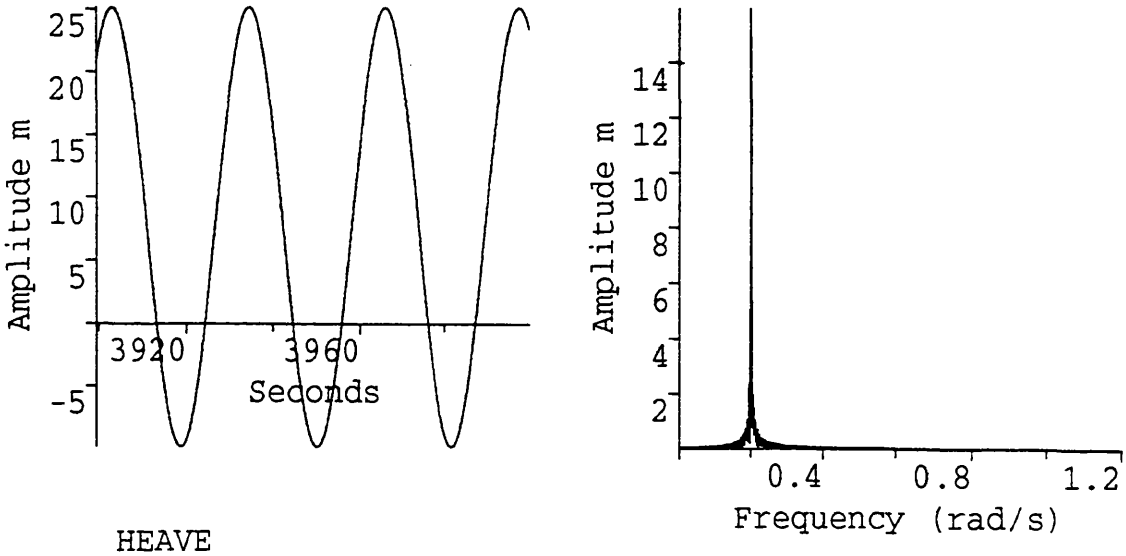

HEAVE

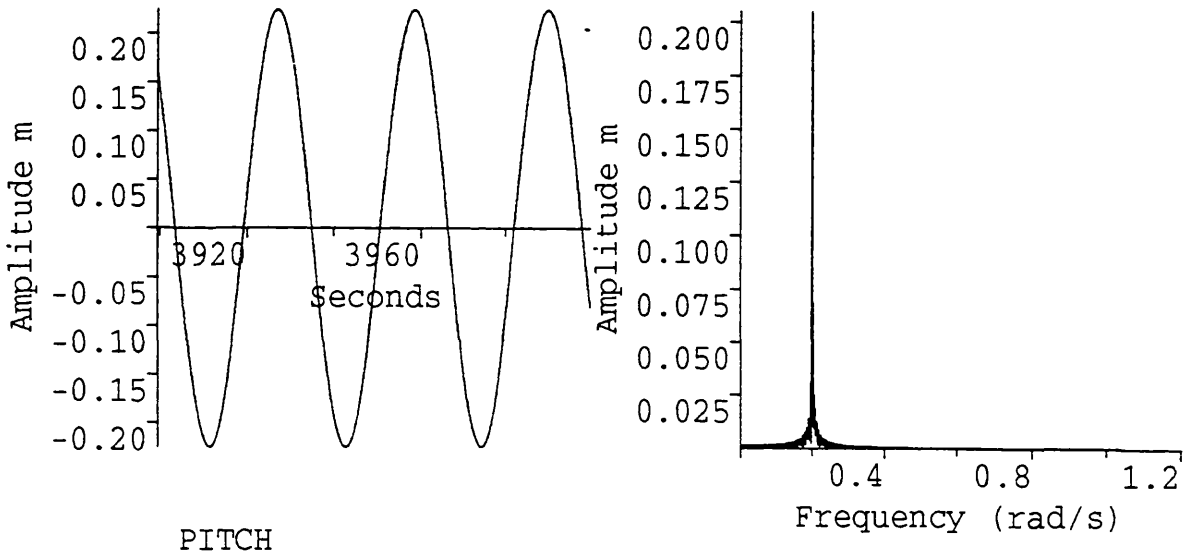

PITCH

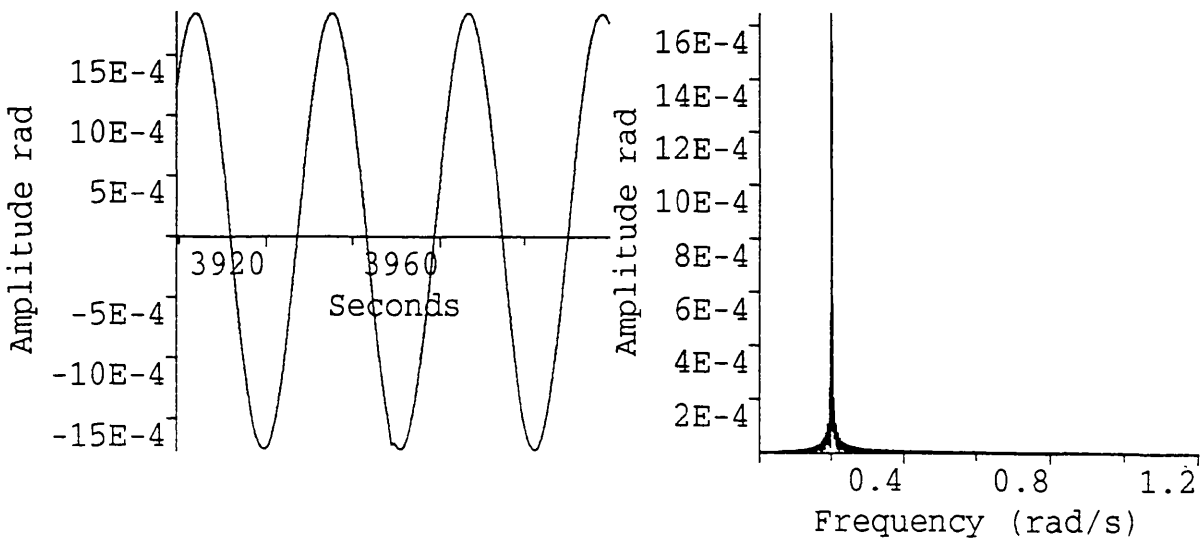

ure 6.1

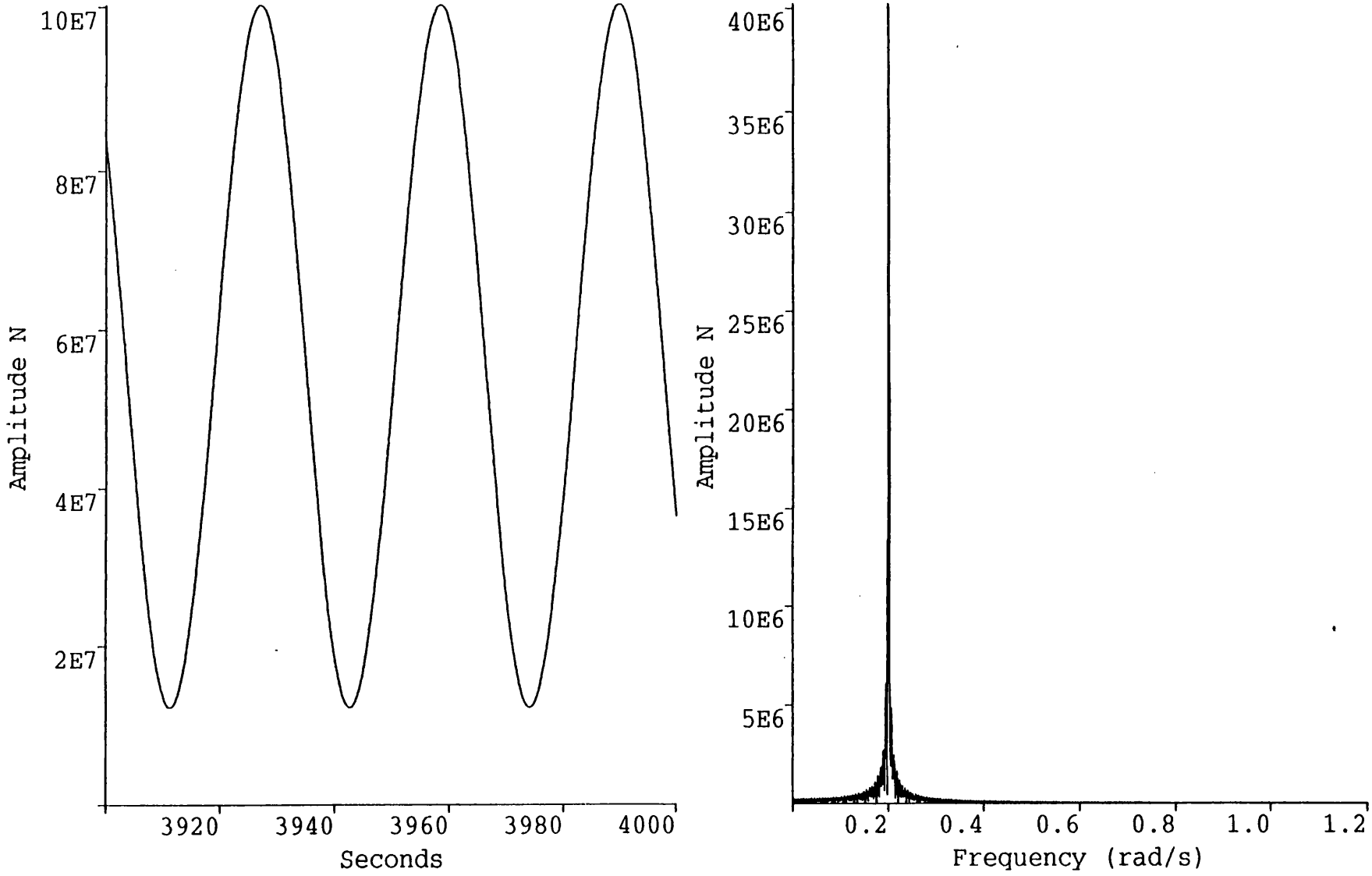
10E7
8E7
6E7
4E7
2E7
Amplitude N
3920
3940
3960
3980
4000
Seconds
40E6
35E6
30E6
25E6
20E6
15E6
10E6
5E6
Amplitude N
0.2
0.4
0.6
0.8
1.0
1.2
Frequency (rad/s)

Figure 6.2

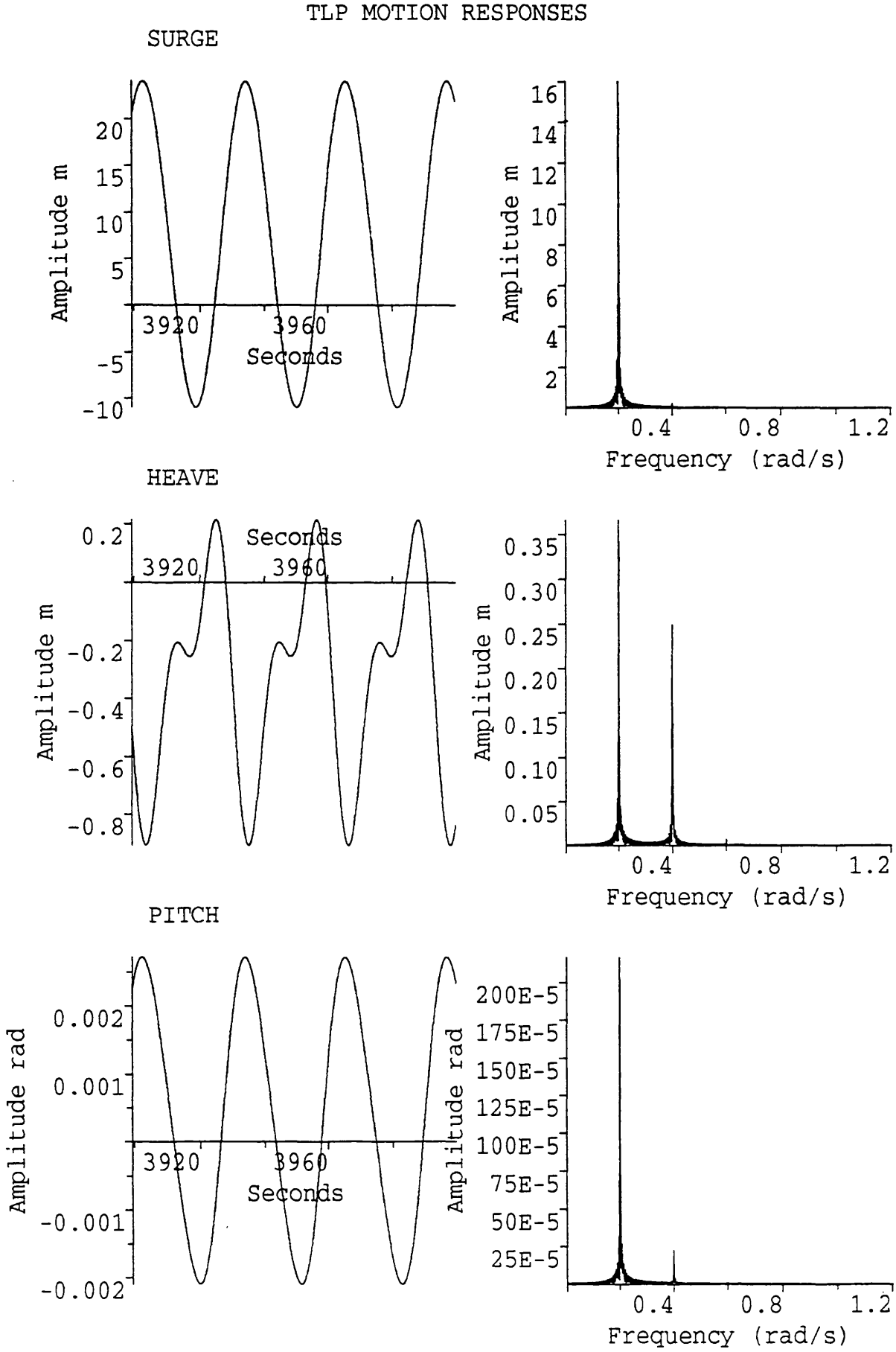
TLP MOTION RESPONSES
SURGE
Amplitude m
20
15
10
5
-5
-10
3920
3960
Seconds
Amplitude m
16
14
12
10
8
6
4
2
0.4
0.8
1.2
Frequency (rad/s)
HEAVE
Amplitude m
0.2
-0.2
-0.4
-0.6
-0.8
3920
Seconds
3960
Amplitude m
0.35
0.30
0.25
0.20
0.15
0.10
0.05
0.4
0.8
1.2
Frequency (rad/s)
PITCH
Amplitude rad
0.002
0.001
-0.001
-0.002
3920
3960
Seconds
Amplitude rad
200E-5
175E-5
150E-5
125E-5
100E-5
75E-5
50E-5
25E-5
0.4
0.8
1.2
Frequency (rad/s)

Figure 6.3

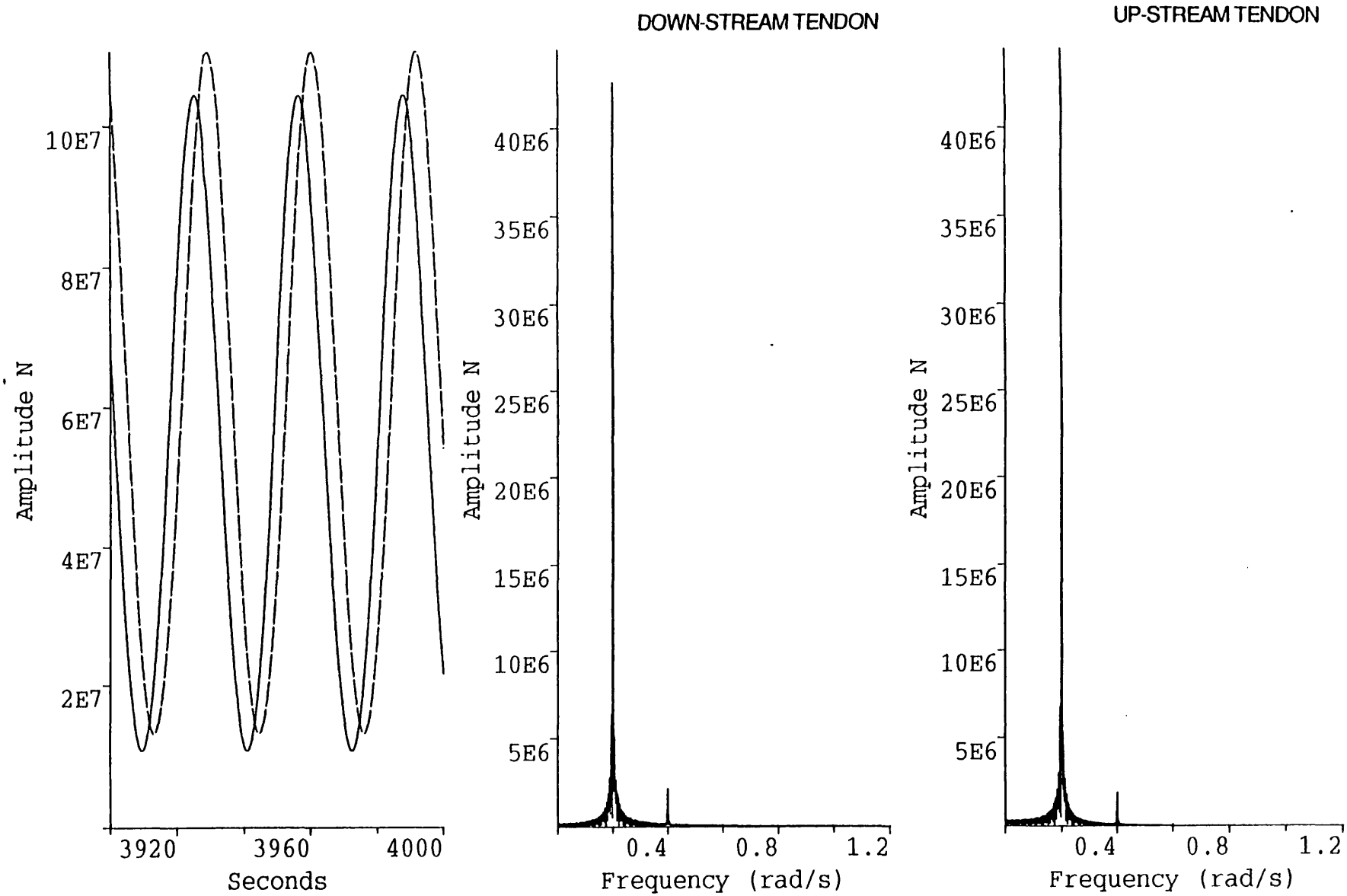
TENDON RESPONSES
DOWN-STREAM TENDON
UP-STREAM TENDON
Amplitude N
10E7
8E7
6E7
4E7
2E7
3920
3960
4000
Seconds
40E6
35E6
30E6
25E6
20E6
15E6
10E6
5E6
0.4
0.8
1.2
Frequency (rad/s)
Down-Stream Tendon
Up-Stream Tendon

Figure 6.4

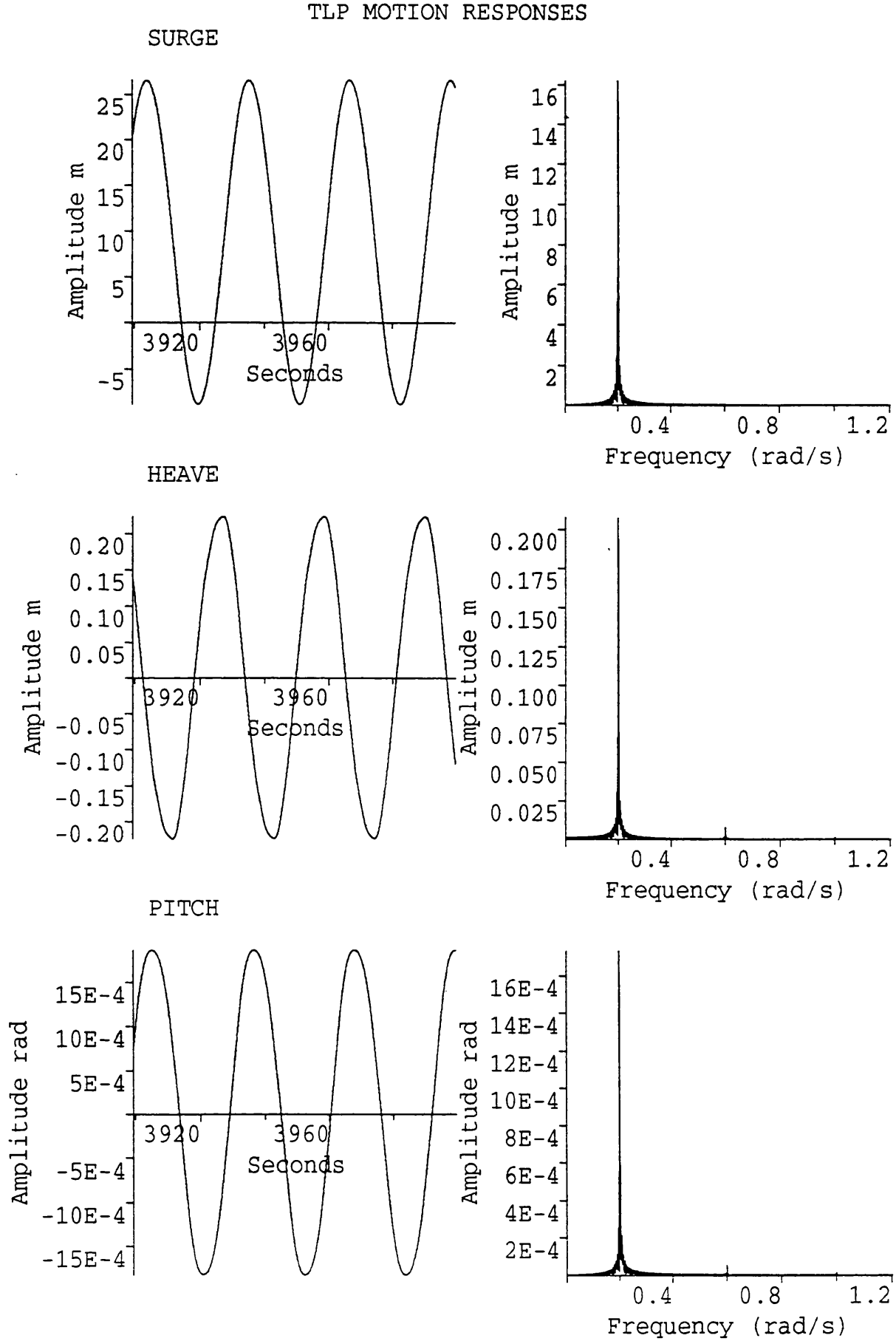
TLP MOTION RESPONSES
SURGE
Amplitude m
25
20
15
10
5
-5
3920
3960
Seconds
Amplitude m
16
14
12
10
8
6
4
2
0.4
0.8
1.2
Frequency (rad/s)
HEAVE
Amplitude m
0.20
0.15
0.10
0.05
-0.05
-0.10
-0.15
-0.20
3920
3960
Seconds
Amplitude m
0.200
0.175
0.150
0.125
0.100
0.075
0.050
0.025
0.4
0.8
1.2
Frequency (rad/s)
PITCH
Amplitude rad
15E-4
10E-4
5E-4
-5E-4
-10E-4
-15E-4
3920
3960
Seconds
Amplitude rad
16E-4
14E-4
12E-4
10E-4
8E-4
6E-4
4E-4
2E-4
0.4
0.8
1.2
Frequency (rad/s)

Figure 6.5

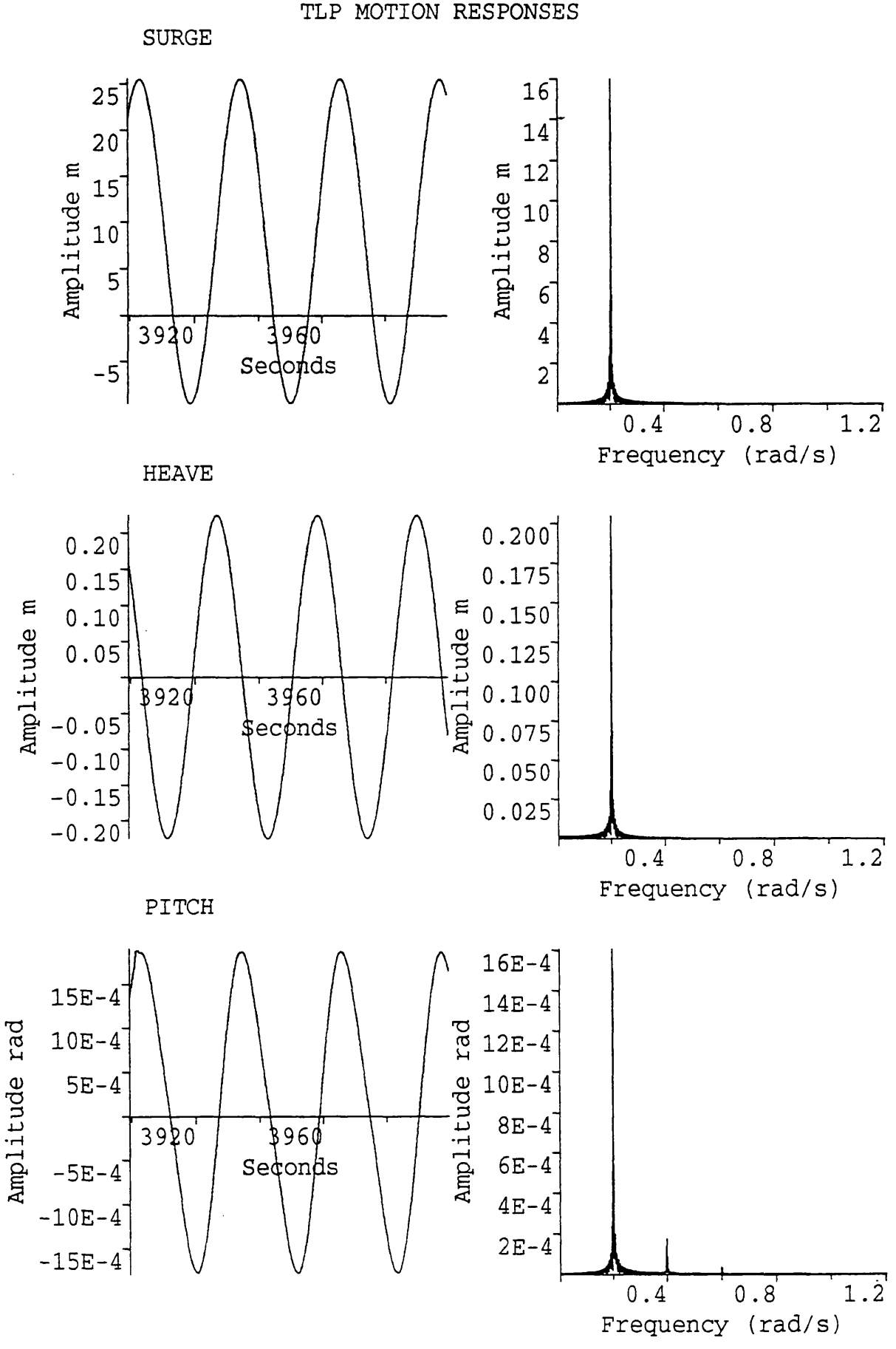
TLP MOTION RESPONSES
SURGE
Amplitude m
25
20
15
10
5
-5
3920
3960
Seconds
Amplitude m
16
14
12
10
8
6
4
2
0.4
0.8
1.2
Frequency (rad/s)
HEAVE
Amplitude m
0.20
0.15
0.10
0.05
-0.05
-0.10
-0.15
-0.20
3920
3960
Seconds
Amplitude m
0.200
0.175
0.150
0.125
0.100
0.075
0.050
0.025
0.4
0.8
1.2
Frequency (rad/s)
PITCH
Amplitude rad
15E-4
10E-4
5E-4
-5E-4
-10E-4
-15E-4
3920
3960
Seconds
Amplitude rad
16E-4
14E-4
12E-4
10E-4
8E-4
6E-4
4E-4
2E-4
0.4
0.8
1.2
Frequency (rad/s)

igure 6.6

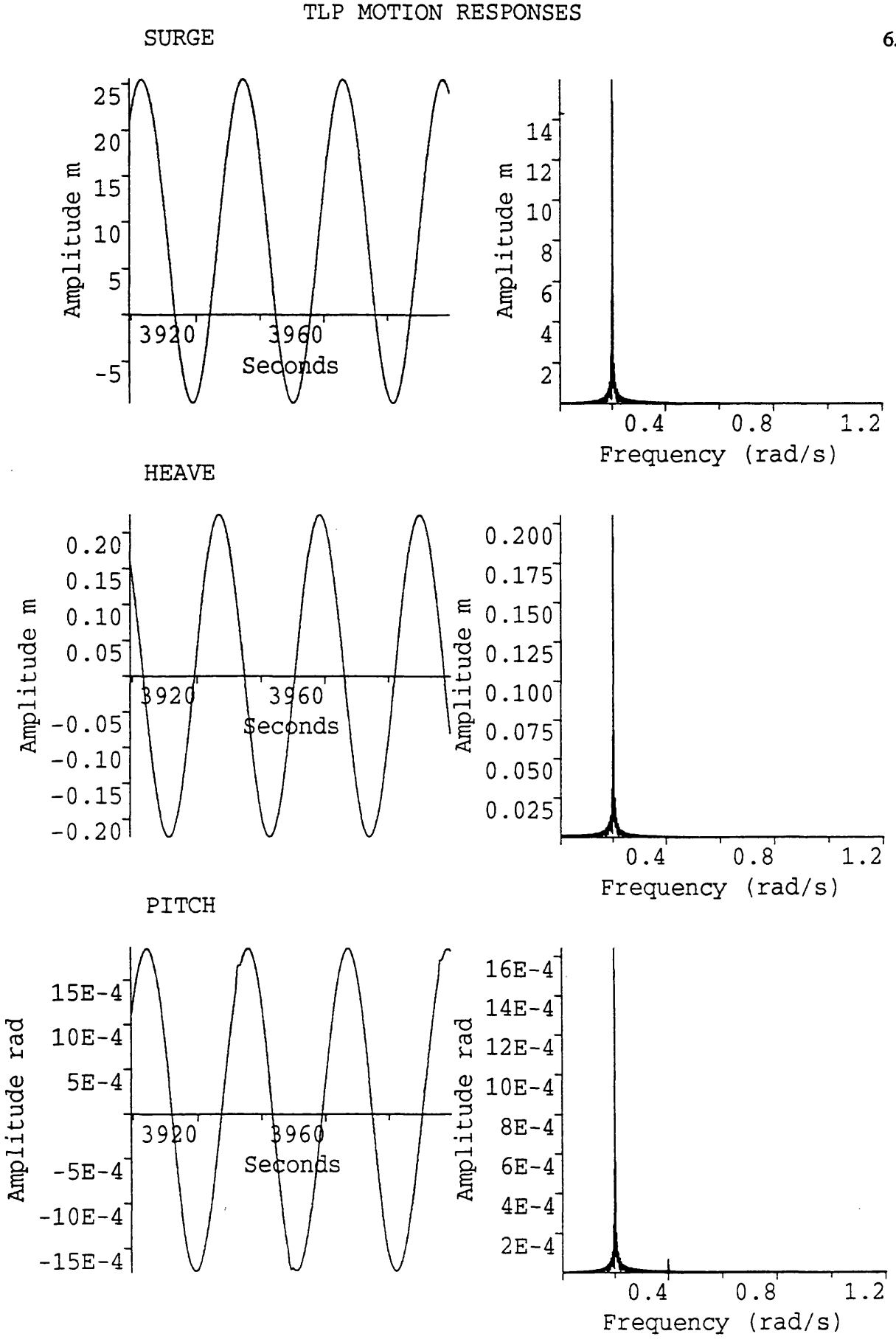
TLP MOTION RESPONSES
SURGE
Amplitude m
25
20
15
10
5
-5
3920
3960
Seconds
Amplitude m
14
12
10
8
6
4
2
0.4
0.8
1.2
Frequency (rad/s)
HEAVE
Amplitude m
0.20
0.15
0.10
0.05
-0.05
-0.10
-0.15
-0.20
3920
3960
Seconds
Amplitude m
0.200
0.175
0.150
0.125
0.100
0.075
0.050
0.025
0.4
0.8
1.2
Frequency (rad/s)
PITCH
Amplitude rad
15E-4
10E-4
5E-4
-5E-4
-10E-4
-15E-4
3920
3960
Seconds
Amplitude rad
16E-4
14E-4
12E-4
10E-4
8E-4
6E-4
4E-4
2E-4
0.4
0.8
1.2
Frequency (rad/s)

ure 6.7

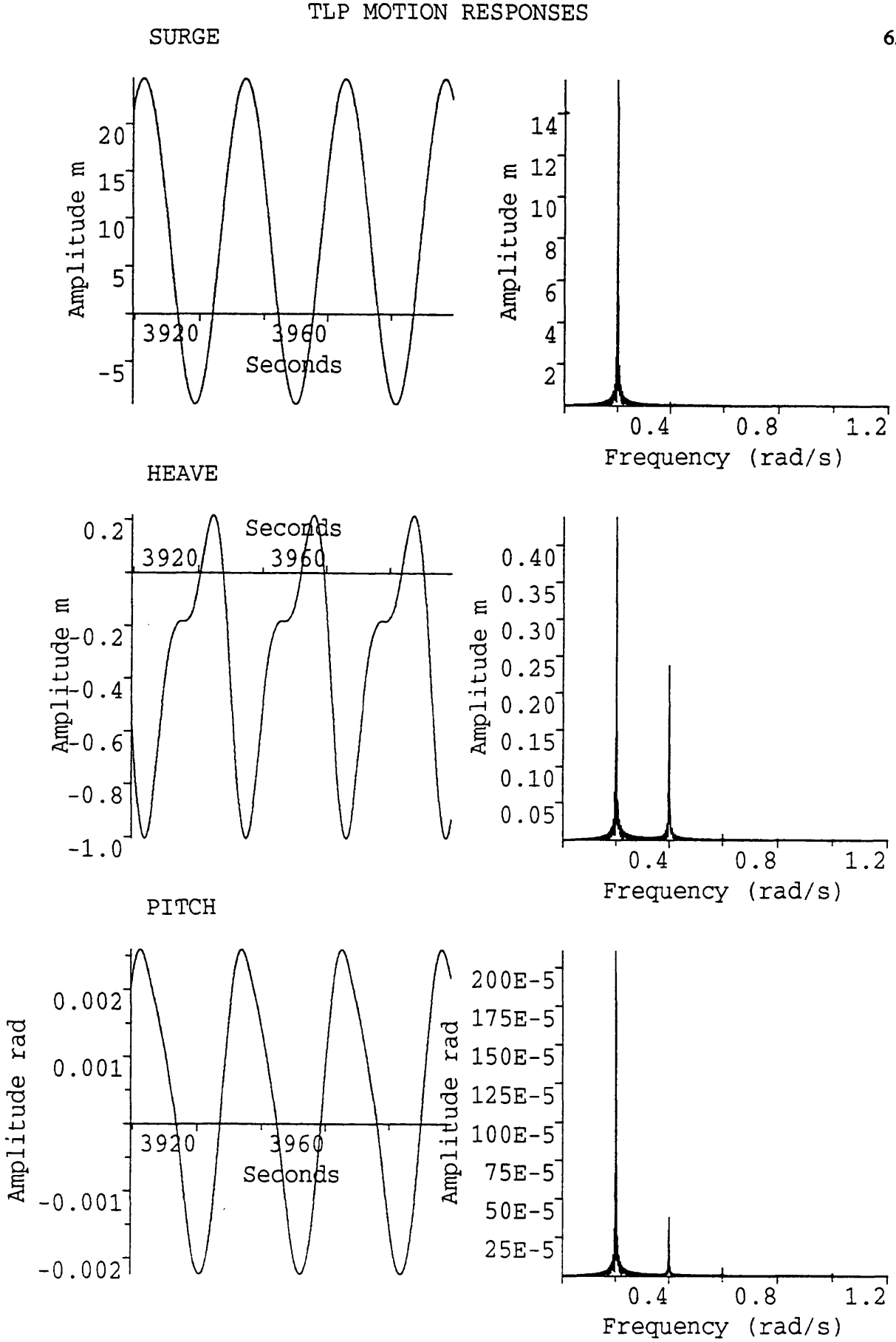
TLP MOTION RESPONSES
SURGE
Amplitude m
20
15
10
5
-5
3920
3960
Seconds
Amplitude m
14
12
10
8
6
4
2
0.4
0.8
1.2
Frequency (rad/s)
HEAVE
Seconds
3920
3960
0.2
-0.2
-0.4
-0.6
-0.8
-1.0
Amplitude m
Amplitude m
0.40
0.35
0.30
0.25
0.20
0.15
0.10
0.05
0.4
0.8
1.2
Frequency (rad/s)
PITCH
Amplitude rad
0.002
0.001
-0.001
-0.002
3920
3960
Seconds
Amplitude rad
200E-5
175E-5
150E-5
125E-5
100E-5
75E-5
50E-5
25E-5
0.4
0.8
1.2
Frequency (rad/s)

ure 6.8

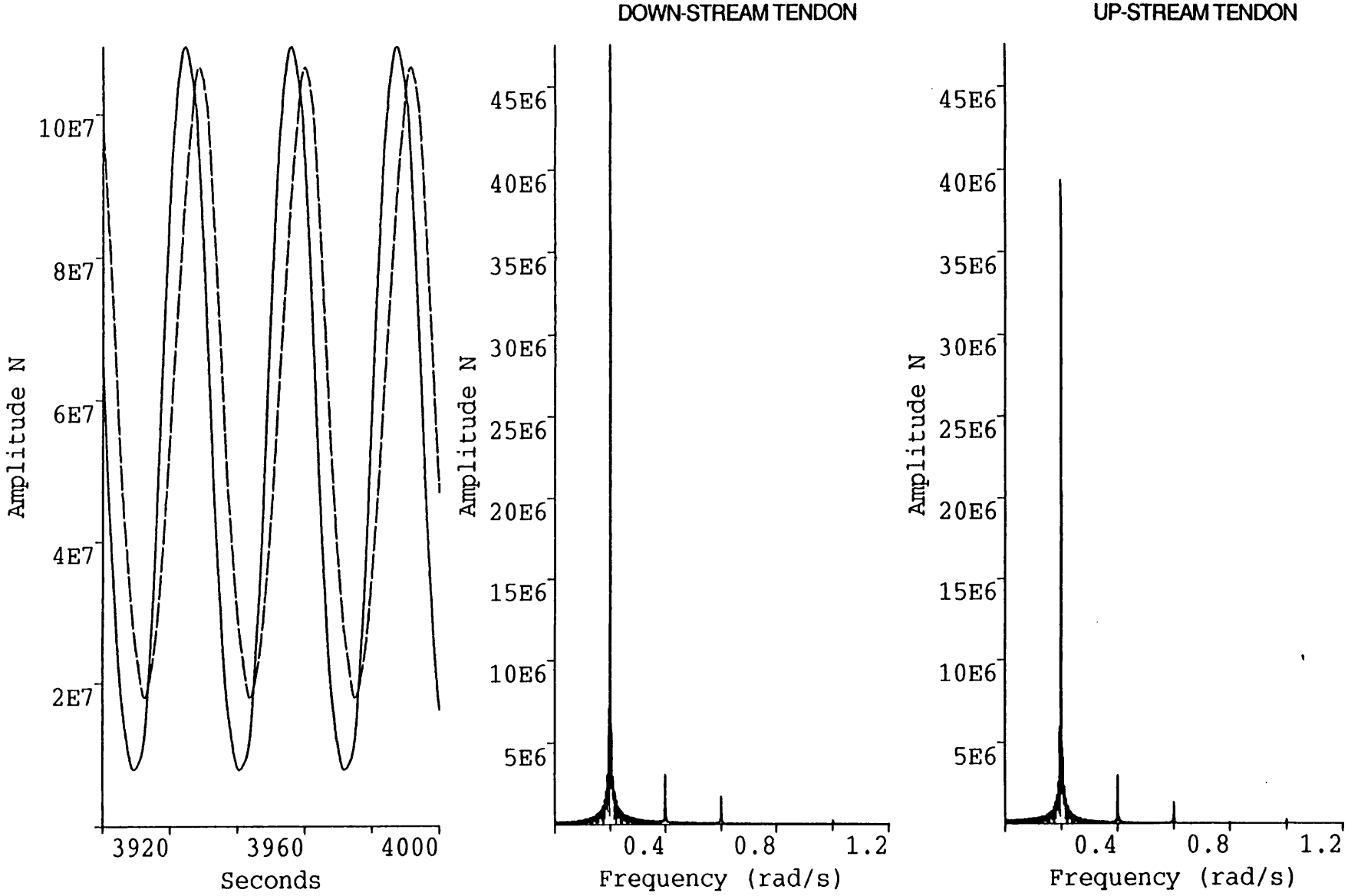
DOWN-STREAM TENDON
UP-STREAM TENDON
Amplitude N
10E7
8E7
6E7
4E7
2E7
3920
3960
4000
Seconds
45E6
40E6
35E6
30E6
25E6
20E6
15E6
10E6
5E6
0.4
0.8
1.2
Frequency (rad/s)
Down-Stream Tendon
Up-Stream Tendon

Figure 6.9

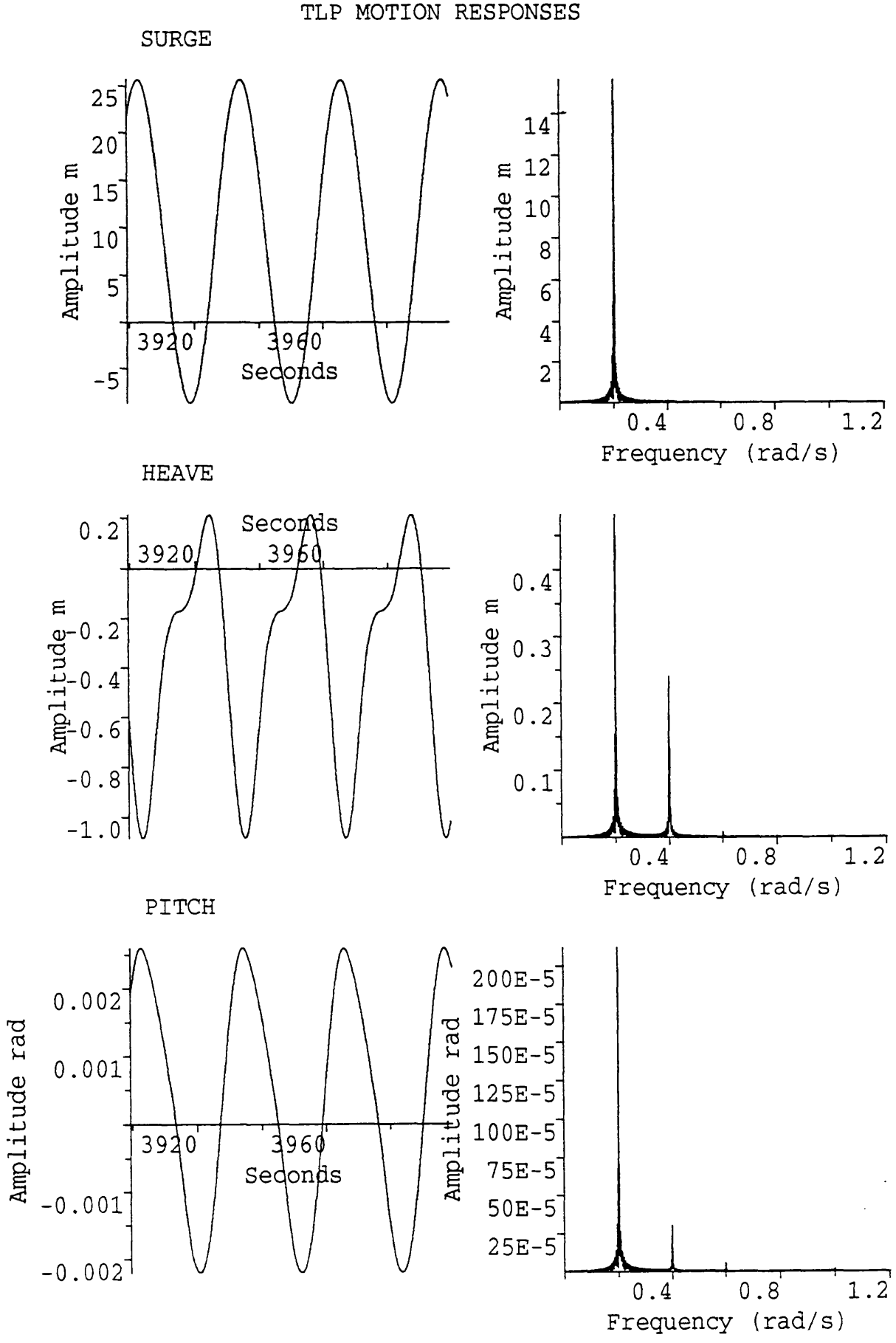
TLP MOTION RESPONSES
SURGE
Amplitude m
25
20
15
10
5
-5
3920
3960
Seconds
Amplitude m
14
12
10
8
6
4
2
0.4
0.8
1.2
Frequency (rad/s)
HEAVE
Seconds
0.2
3920
3960
Amplitude m
-0.2
-0.4
-0.6
-0.8
-1.0
Amplitude m
0.4
0.3
0.2
0.1
0.4
0.8
1.2
Frequency (rad/s)
PITCH
Amplitude rad
0.002
0.001
3920
3960
Seconds
-0.001
-0.002
Amplitude rad
200E-5
175E-5
150E-5
125E-5
100E-5
75E-5
50E-5
25E-5
0.4
0.8
1.2
Frequency (rad/s)

gure 6.10

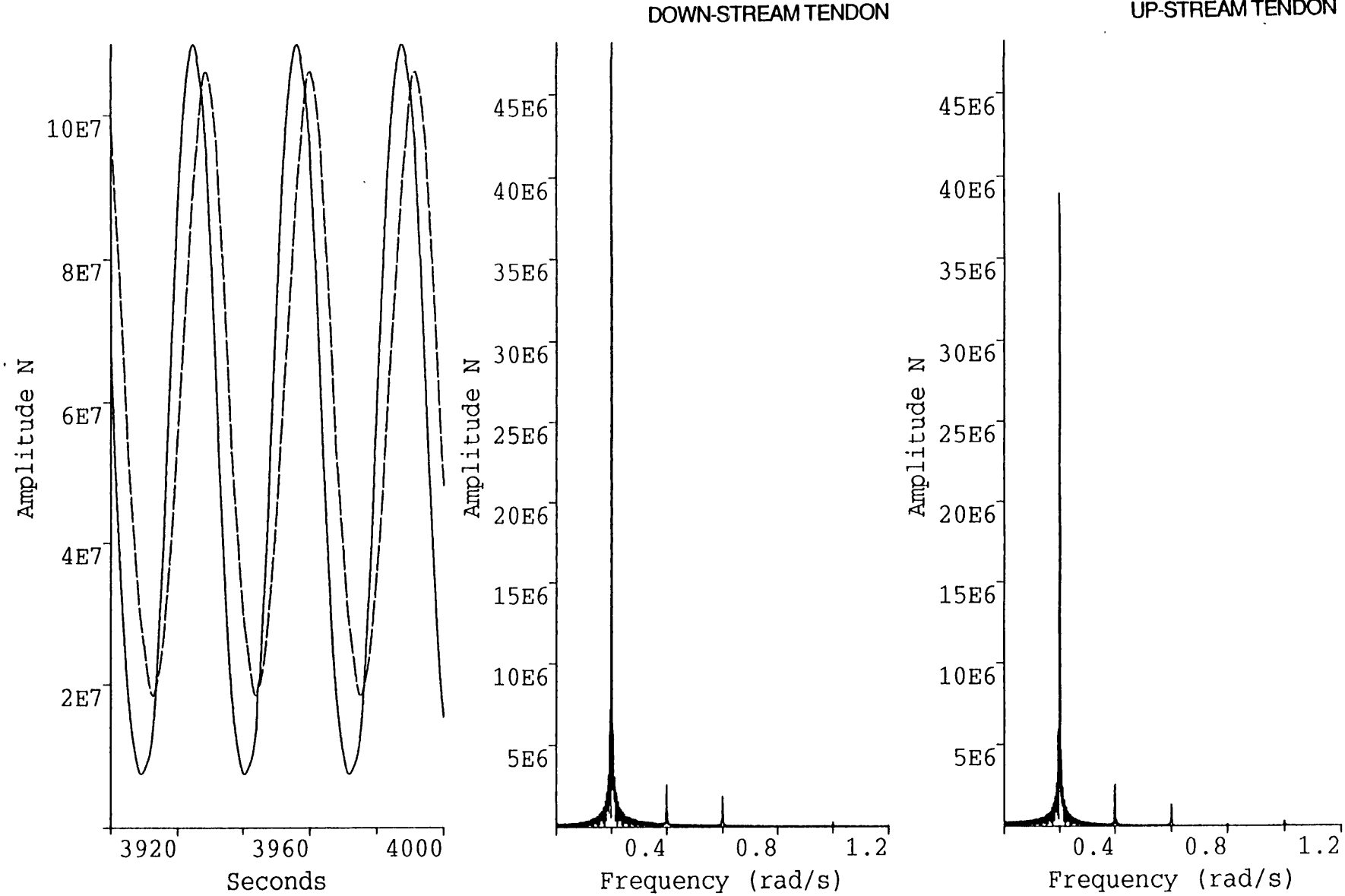
DOWN-STREAM TENDON
UP-STREAM TENDON
Amplitude N
10E7
8E7
6E7
4E7
2E7
3920
3960
4000
Seconds
45E6
40E6
35E6
30E6
25E6
20E6
15E6
10E6
5E6
0.4
0.8
1.2
Frequency (rad/s)
Down-Stream Tendon
Up-Stream Tendon

Figure 6.11

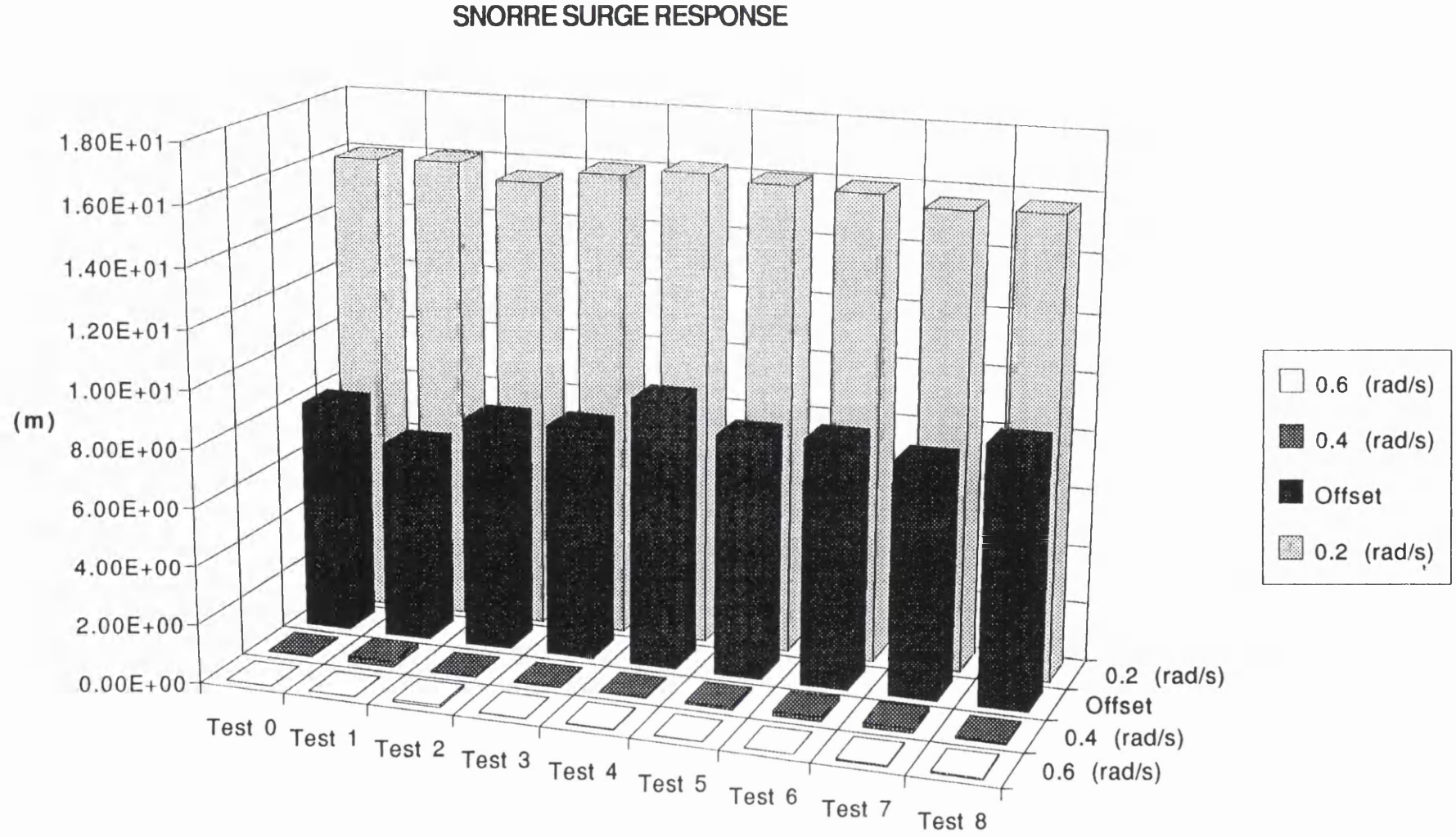
SNORRE SURGE RESPONSE
1.80E+01
1.60E+01
1.40E+01
1.20E+01
1.00E+01
(m)
8.00E+00
6.00E+00
4.00E+00
2.00E+00
0.00E+00
Test 0
Test 1
Test 2
Test 3
Test 4
Test 5
Test 6
Test 7
Test 8
0.2 (rad/s)
Offset
0.4 (rad/s)
0.6 (rad/s)
0.6 (rad/s)
0.4 (rad/s)
Offset
0.2 (rad/s)

Figure 6.12

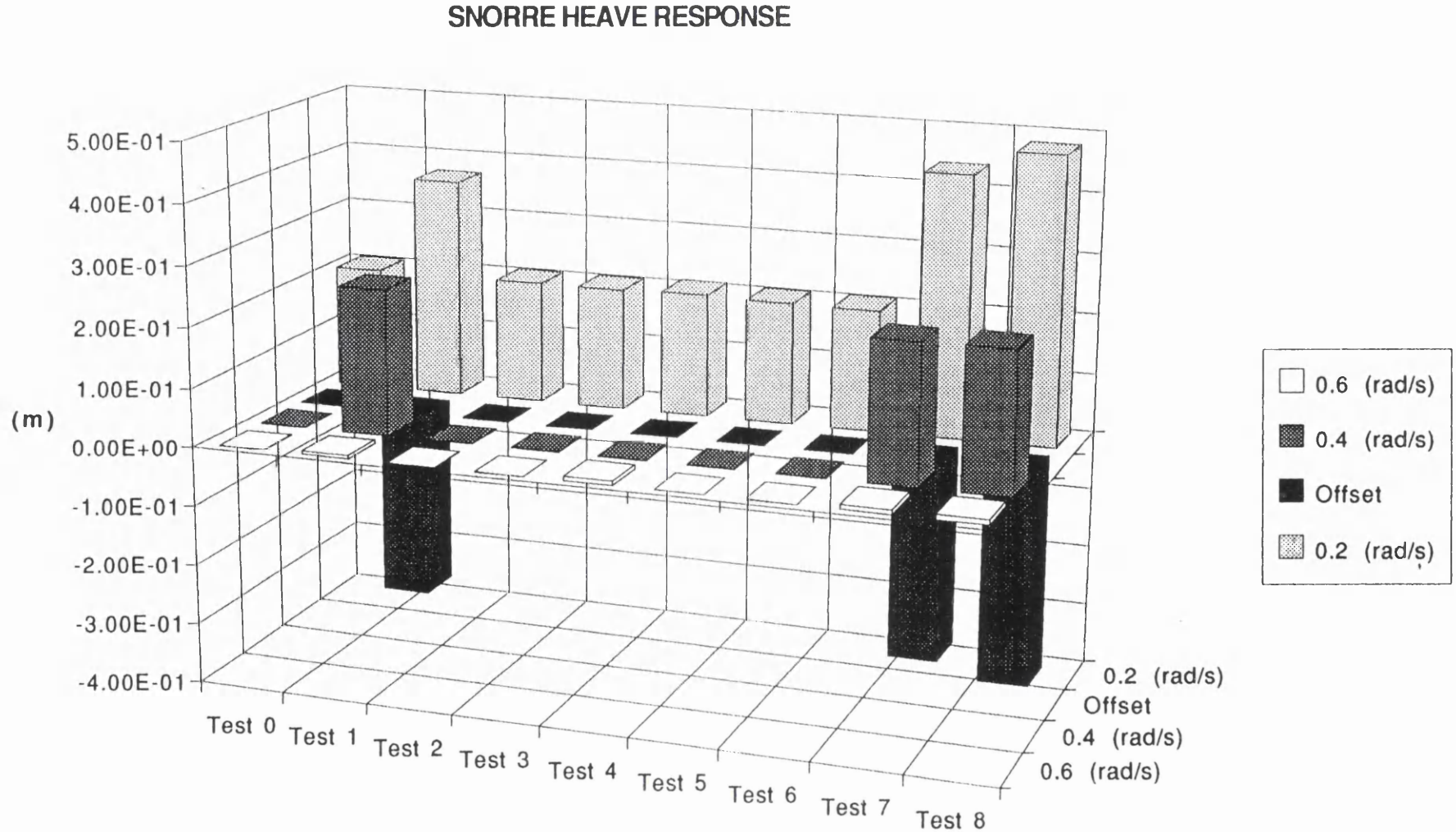
SNORRE HEAVE RESPONSE
5.00E-01
4.00E-01
3.00E-01
2.00E-01
1.00E-01
0.00E+00
-1.00E-01
-2.00E-01
-3.00E-01
-4.00E-01
(m)
Test 0
Test 1
Test 2
Test 3
Test 4
Test 5
Test 6
Test 7
Test 8
0.2 (rad/s)
Offset
0.4 (rad/s)
0.6 (rad/s)
0.6 (rad/s)
0.4 (rad/s)
Offset
0.2 (rad/s)

Figure 6.13

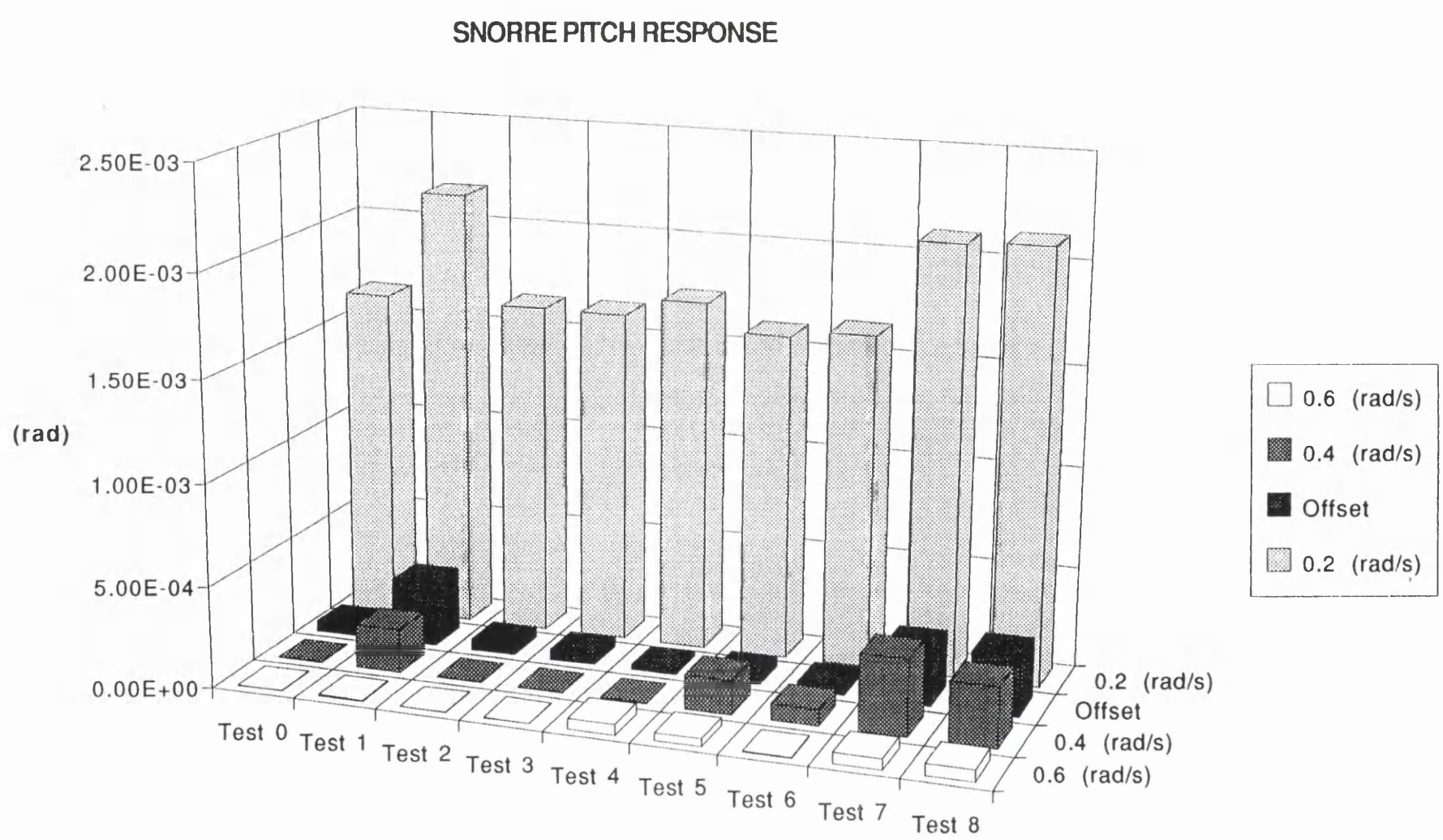
SNORRE PITCH RESPONSE
2.50E-03
2.00E-03
1.50E-03
(rad)
1.00E-03
5.00E-04
0.00E+00
Test 0
Test 1
Test 2
Test 3
Test 4
Test 5
Test 6
Test 7
Test 8
0.2 (rad/s)
Offset
0.4 (rad/s)
0.6 (rad/s)
0.6 (rad/s)
0.4 (rad/s)
Offset
0.2 (rad/s)

Figure 6.14

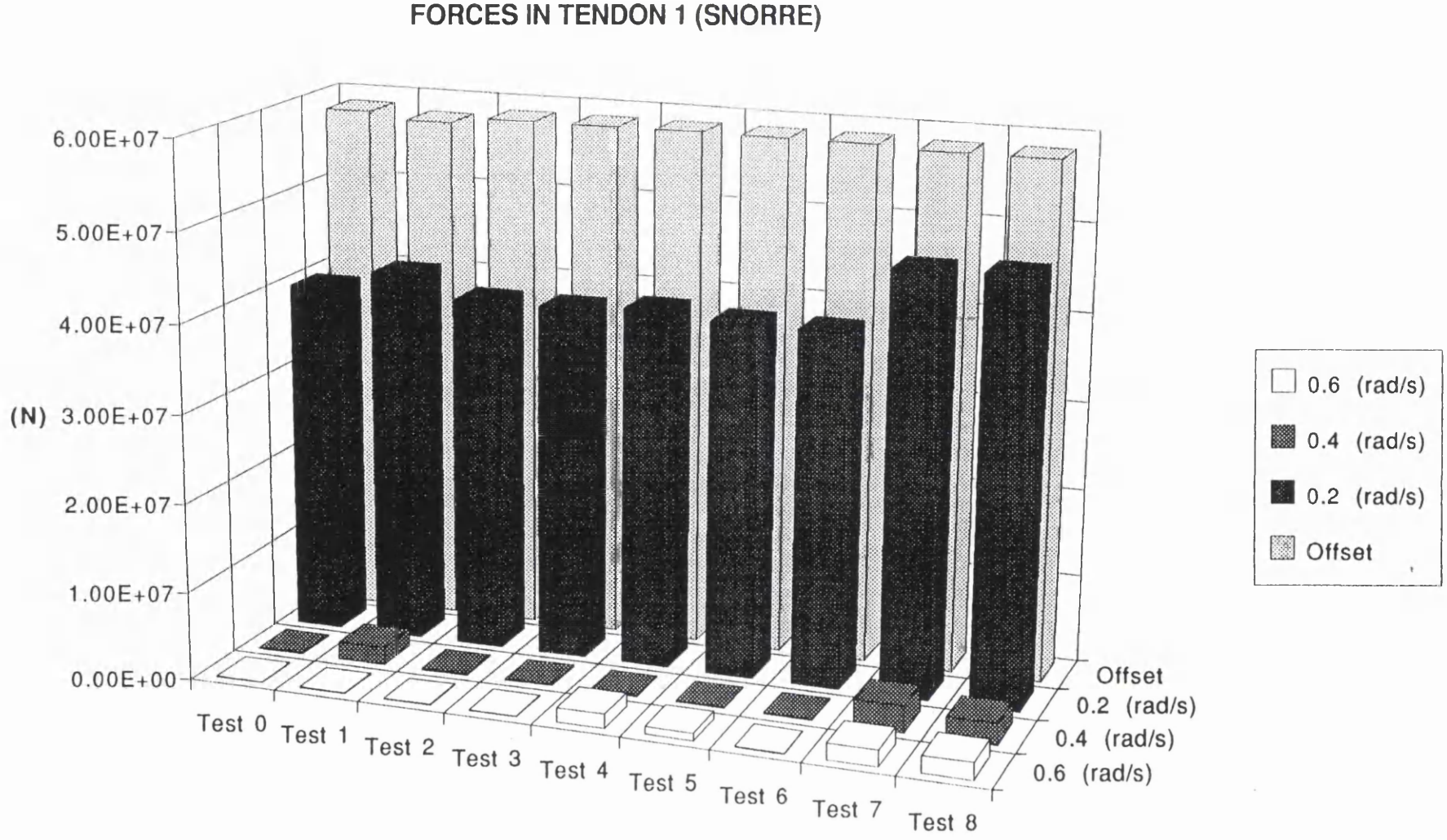
FORCES IN TENDON 1 (SNORRE)
6.00E+07
5.00E+07
4.00E+07
(N) 3.00E+07
2.00E+07
1.00E+07
0.00E+00
Test 0
Test 1
Test 2
Test 3
Test 4
Test 5
Test 6
Test 7
Test 8
Offset
0.2 (rad/s)
0.4 (rad/s)
0.6 (rad/s)
0.6 (rad/s)
0.4 (rad/s)
0.2 (rad/s)
Offset

Figure 6.15

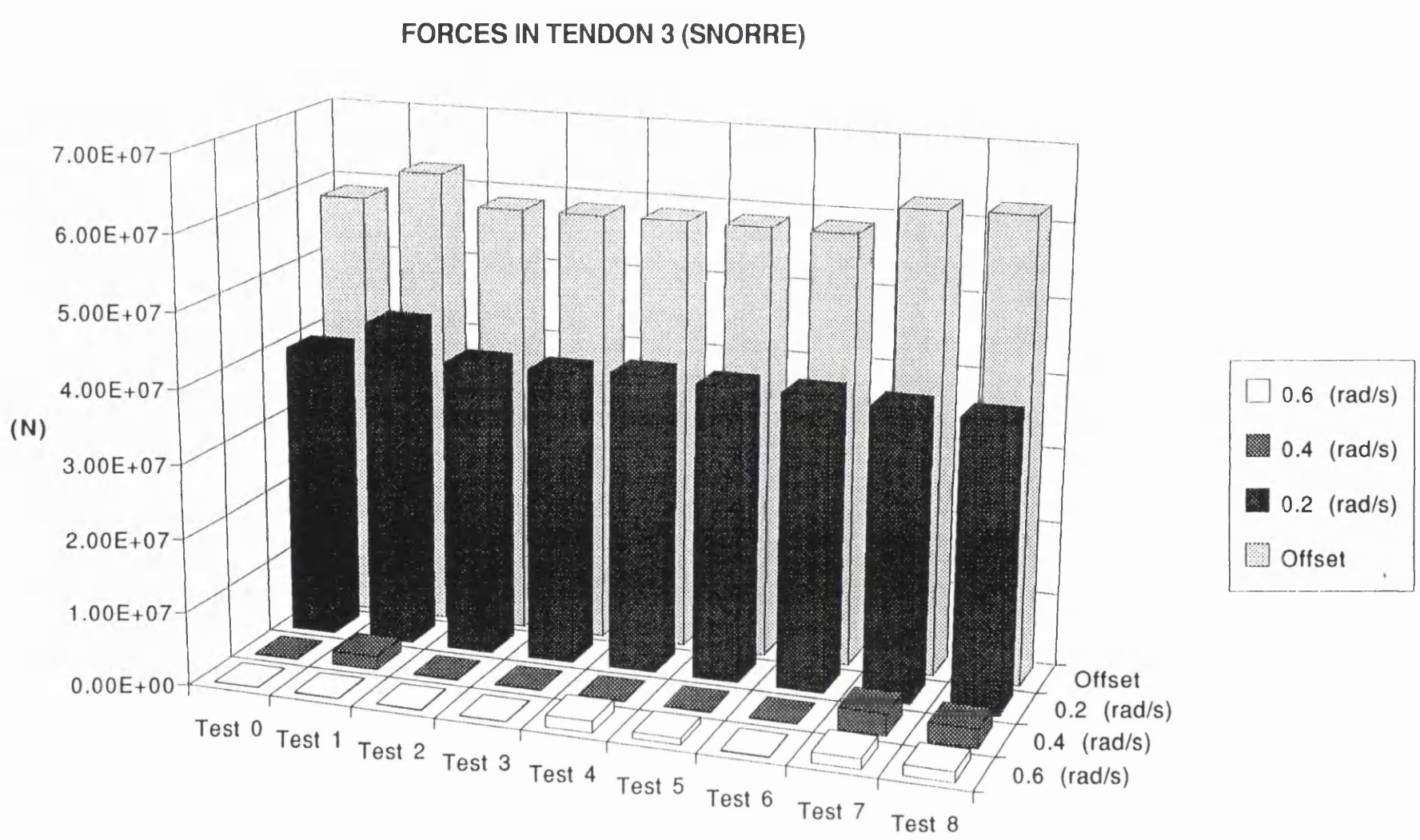
FORCES IN TENDON 3 (SNORRE)
7.00E+07
6.00E+07
5.00E+07
4.00E+07
(N)
3.00E+07
2.00E+07
1.00E+07
0.00E+00
Test 0
Test 1
Test 2
Test 3
Test 4
Test 5
Test 6
Test 7
Test 8
Offset
0.2 (rad/s)
0.4 (rad/s)
0.6 (rad/s)
0.6 (rad/s)
0.4 (rad/s)
0.2 (rad/s)
Offset

Figure 6.16

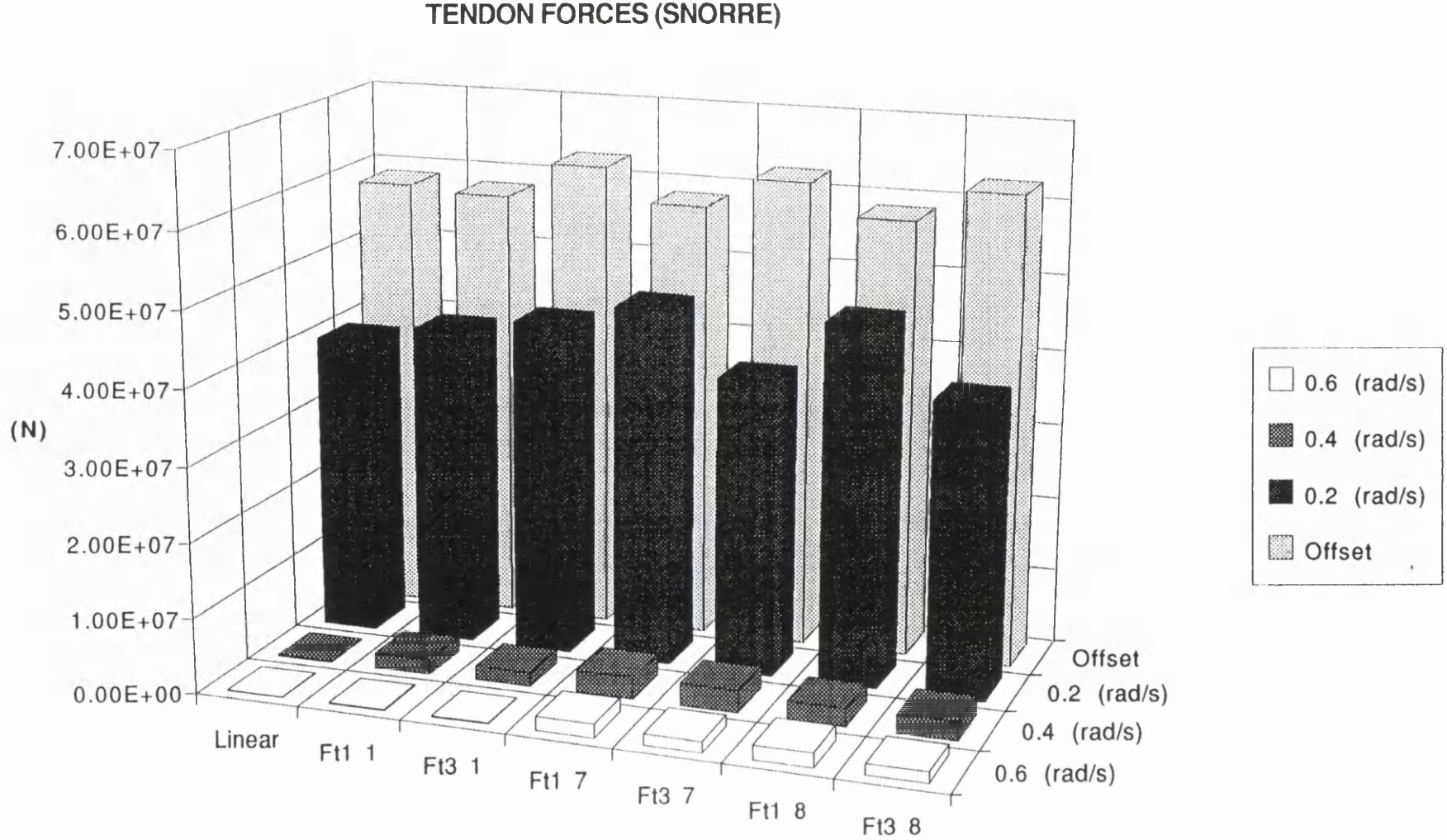
TENDON FORCES (SNORRE)
7.00E+07
6.00E+07
5.00E+07
4.00E+07
(N)
3.00E+07
2.00E+07
1.00E+07
0.00E+00
Linear
Ft1 1
Ft3 1
Ft1 7
Ft3 7
Ft1 8
Ft3 8
Offset
0.2 (rad/s)
0.4 (rad/s)
0.6 (rad/s)
0.6 (rad/s)
0.4 (rad/s)
0.2 (rad/s)
Offset

Figure 6.17

HEIDRUN TLP CHARACTERISTICS

Spacing between the columns centres	80 m
Columns diameter	31 m
Pontoon width	15.95 m
Pontoon height	13 m
Draught	77.3 m
Total Mass	2.52E+08 kg
Tether pretension	3.63E+08 N
Roll moment of inertia	2.40E+12 N.m.s^2
Pitch moment of inertia	2.40E+12 N.m.s^2
Vertical position of CoG above free surface	-18.98 m
Length of the mooring tethers	268.6 m
Section of the tethers	2.06 m^2
Young modulus of the tethers	2.13E+11 N/m^2
Surge Stiffness	1.35E+06 N/m
Heave Stiffness	1.65E+09 N/m
Roll Stiffness	2.62E+12 N/m
Surge natural frequency	4.80E-02 rad/s
Heave natural frequency	2.12 rad/s
Roll natural frequency	1.89 rad/s

Table 6.2

TLP RESPONSE: TIME DOMAIN SIMULATION
Heidrun TLP Amplitude=13.52m Frequency=0.2rad/s Head sea

Motion	Frequency	Linear Test 0	Non Linear Stiffness Test 1	Viscous Damping Test 2	Acceleration Coupling Test 3	Drag Forces Test 4	Free Surface Effects Test 5	Displacement Test 6	All Effects (-Disp) Test 7	All Effects Test 8
	Offset	7.47	6.86	7.438	7.47	8.63	7.76	7.77	8.62	9.2
Surge	0.2 rad/s	13.97	13.99	13.88	13.97	14.04	13.99	13.95	13.92	13.96
Response (m)	0.4 rad/s	4.06E-02	6.53E-02	4.05E-02	4.06E-02	3.70E-02	4.01E-02	1.05E-01	7.59E-02	3.31E-02
	0.6 rad/s	2.24E-02	2.17E-02	2.93E-02	2.24E-02	3.05E-02	1.97E-02	1.98E-02	1.80E-02	1.58E-02
	Offset	0.000	-0.272	0.000	0.000	0.000	0.000	0.000	-0.314	-0.334
Heave	0.2 rad/s	0.145	0.362	0.145	0.145	0.146	0.145	0.145	0.460	0.494
Response (m)	0.4 rad/s	4.19E-04	0.166	4.19E-04	4.11E-04	4.27E-04	4.19E-04	4.19E-04	0.164	0.166
	0.6 rad/s	1.36E-04	1.59E-03	1.35E-04	1.36E-04	3.08E-03	1.36E-04	1.36E-04	3.45E-03	3.15E-03
	Offset	1.67E-04	3.92E-04	1.66E-04	1.67E-04	1.52E-04	1.70E-04	1.64E-04	4.31E-04	4.43E-04
Pitch	0.2 rad/s	1.27E-03	1.70E-03	1.27E-03	1.27E-03	1.30E-03	1.24E-03	1.26E-03	1.65E-03	1.64E-03
Response (rad)	0.4 rad/s	5.97E-06	1.26E-04	5.99E-06	5.98E-06	6.05E-06	1.50E-04	1.48E-05	3.72E-05	7.59E-05
	0.6 rad/s	3.00E-06	4.58E-06	3.00E-06	3.00E-06	2.34E-05	2.79E-05	3.76E-06	3.11E-05	2.35E-05
Force	Offset	9.42E+07	8.99E+07	9.42E+07	9.42E+07	9.42E+07	9.42E+07	9.42E+07	8.97E+07	8.97E+07
in	0.2 rad/s	5.88E+07	6.29E+07	5.88E+07	5.88E+07	5.91E+07	5.88E+07	5.88E+07	6.79E+07	6.86E+07
Tendon 1 (N)	0.4 rad/s	6.14E+05	1.88E+06	6.14E+05	6.14E+05	6.45E+05	6.14E+05	6.14E+05	8.07E+05	1.56E+06
(Down-Stream)	0.6 rad/s	3.84E+05	4.30E+05	3.86E+05	3.84E+05	1.56E+06	3.84E+05	3.83E+05	2.00E+06	1.84E+06
Force	Offset	9.42E+07	1.03E+08	9.42E+07	9.42E+07	9.42E+07	9.42E+07	9.42E+07	1.04E+08	1.04E+08
in	0.2 rad/s	5.88E+07	6.74E+07	5.88E+07	5.88E+07	5.91E+07	5.88E+07	5.88E+07	6.17E+07	6.07E+07
Tendon 3 (N)	0.4 rad/s	6.14E+05	2.45E+06	6.14E+05	6.14E+05	6.45E+05	6.14E+05	6.14E+05	1.22E+06	1.47E+06
(Up-Stream)	0.6 rad/s	3.84E+05	3.28E+05	3.86E+05	3.84E+05	1.56E+06	3.84E+05	3.83E+05	1.13E+06	1.30E+06

Table 6.3

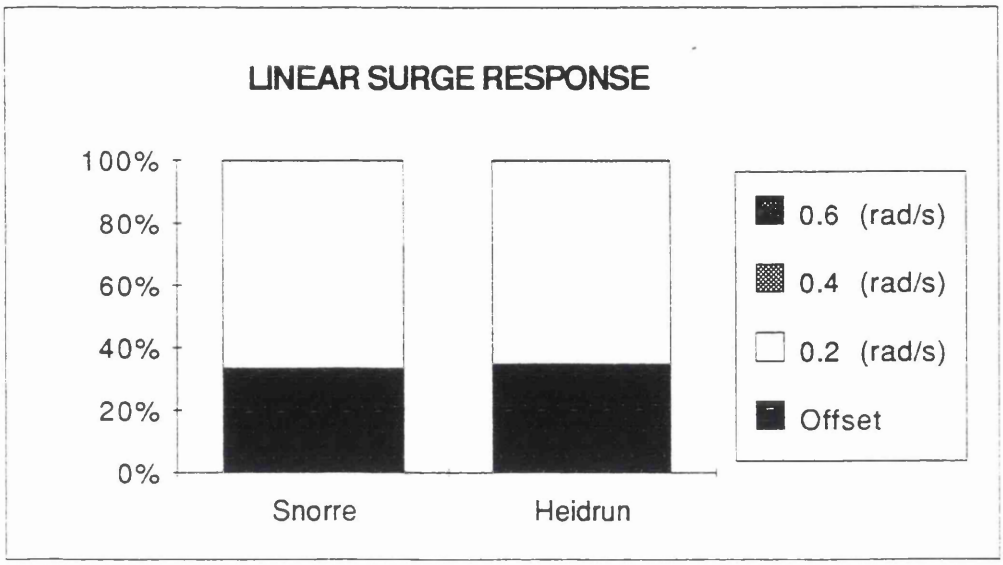

Figure 6.18

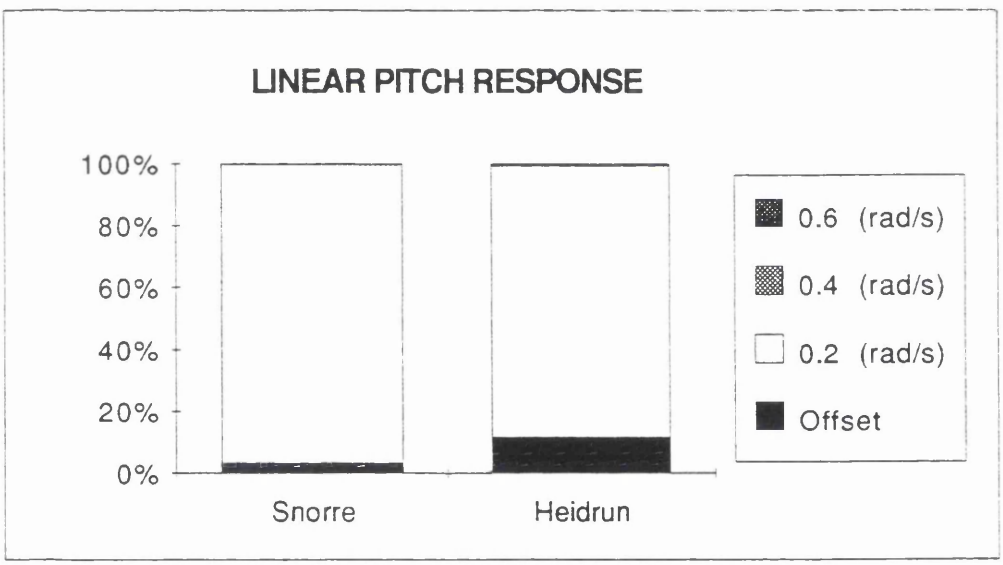

Figure 6.19

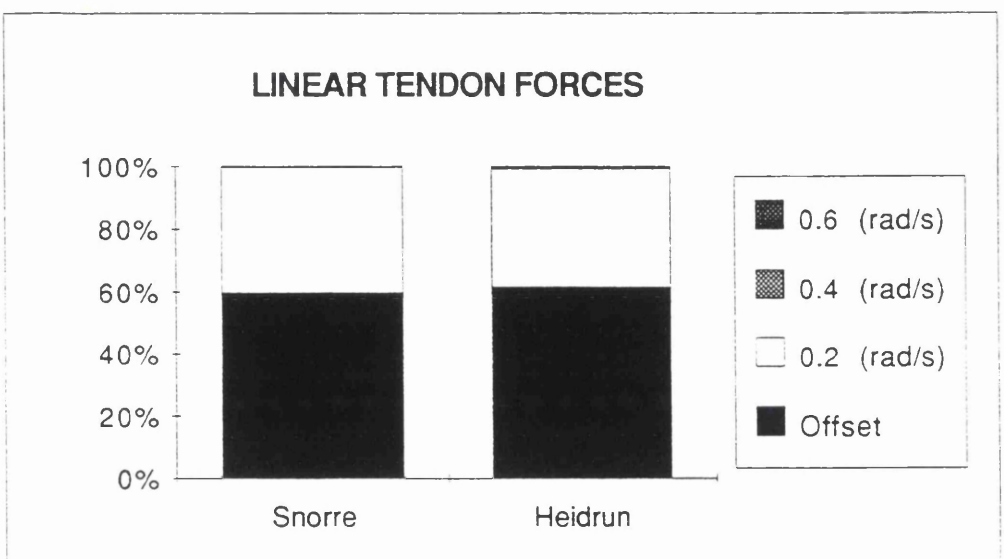

Figure 6.20

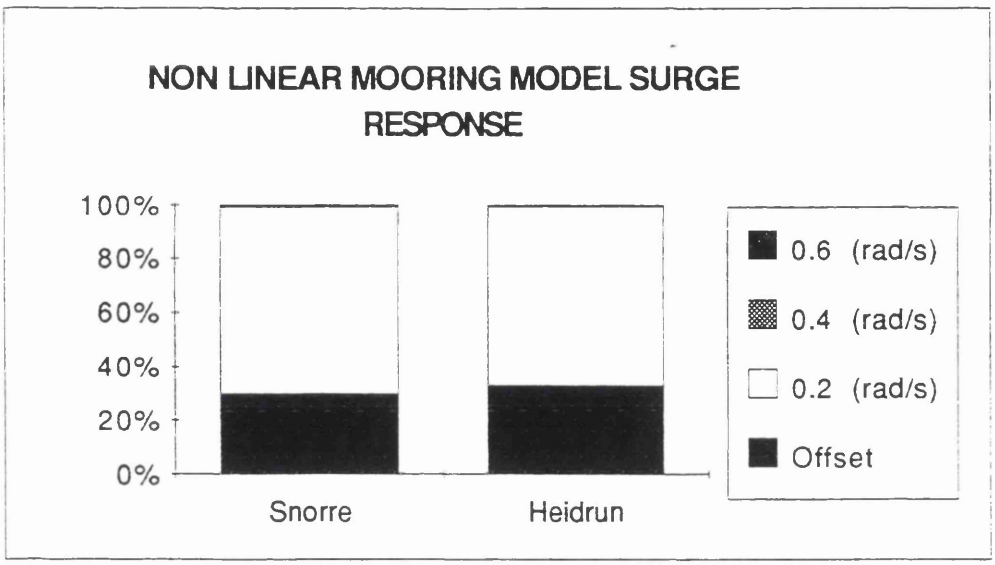

Figure 6.21

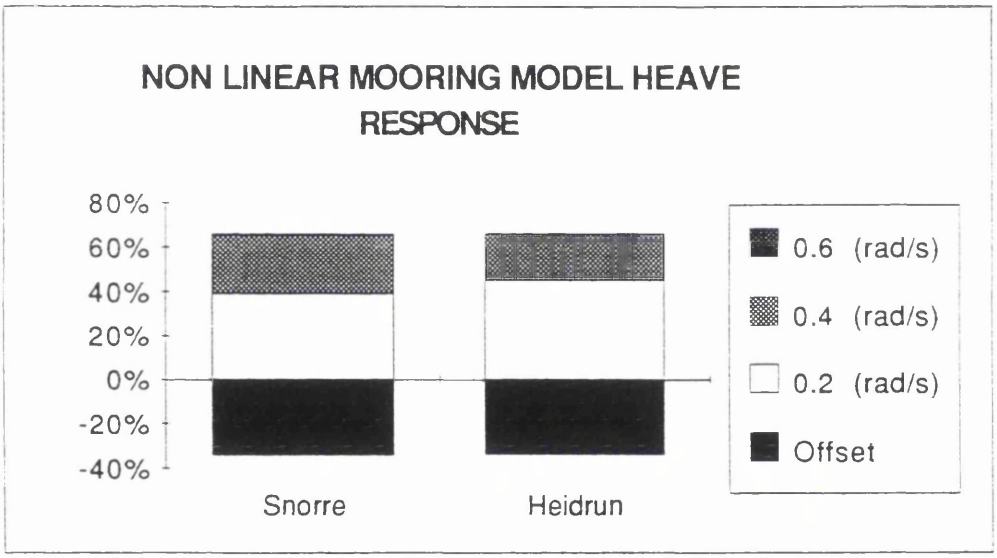

Figure 6.22

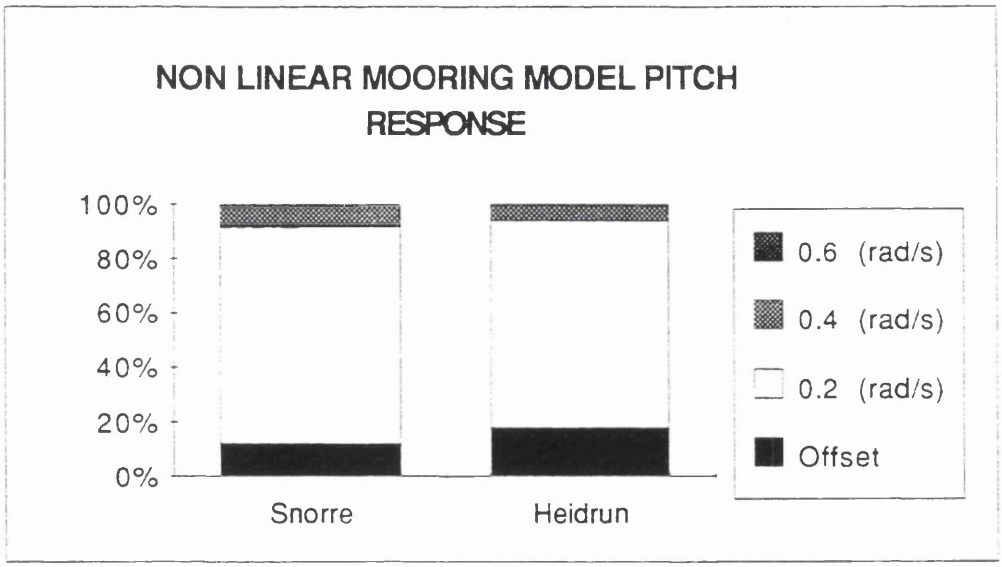

Figure 6.23

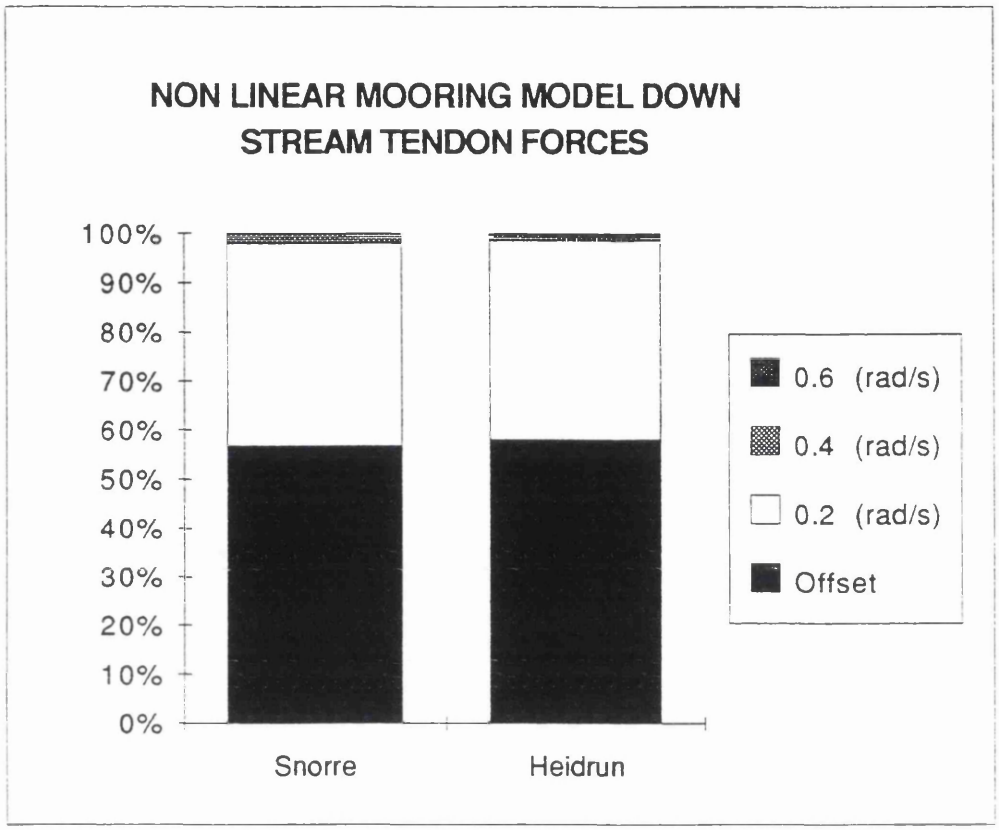

Figure 6.24

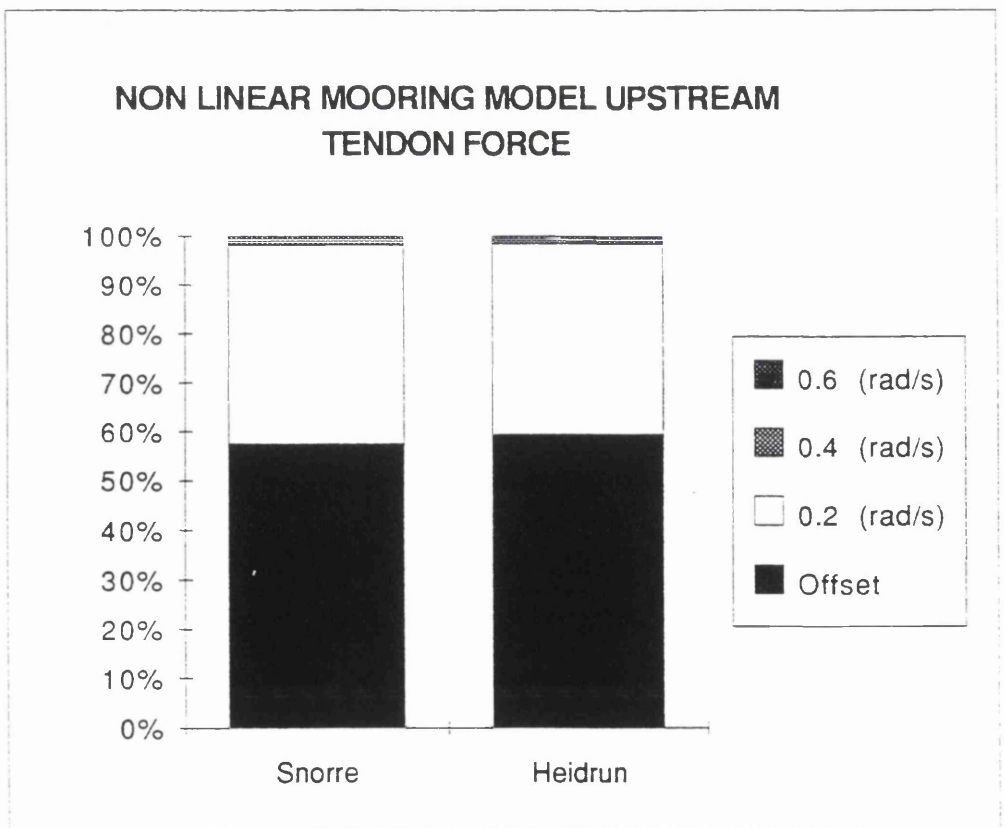

Figure 6.25

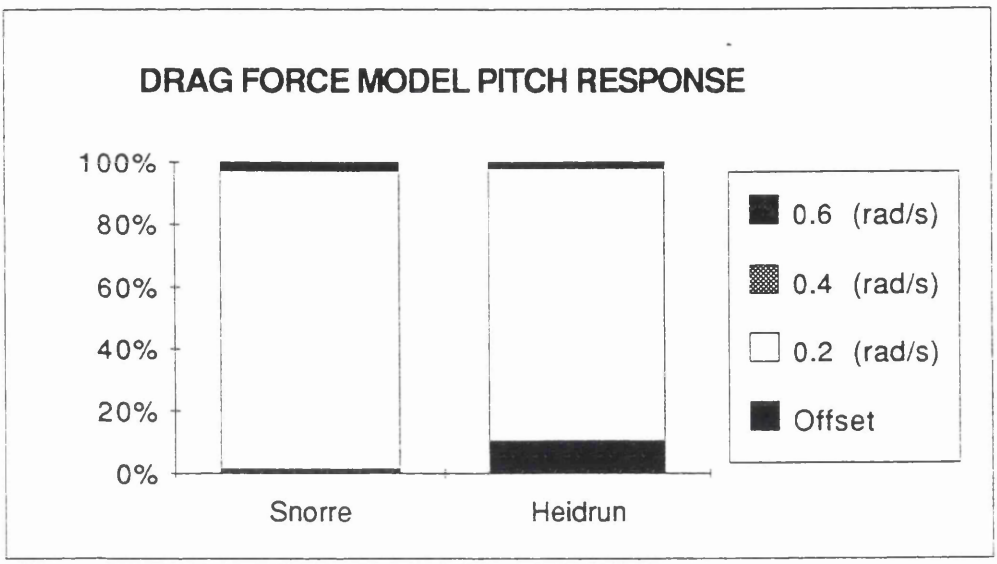

Figure 6.26

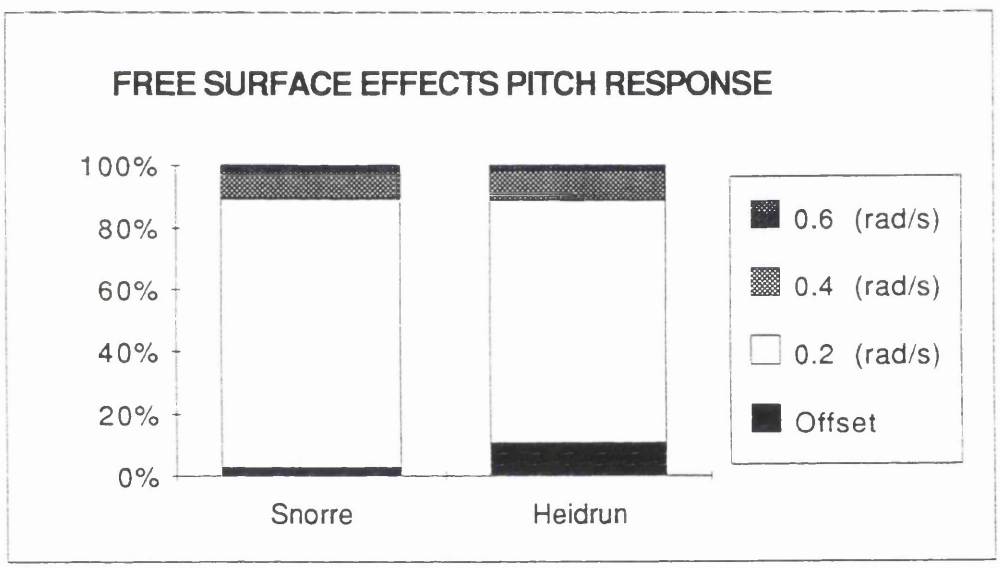

Figure 6.27

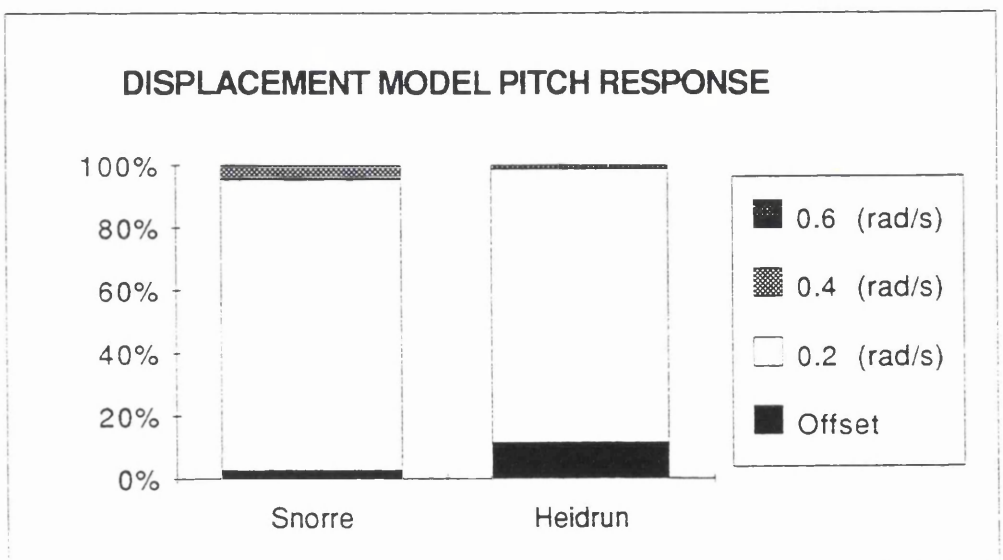

Figure 6.28

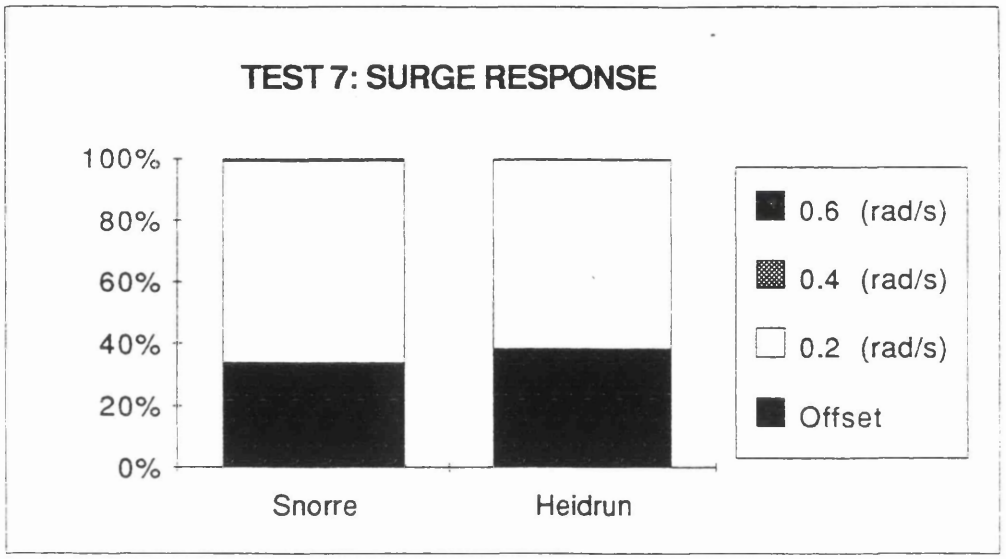

Figure 6.29

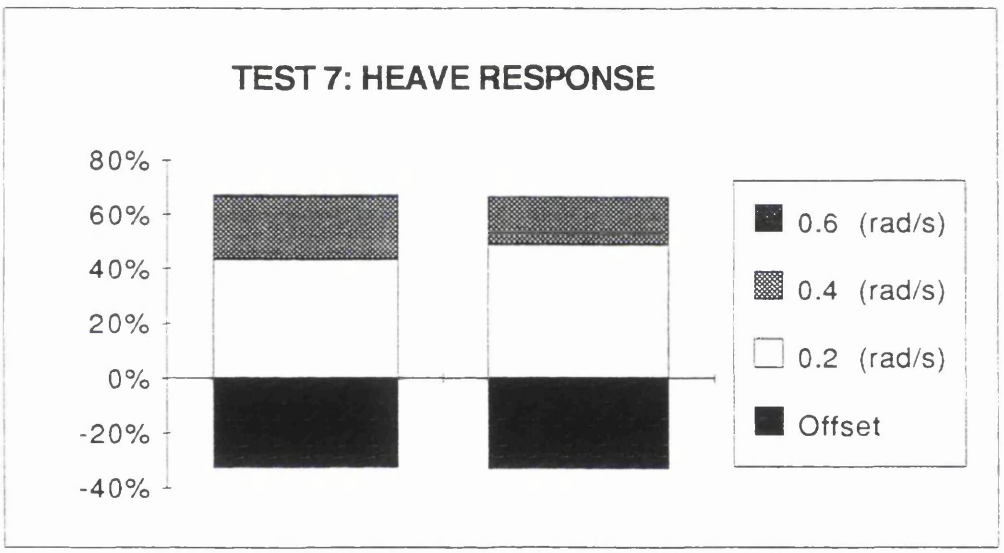

Figure 6.30

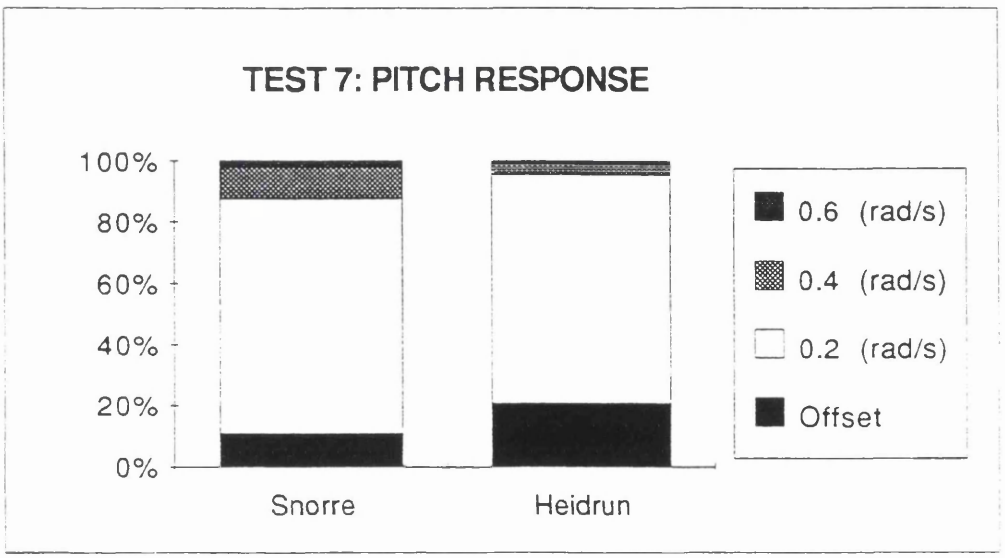

Figure 6.31

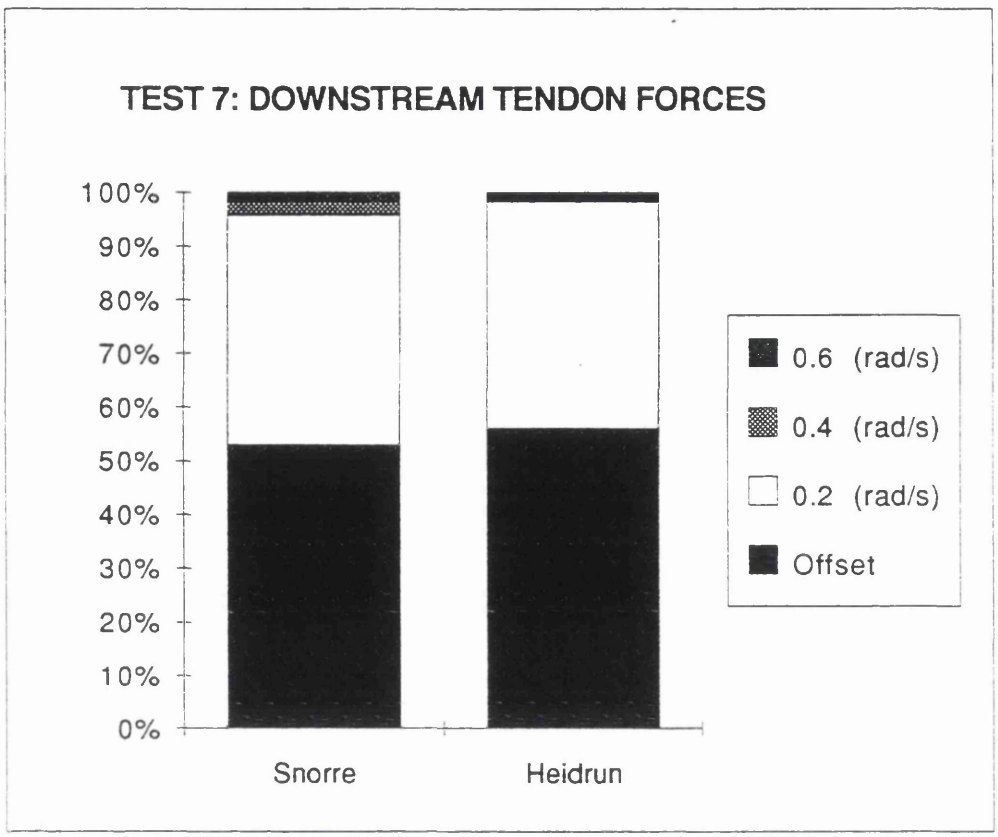

Figure 6.32

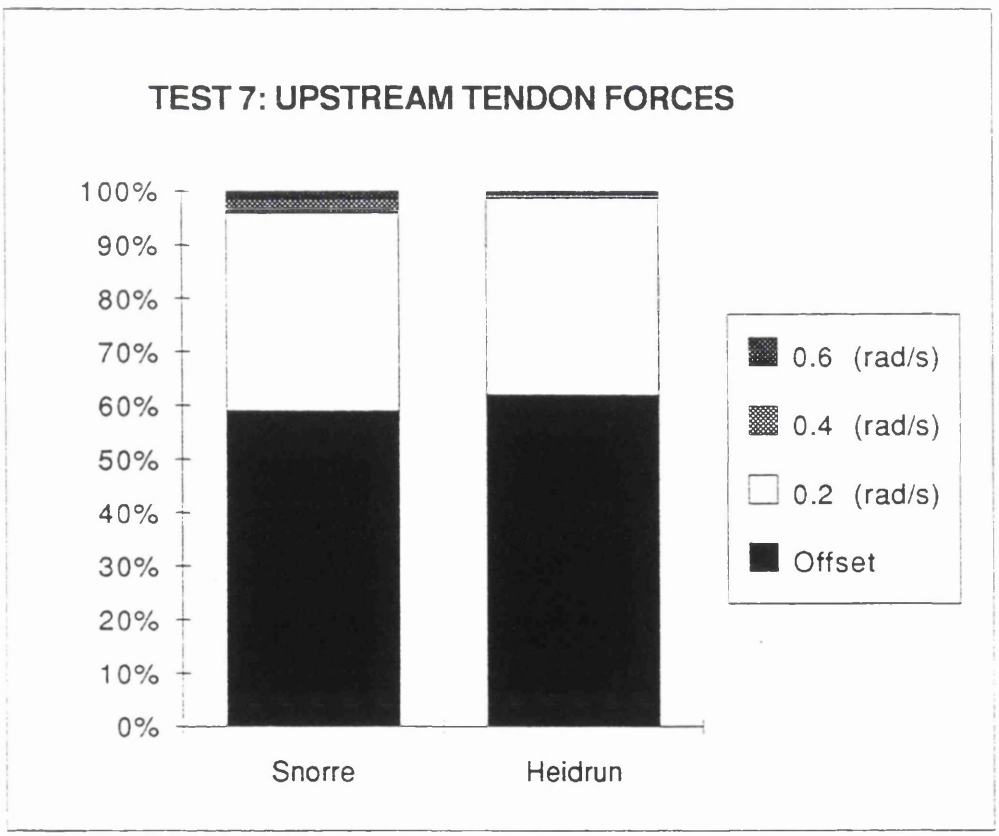

Figure 6.33

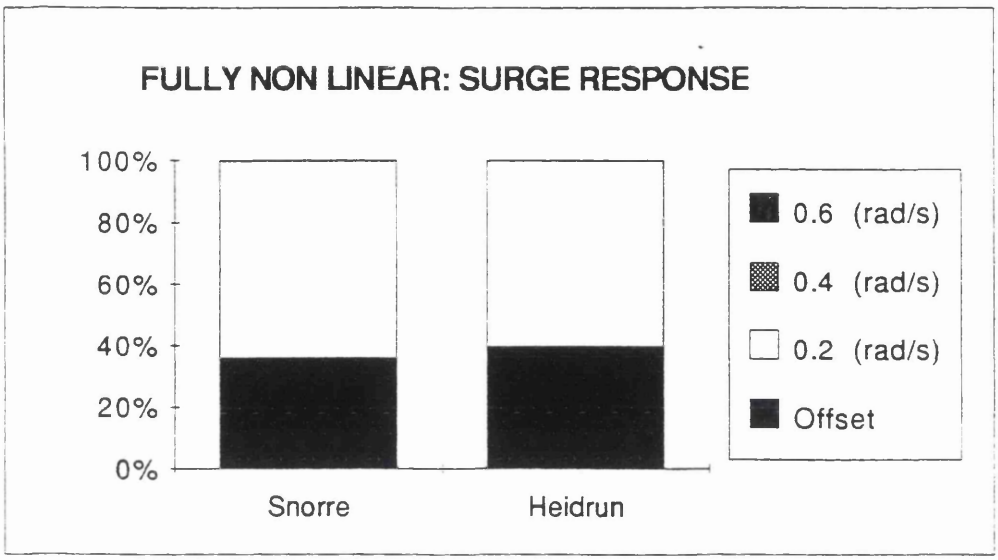

Figure 6.34

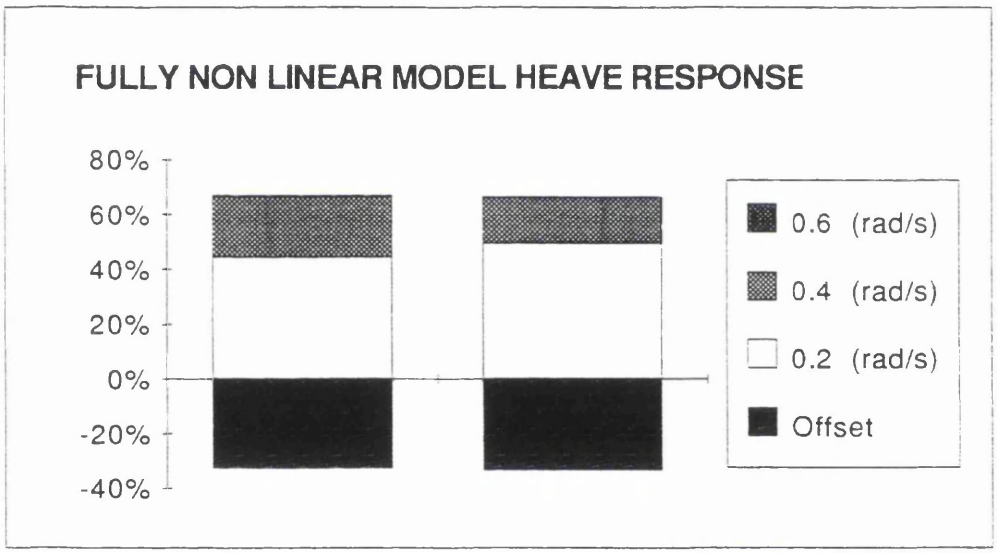

Figure 6.35

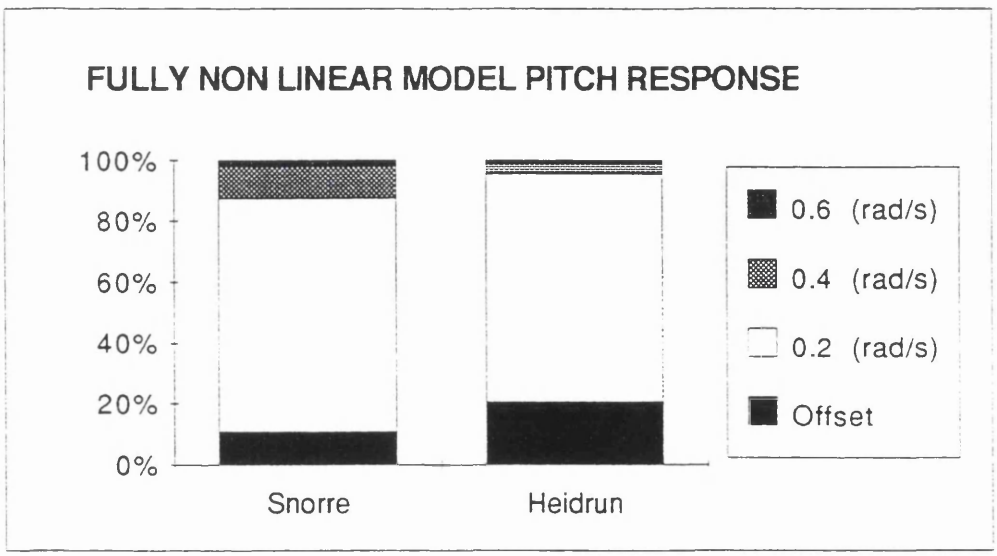

Figure 6.36

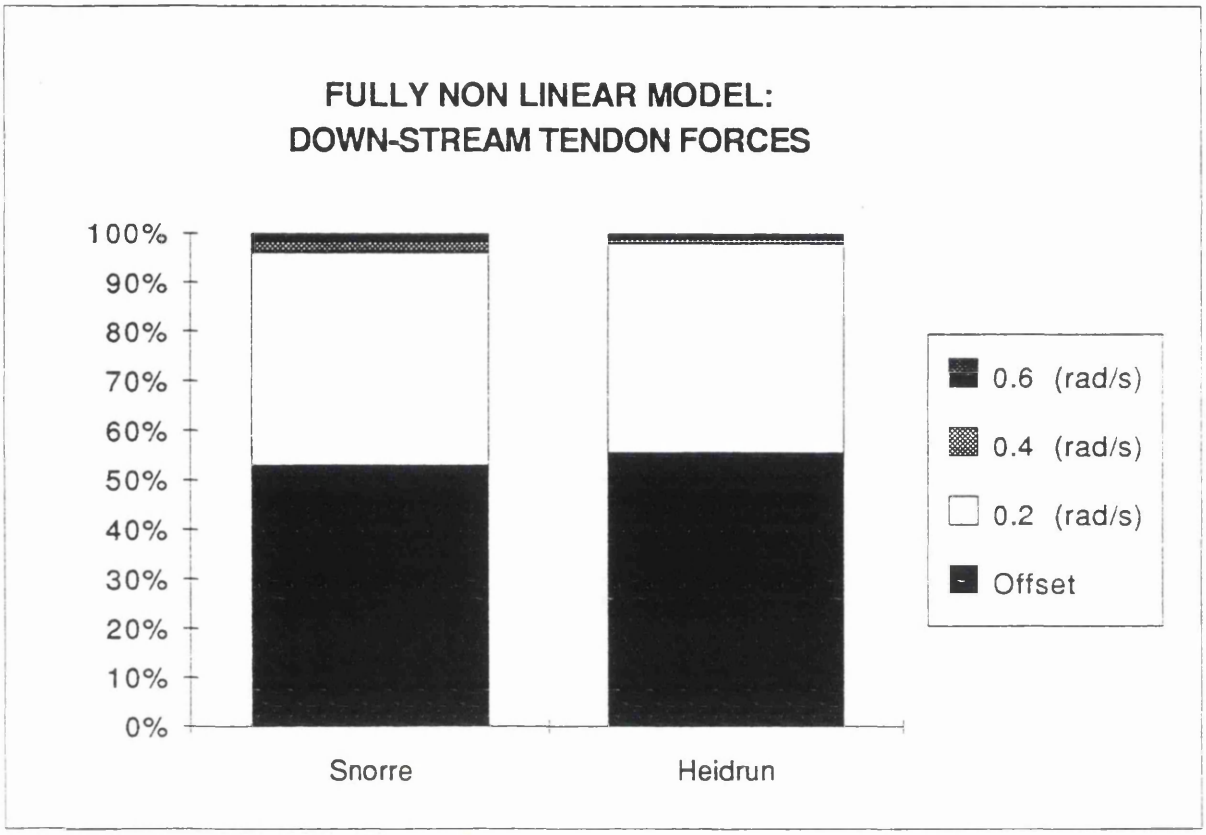

Figure 6.37

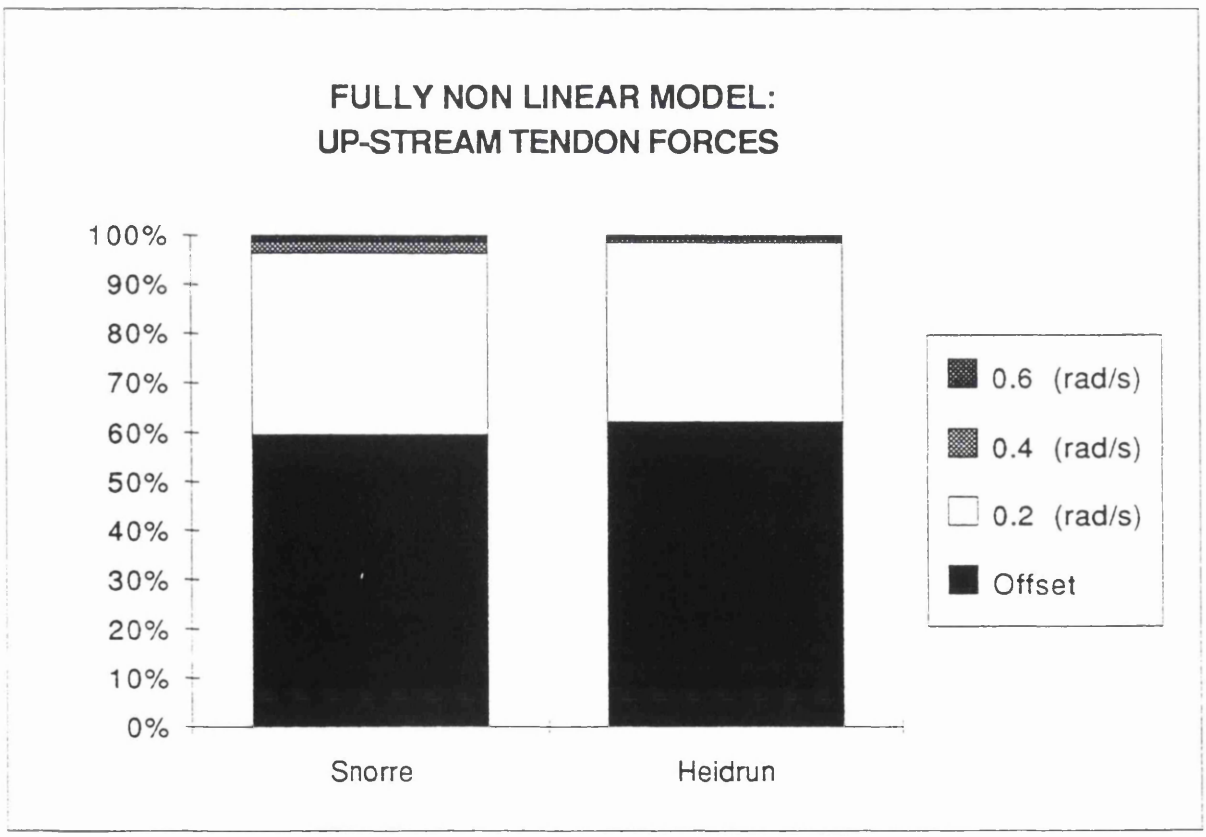

Figure 6.38

LINEAR MODEL RESULTS FOR DIFFERENT WAVE FREQUENCIES

Snorre TLP Wind Velocity: 40m/s Current Velocity: 0.6m/s

Wave Frequency (rad/s)		0.15	0.2	0.25	0.3	0.35	0.4	0.45	0.5	0.55	0.6	0.65	0.7
Wave Amplitude (m)		4.55	13.52	12.68	9.6	7.04	5.24	3.98	3.09	2.45	1.98	1.63	1.35
	Offset	7.97	8.01	7.98	7.95	7.93	7.92	7.92	7.92	7.84	7.92	7.88	7.93
Surge	ω	6.86	15.98	14.94	8.41	6.12	3.68	2.1	1.347	0.67	0.321	5.46E-02	0.129
Response (m)	2ω	7.48E-03	2.38E-02	3.08E-02	2.38E-02	1.40E-02	7.27E-03	4.55E-03	4.21E-03	1.07E-02	5.72E-03	8.24E-03	3.80E-03
	3ω	3.40E-03	1.04E-02	2.04E-02	1.44E-02	8.12E-03	4.70E-03	4.00E-03	3.11E-03	7.00E-03	2.97E-03	5.53E-03	2.62E-03
	Offset	0	0	0	0	0	0	0	0	0	0	0	0
Heave	ω	9.00E-02	0.204	0.164	7.03E-02	2.88E-02	1.08E-03	1.10E-02	1.68E-02	1.53E-02	1.33E-02	9.63E-03	5.53E-03
Response (m)	2ω	2.86E-04	6.03E-04	2.52E-04	6.62E-05	3.06E-05	1.31E-06	9.90E-06	7.75E-06	1.65E-05	1.03E-05	8.10E-06	2.05E-06
	3ω	1.24E-04	3.02E-04	1.28E-04	2.39E-05	1.57E-05	7.01E-07	5.21E-06	3.12E-06	7.50E-06	5.97E-06	3.76E-06	3.70E-06
	Offset	5.03E-05	5.26E-05	5.21E-05	4.93E-05	4.78E-05	4.18E-05	4.92E-05	5.00E-05	5.00E-05	5.03E-05	4.96E-05	5.00E-05
Pitch	ω	2.93E-04	1.64E-03	2.82E-03	2.48E-03	2.69E-03	2.18E-03	1.69E-03	1.35E-03	9.35E-04	5.70E-04	2.56E-04	1.10E-04
Response (rad)	2ω	8.58E-07	2.66E-06	4.71E-06	4.68E-06	2.70E-06	1.42E-06	1.63E-06	1.22E-06	1.67E-06	2.27E-07	3.85E-07	8.00E-08
	3ω	3.19E-07	3.23E-06	2.34E-06	4.76E-06	1.35E-06	9.10E-07	8.81E-07	2.68E-06	9.36E-07	2.45E-07	2.19E-07	1.37E-07
Force	Offset	5.87E+07	5.85E+07	5.85E+07	5.85E+07	5.85E+07	5.85E+07	5.85E+07	5.85E+07	5.85E+07	5.85E+07	5.85E+07	5.85E+07
in	ω	1.75E+07	3.99E+07	3.23E+07	1.39E+07	5.70E+06	3.15E+05	2.30E+06	3.36E+06	3.10E+06	2.65E+06	1.73E+06	1.08E+06
Downstream	2ω	2.04E+05	1.19E+05	1.10E+05	1.25E+05	1.16E+05	9.20E+04	8.60E+04	7.30E+04	7.20E+04	6.50E+04	1.13E+05	5.60E+04
Tendon (N)	3ω	1.40E+05	8.28E+04	6.40E+04	8.60E+04	7.80E+04	6.39E+04	5.30E+04	5.10E+04	4.80E+04	4.50E+04	7.30E+04	3.70E+04
Force	Offset	5.87E+07	5.85E+07	5.85E+07	5.85E+07	5.85E+07	5.85E+07	5.85E+07	5.85E+07	5.85E+07	5.85E+07	5.85E+07	5.85E+07
in	ω	1.75E+07	3.99E+07	3.23E+07	1.39E+07	5.70E+06	3.15E+05	2.30E+06	3.36E+06	3.10E+06	2.65E+06	1.73E+06	1.08E+06
Upstream	2ω	2.04E+05	1.19E+05	1.10E+05	1.25E+05	1.16E+05	9.20E+04	8.60E+04	7.30E+04	7.20E+04	6.50E+04	1.13E+05	5.60E+04
Tendon (N)	3ω	1.40E+05	8.28E+04	6.40E+04	8.60E+04	7.80E+04	6.39E+04	5.30E+04	5.10E+04	4.80E+04	4.50E+04	7.30E+04	3.70E+04

Table 6.4

NON LINEAR MODEL RESULTS FOR DIFFERENT WAVE FREQUENCIES

Snorre TLP Wind Velocity: 40m/s Current Velocity: 0.6m/s

Wave Frequency (rad/s)		0.15	0.2	0.25	0.3	0.35	0.4	0.45	0.5	0.55	0.6	0.65	0.7
Wave Amplitude (m)		4.55	13.52	12.68	9.6	7.04	5.24	3.98	3.09	2.45	1.98	1.63	1.35
	Offset	8.85	7.97	9.38	10.32	9.18	9.09	9.06	9.05	8.97	9.05	9	9.05
Surge	ω	6.9	15.61	14.78	8.38	6.12	3.68	2.1	1.35	0.671	0.32	4.60E-02	0.13
Response (m)	2ω	5.16E-02	0.145	7.47E-02	3.52E-02	1.62E-02	8.59E-03	5.40E-03	4.97E-03	1.21E-02	5.14E-03	9.40E-03	4.37E-03
	3ω	9.63E-03	0.0497	4.52E-02	1.84E-02	1.59E-02	8.06E-03	3.70E-03	4.71E-03	8.12E-03	3.55E-03	6.30E-03	3.05E-03
	Offset	-0.159	-0.332	-0.296	-0.233	-0.156	-0.136	-0.128	-0.126	-0.124	-0.125	-0.127	-0.125
Heave	ω	0.198	0.437	0.482	0.298	0.188	0.11	6.25E-02	4.30E-02	2.57E-02	1.71E-02	1.03E-02	6.36E-03
Response (m)	2ω	3.31E-02	0.234	0.169	7.95E-02	2.81E-02	9.75E-03	4.23E-03	1.57E-03	5.42E-04	1.19E-04	1.36E-04	7.43E-05
	3ω	6.54E-04	7.59E-03	7.93E-03	5.06E-03	1.27E-03	1.61E-04	4.97E-04	5.16E-04	2.70E-04	1.67E-04	1.07E-04	5.80E-05
	Offset	3.21E-04	2.77E-04	3.26E-04	3.32E-04	3.20E-04	3.19E-04	3.19E-04	3.20E-04	3.18E-04	3.20E-04	3.18E-04	3.20E-04
Pitch	ω	5.25E-04	2.10E-03	3.32E-03	2.73E-03	2.90E-03	2.30E-03	1.77E-03	1.47E-03	9.58E-04	5.85E-04	2.59E-04	1.18E-04
Response (rad)	2ω	3.21E-05	3.69E-04	1.37E-04	1.98E-04	1.19E-05	2.30E-06	2.27E-06	2.13E-06	2.00E-06	3.46E-07	7.00E-07	1.24E-07
	3ω	4.53E-06	5.35E-05	3.30E-05	1.09E-05	2.77E-05	2.62E-05	3.38E-05	2.37E-05	1.45E-05	1.78E-06	2.67E-06	1.36E-06
Force	Offset	5.69E+07	5.82E+07	5.77E+07	5.74E+07	5.70E+07	5.69E+07	5.68E+07	5.68E+07	5.68E+07	5.68E+07	5.68E+07	5.68E+07
in	ω	1.75E+07	4.73E+07	4.86E+07	3.05E+07	2.60E+07	1.88E+07	1.39E+07	1.17E+07	7.87E+06	5.25E+06	2.60E+06	1.26E+06
Downstream	2ω	3.00E+05	2.93E+06	9.98E+04	1.82E+06	2.66E+05	2.42E+05	8.20E+04	98657	1.29E+05	6.70E+04	1.09E+05	5.60E+04
Tendon (N)	3ω	1.73E+05	1.81E+06	1.54E+06	1.05E+06	3.04E+05	2.25E+05	3.00E+05	1.57E+05	1.44E+05	4.50E+04	7.00E+04	4.00E+04
Force	Offset	6.17E+07	6.23E+07	6.25E+07	6.23E+07	6.18E+07	6.16E+07	6.16E+07	6.16E+07	6.16E+07	6.15E+07	6.16E+07	6.15E+07
in	ω	1.86E+07	3.92E+07	3.26E+07	1.83E+07	1.83E+07	1.54E+07	1.28E+07	1.12E+07	7.56E+06	4.90E+06	2.57E+06	1.50E+06
Upstream	2ω	4.27E+05	2.93E+06	1.30E+06	2.12E+06	4.26E+05	2.79E+05	1.20E+05	8.15E+04	1.58E+05	6.90E+04	1.18E+05	5.90E+04
Tendon (N)	3ω	2.20E+05	1.42E+06	1.60E+06	8.70E+05	3.69E+05	1.83E+05	2.68E+05	2.45E+05	1.78E+05	2.90E+04	7.90E+04	3.60E+04

Table 6.5

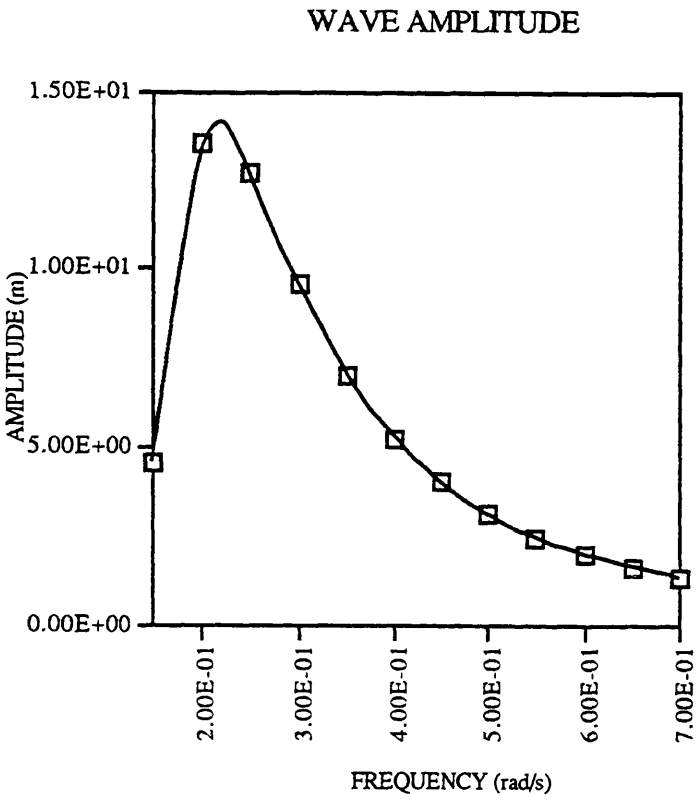

Figure 6.39

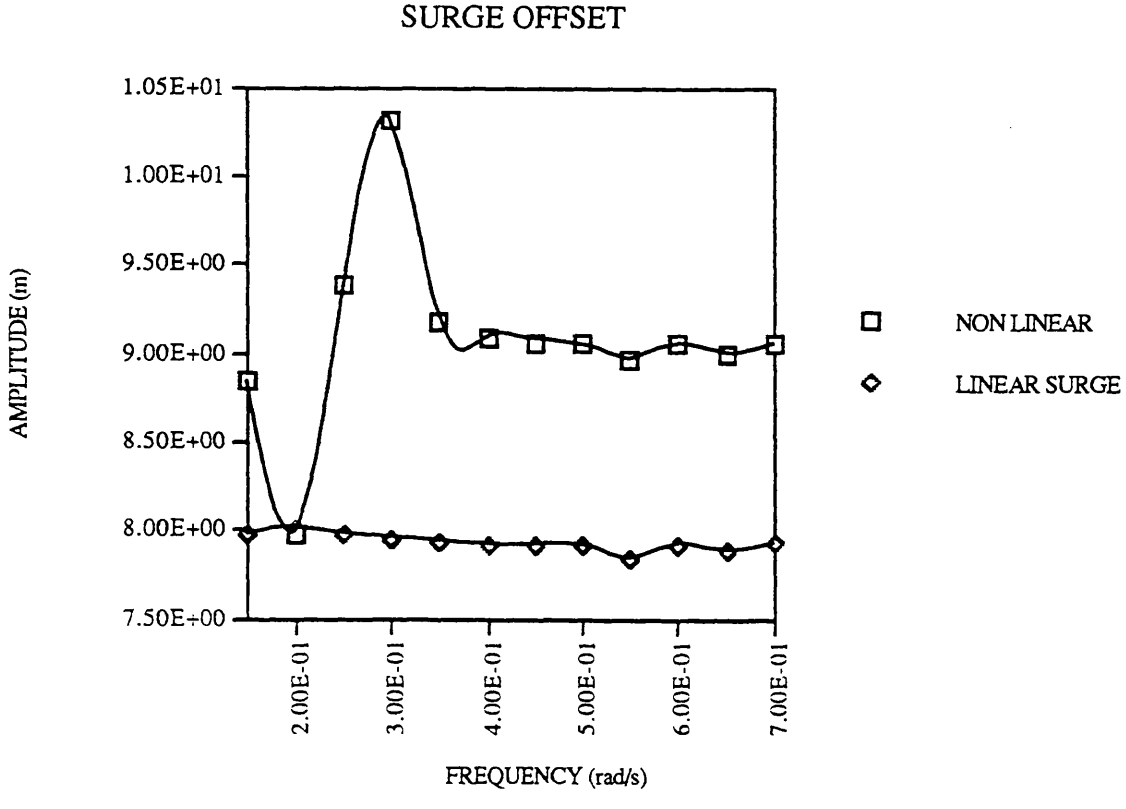

Figure 6.40

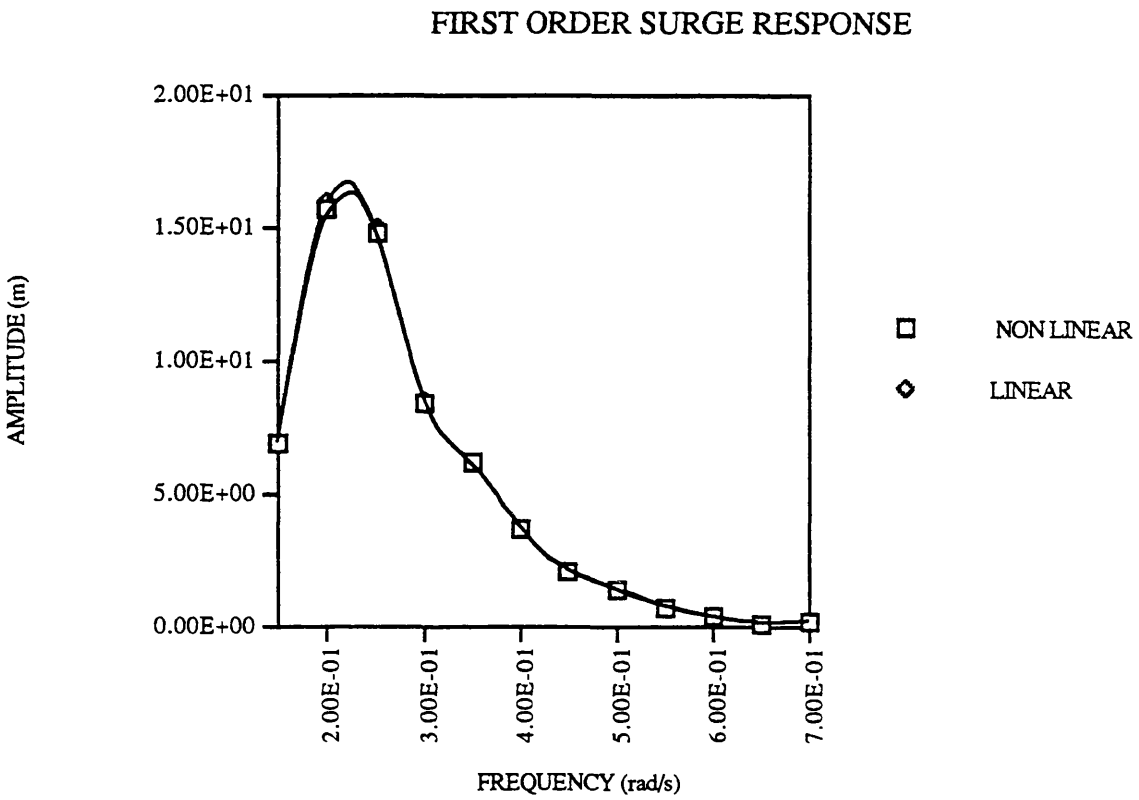

Figure 6.41

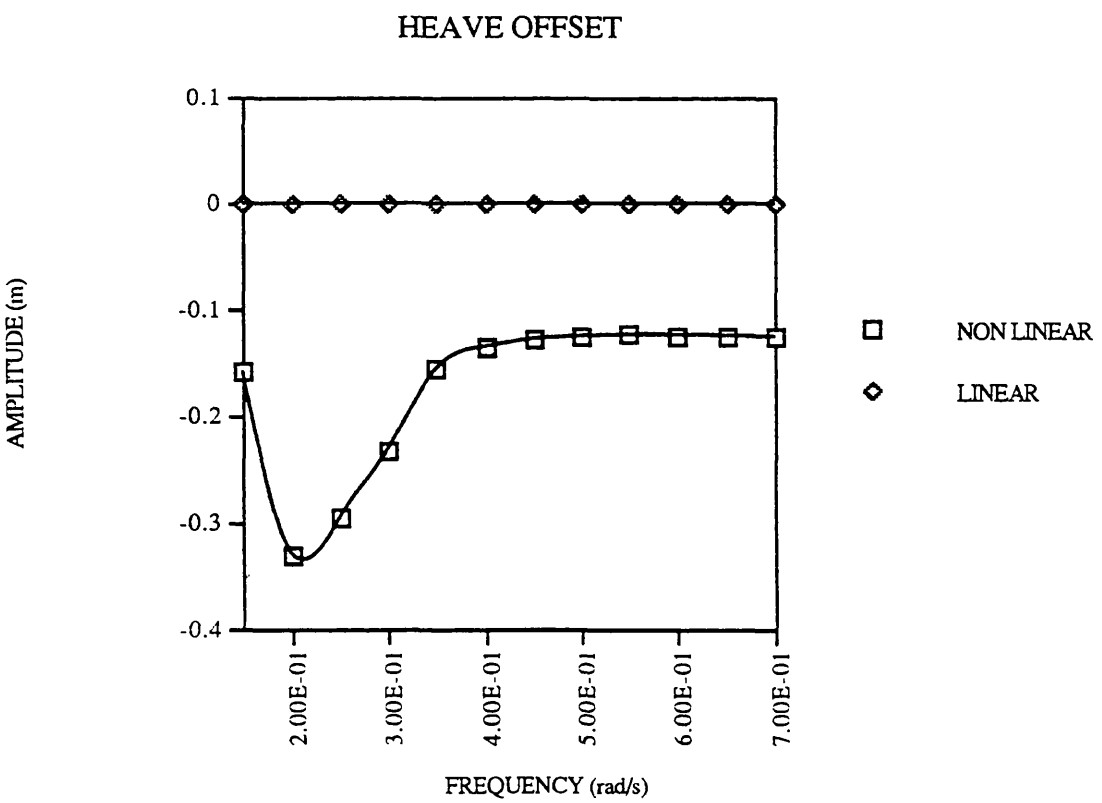

Figure 6.42

FIRST ORDER HEAVE RESPONSE

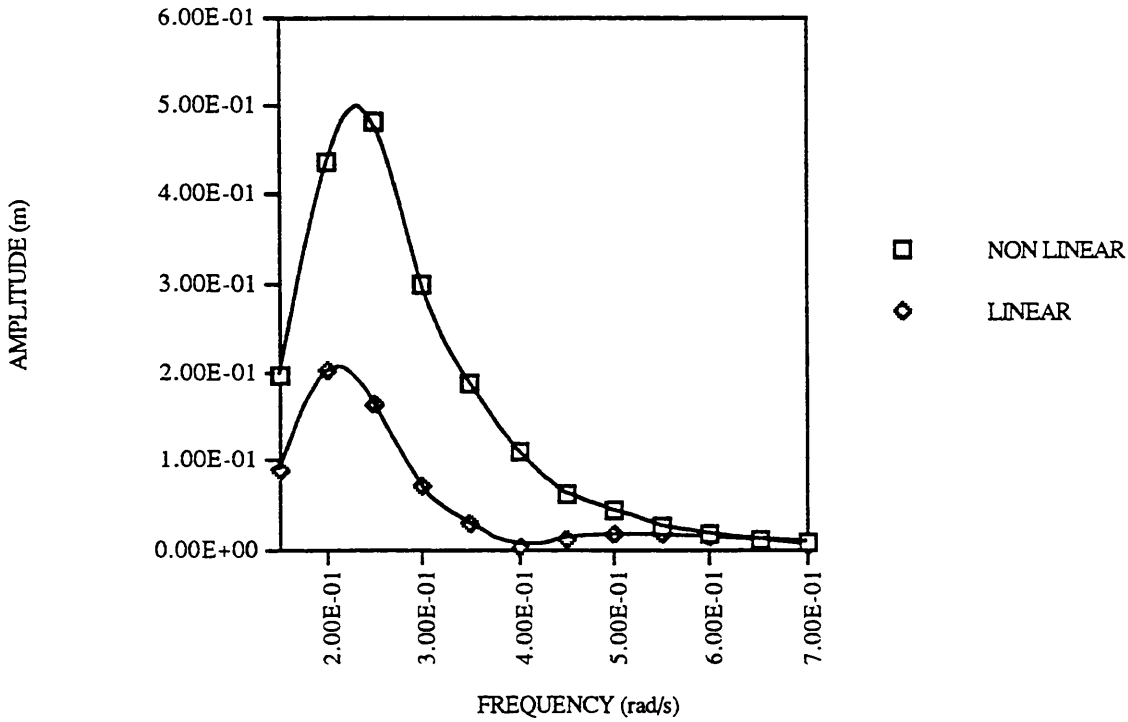

Figure 6.43

SECOND ORDER HEAVE RESPONSE

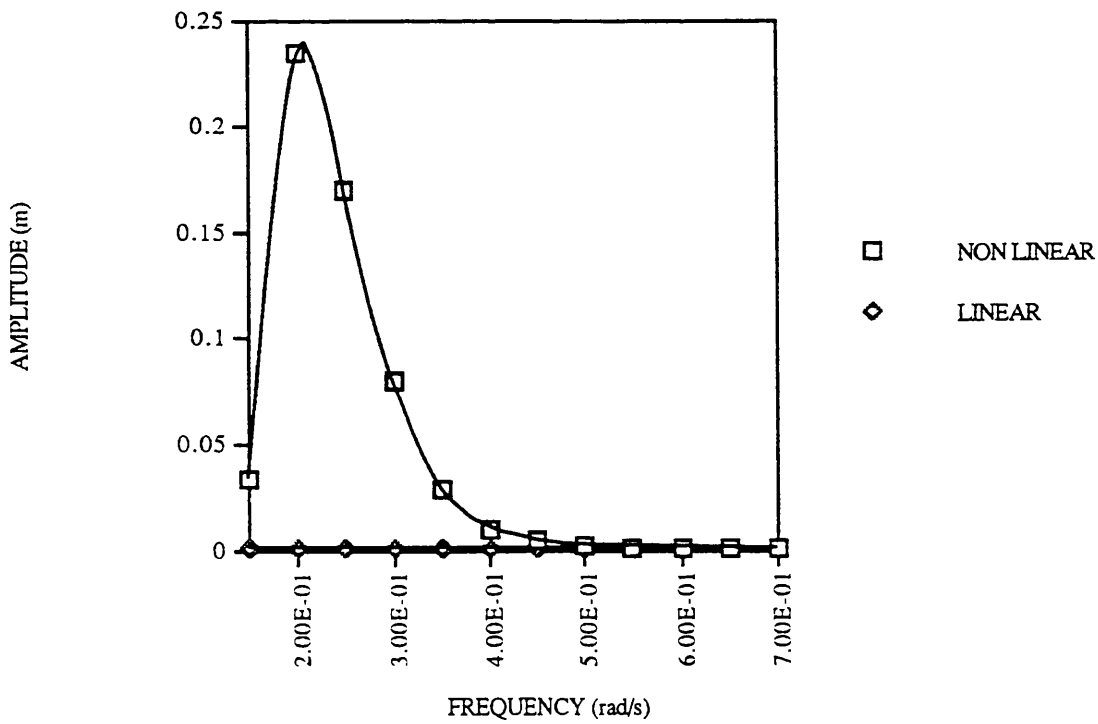

Figure 6.44

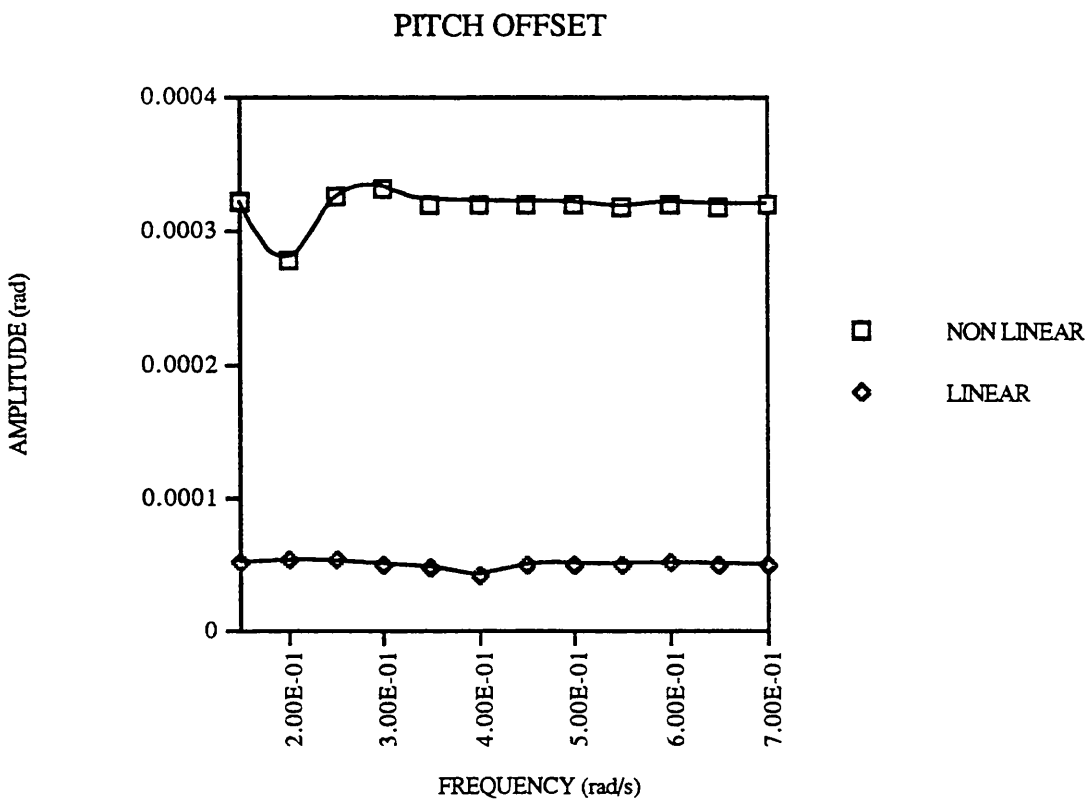

Figure 6.45

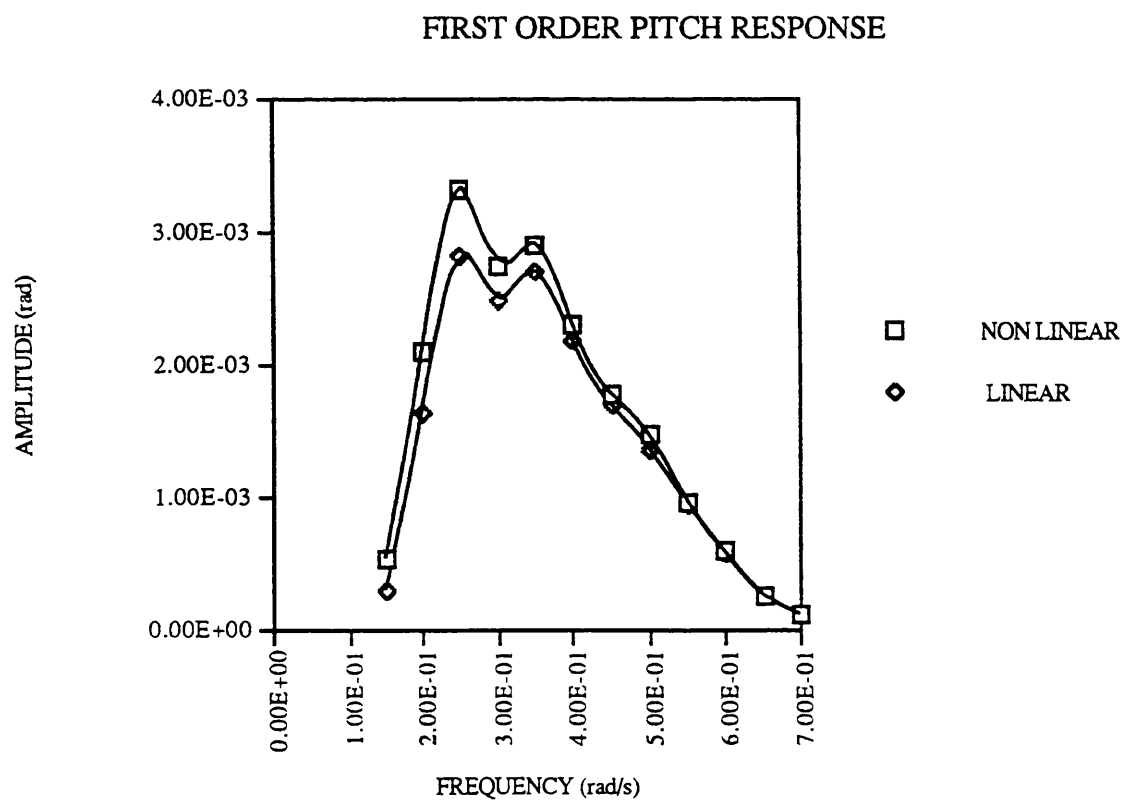

Figure 6.46

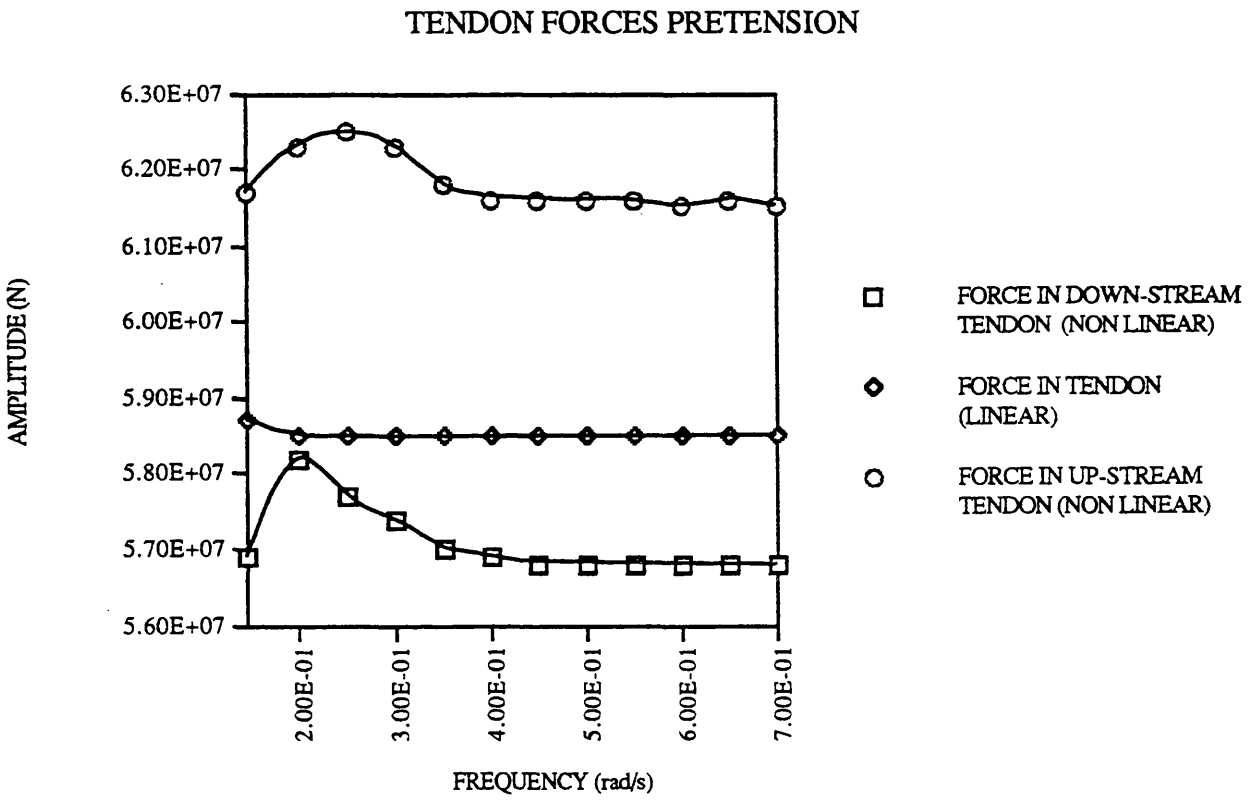

Figure 6.47

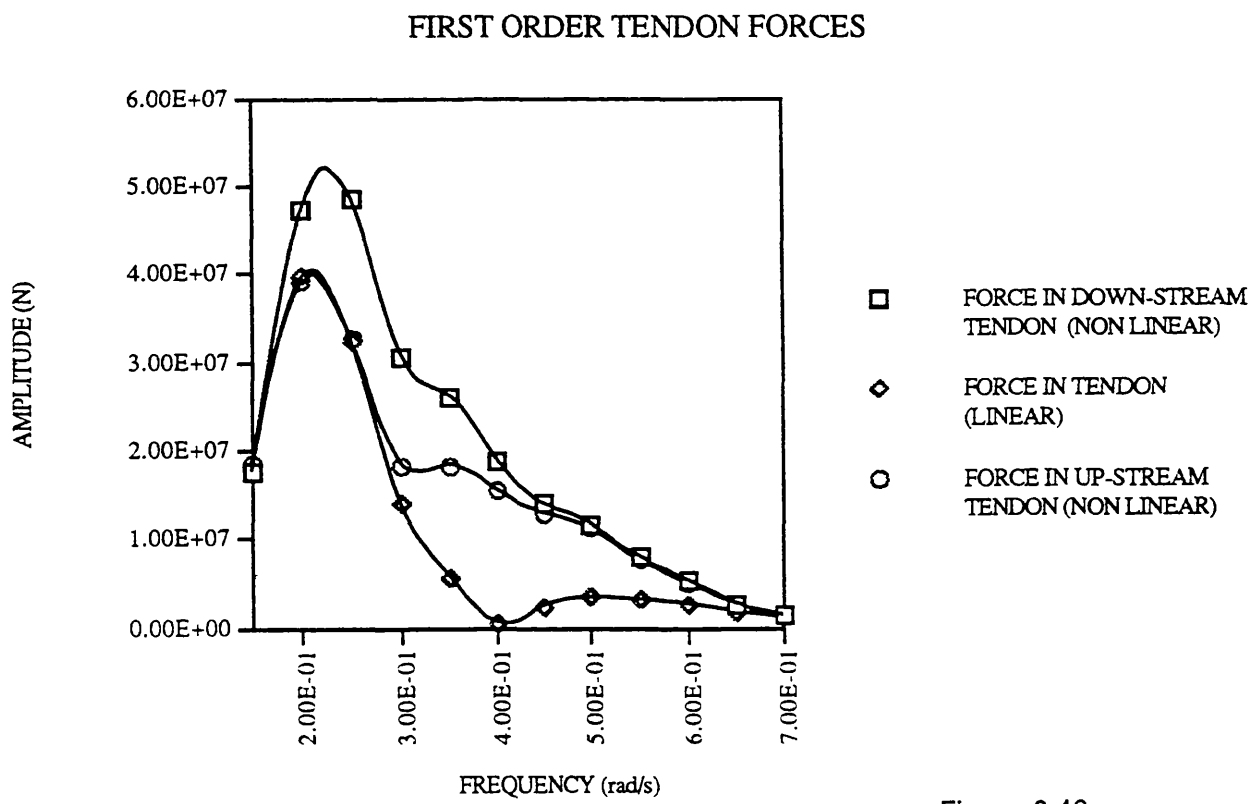

Figure 6.48

NON COLINEAR ENVIRONMENTAL FORCES

Snorre TLP Wave Amplitude: 13.52m Wave Frequency: 0.2rad/s Wind velocity: 40m/s Current Velocity: 0.6m/s

Wave Angle			0	45	90	0	45	90	0	45	90	0	45	90	0	45	0	135	135
Wind Angle			0	0	0	45	45	45	90	90	90	0	0	0	45	45	90	45	45
Current Angle			0	0	0	0	0	0	0	0	0	45	45	45	45	45	45	45	135
Surge	Xo	Offset	7.9	7.42	6.53	5.28	4.73	3.84	2.84	2.02	1.14	7.32	6.89	5.96	4.69	4.186	2.044	2.29	2.17
Response (m)	X1	0.2 rad/s	15.63	11.13	0.59	15.67	11.16	0.338	15.73	11.2	0.084	15.63	11.14	0.55	15.67	11.17	15.73	11.27	11.31
Sway	Yo	Offset	0	0.96	1.4	2.7	3.68	4.05	5.39	6.38	6.69	0.572	1.47	2.04	3.27	4.186	5.96	4.29	4.29
Response (m)	Y1	0.2 rad/s	0	11.24	15.71	0.25	11.19	15.65	0.509	11.15	15.61	4.21E-02	11.22	15.73	0.297	11.17	0.55	11.16	11.16
Heave	Zo	Offset	-0.33	-0.326	-0.308	-0.291	-0.296	-0.285	-0.295	-0.3	-0.305	-0.317	-0.317	-0.301	-0.288	-0.294	-0.301	0.279	0.279
Response (m)	Z1	0.2 rad/s	0.432	0.351	0.204	0.329	0.357	0.281	0.238	0.356	0.38	0.407	0.352	0.221	0.306	0.355	0.22	0.212	0.212
	Z2	0.4 rad/s	0.229	0.234	0.231	0.23	0.234	0.23	0.232	0.234	0.229	0.229	0.234	0.231	0.23	0.234	0.232	0.235	0.235
Roll	Ωo	Offset	0	1.58E-05	2.16E-05	-1.20E-04	-1.40E-04	-1.43E-04	-2.40E-04	-2.60E-04	-2.65E-04	-6.02E-06	2.55E-05	2.76E-05	-1.26E-04	-1.46E-04	-2.46E-04	-1.45E-04	-1.45E-04
Response (rad)	Ω1	0.2 rad/s	0	1.52E-03	3.81E-04	6.90E-05	1.51E-03	2.13E-03	1.38E-04	1.49E-03	2.12E-03	1.35E-05	1.52E-03	2.16E-03	8.26E-05	1.50E-03	1.51E-04	1.50E-03	1.50E-03
Pitch	Ωo	Offset	2.77E-04	2.72E-04	2.52E-04	1.55E-04	1.52E-04	1.32E-04	3.38E-05	-3.15E-05	1.20E-05	-2.70E-04	2.66E-04	2.46E-04	-1.49E-04	1.46E-04	-2.77E-05	1.08E-04	1.08E-04
Response (rad)	Ω1	0.2 rad/s	2.12E-03	1.48E-03	1.65E-04	2.14E-03	1.50E-03	9.60E-05	2.16E-03	1.51E-03	2.71E-05	2.12E-03	1.49E-03	6.35E-06	2.14E-03	1.50E-04	2.16E-03	1.54E-03	1.56E-03
Force	Fo	Offset	5.82	5.81	5.81	5.8	5.79	5.8	5.8	5.8	5.81	5.81	5.8	5.81	5.8	5.79	5.8	5.81	5.81
in Tendon 1	F1	0.2 rad/s	4.7	4.96	4.68	4.71	4.96	4.66	4.73	4.96	4.65	4.68	4.94	4.72	4.7	4.94	4.71	3.9	3.84
(10E-7 N)		Fo-F1	1.12	0.85	1.13	1.09	0.83	1.14	1.07	0.84	1.16	1.13	0.86	1.09	1.1	0.85	1.09	1.91	1.97
Force	Fo	Offset	5.82	5.84	5.84	5.98	6	6.01	6.16	6.18	6.2	5.82	5.83	5.85	5.98	6	6.17	6.03	6.02
in Tendon 2	F1	0.2 rad/s	4.7	3.86	3.71	4.81	3.96	3.82	4.92	4.07	3.93	4.7	3.93	3.69	4.81	4.03	4.93	4.1	4.04
(10E-7 N)		Fo-F1	1.12	1.98	2.13	1.17	2.04	2.19	1.24	2.11	2.27	1.12	1.9	2.16	1.17	1.97	1.24	1.93	1.98
Force	Fo	Offset	6.23	6.24	6.22	6.21	6.22	6.2	6.21	6.23	6.22	6.22	6.23	6.21	6.21	6.22	6.21	6.19	6.19
in Tendon 3	F1	0.2 rad/s	3.91	4.23	3.93	3.89	4.23	3.95	3.88	4.22	3.97	3.92	4.24	3.9	3.91	4.24	3.89	4.15	4.21
(10E-7 N)		Fo-F1	2.32	2.01	2.29	2.32	1.99	2.25	2.33	2.01	2.25	2.3	1.99	2.31	2.3	1.98	2.32	2.04	1.98
Force	Fo	Offset	6.23	6.21	6.18	6.03	6.02	5.99	5.85	5.84	5.82	6.21	6.2	6.17	6.02	6	5.85	5.97	5.97
in Tendon 4	F1	0.2 rad/s	3.91	4.2	4.91	3.8	4.09	4.8	3.69	3.99	4.69	3.91	4.13	4.93	3.8	4.029	3.69	5.08	5.14
(10E-7 N)		Fo-F1	2.32	2.01	1.27	2.23	1.93	1.19	2.16	1.85	1.13	2.3	2.07	1.24	2.22	1.971	2.16	0.89	0.83
Total Steady Force:		ΣFo	24.1	24.1	24.05	24.02	24.03	24	24.02	24.05	24.05	24.06	24.06	24.04	24.01	24.01	24.03	24	23.99
Mean of F1 in the 4 Tendons			4.305	4.3125	4.3075	4.3025	4.31	4.3075	4.305	4.31	4.31	4.3025	4.31	4.31	4.305	4.30975	4.305	4.3075	4.3075
Mean of (Fo-F1) for the 4 Tendons			1.72	1.7125	1.705	1.7025	1.6975	1.6925	1.7	1.7025	1.7025	1.7125	1.705	1.7	1.6975	1.69275	1.7025	1.6925	1.69

Table 6.6

CHAPTER 7: CONCLUSION AND POSSIBLE FUTURE DEVELOPMENTS

This thesis presents a prediction model to calculate the environmental forces on a tension leg platform. After validation, this model is used in a time domain program to calculate the displacements of the structure, and the forces in the tendon lines.

1. WAVE MODEL

The wave force model based on analytical solutions is a particularly useful contribution. It gives more accurate results than the conventional Morison approach and can be extended to calculate the steady drift.

It is not as precise as a diffraction radiation code, but it is much faster, and does not require mesh generation.

It can be of great help, for the early design stage of a TLP. A computer program based on this model has been developed which gives results with reasonable precision, and allows fast calculations. It is very helpful to carry out a parametric study. The input data can be changed easily, and a new calculation can be run in a few minutes.

With some minor modifications to the program, it can be used to calculate other important values for the design of a TLP. For example, it would be relatively easy, to calculate the diffracted free surface under the deck of the platform. It is also possible to calculate local loads on the columns for a structural design study.

In a recent paper, Kim et al [7.1] presented the latest developments in predicting the wave forces on circular cylinders. He proposes a method to calculate the drift damping, the difference and the sum frequency QTFs. The method has not been fully tested yet, in particular the sum frequency problem.

However, this method could be very appropriate for the TLP study since the second order poses problems in the dynamic responses of the TLP. At the moment, it is almost impossible to include the influence of the second order forces in design since the programs available to carry out these computations are very complicated and require enormous computational facilities.

2. WIND AND CURRENT MODEL

The wind force calculations show that the wind forces play an important role in the steady surge displacement of the TLP. This is particularly important because they cause a set down of the TLP in heave. The set down has to be taken into account for the design of the deck height.

The varying wind has also an important effect in surge since it can excite the TLP at its natural frequency. However, a precise calculation of this force is quite difficult due to the uncertainties in the description of the wind. Wind spectra give a representation of the energy carried by the fluctuating wind over a range of frequencies. In the frequency range around the surge natural frequency of the TLP, the wind gusts energy is not very well known, and the different wind spectra developed until now are not completely satisfactory for design.

The dynamic responses of the platform vary largely from one wind spectrum formulation to the other, both in terms of response spectra or significant values.

The prediction model developed in this thesis for the wind is very simple. It could be improved in several ways. A non correlated flow could be considered by using a multiple loading method. The geometry of the deck has been crudely represented as a rectangular box. A more suitable geometry could be taken into account. The variation of the wind velocity with the altitude could also be implemented more carefully specially in the Ochi-Shin, Kaimal and Slettringen wind spectrum formulations.

However, the more urgent improvement concerning slowly varying wind calculations would be a better modelling of the wind gusts in the low frequency region.

In this study, the influence of the current has also been investigated. The analysis shows that taking a constant or varying velocity profile does not make significant changes in the results.

However, the current loading is important for the calculation of the steady rotations of the TLP. This has a direct influence on the asymmetry of the forces in the tendons. High velocity currents can also have a significant influence on the surge offset and thus on the set down of the TLP.

Some uncertainties remain in the current force calculations. The influence of the wind on the storm surge current for example. For the moment, only empirical formulae are available. The influence of the current on the waves could also be investigated. The waves could become steeper and the free surface effects could be increased by high velocity currents.

3. TIME DOMAIN MODEL

The time domain model presents two advantages over the frequency domain study.

It can be used to calculate the loads in the tendons that are one of the main important design parameters for a TLP. It also enables us to include non linearities in the prediction model.

The analysis carried out here shows that the most important non linearity is the non linear behaviour of the mooring system. It radically changes the response of the platform in heave. It enables us to evaluate the set down. In terms of tendon forces, it gives higher values of the pretension and the first order forces. It introduces some asymmetry between the different tendons. Finally, it shows second order effects that could play some role in springing.

The analysis on the influence of the directionality of the environmental forces shows that the loads and responses are not very sensitive to the directionality. However, it should be noticed that all the effects have not been taken into account. In particular, directionality of the waves seems to play an important role in the ringing phenomenon. The sum-frequency

forces are also expected to vary with the wave direction. Thus, the direction of the sea does not have significant influence on the steady and first order forces of the tendons, but higher order forces and responses should be investigated.

The time domain model developed here, could be improved. An irregular sea state could be taken into account. Then, the slowly varying drift could be added to the model, as well as the slowly varying wind.

This would imply careful modifications in the free surface effect calculations. Indeed the Airy theory would overestimate the kinematics in the wave crests. A suitable stretching formula would have to be used. Yet the Wheeler stretching formula is said to pose problems too. An alternative would be to use a non linear wave crest model such as the Longuet Higgins model.

A more careful study could also be carried out on the slapping effects on the TLP. At the moment, the model implemented to predict slapping forces is indeed very simplistic.

Finally, if the sum frequency QTFs can be approximated, it would be useful to implement them in the time domain program to see their effects. They would induce super-harmonic responses in heave and pitch, and more importantly the springing effect on the tendon forces could be calculated.

REFERENCE OF CHAPTER 7

[7.1] Kim M.H., Natvig B.J., Mercier R.S., Gu G., Wu C., 1995, PC Computation for Second Order Wave Loads on Large Volume Multi-Column Structures, Proc. of the Fifth ISOPE Conference.